Summer 2014

Studies of fungal natural products and the degradation of A- and SS-trenbolone

Sarah Ann Long
University of Iowa

STUDIES OF FUNGAL NATURAL PRODUCTS AND THE DEGRADATION OF α– AND ß–TRENBOLONE

by

Sarah Ann Long

A thesis submitted in partial fulfillment
of the requirements for the Doctor of
Philosophy degree in Chemistry
in the Graduate College of
The University of Iowa

August 2014

Thesis Supervisor: Professor James B. Gloer

Graduate College
The University of Iowa
Iowa City, Iowa

CERTIFICATE OF APPROVAL

_____

PH.D. THESIS

_____

This is to certify that the Ph.D. thesis of

Sarah Ann Long

has been approved by the Examining Committee
for the thesis requirement for the Doctor of Philosophy
degree in Chemistry at the August 2014 graduation.

Thesis Committee: _____
James B. Gloer, Thesis Supervisor

_____
David M. Cwiertny

_____
Amanda J. Haes

_____
Daniel M. Quinn

_____
David F. Wiemer

ACKNOWLEDGMENTS

First, I would like to thank my amazing advisor and thesis supervisor, Dr. Gloer. You are the best advisor I could have ever hoped for. Your patience and understanding really helped me through some tough times, and your caring and laid–back teaching style helped me to worry less, sometimes, even in the most stressful of times. Thank you so much for ALWAYS taking the time to talk and help me out with my research no matter how busy you were, and we all know that there is never a point when you weren't juggling multiple projects and deadlines.

Thank you to my committee members for their time and helping me throughout my graduate career. I would also like to thank all the collaborators that made the work discussed within this thesis possible. Thank you to Dr. Wicklow and colleagues at the United States Department of Agriculture (USDA) National Center for Agricultural Utilization Research (NCAUR) in Peoria, Illinois. These researchers were responsible for the collection, isolation, identification, fermentation, extraction, and the antifungal and antiinsectan bioactivity screening of the isolates. Thank you to Dr. Cwiertny of the Department of Civil Engineering at the University of Iowa, and all the collaborators that I refer to as "Team Trenbolone," for reaching out to us to provide NMR data to further support their conclusions about the degradation of both 17α– and 17β–trenbolone. Without "Team Trenbolone" the dream of being published in such a prestigious journal as *Science* may not have come to fruition, especially not this early in my career. Dr. Jonas Baltrusaitis, thank you for your work calculating ECD spectra for multiple compounds and multiple isomers of each compound.

Thank you to the people that run the NMR, MS, and X–ray crystallography facilities. Dr. Santhana Velpuillai, thank you for always helping me troubleshoot the parameters of different NMR experiments to insure the best data possible was collected. Dr. Lynn Teesch and Vic Parcell, thank you for the countless hours of expanding

different regions, optimizing conditions, and going over the MS data until the ions of interest were found. Thank you to Dr. Dale Swenson for collecting and analyzing the crystal data, and for your patience and willingness to look at many "crystals" until I was finally able to obtain one of use.

Thank you to the staff of the Department of Chemistry, especially Earlene Erbe, Janet Kugley, and Sharon Robertson, for always finding time to make our lives as graduate students easier, even when it probably made your jobs more difficult. These three women are always there for students in need of help starting from the day we apply all the way up to our graduation.

Thank you to all of the Gloer group members past and present for teaching me the ropes, learning with me, and providing a lot of fun and memories along the way.

Thank you to Dr. Leo Sternbach. We never met, but your work made mine possible.

Last, but certainly not least, I would like to thank my family and friends. They have provided so much love and support throughout the years that without them I honestly don't know if I would have made it to this point. Being a third generation chemist, I thought I knew what I was getting myself into when I started this journey, but I couldn't have been more wrong. Surviving graduate school is the biggest accomplishment in my life, up until this point. I am sure there will be many more hurdles and life changing events ahead, but with my amazing support system I know we can get through those as well. Jolene and Meagan you two are the sisters I never had. I am so grateful that we continue to be as close, if not closer, than we were in undergrad. Our girls' weekends were always, and will continue to be, a welcome and needed escape. "Iowa family" you made grad. school a fantastic experience outside of the chemistry building. Our ridiculous study sessions and "family dinners" will be memories I will always cherish. Mom and Dad, thank you comforting me and/or giving me the tough–love pushes I needed, and trying to figure out which one I needed in each instance. Tyler,

trying to write our theses at the same time was a bad plan, but we made it! I love you and cannot wait for the next chapter of our lives to begin.

TABLE OF CONTENTS

LIST OF TABLES vi

LIST OF FIGURES vii

LIST OF ABBREVIATIONS xii

CHAPTER

1. INTRODUCTION 1

2. SCREENING OF FUNGAL ISOLATES 22

3. KIPUKASIN AND OXEPINAMIDE DERIVATIVES FROM ASPERGILLUS PUULAAUENSIS 32

4. CHEMICAL INVESTIGATION OF A TRICHOTHECIUM CROTOCINIGENUM ISOLATE 49

5. PHOTODEGRADATION AND REGENERATION OF 17A– AND 17B– TRENBOLONE 60

6. SUMMARY AND CONCLUSIONS 78

7. EXPERIMENTAL 82

General Experimental Procedures 82
General Procedures for NMR Experiments 85
General Procedures for Collection and Refinement of X–Ray Data 89
GCMS Conditions for Amino Acid Derivative Analysis 89
General Procedures for Isolation of Fungal Species from Wood–Decay Fungal Hosts 90
General Procedures for Solid–Substrate Fermentations 90
General Procedures for Antifungal Assays 91
General Procedures for Antiinsectan Assays 92
General Procedures for Antibacterial Assays 94
Procedures for Isolation and Characterization of Metabolites from an isolate of *Aspergillus puulaauensis* (MYC–2152 = NRRL 62124) 95
Procedures for Isolation and Characterization of Metabolites from an Isolate of *Trichothecium crotocinigenum* (MYC–2235) 99

APPENDIX A. SELECTED NMR AND MASS SPECTRA 107

APPENDIX B. X–RAY CRYSTALLOGRAPHIC DATA OF 15-EPI-OXEPINAMIDE E (GLO11_6) 180

REFERENCES 198

LIST OF TABLES

Table

2.1. Bioactivity of Endophytic Fungal Extracts....24

2.2. Endophytic Sample Hosts and Geographic Origins....24

2.3. Bioactivity of Fungicolous/Mycoparasitic Fungal Extracts....24

3.1. NMR Comparison of 15-*epi*-Oxepinamide E (**3.1**), Brevianamide L (3.15), and Oxepinamide E (3.14)....36

3.2. NMR Data for Artifact **3.4**....40

3.3. NMR Data for Kipukasin H (**3.2**)....45

4.1. NMR Data for **4.1** in Methanol–d_4....52

5.1. NMR Data for 17β–Trenbolone (**5.3**) in CD_3OD....63

5.2. NMR Data for **5.5** in CD_3OD....65

5.3. NMR Data for **5.6** in CD_3OD....66

5.4. NMR Data for **5.7** and **5.8** in CD_3OD....69

5.5. NMR Data for 17α–Trenbolone (**5.4**) in CD_3OD....72

B1. Crystal Data and Structure Refinement for Glo11_6....181

B2. Atomic Coordinates (x 10^4) and Equivalent Isotropic Displacement Parameters (A^2 x 10^3) for Glo11_6....182

B3. Bond Lengths [A] and Angles [deg] for Glo11_6....184

B4. Anisotropic Displacement Parameters (A^2 x 10^3) for Glo11_6....191

B5. Hydrogen Coordinates (x 10^4) and Isotropic Displacement Parameters....192

B6. Torsion Angles [deg] for Glo11_6....194

B7. Hydrogen Bonds for Glo11_6 [A and deg.]....197

LIST OF FIGURES

Figure

1.1. H2BC (left) Compared to the HMBC (right) Spectra of Cyclosporin A (Spectra from ref. 27) 9

1.2. Traditional HMBC (a) and IMPACT–HMBC (b) Spectra of Isopropylidene Glycerol (Spectra from ref. 36) 12

1.3. Flow Chart of Automated HPLC–CapNMR Process 17

1.4. Flow Chart of Bruker's HPLC–SPE–NMR Setup....18

3.1. Structure and $[\alpha]_D$ –value Comparisons of Stereoisomers **3.1**, **3.14**, and **3.15** 35

3.2. ORTEP Image of 15-*epi*-Oxepinamide E (**3.1**) 37

3.3. Experimental ECD Spectrum (left), and TDDFT–Calculated ECD Spectrum Based on the Conformation of **3.1** in the X–ray Crystal Structure....38

3.4. ECD Spectrum of **3.4** (top) Compared to Those Calculated for the Two Possible Diastereomers (bottom left and right) 42

3.5. Key HMBC Correlations for Kipukasin H (**3.2**)....44

3.6. ECD Spectra of Kipukasins F (**3.21** top), H (**3.2**, left), and I (**3.3**, right)....46

4.1. Comparison of the Upfield ^{1}H NMR Signals observed for Compound **4.1** in $CDCl_3$ (left) and Methanol-d_4 (right)....51

4.2. Expansion of the Upfield Region of the HSQC Spectrum of **4.1** 53

4.3. Key HMBC Correlations Supporting the Assignment of Structure **4.1**....54

4.4. Co-injection of FDAA–derivatized D– and L–Pip Standards (1:1) with the Sample Derived from **4.1**....55

5.1. Trenbolone Acetate (**5.1**) and its Excreted Metabolites....61

5.2. Key HMBC (arrows) and COSY (boldface) Correlations for **5.3** 64

5.3. Key HMBC (arrows) and COSY (boldface) Correlations for **5.5** 66

5.4. Key HMBC Correlations Useful in Locating the Two Aldehyde Units in **5.6**.....66

5.5. Summary of NMR Shift Data and HSQC, HMBC (arrows), and COSY (boldface) Correlations for the as-yet Unidentified Decomposition Product (δ_H in black; δ_C in red)....74

5.6. Structure of **5.10** Obtained Upon Reaction of **5.4** in D_2O (left) and H_2O (right). 75

5.7. Proposed Mechanism for the Conversion of **5.4** to **5.10** in D_2O 75

5.8. Proposed Mechanism for the Reversion of **5.10** to Deuterated 17α–Trenbolone (**5.4'**) 76

A1. ^{1}H NMR Spectrum of 15–*epi*–Oxepinamide E (**3.1**; $CDCl_3$, 600 MHz) 108

A2. ^{1}H NMR Spectrum of 15–*epi*–Oxepinamide E (**3.1;** 500 MHz, DMSO–d_6).....109

A3. ^{13}C NMR Spectrum of 15–*epi*–Oxepinamide E (**3.1**; $CDCl_3$, 100 MHz).....110

A4. DEPT Spectrum of 15–*epi*–Oxepinamide E (**3.1**; $CDCl_3$, 100 MHz) 111

A5. HSQC Spectrum of 15–*epi*–Oxepinamide E (**3.1**; $CDCl_3$, 600 MHz).....112

A6. HMBC Spectrum of 15–*epi*–Oxepinamide E (**3.1**; $CDCl_3$, 600 MHz).....113

A7. Co-injection of the TFA(+)–*S*–2–butyl Ester Derivatives of the D– and L–Standards (1:1) with the Derivative Mixture Prepared from the Hydrolyzate of Compound **3.1** 114

A8. ^{1}H NMR Spectrum of Fraction 5 of the MYC–2152 Extract Before HPLC ($CDCl_3$, 500 MHz).....115

A9. ^{1}H NMR Spectrum of Fraction 5 of the MYC–2152 Extract Before HPLC; Expansion of the Downfield Region ($CDCl_3$, 500 MHz).....116

A10. ^{1}H NMR Spectrum of Artifact **3.4** ($CDCl_3$, 500 MHz).....117

A11. ^{1}H NMR Spectrum of **3.4**; Expansion of the Downfield Region ($CDCl_3$, 500 MHz).....118

A12. ^{1}H NMR Spectrum of Kipukasin H (**3.2**; $CDCl_3$, 400 MHz).....119

A13. ^{13}C NMR Spectrum of Kipukasin H (**3.2**; $CDCl_3$, 100 MHz).....120

A14. HSQC NMR Spectrum of Kipukasin H (**3.2**; $CDCl_3$, 600 MHz) 121

A15. HMBC NMR Spectrum of Kipukasin H (**3.2**; $CDCl_3$, 600 MHz).....122

A16. ^{1}H NMR Spectrum of Kipukasin I (**3.3**; $CDCl_3$, 600 MHz) 123

A17. ^{1}H NMR Spectrum of Kipukasin I (**3.3**; CD_3OD, 400 MHz) 124

A18. ^{1}H NMR Spectrum of Cyclo-(L-pipecolinyl-aminocyclopropane-carboxylic acid) (**4.1**; $CDCl_3$, 500 MHz).....125

A19. ^{1}H NMR Spectrum of Cyclo-(L-pipecolinyl-aminocyclopropane-carboxylic acid) (**4.1**; CD_3OD, 500 MHz).....126

A20. ^{13}C NMR Spectrum of Cyclo-(L-pipecolinyl-aminocyclopropane-carboxylic acid) (**4.1**; CD_3OD, 150 MHz).....127

A21. DEPT NMR Spectrum of Crude Extract of *Trichothecium crotocinigenum* (NRRL 62714) with Diagnostic CH_2 Signals from **4.1** Overlaid in Red (CD_3OD, 100 MHz).....128

A22. COSY NMR Spectrum of Cyclo-(L-pipecolinyl-aminocyclopropane-carboxylic acid) (**4.1**; CD_3OD, 600 MHz).....129

A23. HSQC NMR Spectrum of Cyclo-(L-pipecolinyl-aminocyclopropane-carboxylic acid) (**4.1**; CD_3OD, 600 MHz).....130

A24. HMBC NMR Spectrum of Cyclo-(L-pipecolinyl-aminocyclopropane-carboxylic acid) (**4.1**; CD_3OD, 600 MHz).....131

A25. ^1H NMR Spectrum of Pentadepsipeptide **4.4** ($CDCl_3$, 500 MHz).....132

A26. ^1H NMR Spectrum of Pentadepsipeptide **4.4** (Benzene–d_6, 500 MHz).....133

A27. ^1H NMR Spectrum of Pentadepsipeptide **4.4** (Acetone–d_6, 500 MHz).....134

A28. HRESITOFMSMS Data for Pentadepsipeptide **4.4**.....135

A29. Chromatogram of the Co-injection of Derivatized Hydrolyzate from Pentadepsipeptide **4.4** with the D– and L–Standards of Ala and Thr.....136

A30. Chromatogram of the Co-injection of Derivatized Hydrolyzate from Pentadepsipeptide **4.4** with the D– and L–Standards of Ile.....137

A31. ^1H NMR Spectrum of the CH_2Cl_2 partition of the Hydrolyzate of **4.5** ($CDCl_3$, 500 MHz).....138

A32. ^1H NMR Spectrum of Pentadepsipeptide **4.5** ($CDCl_3$, 500 MHz).....139

A33. HRESITOFMSMS Data for Pentadepsipeptide **4.5**.....140

A34. ^1H NMR Spectrum of β–Trenbolone (**5.4**; CD_3OD, 600 MHz) 141

A35. COSY NMR Spectrum of β–Trenbolone (**5.4**; CD_3OD, 600 MHz).....142

A36. HSQC NMR Spectrum of β–Trenbolone (**5.4**; CD_3OD, 600 MHz).....143

A37. HMBC NMR Spectrum of β–Trenbolone (**5.4**; CD_3OD, 600 MHz).....144

A38. ^1H NMR Spectrum of **5.5** (CD_3OD, 500 MHz).....145

A39. COSY NMR Spectrum of **5.5** (CD_3OD, 600 MHz).....146

A40. HSQC NMR Spectrum of **5.5** (CD_3OD, 600 MHz).....147

A41. HMBC NMR Spectrum of **5.5** (CD_3OD, 600 MHz).....148

A42. ^1H NMR Spectrum of **5.6** Before 2D NMR Data Collection (CD_3OD, 500 MHz).....149

A43. ^{1}H NMR Spectrum of **5.6** After 2D NMR Data Collection (CD_3OD, 600 MHz).....150

A44. COSY NMR Spectrum of **5.6** (CD_3OD, 600 MHz).....151

A45. HSQC NMR Spectrum of **5.6** Acquired using Standard Parameters (CD_3OD, 600 MHz).....152

A46. HSQC NMR Spectrum of **5.6** with Parameters Optimized for Aldehyde $^{1}J_{CH}$ of 170 Hz (CD_3OD, 600 MHz).....153

A47. HMBC NMR Spectrum of **4.6** (CD_3OD, 600 MHz).....154

A48. Original ^{1}H NMR Spectrum of **5.7** (CD_3OD, 500 MHz).....155

A49. ^{1}H NMR Spectrum of **5.7** Before 2D NMR Data Collection (CD_3OD, 600 MHz).....156

A50. ^{1}H NMR Spectrum of **5.7** After 2D NMR Data Collection (CD_3OD, 600 MHz).....157

A51. COSY NMR Spectrum of **5.7** (CD_3OD, 600 MHz).....158

A52. HSQC NMR Spectrum of **5.7** (CD_3OD, 600 MHz).....159

A53. HMBC NMR Spectrum of **5.7** (CD_3OD, 600 MHz).....160

A54. ^{1}H NMR Spectrum of **5.8** (CD_3OD, 500 MHz).....161

A55. ^{1}H NMR Spectrum of β–Trenbolone (**5.3**); NMR Tube Experiment, Before Photolysis (D_2O, 500 MHz).....162

A56. ^{1}H NMR Spectrum of β–Trenbolone (**5.3**); NMR Tube Experiment, Immediately After Photolysis (D_2O, 500 MHz).....163

A57. ^{1}H NMR Spectrum of β–Trenbolone (**5.3**); NMR Tube Experiment, Three Days After Photolysis (D_2O, 500 MHz).....164

A58. ^{1}H NMR Spectrum of β–Trenbolone (**5.3**); NMR Tube Experiment, Eight Days After Photolysis (D_2O, 500 MHz).....165

A59. ^{1}H NMR Spectrum of α–Trenbolone (**5.4**; CD_3OD, 600 MHz).....166

A60. COSY NMR Spectrum of α–Trenbolone (**5.4**; CD_3OD, 600 MHz).....167

A61. HSQC NMR Spectrum of α–Trenbolone (**5.4**; CD_3OD, 600 MHz).....168

A62. HMBC NMR Spectrum of α–Trenbolone (**5.4**; CD_3OD, 600 MHz).....169

A63. ^{1}H NMR Spectrum of α–Trenbolone (**5.4**); NMR Tube Experiment, Before Photolysis (D_2O, 500 MHz).....170

A64. ^{1}H NMR Spectrum of α–Trenbolone (**5.4**); NMR Tube Experiment, Immediately After Photolysis (D_2O, 500 MHz).....171

A65. ^{1}H NMR Spectrum of α–Trenbolone (**5.4**); NMR Tube Experiment, Five Days After Photolysis (D_2O, 500 MHz) 172

A66. ^{1}H NMR Spectrum of α–Trenbolone (**5.4**) After Photolysis in H_2O, and Extraction with CH_2Cl_2 (CD_3OD, 500 MHz) 173

A67. ^{1}H NMR Spectrum of α–Trenbolone (**5.4**) After Photolysis in D_2O, and Extraction with CH_2Cl_2 (CD_3OD, 500 MHz) 174

A68. COSY NMR Spectrum of α–Trenbolone (**5.4**) After Photolysis in D_2O, and Extraction with CH_2Cl_2 (CD_3OD, 600 MHz) 175

A69. HSQC NMR Spectrum of α–Trenbolone (**5.4**) After Photolysis in D_2O, and Extraction with CH_2Cl_2 (CD_3OD, 600 MHz) 176

A70. HMBC NMR Spectrum of α–Trenbolone (**5.4**) After Photolysis in D_2O, and Extraction with CH_2Cl_2 (CD_3OD, 600 MHz) 177

A71. ^{1}H NMR Spectrum of α–Trenbolone (**5.4**) After Photolysis in D_2O, Extraction with CH_2Cl_2, Dried and Stored in the Dark, After 23 Days (CD_3OD, 500 MHz) 178

A72. ^{1}H NMR Spectrum of α–Trenbolone (**5.4**) After Photolysis in D_2O, Dried, and Dissolved in CD_3OD (500 MHz) 179

LIST OF ABBREVIATIONS

$[\alpha]_D^{25}$	specific optical rotation
β-Ala	beta-alanine
Å	Angstrom
Ac	acetyl
Ala	alanine
ARS	Agricultural Research Service
ATCC	American Type Culture Collection
ax	axial
br	broad
°C	degrees Celsius
C_{18}	octadecylsilyl
calcd	calculated
CASE	computer–assisted structure elucidation
CC	column chromatography
CCDC	Cambridge Crystallographic Data Centre
CD	circular dichroism
C_6H_6	benzene
$CHCl_3$	chloroform
CH_2Cl_2	dichloromethane
cm	centimeter(s)
cm^{-1}	wavenumber
cz	clear zone
δ	chemical shift
d	doublet

1D	one-dimensional
2D	two-dimensional
DEPT	distortionless enhancement by polarization transfer
DS	dummy scans
DW	dwell time
ECD	electronic circular dichroism
ε	extinction coefficient
EF	elongation factor
EIMS	electron impact mass spectrometry
ENDO	endophytic culture collection
ESIMS	electrospray ionization mass spectrometry
EtOAc	ethyl acetate
eV	electron volt
EtOAc	ethyl acetate
FABMS	fast atom bombardment mass spectrometry
FID	free induction decay
Fr	fraction
FT	Fourier transform
g	gram(s)
GCMS	gas chromatography mass spectrometry
GenBank	National Center for Biotechnology Information
Hex	hexanes
h	hour(s)
H2BC	heteronuclear 2 Bond Correlation
HETCOR	heteronuclear correlation
HMBC	heteronuclear multiple bond correlation
HMQC	heteronuclear multiple quantum correlation

HPLC	high performance liquid chromatography
HREIMS	high resolution electron impact mass spectrometry
HRESIMS	high resolution electrospray ionization mass spectrometry
HRESITOFMS	high resolution electrospray ionization time-of-flight mass spectrometry
Hz	hertz
INEPT	insensitive nuclei enhanced by polarization transfer
INADEQUATE	incredible natural–abundance double–quantum transfer experiment
IR	infrared
ITS	internal transcribed spacer region
J	coupling constant
L	liter(s)
LC	liquid chromatography
LREI	low resolution electron impact
LRESI	low resolution electron spray ionization
μ	micro
m	multiplet
M	mortality
$M^{+\bullet}$	molecular ion
MaxEnt	maximum entropy reconstruction
MeCN	acetonitrile
mg	milligram(s)
MHz	megahertz
MIC	minimum inhibitory concentration
min	minute(s)
mL	milliliter(s)
mm	millimeter(s)

MeOH	methanol
MS	mass spectrometry
MTPA	α-methoxy-α-trifluoromethylphenylacetic acid
MYC	mycoparasitic/fungicolous culture collection
mz	mottled zone
m/z	mass-to-charge ratio
NOE	nuclear Overhauser effect
NOESY	nuclear Overhauser effect spectroscopy
NP	natural product
NRRL	Northern Regional Research Laboratory
NCAUR	National Center for Agricultural Utilization Research
NMR	nuclear magnetic resonance
NRRL	USDA Agricultural Research Service Culture Collection/Northern Regional Research Laboratory
obsd	observed
PAF	platelet activating factor
PANACEA	parallel acquisition NMR all-in-one combination of experimental applications
PANSY	parallel acquisition NMR spectroscopy
PDA	potato dextrose agar
PDB	potato dextrose broth
ppm	parts per million
q	quartet
rg	reduced growth
RG	receiver gain
ROESY	rotating frame Overhauser effect spectroscopy
RP	reversed phase

RP HPLC	reversed-phase high pressure liquid chromatography
rpm	rotations per minute
RT	room temperature
s	singlet
SF	spectral frequency
SI	size
SW	spectral width
t	triplet
TD	number of data points to acquire
TFA	trifluoroacetyl
TFAA	trifluoroacetic anhydride
TLC	thin-layer chromatography
TOCSY	total correlation spectroscopy
TOF	time of flight
t_R	retention time
USDA	United States Department of Agriculture
UV	ultraviolet
Vis	visible
ZG	zero and go
VCD	vibrational circular dichroism
YMG	yeast–malt–glucose
wk	weak

CHAPTER 1

INTRODUCTION

Natural products (NPs) are compounds that come from natural sources, and display a wide variety of bioactivities and structural features. These compounds have proven to be vital for biomedical research and are likely to continue to provide starting points for the development of new drugs to combat a variety of diseases, infections, and illnesses.[1] NPs and compounds derived from them are among the top therapeutic agents in current treatments for cancer and malaria as well as bacterial and fungal infections.[2] Well known examples include compounds **1.1**–**1.4**. Out of 1010 new chemical entities with medical applications discovered between 1991 and 2006, 53% were NPs or synthetic derivatives of NPs.[3,4] If one focuses on the compounds specifically used in cancer treatment, the percentage rises to 65%,[3] while almost 70%[1] of the anti-infective (antibacterial, antifungal, antiparasitic, and antiviral) agents marketed during this period were inspired by NPs.[4] Thus, NPs have a major impact in the medical and pharmaceutical fields, but there are also agricultural applications for NPs , e.g., as pesticides, herbicides, and fungicides.[2]

The main sources utilized to discover new NPs are plants, fungi, and bacteria. These are the most studied because of the vast diversity among species, suggesting a parallel diversity of classes of compounds with varying bioactivities produced by these sources. When focusing on plants specifically, it is estimated that only a small percentage of the known 350,000 species have been chemically investigated for their potential pharmacological uses.[1] The fungal kingdom contains a diverse selection of mushrooms, yeasts, and molds. It is estimated that there are somewhere between one to two million fungal species, and less than 5% of these species have been characterized, let alone chemically investigated.[5]

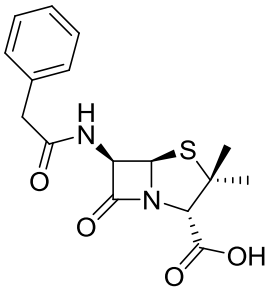

1.1
Penicillin G
Antibacterial

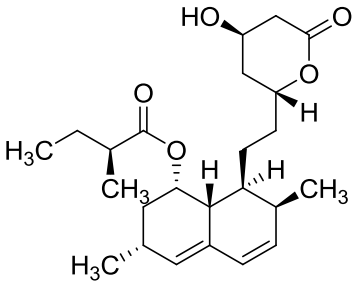

1.2
Lovastatin
Cholesterol-Lowering

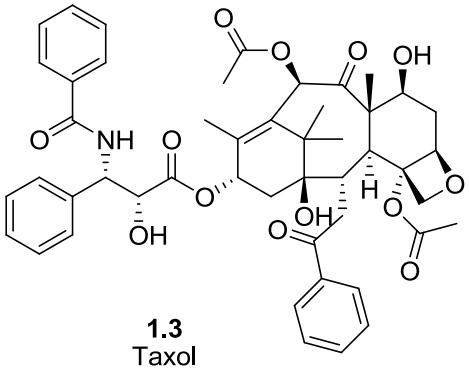

1.3
Taxol
Anticancer

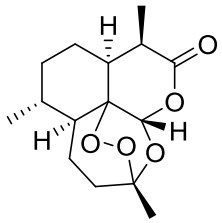

1.4
Artemisinin
Antimalarial

In this introductory chapter, different techniques used in the identification of NPs will be discussed, including many advancements that have been made over the past half–century. Some of the techniques available include mass spectrometry (MS) techniques, electronic circular dichroism (ECD), X–ray crystallography, and computational analysis. However, 1D, 2D, and "hyphenated technique" NMR experiments will be the main focus, as NMR is the most predominant and universally applicable tool in NP structure determination. Application of NMR techniques usually enables complete characterization of NP structure, including conformation, with little or no sample destruction.

Before a NP can be evaluated for its bioactivity or characterized, it must first be isolated from its source. The isolation process generally involves several steps, including, but not limited to: liquid–liquid partitioning, column chromatography (CC) on

various stationary phases, reversed–phase, and/or normal–phase HPLC using a variety of methods for detection. Once a compound is isolated, the structure must be determined. Until 50 years ago, NP structures were typically determined through a painstaking series of synthetic and degradation steps. When all the clues from this lengthy process were analyzed as a whole, researchers were able to eventually propose a structure for the NP.[6] As spectroscopic methods were developed and became more sophisticated, sensitive, and capable, the ability to determine the structures of NPs dramatically increased.[6] This began in the early 1950's with the advent of commercially available IR and UV/Vis spectrometers, which allowed for easier functional group determination. Before this time these instruments were not routinely used, but manufactures such as Beckman and Cary offered instruments that could be calibrated with chart papers making them much more user friendly.[6]

The development of mass spectrometry (MS) began in the 1920's with separate reports from Aston and Dempster.[7] The principle of MS is that ions produced from a compound, in this case, an NP, can be characterized in terms of their *mass–to–charge ratio* (*m/z*). Careful analysis of those ions can usually provide molecular weight information through the observation of the molecular ion peak or a pseudo–molecular ion peak (i.e., $[M+H]^+$, $[M-H]^-$, $[M+Na]^+$).[7] By the late 1950s, high resolution mass spectrometers (HRMS) were able to determine exact masses, thus helping to assign the molecular formulas of compounds. HRMS was limited by its commercial availability until the 60's.[6] Now, HRMS is widely available and is considered a vital technique for NP identification and structure elucidation.[7]

X–ray crystallographic techniques[8] were also not heavily utilized before the 1960's because of the low resolution images obtained, which required extensive and laborious calculations, not to mention considerable time. However, by the mid 1960's these limitations had been mostly overcome by commercial diffractometers and higher quality computers with more memory and faster processing speeds.[6] Despite its power,

X–ray crystallography is not used more routinely as a front–line technique in NP structure determination because many NPs are not crystalline or do not produce crystals suitable for analysis, especially given the small quantities typically available in discovery stages, and the fact that NP samples initially obtained are often not completely pure.[9] In NP research, this technique is generally used late in the process, and only for compounds found to be new, in order to confirm an assigned new structure and to help in stereochemical/conformational assignment.[9]

During this same time period, the potential of NMR aid in structure determination of organic molecules was gradually explored and developed. In 1961, Varian released the A-60, a 60–MHz (^{1}H NMR) instrument, which was made user–friendly by incorporating calibrated chart paper and a field/frequency lock. With the advent of an NMR instrument that no longer required a specialist for operation, the use of this technique skyrocketed from only one paper mentioning the use of NMR in 1960 to 220 by 1967.[6]

By the mid 60's, NMR was commonly being used to supplement the traditional methods of NP structure elucidation, however, there were still many limitations. One major limitation initially faced by NMR was sensitivity. For instance, the first commercial NMR instruments produced a spectrum with a signal–to–noise ratio (S/N) of approximately 10:1 using a 1% sample of ethylbenzene. Today's modern spectrometers can achieve a S/N of 10,000:1 with a 0.1% sample. This dramatic improvement was largely due to the introduction of pulsed Fourier transform in NMR processing, by Ernst and Anderson, which was made commercially available in 1970 by both Bruker and Varian (HX-90 and XL-100 instruments, respectively), and the higher field strengths of the modern instruments.[6] High–field FT NMR instruments using superconducting solenoids were commercially introduced relatively soon after the FT advancement, starting with the Bruker WH–270, which again dramatically increased spectrometer sensitivity. These advances not only made the acquisition of ^{13}C NMR spectra more

routine, but allowed for the development of multiple pulse sequences, which ultimately led to the introduction of 2D NMR by Ernst *et al*.[6]

The original 2D NMR techniques developed included correlation spectroscopy (COSY; $^{1}H–^{1}H$ correlation through coupling), heteronuclear correlation (HETCOR; 1–bond $^{1}H–^{13}C$ correlation), and nuclear Overhauser effect spectroscopy (NOESY; $^{1}H–^{1}H$ correlation through space). Researchers quickly realized that structural fragments composed entirely of protonated carbons (spin–systems) could be determined and assigned through the use of COSY and HETCOR, however, if there were heteroatoms or non–protonated carbons separating these segments, as there often are, the full structure could not be determined by these techniques alone.[6, 10] This problem was solved in 1984 by three independent researchers who realized that, through optimization of the pulse programs for smaller heteronuclear *J*–values, $^{1}H–^{13}C$ correlations could be obtained even if the hydrogen and carbon were separated by two or three bonds (i.e., "long–range" correlations).[11-13]

Other pulse sequences were developed in order to edit ^{13}C NMR spectra based on the number of attached hydrogens. There are three main experiments that utilize ^{13}C spectral editing; attached proton test (APT),[14] insensitive nuclei enhanced by polarization transfer (INEPT),[15] and distortionless enhancement by polarization transfer (DEPT).[16] The APT is the simplest ^{13}C spectral editing technique. The pulse sequence provides a spectrum in which the methyl and methine carbons appear inverted, while methylene and non–protonated carbons appear upright.[14] Unfortunately, this experiment is less sensitive than a traditional ^{13}C NMR spectral acquisition sequence and is also somewhat unreliable due to its sensitivity to variations in one bond $^{1}H–^{13}C$ coupling constants ($^{1}J_{CH}$). It is thus rarely used. Since both INEPT and DEPT employ polarization transfer from protons to attached ^{13}C nuclei, they are both significantly more sensitive on a per–scan basis than a standard ^{13}C NMR spectrum.[6] Unlike APT, neither of these options provides signals for non-protonated carbons, and must therefore be used in conjunction with a regular ^{13}C

NMR spectrum.[15,16] DEPT is generally preferred over INEPT because it is less sensitive to $^{1}J_{CH}$ variations.[16] In a DEPT–135 spectrum, methyl and methine signals are upright while methylene signals are inverted.[16] More recently, an alternative to DEPT called DEPT–Q, which overcomes the limitations of not detecting non-protonated carbons was described.[17] The output is similar to APT, but with increased sensitivity. While the non-protonated carbon signals are still weaker than those of a standard ^{13}C NMR spectrum, it takes less time to collect a DEPT–Q spectrum than it does for a standard ^{13}C and DEPT combined.[17] It should be noted that the information obtained from a DEPT or a DEPT–Q spectrum can also be indirectly obtained from an HSQC or HMQC spectrum, a technique which will be discussed in detail later, which would also provide the proton assignments corresponding to each protonated carbon signal.

Just as the sensitivity of NMR spectrometers has increased, and pulse sequences to gain valuable information using spectral editing have proliferated and improved, so has the technology for acquiring 2D data. The original COSY experiment operated on a phase-cycling coherence pathway selection basis,[18] which has been almost completely replaced by a gradient–selection type pulse program approach.[19] Simply put, instead of relying on phase–cycling, a method used to cancel out unwanted signals and artifacts while increasing the intensity of the desired signals accomplished by varying the phases of the pulses and the receiver, a field gradient pulse is used to excite only the relevant nuclei, which is accomplished by applying an inhomogeneous magnetic field to remove all signals, and applying a gradient (linear magnetic field) to restore the desired signals. The use of a field gradient pulse results in a need for fewer scans, faster acquisitions, and better suppression of artifacts.[19] A variant of the COSY experiment (COSY–45) employs a 45° pulse at the end of the pulse program that can allow one to distinguish geminal and vicinal correlations, due to their different phases, with only a minor loss in sensitivity.[18] Another COSY variant, called double–quantum filtered COSY (DQ–COSY), is more

sensitive, making this technique particularly useful to help distinguish correlations that are close to the diagonal.[20]

Total correlation spectroscopy (TOCSY) is similar to COSY in that it is a homonuclear ^{1}H–^{1}H correlation technique, but it provides correlations for all protons in a spin–system, not just those that are directly coupled. Like the COSY experiment, TOCSY programs have also gone through similar enhancements to increase sensitivity and decrease artifacts and distortion. In addition, an advanced adjunct technique is selective 1D TOCSY. This involves manual variation of the mixing times, unlike a tradition TOCSY, which employs a general mixing time range between 60 and 100 ms.[6] This 1D technique allows accurate measurement of *J*–values in overlapping signals if the two are in separate spin–systems.[21]

Another important set of 2D NMR experiments developed were the so–called inverse detection techniques. By the 1990's, the HETCOR experiment had been completely replaced by heteronuclear multiple-quantum correlation spectroscopy (HMQC) and heteronuclear single-quantum correlation spectroscopy (HSQC) methods, because of their ten–fold sensitivity increase due to the employment of ^{1}H detection rather than ^{13}C detection.[6] HMQC and HSQC give similar information, however, the data are collected in different ways. The main difference between the two is that HSQC uses far more pulses than HMQC, making HSQC more prone to sensitivity loss. On the other hand, HSQC provides cross-peaks that appear as singlets, while HMQC produces cross peaks that mirror the multiplicity of the corresponding ^{1}H signals, therefore degrading the resolution.[10] As is the case with COSY, both of these experiments have been greatly improved by the use of gradients.[10] One limitation of these techniques is that the sequence incorporates a fixed value corresponding to the approximate coupling constants of interest (typically 140-150 Hz). However, the range of $^{1}J_{CH}$ in organic compounds is from 125 to almost 200 Hz depending on the type of structure and functional group(s) present. This can lead to a significant loss of sensitivity for signals

far removed from the set value.[6] However, if an out–of–range $^{1}J_{CH}$ is suspected, the experiment can be optimized for a different $^{1}J_{CH}$ if needed. Krishnamurthy et al. developed a program that sweeps through different pulses in order to adjust to the size of the expected coupling based on the chemical shift range that is being swept (i.e., reflecting the difference between sp^2 and sp^3 $^{1}J_{CH}$ values), eliminating the need for $^{1}J_{CH}$ optimization.[22,23] Both HMQC and HSQC also have variations that show heteronuclear ^{1}H–^{15}N correlations, however, the multitude of pulses that HSQC requires make data acquisition more lengthy and less sensitive, and ^{15}N is much less naturally abundant than ^{13}C, so HMQC is preferred in this situation.

The next set of 2D experiments to be developed, and later improved, are those that detect so–called "long range" correlations between ^{1}Hs and ^{13}Cs that are two to three bonds away. The original 2D experiment used to obtain this information was a HETCOR pulse sequence modified and optimized for long–range couplings.[11,12] Other, less commonly used programs were also independently developed based on ^{13}C–detection for this purpose.[13] However, such information is now almost exclusively obtained by a ^{1}H–detected heteronuclear multiple bond correlation (HMBC) sequence that uses a gradient to selectively suppress ^{1}H–^{13}C magnetization.[24] Improvements made in HMBC experiments in recent years include the suppression of residual $^{1}J_{CH}$ cross peaks by using a *J*–filter, and improvement of general sensitivity to detect long–range couplings by using a set of varying delay values rather than a fixed delay value (traditionally optimized for J_{CH} of 8 Hz). Many attempts have been made to distinguish $^{2}J_{CH}$ and $^{3}J_{CH}$ correlations through many variations in the pulse sequence and the data processing techniques, but these have rarely been very sucessful.[25-27] An example of a recent effort in this area (H2BC) suppresses both the $^{1}J_{CH}$ and the $^{3}J_{CH}$ leaving (theoretically) only the $^{2}J_{CH}$ correlations.[26] However, to gain the $^{3}J_{CH}$ information, a traditional HMBC experiment must also be acquired.[26] Since H2BC relies on J_{HH}–values, it is possible to still obtain a cross peak that does not represent a $^{2}J_{CH}$. Researchers have developed a "rule–of–thumb"

to verify if a cross–peak is due to a $^{2}J_{CH}$ coupling by comparing the intensities of the respective cross peaks in the H2BC and HMBC. If a peak is weak in the H2BC and strong in the HMBC, it is indicative of a $^{3}J_{CH}$, but if it is strong in the H2BC and weak in the HMBC, the peak corresponds to a $^{2}J_{CH}$.[27] An example of this technique and its comparison to traditional HMBC can be seen in Figure 1.1.[27] It should be noted that in the H2BC spectrum below the $^{2}J_{CH}$ correlations to non–protonated carbons were not observed. Furrier did not discuss this aspect, so it is not clear if this is an anomalous event or typical of H2BC.

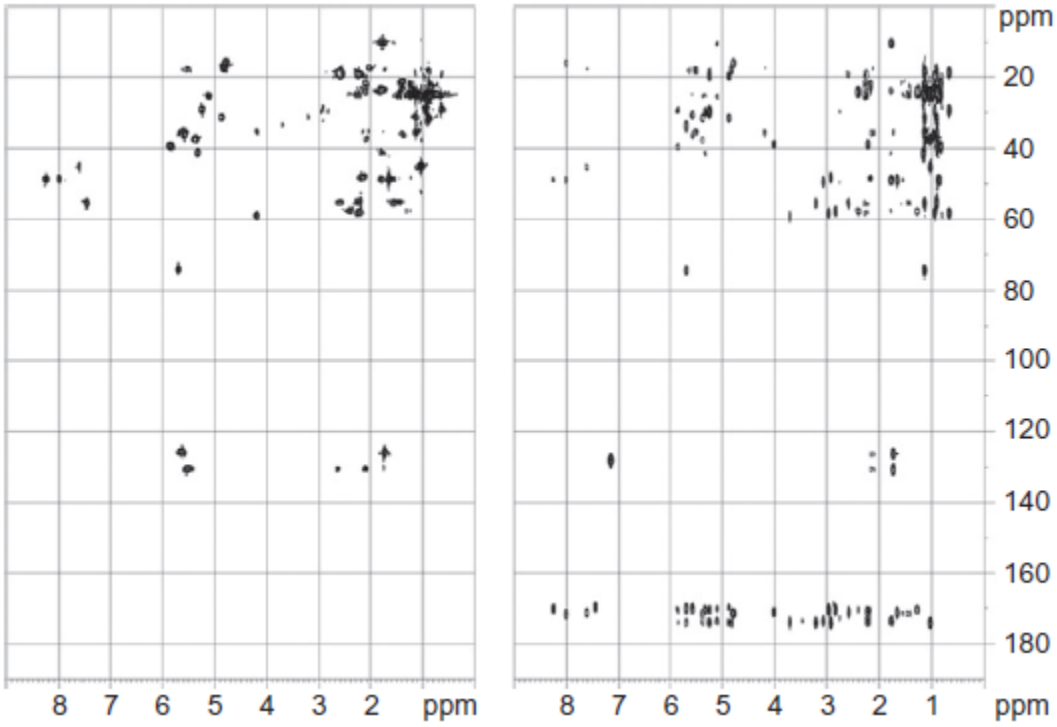

Figure 1.1. H2BC (left) Compared to the HMBC (right) Spectra of Cyclosporin A (Spectra from ref. 27)

One additional through–bond 2D NMR experiment worthy of note is the so–called incredible natural–abundance double–quantum transfer experiment (2D

INADEQUATE) which detects natural abundance 2D ^{13}C–^{13}C correlations. The major downfall of this experiment is the amount of sample required to acquire a spectrum with adequate S/N because of the approximately 1% natural abundance of ^{13}C, resulting in a 0.01% probability of adjacent ^{13}C atoms, together with the dramatically lower sensitivity of the individual ^{13}C nucleus compared to ^{1}H.[10] Continuing advancements in the sensitivity of NMR probes, improvements in the INADEQUATE acquisition sequence, and upgrades in processing techniques, have also undergone changes to improve sensitivity. This technique would prove to be especially useful in the structure elucidation of compounds that contain network(s) of non–protonated carbons, however, it still remains the least sensitive NMR technique, and seems unlikely to become routine due to the limited natural ^{13}C isotope abundance.[10] Recently, in attempts to ameliorate the natural abundance issue and to enable greater use of INADEQUATE experiments, uniformly labelled ^{13}C–glucose has been utilized during microbial fermentation processes, resulting in an approximately 35% incorporation of ^{13}C in NPs of interest.[28]

The array of NMR experiments summarized above focuses on the determination of a NPs skeletal structure, but there are other types of NMR experiments that can help researchers elucidate elements of three–dimensional (stereochemical and/or conformational) structure as well. One type of data that can assist in determination of a compound's stereochemical configuration is vicinal coupling constant values. This *J*–based analysis utilizes either the Karplus equation,[29] or a modified Karplus equation (Altona equation)[30] to estimate the dihedral angle between vicinal protons based on their coupling constants. The Altona equation is somewhat more sophisticated in that it also takes into account the electronegativity of the nearby atoms. The limitations of these equations lie in the fact that the equations allow for a 5–10° window of error, and in many cases the observed *J*–values are not necessarily equivalent to the calculated coupling constants.[29,30] This type of analysis is also difficult when proton signals are

overlapped, and only applies well to structures where geometry is restricted and well defined.

Other NMR experiments can provide less ambiguous conformational and stereochemical information. Both NOESY, mentioned earlier, and ROESY (rotating frame nuclear Overhauser effect spectroscopy), give correlations for protons that are close to each other in space (≤5 Å apart). NOESY uses mixing times without pulses to build up NOEs,[31] while ROESY accomplishes this by using multiple pulses of alternating phase.[32] NOESY experiments tend to produce COSY artifacts, while ROESY produces TOCSY artifacts, but both undesired effects can be minimized by varying the mixing times or pulse sequences, respectively. Traditionally, NOESY is used for small molecules and ROESY is more apt to be used for molecules of more moderate mass (approximately 700–1500 Da).[10] These techniques are commonly used to locate two groups on the same face of a cyclic structure.

Sometimes NMR based methods can also be used to assign absolute stereochemistry of a molecule. Such methods typically employ chemical derivatization of the NP. There are many derivatizing agents and approaches utilized for making stereochemical assignments by NMR.[33] One common example is Mosher's method.[33] Mosher's method is employed to determine the stereochemistry of a secondary alcohol by esterifying it with both isomers of a chiral reagent that contains an aromatic ring near the derivatization site. The differences in chemical shifts for the two resulting diastereomers associated with the proximity of nearby ^{1}H's to the aromatic ring allow for the configuration to be assigned.[33] If the relative configuration has already been determined, assignment of this stereocenter affords an overall stereochemical assignment for the molecule.

Recently, there have been great strides in efforts to decrease the amount of time required to acquire 2D NMR data without sacrificing sensitivity or resolution. For example, two time–saving HMQC experiments have been proposed. SOFAST–HMQC is

best suited for large molecules such as proteins and biopolymers, because it relies on the corresponding very short relation times shown by such molecules.[34] ASAP–HMQC, on the other hand, uses homonuclear mixing similar to TOCSY experiments during the relaxation delay, which allows for better transfer of magnetization from the ^{1}H to the ^{13}C.[35] This sequence modification results in greater signal enhancement and a shorter relaxation delay, leading to shorter data acquisition times.[35] Traditional HSQC still provides better resolution than the ASAP–HMQC technique, but the latter can be useful as a more rapid screening tool. This same type of homonuclear mixing has not been incorporated into HSQC experiments because of the multiple pulses and pulse angles utilized, but it has been incorporated into a modified HMBC sequence called IMPACT–HMBC.[36] Sensitivity of the IMPACT–HMBC is slightly increased considering the time element, and almost completely suppresses the $^{1}J_{CH}$ artifacts, as is apparent in Figure 1.2.[36]

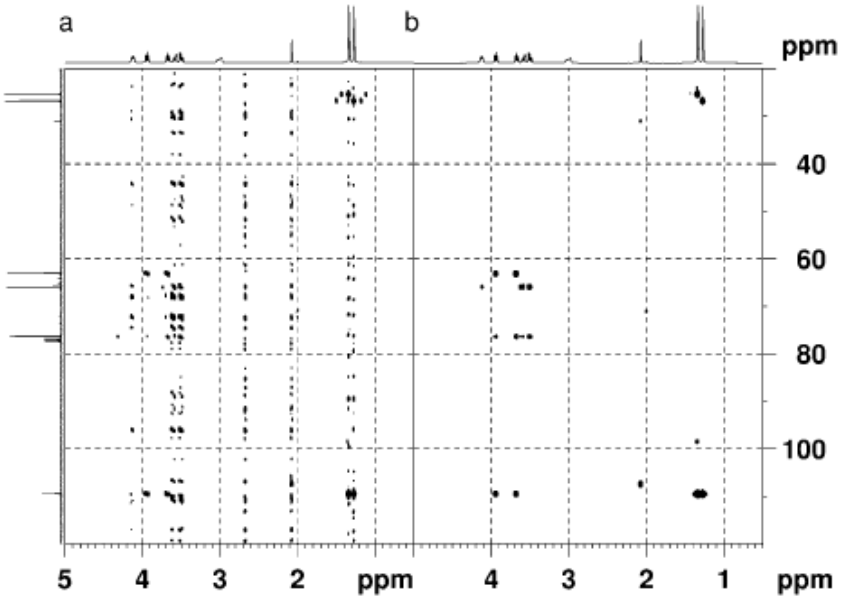

Figure 1.2. Traditional HMBC (a) and IMPACT–HMBC (b) Spectra of Isopropylidene Glycerol (Spectra from ref. 36)

Another new technique, parallel acquisition NMR spectroscopy (PANSY), proposes to do exactly as the name implies. The original PANSY experiment combined a COSY and a NOESY experiment.[37] The premise behind this experiment was that the data for the COSY experiment could be collected during the mixing time needed for NOESY. However, researchers could simultaneously collect data for different types of 2D experiments through the use of two or more independent receivers, which many of the newest spectrometers possess. Very recently, a sequence was developed that was designed to obtain all the data necessary for small molecule structure elucidation in a single experiment called PANACEA.[38] This experiment simultaneously collects HSQC and HMBC data on the ^{1}H channel and a ^{13}C NMR spectrum and 2D INADEQUATE (where feasible given the sample size) on the ^{13}C channel. One potential drawback of this approach is that all the samples used to date have been highly concentrated, so it is unclear how applicable this will be in the NP field.[6]

One further NMR improvement currently in the developmental stage involves the concept of non-uniform sampling. The concept relies on the collection of data at irregularly spaced time intervals. This requires that the time intervals used in the non-uniform sampling be a subset of interval times used in traditional 2D experiments, which could, in theory, yield a spectrum in one quarter of the standard time with no loss of resolution.[6] The idea itself is not new, however, this sampling technique has rarely been used due to the requirement for suitably specialized software not included in spectrometer software packages, because traditional Fourier transform (FT) analysis of the data cannot be employed, but a maximum entropy reconstruction (MaxEnt) must instead be used.[39,40]

This idea of a non-Fourier method of data processing could result in significant improvements in computer power and software that can allow for the continuing enhancements in data collection and processing methods for all NMR techniques. Another area in which dramatically improving computer capabilities has allowed for considerable advancement is computer–assisted structure elucidation (CASE).[41] The

corresponding programs often allow for structure confirmation, insight into stereochemical and conformational arrangements of compounds, and even revision of proposed NP structures. Two such commercial software packages that can offer such insights are StrucEluc and ACD/Labs Structure Elucidator.[41] These programs are capable of generating a list of possible structures based off of the 1D and 2D data collected.[41] A commonly used program that aids in conformational analysis is Spartan. These data can be linked together with NOESY data to help refine the calculated conformers generated.[42]

While advances in NMR resolution and sensitivity have been remarkable and improvements in 2D data collection have evolved to the point where sample limitations can usually be overcome, other techniques to speed up the overall process of data collection have been developed and employed. Perhaps the most common involves the idea of combining isolation techniques with NMR instruments effectively serving as detectors. The development of HPLC–NMR started in 1978, but it has taken many years for the technique to evolve to approach the point of routine analysis.[43]

The first two approaches to HPLC–NMR that were developed are on–flow and stop–flow. The on–flow process allows only rapid acquisition of data, so only ^{1}H NMR spectra could be acquired, and is thus primarily used in rapid screening for major metabolites. Stop–flow HPLC–NMR, on the other hand, is capable of carrying out longer acquisitions, including 2D NMR experiments, on one or more selected components of an injected sample. Unfortunately, there is a lack of sensitivity due to the limited volume of the flow probe used (to minimize peak spreading) and sensitivity is also dependent on the field strength of the NMR instrument used.[43] In 2003, it was reported that a compound of 500 molecular weight could be analyzed at a level of 100 ng on a 600 MHz NMR spectrometer using the stop–flow technique.[43] In 2009, two new compounds, cycloisoallolaurinterol (**1.5**) and isoallolaurinterol (**1.6**), were isolated from a crude extract of the marine alga *Laurencia filiformis* after they had been screened and

characterized via on–flow and off–flow HPLC–NMR, respectively, using a 60–μL flow probe.[44]

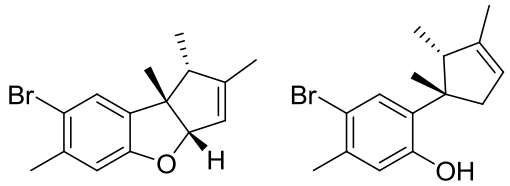

1.5 **1.6**

More recently, however, desire for additional sensitivity improvements led to the advent of microcoil HPLC–NMR and capillary NMR (CapNMR). Both microcoil HPLC–NMR and capillary NMR development led to flow probes that utilize a much smaller sample volume, 2.5–5 μL, versus the traditional flow probe volume of 40–120 μL. This decrease in cell and receiver coil size allows for an observed 5–fold sensitivity increase.[43] Microcoil HPLC–NMR is best suited for on–line analysis in which the components are separated and analyzed in a traditional HPLC–NMR step used in either on–flow or stop–flow mode.[43] This on–line analysis requires the use of deuterated solvents throughout the entire process. However, combining this technique with a cryoprobe can increase the limit of detection and sensitivity by 20–fold.[43] Using a 1.5–μL microcoil flow probe, six tocopherol homologues (**1.7–1.12**) were identified from a standard solution mixture using microcoil HPLC–NMR.[45]

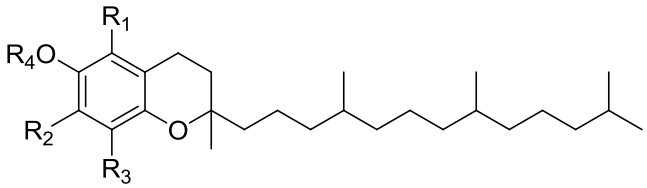

1.7 R_1=H, R_2=H, R_3=H R_4=H
1.8 R_1=H, R_2=H, R_3=CH_3 R_4=H
1.9 R_1=H, R_2=CH_3, R_3=CH_3 R_4=H
1.10 R_1=CH_3, R_2=H, R_3=CH_3 R_4=H
1.11 R_1=CH_3, R_2=CH_3, R_3=CH_3 R_4=H
1.12 R_1=CH_3, R_2=CH_3, R_3=CH_3 R_4=$COCH_3$

CapNMR involves an off–line type of protocol (Figure 1.3)[43] that allows NMR analysis of previously isolated single components or mixtures after automated collection from one or many separations, providing a higher concentration of the isolated material to be analyzed. This also allows for the use of non–deuterated solvents during the HPLC step, which significantly reduces the cost of operation and also allows for a larger variety of solvents to be used. Using this technique, a ^{1}H NMR spectrum can be obtained using only approximately 2–30 μg of an individual component.[43] CapNMR was used in 2005 to identify 13 new steroidal compounds extracted from fireflies, an example of which is compound **1.13**.[46]

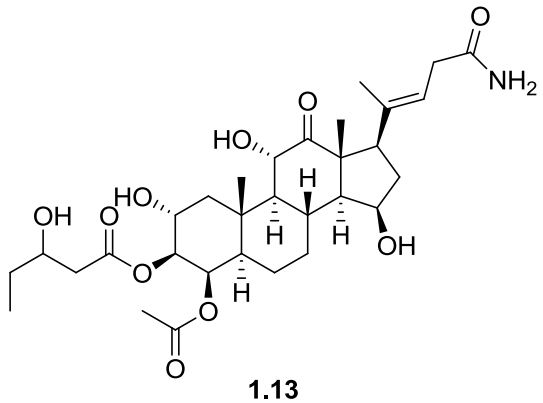

1.13

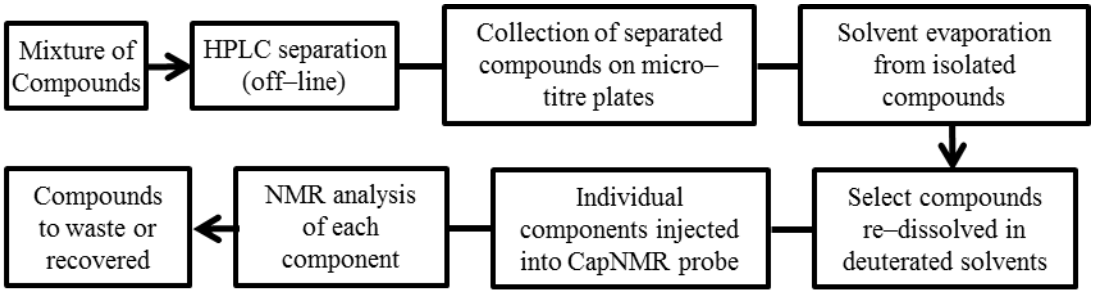

Figure 1.3. Flow Chart of Automated HPLC–CapNMR Process

Recently, another hyphenated technique, HPLC–SPE–NMR, which incorporates the use of solid phase extraction (SPE) has been introduced in Bruker systems. SPE cartridges are placed in–line after the HPLC separation which allows for individual isolated compounds to accumulate on the cartridge after single or repeated HPLC steps. This method only requires deuterated solvents to be used to wash analytes off of the SPE cartridges, and not during the separation process itself. Prior to removing a sample from a cartridge, it can be stored under nitrogen to prevent degradation. The Bruker HPLC–SPE–NMR system flow chart is summarized in Figure 1.4.[43] One representative study used this method to rapidly isolate and identify major metabolites extracted from a plant of the genus *Hubertia* (**1.14-1.16**).[47] Further study demonstrated that even components comprising as little as 0.5% or less of the crude extract could be identified using this process.[48]

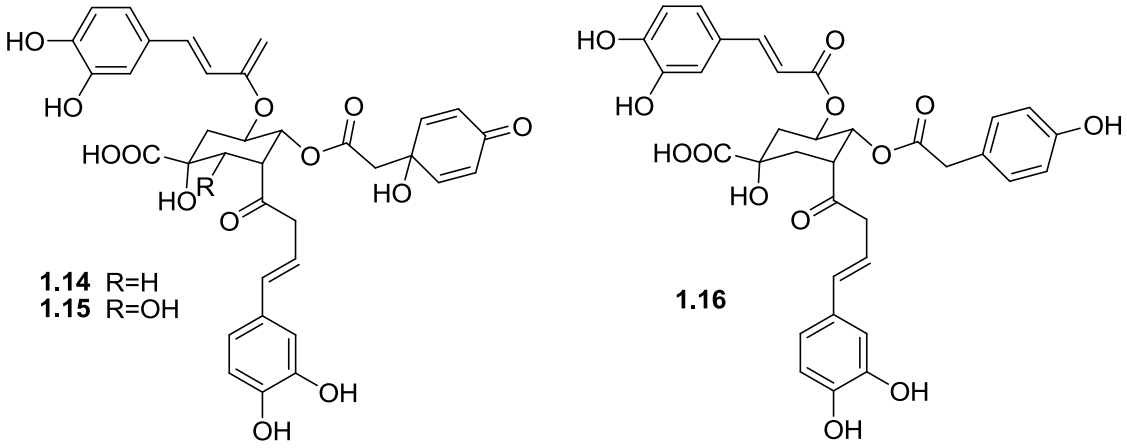

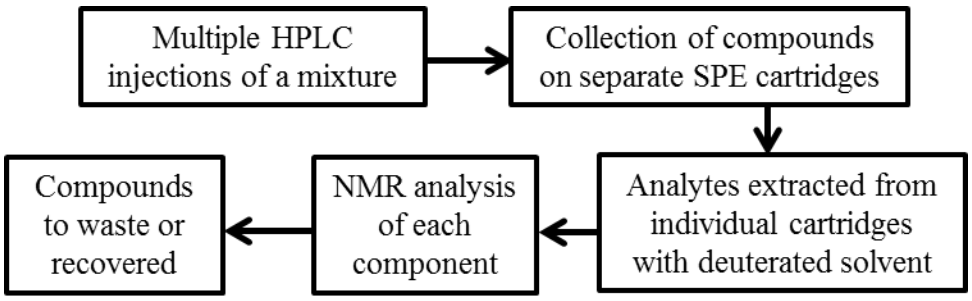

Figure 1.4. Flow Chart of Bruker's HPLC–SPE–NMR Setup

Lastly, since in some cases NMR data alone are insufficient to enable a compound's identification, HPLC–NMR has recently been "hyphenated" with MS in an HPLC–NMR–MS system. This hyphenated technique uses a splitter to divert some of the eluent of the HPLC column to the MS and the rest to the NMR. Typically, a 1:20 split is used, which allows sufficient material for NMR detection. This is known as a parallel configuration. Alternatively, an HPLC–NMR–MS system can also be set up in series, whereupon leaving the NMR after HPLC separation, the analyte then flows to the MS. The series configuration is simpler and allows for easy separation of the NMR and

MS components so they can also be used as standalone instruments, providing a distinct logistical advantage. However, this instrumental configuration can also cause significant analyte peak–broadening by the time individual components reach the MS. Both series and parallel configurations can allow for rapid screening of analytes in crude mixtures.[43]

As previously discussed, NMR and/or X–ray techniques can be employed to help researchers determine the relative, and in some cases, the absolute configuration of natural products. However, this remains a challenging aspect of NP structure elucidation. One non–destructive method that can be employed, if the chiral compound has a chromophore, is electronic circular dichroism (ECD).[49] Historically when using ECD, researchers would compare the spectrum of the new compound to that of a known compound with a similar structure, or employ empirical rules such as the octant or exciton chirality rules to help assign NP(s) configuration. However, many NPs are complex and can have multiple chromophores and stereocenters making these rules difficult to apply. The rapid emergence of powerful computational methods has significantly expanded the utility of ECD for stereochemical analysis. Computationally calculated ECD spectra can be obtained by first performing conformational analysis on a compound to determine the most stable possible conformer(s). This can be accomplished with programs like Spartan 10 via energy–minimization calculations, commonly using Monte Carlo methods. After this analysis is complete, the most prevalent conformer(s) are further optimized using density functional theory (DFT). Next, time–dependent density functional theory (TDDFT) calculations are performed to obtain calculated UV/ECD spectra of the most stable (i.e., the most populated) conformers. If multiple conformers are expected to be present in significant concentrations, their respective calculated spectra can be Boltzmann–averaged to give an aggregate spectrum.[49]

Once calculated ECD spectra are generated for each of the possible enantiomers in their respective energy–minimized conformers, they can be compared to the experimental ECD spectrum. If X–ray crystallographic data are available, researchers

may choose to use the conformation observed in the crystal, rather than using energy–minimizing calculations. The use of calculated ECD spectra to determine the absolute configuration of NPs has gained popularity in recent years with rapid improvement in the optimization of the calculations that predict energy–minimized conformers and the TDDFT calculations of the spectra themselves. This method has been proven successful for a broad variety of classes of compounds recently, with many published studies emerging in the NP field in just the last two years.[49]

Since the beginning of efforts to isolate and identify NPs, applicable aspects of science and technology have progressed by orders of magnitude. Researchers now have the capability to isolate and completely characterize the gross structure of a molecule with one "hyphenated" technique in some instances, and keep the majority of the sample intact. In the last half–century, the scientific community has gone from having instruments so complicated that a specialist was required for their operation, to now having scientists routinely able to use the instruments themselves for their own research. The sensitivity of ^{1}H NMR data collection has increased ten thousand–fold, while ^{13}C NMR data, which were originally unobtainable, are now routine.[6] The advent of 2D NMR with different series of selected pulses, pulse angles, mixing times, relaxation times, and processing parameters enables researchers to determine $^{1}J_{CH}$ and $^{2}J_{CH}/^{3}J_{CH}$ correlations (HSQC and HMBC), correlations among scalar–coupled protons (COSY and TOCSY), and correlations between hydrogens through space (NOESY and ROESY). All of these techniques have been improved upon, and even combined, cutting down on the time needed to acquire data. Other spectroscopic techniques, along with rapidly developing calculation methods, have also allowed for the determination of absolute configuration without destroying the sample (e.g., via ECD). There are still cases where degradation or derivatization is the preferred technique for determining absolute configuration (e.g., peptides), but in many cases, destructive processes are no longer required for determination of configurations. Preserving the maximum possible quantity

of NP material after characterization is very important, so that these rare compounds can be tested as extensively as possible for biological activity suggestive of potential utility.

Many of the spectroscopic methods discussed in this chapter were utilized in two very different projects described in this thesis. One project was directed toward isolation and identification of bioactive secondary metabolites produced by a number of different fungal isolates. Chapter two will discuss the screening of two types of fungal fermentation extracts as well as the identification of many known compounds encountered therein. Chapters three and four will detail the isolation and characterization of seven new secondary fungal metabolites and several known compounds encountered in two of the extracts. Chapter five focuses on the second project, which involved exploration of the degradation products of the excreted metabolites of trenbolone acetate (TbA), a steroid commonly used to promote growth in beef cattle.

CHAPTER 2

SCREENING OF FUNGAL ISOLATES

As discussed in chapter one, the discovery of natural products begins with the selection of a source to chemically investigate. While there are many different source options, the studies described in this thesis focus on fungi, which have proven to be productive sources of new secondary fungal metabolites.[50-52] The fungal kingdom, as previously mentioned, is extremely vast, but only a very small percentage of the fungi have been characterized, let alone chemically investigated. One ecological group of fungi that our research investigates includes endophytic fungi. These types of fungi colonize the tissues of plants, generally without causing visible symptoms in the host. Such fungi can sometimes cause disease after long–term infestation, indicating that the relationship may or may not be symbiotic.[53] The colonizing fungi may impact the development, growth, and/or survival of the host plant and may do so in a positive or negative way. A positive effect, for example, could arise from compounds produced by the endophytes that could provide protection for the host against various pathogens or insect attack.[53]

Another group of fungi that is of interest to our research group includes fungicolous and mycoparasitic fungi.[54] A fungicolous fungus is one that is found growing on another fungal species. When the relationship to the host fungus is found to be parasitic, the colonizer is classified as mycoparasitic. Due to the complexity of fungal species' relationships in nature, it is difficult to reproduce these conditions in a laboratory environment, and thus difficult to classify a true mycoparasitic relationship without extensive ecological studies. Thus, the term fungicolous is a more general categorization for fungi that are found as colonists of others. In order for one fungal species to colonize a host fungal species, the colonist needs to overcome the host's defenses. Such a process could be aided by the production of antifungal compounds. It is for this reason that

fungicolous and/or mycoparasitic fungi are viewed as potential sources of antifungal agents in our research. Indeed, over the years, many new bioactive compounds have been isolated from these types of sources.[50,51,55]

The research described in this thesis involves studies of fungicolous, mycoparasitic, and endophytic fungal isolates which were collected and identified by Dr. Donald T. Wicklow at the United States Department of Agriculture (USDA) National Center for Agricultural Utilization Research (NCAUR) in Peoria, Illinois. Fungicolous/mycoparasitic isolates were generally collected from the surfaces of the long–lived fungal host fruiting bodies, which tend to be rich in nutrients and are relatively easy to recognize and collect. The geographic locations and hosts from which the endophytic samples were collected are listed in Table 2.2.

Source material was typically plated on potato dextrose agar (PDA) and the individual fungal colonies that emerged were isolated. Preliminary identification and culture dereplication was done (by Dr. Wicklow) in an effort to select a diverse array of fungal isolates for study. Selected isolates were subjected to solid–substrate fermentation on rice, followed by extraction with ethyl acetate (EtOAc). The resulting extracts were dried and screened for antifungal activity in disc assays against *Aspergillus flavus* (NRRL 6541) and *Fusarium verticillioides* (NRRL 25457).[56] These test organisms are used because they are agriculturally problematic, and they are also opportunistic human pathogens. The crude extracts are also tested against *Spodoptera frugiperda* (fall army worm, FAW) for antiinsectan activity.[57,58] The fall army worm is a crop pest that has great economic impact, as it is a major cause of damage to leaves and ears of corn. Many extracts were screened for their biological activity in these assays. Eight endophytic fungal extracts and seven fungicolous/mycoparasitic fungal extracts were selected for chemical investigation in the work described here (Tables 2.1-2.3).

Table 2.1. Bioactivity of Endophytic Fungal Extracts

		A. flavus		*F. verticillioides*		FAW
ENDO	**Taxonomy**	**1-da**	**2-da**	**1-da**	**2-da**	**(% rgr)**
3470	Unknown	(-)	(-)	(-)	(-)	(-)
3476	Possible *Penicillium*	mz=3 wk	(-)	mz=15	mz=5	(-)
3481	Possible *Mortierella*	(-)	(-)	(-)	(-)	(-)
3503	Unknown	mz=6	mz/rg=6	cz3+mz10	mz=10	(-)
3109	*Chaetomium* sp.	mz/rg=3	(-)	mz=10	(-)	25%rgr
3115	Unknown	(-)	(-)	(-)	(-)	90%rgr
3176	Unknown	cz7+mz5	(-)	cz=12	(-)	50%rgr
3461	Unknown	cz=3	cz=3	cz=3	(-)	(-)

Note: rg–reduced growth, mz–mottled zone, cz–clear zone, wk–weak, rgr–reduced growth rate, (-)–not active , FAW–Fall Army Worm

Table 2.2. Endophytic Sample Hosts and Geographic Origins

ENDO	**Host Taxon**	**Common Name**	**Tissue**	**Location**
3470	*Secale cerealis*	Rye	stem	Kilbourne, IL
3476	*Secale cerealis*	Rye	stem	Kilbourne, IL
3481	*Secale cerealis*	Rye	stem	Kilbourne, IL
3503	*Secale cerealis*	Rye	stem	Kilbourne, IL
3109	*Triticum* sp.	Wheat	seed	Patagonia, AZ
3115	*Triticum* sp.	Wheat	seed	Patagonia, AZ
3176	*Zea Mays*	Corn	xylem sap	Peoria, IL
3461	*Secale cerealis*	Rye	stem	Kilbourne, IL

Table 2.3. Bioactivity of Fungicolous/Mycoparasitic Fungal Extracts

		A. flavus		*F. verticillioides*		FAW
MYC	**Taxonomy**	**2-da**	**4-da**	**2-da**	**4-da**	**(% rgr)**
2152	*Aspergillus puulaauensis*	(-)	(-)	(-)	rg=3	71M; >75%
2117	Possible *Penicillum* sp.	(-)	(-)	mz=10	mz=8	75%
2012	Unknown	na	rg=5	rg=7	(-)	(-)
2102	*Aspergillus ochraceus* group	cz=4	cz=3	mz=3	mz=2	100M
2235	*Trichothecium crotocinigenum*	cz=10	mz/rg=7	mz=6	mz2+rg8	100M
2274	*Pestalotia* sp.	mz=13	mz/rg=13	(-)	rg=8	(-)
2292	*Paecilomyces lilacinus*	cz=3	cz=3	cz=7	cz=3	(-)

Note: rg–reduced growth, mz–mottled zone, cz–clear zone, wk–weak, rgr–reduced growth rate, M–mortality, (-)–not active, FAW–Fall Army Worm

The crude extracts were subjected to various isolation techniques including liquid–liquid partitioning, silica gel column chromatography, and/or Sephadex LH–20 column chromatography, as well as reversed–phase HPLC. The liquid–liquid partitioning step is initially done between hexanes and acetonitrile to separate the lipids (generally not active in the assays and therefore not of interest) from the more polar compounds. Compounds isolated from the resulting acetonitrile partition fractions were characterized using NMR, MS, ECD, X–ray crystallography, and/or derivatization techniques depending on the nature of their structures and properties. Over three quarters of the metabolites encountered were previously described in the literature. Comparison of the collected NMR, MS, and/or ECD data to reported values enabled identification of these known metabolites. These results are summarized briefly in the remainder of this chapter. Chapters three and four will discuss new compounds encountered (and known compounds also encountered from the corresponding fungal isolates) in detail.

Of the eight endophytic isolate extracts, three were composed mostly of fatty acids and related lipids on the basis of NMR analysis (over 95%) and were not investigated further (ENDO 3470, 3481, and 3109). The extract from ENDO 3461, after partitioning, was also found to be mostly lipids, and the remaining portion was too sample–limited (<30 mg) and too complex a mixture, still containing lipids, to be investigated further.

Chemical investigation of the EtOAc extract from isolate ENDO 3476 exhibited weak antifungal activity against *A. flavus* and was found to contain the known compound mitorubrin (**2.1**) based on ^{1}H NMR comparison to literature data.[59] Mitorubrin is an azaphilone–type natural product that was originally isolated from *Penicillium rubrum*.[59] The azaphilones are very structurally diverse and exhibit a wide variety of bioactivities. Mitorubrin is known to be a geranylgeranyl transferase inhibitor.[60] Inhibitors of this type are under investigation for their anticancer effects.[61] Azaphilone–type natural products often stand out in out isolation protocols because of their bright yellow–orange color.

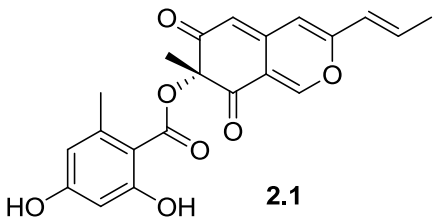

2.1

The EtOAc extract from ENDO 3503 was chemically investigated due to its moderate activity against both *A. flavus* and *F. verticillioides*, and two known compounds were encountered; enniatin B (**2.2**) and chlamydosporol (**2.3**). Enniatin B precipitated from acetonitrile solution during the liquid–liquid partitioning step, and accounted for approximately 50% of the extract. This compound was identified by comparison of both ^{1}H and ^{13}C NMR data to literature values.[62] The enniatins comprise a class of hexadepsipeptide metabolites known to come from many *Fusarium* spp., and are known to exhibit antibiotic activity.[62] Chlamydosporol (**2.3**), a known mycotoxin, was also encountered in this extract and was identified by comparison of HRESITOFMS, ^{1}H NMR, and ^{13}C NMR data with literature values.[63] Compound **2.3** was originally isolated from *Fusarium chlamydosporum*, and since has been isolated from other *Fusarium* spp. as well.[63-65]

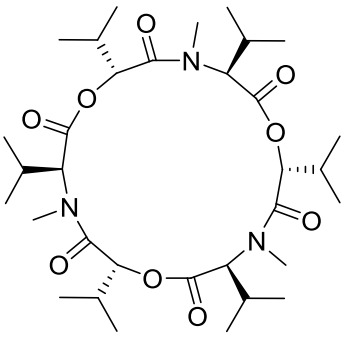

2.2

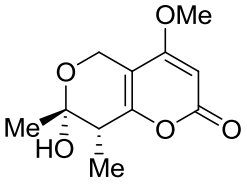

2.3

Studies of the EtOAc extracts of isolates ENDO 3115 and ENDO 3167 afforded only one major metabolite in each case. The antibiotic cochliodinol (**2.4**), originally reported from a *Chaetomium* sp., was isolated from ENDO 3115 and identified by comparison of literature data with the experimental HRESITOFMS, ^{1}H, and ^{13}C NMR data.[66, 67] Equisetin (**2.5**), isolated from ENDO 3167, was originally characterized after isolation from a *Fusarium* sp., and was reported to show potent antibiotic activity against gram–negative bacteria and inhibition of HIV–1.[68,69] Identification of equisetin in ENDO 3167 was accomplished by comparison of HRESITOFMS, ^{1}H NMR, and ^{13}C NMR data to those in the literature.[68]

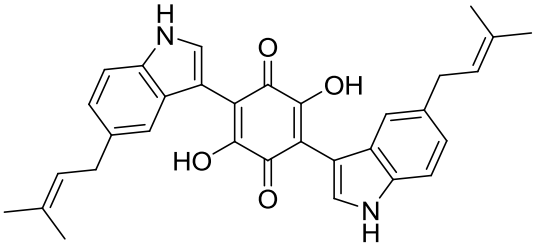

2.4

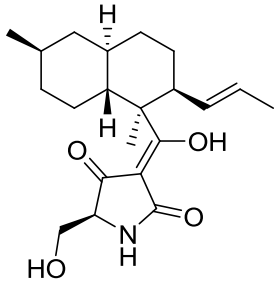

2.5

While all of the metabolites encountered from the investigated endophytic samples were previously reported, the majority of these compounds were reported to exhibit significant bioactivity of some sort. In each case, the activity observed for each extract in the initial screening could be accounted for by the presence of these known metabolites. Of the seven fungicolous and/or mycoparasitic isolate extracts investigated, two produced new compounds, as well as several compounds previously described in the literature. Those isolates are discussed in detail in chapters three and four. The other five afforded only known compounds, and these findings are summarized below.

The major metabolites of the MYC 2117 extract, which exhibited moderate activity against *F. verticillioides* and the fall army worm, were identified as orbuticin

(**2.6**) and pseurotin A (**2.7**). Pseurotin A is a relatively common fungal metabolite originally isolated from *Pseudeurotium ovalis*.[70] It is known to display cytotoxic and antibiotic activities, and is likely the cause of the activity observed in the initial screening. The sample of pseurotin A obtained from MYC 2117 was identified by comparison of ^{1}H NMR data to those of an authentic standard isolated from another fungal source by a member of our group. Orbuticin (**2.6**) was identified by comparison of the literature data[71] to the experimental ^{1}H and ^{13}C NMR data obtained from the MYC 2117–derived sample. Orbuticin was originally reported from *Acremonium butyri*, and exhibited weak activity against the fungal phytopathogens *Phytophthora infestans*, *Pyricularia oryzae*, and *Erysiphe graminis p.v. hordei*.[71]

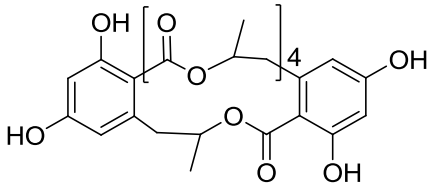

2.6

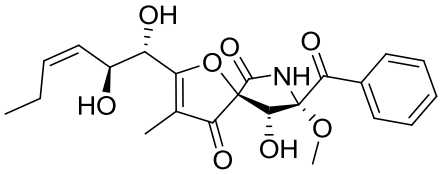

2.7

The extract from MYC 2012 displayed moderate activity against *F. verticillioides* and the fall army worm, while that from MYC 2274 exhibited activity against *A. flavus*. Each extract afforded only one compound through chemical investigation. An isocoumarin derivative, 3,4–dihydro–4,6,8–trihydroxy–7–methoxy–3–methylisocoumarin (**2.8**) was isolated from MYC 2012 and was identified by analysis of HRESITOFMS, ^{1}H–^{1}H decoupling, ^{1}H NMR, and ^{13}C NMR data in comparison with literature values.[72] Cladoacetal A (**2.9**) was encountered in the extract from isolate MYC 2274. This compound was originally reported by our research group in 2002 from a fungicolous *Cladosporium* sp.[73]

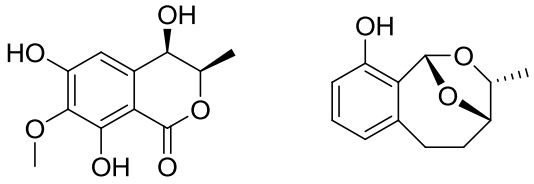

2.8 **2.9**

The MYC 2102 extract exhibited very good activity against the fall army worm, and moderate activity against both *A. flavus* and *F. verticillioides.* Chemical investigation of this extract yielded four major metabolites; mellein (**2.10**), dimorphecolic acid (**2.11**), penicillic acid (**2.12**), and dihydropenicillic acid (**2.13**). Compounds **2.10**, **2.12**, and **2.13** are extremely common fungal metabolites and standards already available in our laboratory were used for ^{1}H NMR data comparison. It is common to encounter penicillic acid and dihydropenicillic acid as a mixture and they were identified as such in this instance by ^{1}H NMR analysis.[74] Both are known to exhibit phytotoxic and antibiotic activities, and likely were responsible for the majority of the activity observed in the initial screening.[75] Dimorphecolic acid (**2.11**) was identified by comparison of HRESITOFMS, ^{1}H–^{1}H decoupling, ^{1}H NMR, and ^{13}C NMR data to those in the literature.[76]

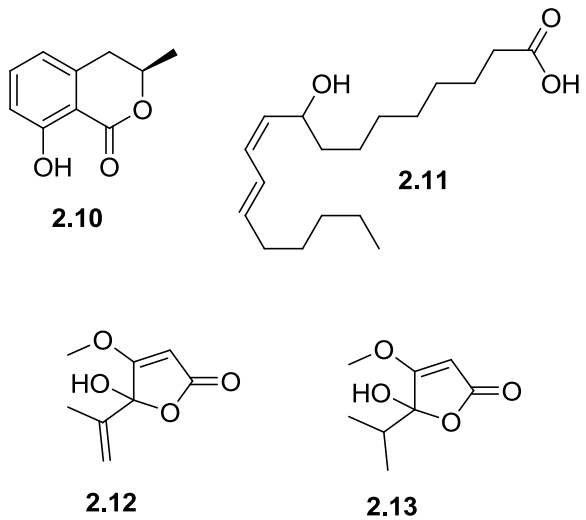

2.10 **2.11**

2.12 **2.13**

The extract from MYC 2292 displayed moderate activity against *A. flavus* and *F. verticillioides* in initial screening. Viridacatumtoxin (**2.14**) and colletofragarone A (**2.15**) were isolated from this extract and identified by comparison of literature data[77-79] to experimental HRESITOFMS, ^{1}H, and ^{13}C NMR data. Viridicatumtoxin (**2.14**) was originally isolated from a *Penicillium* sp. and was found to be a potent antibiotic effective against several strains of *Staphlococcus aureus*, including methicillin–resistant isolates.[78] The triene side chain of compound **2.15** readily converts between the inseparable *cis*– and *trans*– configurations. The resulting mixture leads to complexity in the NMR data, and likely explains why the configurations of the stereocenters have not been assigned. Colletofragarone A (**2.15**) is known to exhibit antifungal properties, and interestingly, inhibits the growth of the source fungus from which it was originally isolated, *Colletotrichum fragariae*.[77] Due to the bioactivity of lactone **2.15**, synthetic methods have been used to attempt to produce this compound, however, so far, only the tricyclic ring system, without the unassigned stereocenters, has been synthesized.[80]

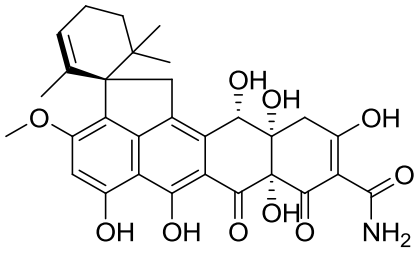

2.14

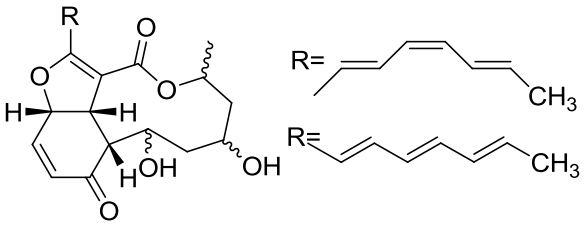

2.15

Chapters three and four will describe in detail studies of two fungicolous and/or mycoparasitic extracts that led to the isolation and identification of seven new compounds, as well as several known metabolites encountered along with them. The natural products described here (and in later chapters) represent many different types of

biogenetic origin, including peptides, nucleosides, polyketides, and mixed biosynthesis, and are reflective of the considerable diversity of chemistry that fungi can produce. Chapter five explores a different kind of topic, as it describes the isolation and characterization of degradation products of two economically important steroids. While the compounds studied in that project are not related to fungal natural products, many of the same spectroscopic and chromatographic techniques employed in our studies of fungal metabolites were used in that project as well.

CHAPTER 3

KIPUKASIN AND OXEPINAMIDE DERIVATIVES FROM *ASPERGILLUS PUULAAUENSIS*

In the course of our ongoing studies of fungicolous fungi as a source of new bioactive natural products,[50-52] an isolate of *Aspergillus* sp. (MYC–2152 = NRRL 62124) was obtained from a basidioma of an *Inonotus* sp. found on a dead soapberry tree in a forest in Kipuka ki (Volcanoes National Park) in the Ka'u District of Hawaii. Sequencing studies later showed that this isolate is a representative of a previously undescribed species of *Aspergillus* Section Versicolores (GenBank Accession No. JN093265), now named *Aspergillus puulaauensis* (Trichocomaceae).[81] The culture was incubated on rice (2 x 50 g) at 25^{0}C for 30 days and the resulting fermentation mixtures were extracted with EtOAc. The filtered EtOAc solution was evaporated to dryness, yielding 590 mg of crude extract.

The EtOAc extract obtained from solid-substrate fermentation cultures of this isolate showed antifungal activity against *Fusarium verticillioides* and antiinsectan activity against *Spodoptera frugiperda* (fall armyworm). Chemical investigation afforded three new compounds (**3.1-3.3**), one artifact (**3.4**), and nine additional known metabolites (**3.5-3.13**). The major metabolite encountered was the known compound sterigmatocystin, **3.5**, which accounted for the majority of the activity observed for the extract, although one of the new compounds (**3.1**) also showed antiinsectan effects. Details of the isolation, structure elucidation, and stereochemical assignments for **3.1-3.4** are described here, as well as a brief discussion of the known compounds.

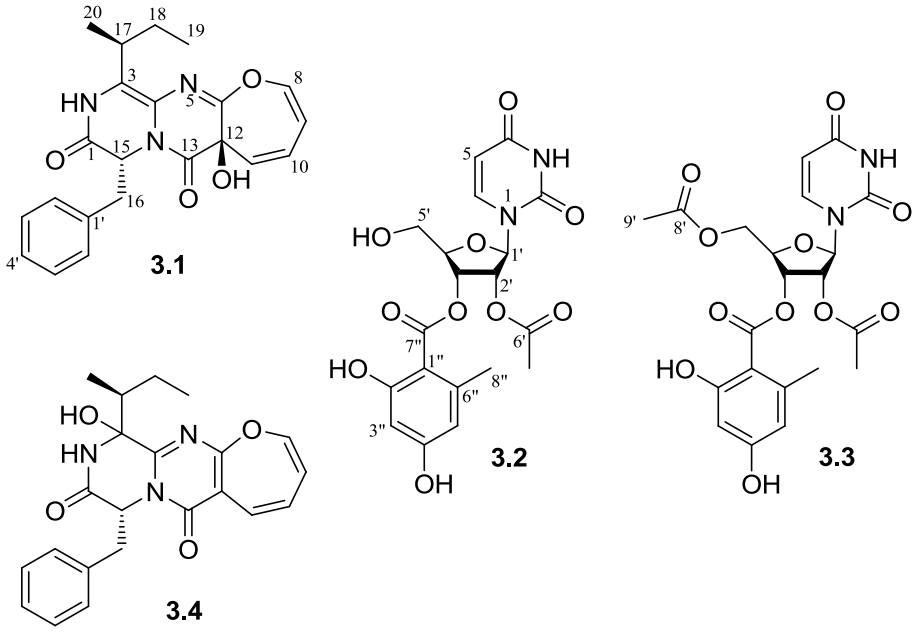

The EtOAc extract described above was subjected to liquid partitioning, silica gel chromatography, and reversed–phase HPLC to afford samples of 15-*epi*-oxepinamide E (**3.1**), kipukasins H (**3.2**) and I (**3.3**), artifact **3.4**, sterigmatocystin (**3.5**), 6,8-di-O-methylnidurufin (**3.6**),[82] and seven known indole alkaloids; aspergamide A (**3.7**),[83] avrainvillamide (**3.8**),[84] notoamides D-F and K (**3.9**–**3.12**),[85-87] and stephacidin A (**3.13**). The absolute configurations of the stephacidin A and notoamide F samples encountered were assigned to match those previously reported by analysis of their ECD spectra in comparison with literature data.[85]

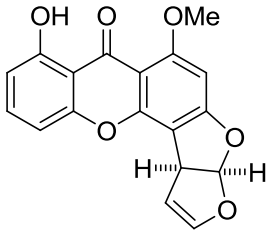

3.5

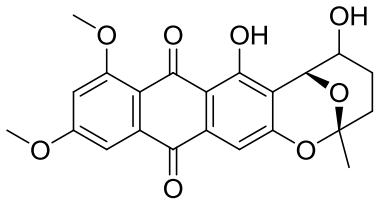

3.6

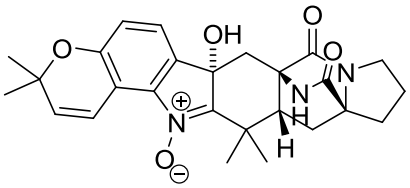

3.7

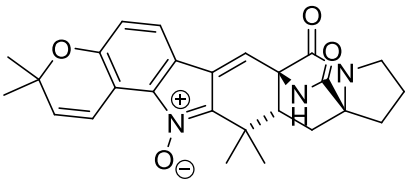

3.8

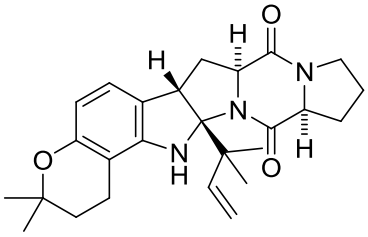

3.9

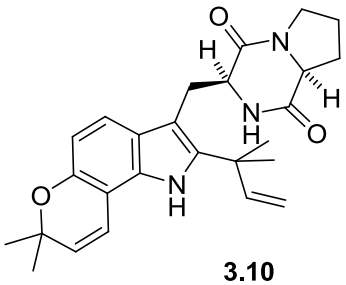

3.10

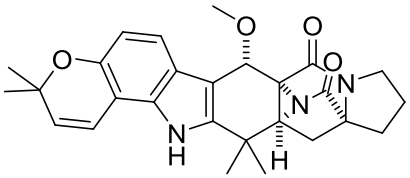

3.11

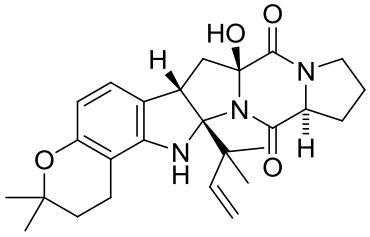

3.12

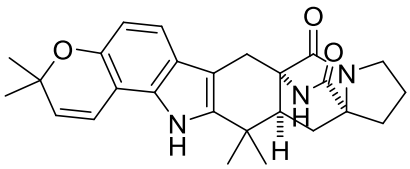

3.13

The molecular formula of **3.1** was determined to be $C_{22}H_{23}N_3O_4$ (12 unsaturations) by HRESITOFMS. The ^{1}H NMR spectrum indicated the presence of a benzyl group, an isolated *sec*-butyl unit, and an oxygenated diene system. A literature

search of these fragments in conjunction with the molecular formula led to reports of a pair of independently described diastereomers called oxepinamide E[88] (**3.14**) and brevianamide L,[89] (**3.15**) which were isolated from *Aspergillus puniceus* and *Aspergillus versicolor*, respectively. Interestingly oxepinamide E was originally patented in 2009, without any stereochemistry reported, by the same group that reported the complete structure in 2011.[88] Oxepinamide E was patented for its ability to inhibit liver X receptors (LXRs) which may signal potential use in the treatment of many diseases including diabetes, Alzheimer's, and atherosclerosis.[88]

Careful comparison of the ^{1}H and ^{13}C NMR data and $[\alpha]_D$ values for **3.1** revealed that the data did not match those of either of the precedents **3.14** or **3.15**, suggesting that **3.1** is a diastereomer of both literature compounds (Figure 3.1, Table 3.1). NMR differences between the compounds in their respective solvents are highlighted in Table 3.1 (**3.1** vs **3.14** (red); **3.1** vs **3.15** (blue)). The major differences between **3.1** and **3.14** can be seen by comparing the δ_H values for H–8, H–11, H–15, H–18, H–19 and H–20, while key differences between **3.1** and **3.15** can be seen in the δ_H values for H–11, H –15, H–18, and H–20, as well as the δ_C of C–16. Interestingly, the ^{1}H NMR signals for the minor component of the fraction containing **3.1** appeared to match those reported for **3.14**.[88] HMBC and HSQC experiments independently confirmed that **3.1** has the same gross structure as both oxepinamide E and brevianamide L.

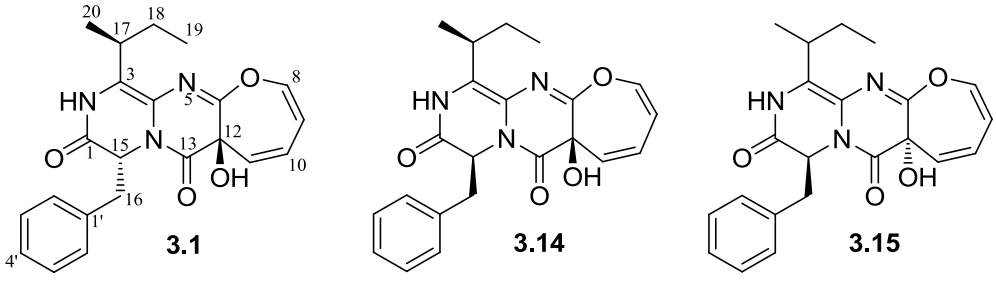

$[\alpha]^{20}_D$ +11.5° (*c* 0.12, acetone)
$[\alpha]^{20}_D$ +129° (*c* 0.25, chloroform)

$[\alpha]^{20}_D$ +500° (*c* 0.25, chloroform)

$[\alpha]^{20}_D$ +190° (*c* 0.10, acetone)

Figure 3.1. Structure and $[\alpha]_D$ –value Comparisons of Stereoisomers **3.1**, **3.14**, and **3.15**

Table 3.1. NMR Comparison of 15-*epi*-Oxepinamide E (**3.1**), Brevianamide L (**3.15**), and Oxepinamide E (**3.14**)

	3.1			**3.14**	**3.15**	
Position	δ_H[a] (mult., J_{HH})	δ_C[a]	δ_H[b] (mult., J_{HH})	δ_H[b] (mult., J_{HH})	δ_H[a] (mult., J_{HH})	δ_C[a]
1		165.4				164.7
2	7.65 (br s)		9.67	9.77 (s)	8.40 (s)	
3		120.8				120.7
4		117.0				117.0
6		152.9				153.4
8	6.59 (d, 7.3)	144.4	6.45 (d, 7.0)	6.72 (d, 7.3)	6.61 (d, 8.3)	144.3
9	5.51 (t, 7.3)	105.4	5.49 (t, 7.0)	5.48 (t, 7.3)	5.52 (t, 7.3)	105.2
10	6.16 (dd; 7.3, 10.5)	129.8	6.12 (dd, 7.0, 10)	6.16 (dd, 10.0, 7.0)	6.19 (dd, 10.3, 7.3)	128.9
11	5.66 (d, 10.5)	131.8	5.71 (d, 10)	5.88 (d, 10.0)	5.83 (d, 10.3)	132.0
12		69.8				70.2
12-OH			6.55 (br s)	6.38 (s)		
13		166.0				165.8
15	5.48 (t, 5.0)	56.6	5.19 (t, 5.0)	5.01 (dd, 6.0, 7.5)	5.30 (t, 5.3)	56.3
16	3.14 (dd; 5.5, 14.0)	37.5	3.00 (dd, 5.3, 14)	2.94 (dd, 5.5, 13.5)	3.09 (dd, 13.8, 5.3)	36.9
	3.26 (dd; 5.5, 14.0)		3.12 (dd, 5.0, 14)	3.03 (dd, 6.5, 13.5)	3.21 (dd, 13.8, 5.3)	
17	3.02 (m)	31.8	2.8 (dq, 2.0, 7.2)	2.80, (m)	3.03 (m)	31.9
18	1.28 (m)	26.9	1.29 (m)	1.16 (m, 7.5)	1.42 (m)	26.3
	1.39 (m)		1.38 (m)		1.51 (m)	
19	0.79 (t, 7.5)	12.0	0.66 (t, 7.2)	0.60 (t, 7.5)	0.77 (t, 7.2)	11.1
20	0.66 (d, 7.0)	17.7	0.61 (d, 7.2)	0.88 (d, 7.5)	0.75 (d, 7.2)	16.8
1'		134.4				135.4
2', 6'	7.04 (m)	129.7	6.99 (m)	7.04 (d, 7.0)	7.07 (m)	129.9
3', 5'	7.18-7.20 (m)	128.5	7.20 (m)	7.20 (t, 7.0)	7.20 (m)	128.2
4'	7.18-7.20 (m)	127.3	7.20 (m)	7.20 (t, 7.0)	7.20 (m)	126.9

Note: [a] $CDCl_3$ [b] DMSO-d_6

Crystallization of **3.1** from $CHCl_3$-MeOH produced yellow/orange needle-like crystals that diffracted poorly, but well enough to enable establishment of the structure and relative configuration by X-ray crystallographic analysis (Figure 3.2).

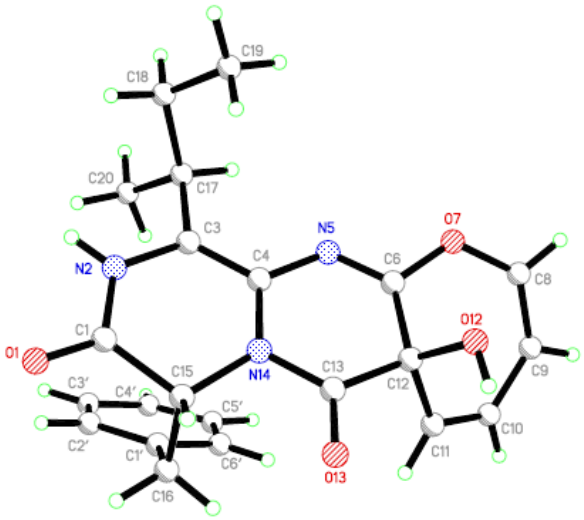

Figure 3.2. ORTEP Image of 15-*epi*-Oxepinamide E (**3.1**)

Acid hydrolysis of a sample of compound **3.1** afforded D-Phe, based on GCMS analysis of its *N*-TFA-2-butyl ester in comparison with standards of derivatized D- and L-Phe. Oxepinamide E (**3.14**) and brevianamide L (**3.15**) had been determined to contain L-Phe units.[88,89] A small amount of L-Phe derivative present can be attributed to the presence of **3.14** as a minor component of the original sample of **3.1**, and this was supported by ^{1}H NMR data. This result, along with the crystallographic results, led to assignment of the 12*R*, 15*R*, 17*S* absolute configuration for **3.1**. This absolute configuration was independently supported by comparison of the ECD spectrum to that of the gas phase-calculated ECD spectrum for the 12*R*, 15*R*, 17*S* isomer generated using the conformation of **3.1**'s observed in the crystal structure (Figure 3.3).

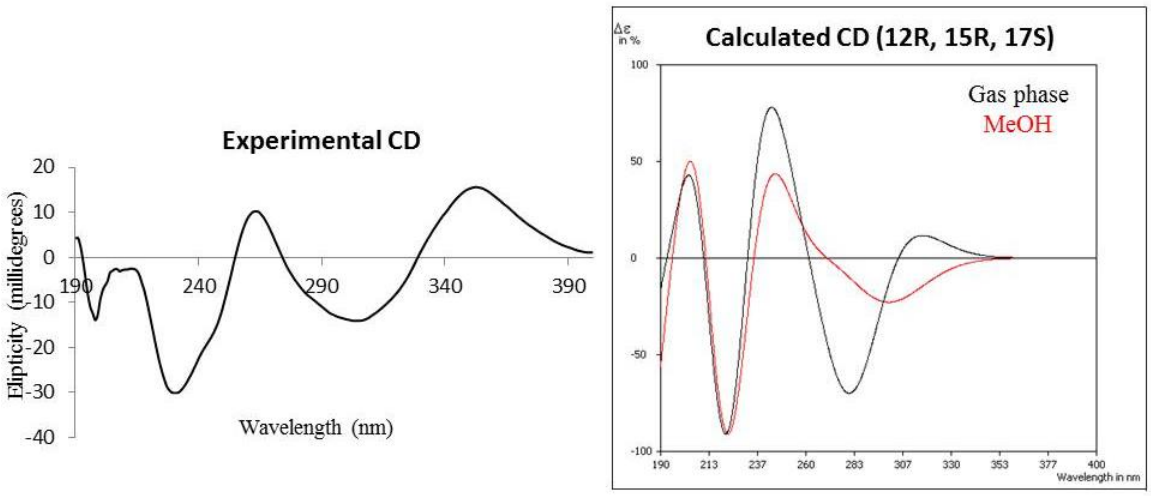

Figure 3.3. Experimental ECD Spectrum (left), and TDDFT–Calculated ECD Spectrum Based on the Conformation of **3.1** in the X–ray Crystal Structure

The absolute configuration of oxepinamide E was determined by Lu *et al*. to be 12*R*, 15*S*, 17*S* on the basis of crystallographic data analysis and the GCMS analysis of the *N*-TFA-2-butyl ester of the phenylalanine obtained upon acid hydrolysis of **3.14**.[88] The conformation of the 17–position of brevianamide L could not be assigned due to the non-crystalline nature of the sample, and because this stereocenter is isolated from the other two, precluding assignment by analysis of NOESY data. However, Li *el al*. determined that H–17 and H–15 were on opposite faces, as in structure **3.1**, by NOE analysis.[89] Thus, their results enabled the assignment of the absolute configurations at two of the centers as 12*S* and 15*S*. In the publication by Li *et al*., the authors stated that the absolute configurations at positions 12 and 15 were *S* and *R* respectively, however, they concluded that the phenylalanine unit was the L–isomer by analysis of its *N*-TFA-2-butyl ester, which would correspond to a 12*S*, 15*S* overall structure. Differences in ^{1}H NMR data and $[\alpha]_D$ values indicated that **3.1** and **3.14** are diastereomers, not enantiomers, therefore, the absolute configuration of brevianamide L (**3.14**) must be 12*S*, 15*S*, 17*S*.

Multiple attempts to obtain a larger, better diffracting crystal of **3.1** in hopes of obtaining another crystal for additional crystallographic studies to obtain higher

resolution X–ray data, as well as to determine a melting point, led to degradation of the original sample obtained. A neighboring silica gel fraction contained **3.1** along with some impurities, and was subjected to HPLC in an attempt to obtain a pure sample of **3.1**. However, compound **3.4** was obtained instead. Comparison of the ^{1}H NMR data for **3.4** with those of the fraction before HPLC indicated that **3.4** was not present in the sample prior to the HPLC step, indicating that it was an artifact of the isolation process. Key differences between the ^{1}H NMR spectra of **3.1** and **3.4** included shifts of the benzyl group multiplet and the signals for the CH_2 of the *sec*–butyl unit, as well as significantly better resolution of the signals for H–9 and H–15. These differences did not clearly reveal the change in the structure that had occurred, so HSQC and HMBC data were collected for **3.4 (**Table 3.2).

These experiments revealed that three carbons (C–3, C–4, and C–12) had radically different chemical shifts in **3.4** than they had in **3.1**. C–3 shifted from δ120.8 to δ84.8, suggesting that it was no longer sp^2 hybridized, but rather an oxygenated sp^3 hybridized carbon. C–12 shifted downfield from δ69.8 to δ111.5, revealing that it now was olefinic and not an oxygenated sp^3 carbon. This change in location of the oxygenated substitution accompanied by a double bond shift was consistent with the downfield shift of C–4 to δ156.3 from δ117.0 caused by the formation of a C–4 to N–5 double bond in compound **3.4,** rather than the C–3 to N–5 double bond in **3.1**. A literature search revealed a publication describing another compound called brevianamide O (**3.16**), a stereoisomer of artifact **3.4.**[90] Brevianamide O was reported to contain L–Phe (15*S*), as did both brevianamide L (**3.15**) and oxepinamide E (**3.14**). While both brevianamides L and O were isolated and identified by the same group,[89,90] they came from fermentations of different *Aspergillus versicolor* isolates.

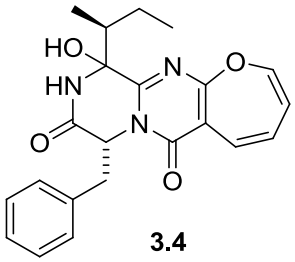

3.4

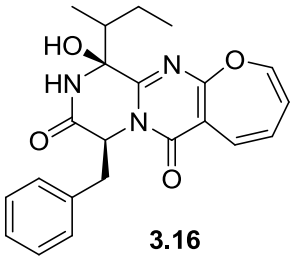

3.16

Table 3.2. NMR Data for Artifact **3.4**

Position	δ_H[a] (mult., J_{HH})	δ_C[b]	HMBC[a] (H→C#)
1		166.4	
2	6.30 (br s)		1[w], 4, 15
3		84.8	
4		156.3	
6		163.6	
8	6.05 (dd, 5.7, 0.6)	143.3	6, 9, 10, 11, 12
9	5.65 (t, 5.7)	117.3	8, 11
10	6.21 (dd; 5.7, 11.2)	128.7	6[w], 8, 9, 12
11	6.78 (d, 11.2)	124.9	6, 8, 9, 12, 13
12		111.5	
13		160.8	
15	5.44 (t, 5.0)	57.3	1, 4, 16, 1'
16	3.43 (dd; 3.4, 14) 3.54 (dd; 5.3, 14)	36.8	1, 15, 1', 2', 6'
17	2.35 (sextet, 7.0)	43.3	3, 4, 18, 19
18	0.82 (m)	24.5	3, 17, 19
19	0.77 (m)	11.6	17, 18
20	0.90 (d, 7.0)	10.5	3, 17, 18
1'		134.5	
2', 6'	6.96 (m)	130.2	16, 3', 4', 5'
3', 4', 5'	7.31 (m)	129.0	1', 2', 6'

Note: [a]600 MHz. [b]150 MHz. [w] Weak correlation

It is assumed that artifact **3.4** would retain its configuration at positions 15 and 17, leaving only two possible diastereomeric products: 3*S*, 15*R*, 17*S* or 3*R*,15*R*, 17*S*. Interestingly, energies of the Spartan 10–minimized conformers of the two possible

artifact diastereomers are much lower than that calculated for the original molecule, **3.1**, by more than 14 kcal/mol. The energy difference between the two possible artifact stereoisomers is less than 0.5 kcal/mol. One possible reason for this energy difference between **3.1** and **3.4** is that **3.4** is more highly conjugated than **3.1**, which contains two isolated diene systems and an isolated ketone. On the other hand, at first glance, the seven–membered oxepin ring appears to meet the criteria for being antiaromatic which would make it highly disfavored. However, the relatively large ring size can provide some limited flexibility, which could enable it to twist out of planarity, making the ring non-aromatic rather than anti–aromatic. This would be analogous to the well–known behavior observed for cyclooctatetraene. Indeed, a "boat–like" conformation was obtained after energy–minimization of **3.4** using Spartan 10. It is interesting to note that oxepin itself is considered to be in rapid equilibrium with benzene oxide, but this behavior is highly dependent on solvent effects, and is also influenced dramatically by the presence of substituents on the ring.[91,92] While the cited studies did not investigate the tautomerism equilibrium effects of an oxepin system fused to another ring, as in **3.4**, the data seems to indicate that the ring system in **3.4** exists as an oxepin rather than a benzene oxide ring system.[90,92] This conclusion is supported by an X–ray structure reported in the literature for a related compound (oxepinamide D).[88]

Comparison of the experimental ECD spectrum of **3.4** to that of the calculated ECD spectra of the two possible diastereomers of **3.4** did not provide substantial confirmation the stereochemistry at position C3 (Figure 3.4). Even though the two calculated spectra are quite different from one another, neither matched the experimental spectrum well. Most notably, the calculated spectra included a prominent peak at 330 nm that was not observed in the experimental data. Even so, the calculated spectrum for the 3*S*, 15*R*, 17*S* isomer did display a negative Cotton effect near 250 nm similar to that observed in the experimental spectrum. Possible explanations for the discrepancy may lie in the unusual nature of the oxepin, which could lead to inaccurate calculation results.

It has been reported that different types of energy–minimization calculations produce significantly different conformers and tautomers in this type of system.[93]

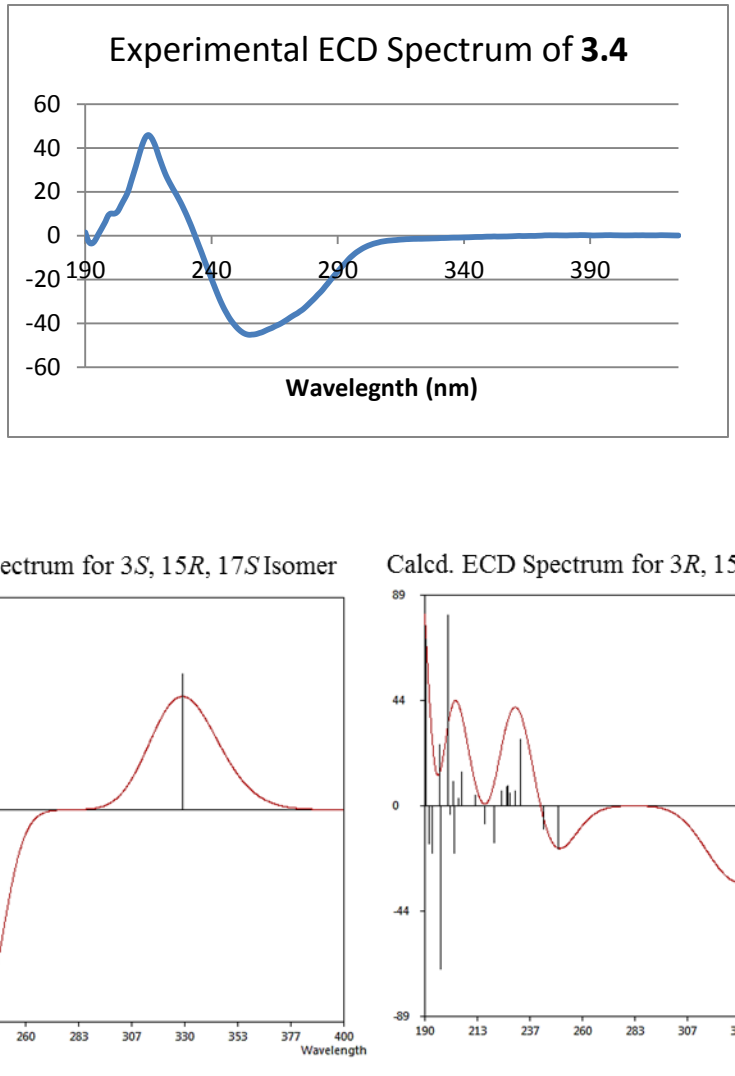

Figure 3.4. ECD Spectrum of **3.4** (top) Compared to Those Calculated for the Two Possible Diastereomers (bottom left and right)

Kipukasins A-G (**3.16**–**3.22**) are a group of modified nucleotides first reported by our group in 2007[52] from two different fungal isolates, one of which (NRRL 35641) was later determined by sequence analysis to be a representative of the same new species[81] as

the isolate described here, while the other (NRRL 35600) was determined to be *Aspergillus amoenus*. Two of the other compounds obtained from MYC–2152 were clearly members of this compound class based on their NMR data, which showed characteristic uracil, furanose, and benzenoid aromatic signals. However, neither molecule contained any methoxy groups, a common characteristic of all the previously reported kipukasins.

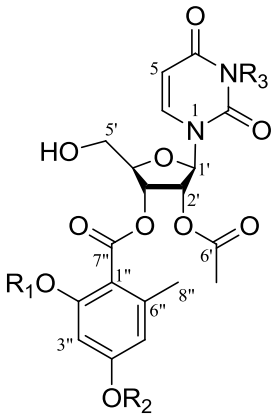

3.16 $R_1 = R_2 = CH_3$; $R_3 = H$
3.17 $R_1 = CH_3$; $R_2 = R_3 = H$
3.18 $R_1 = R_3 = H$; $R_2 = CH_3$
3.21 $R_1 = R_3 = CH_3$; $R_2 = H$

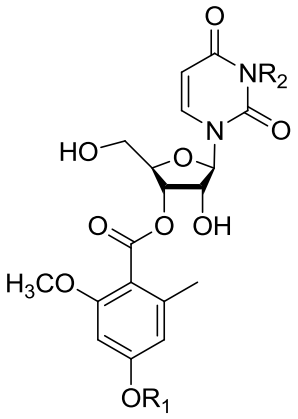

3.19 $R_1 = CH_3$; $R_3 = H$
3.22 $R_1 = H$; $R_2 = CH_3$

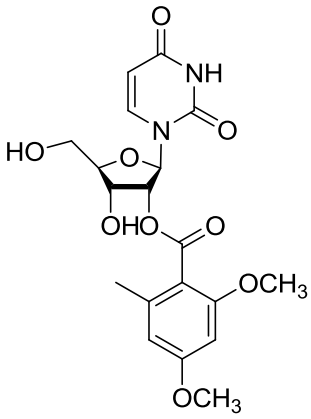

3.20

HRESITOFMS data for kipukasin H (**3.2**; *m/z* 501.1110 [M+Na^+]) indicated a molecular formula of $C_{21}H_{22}N_2O_{11}$ (12 unsaturations; kipukasins A-G have either 10 or 11). The ^1H NMR spectrum indicated the presence of two acetate groups along with the other characteristic signals noted above. Analysis of the HMBC data (Figure 3.5 and Table 3.3) for the acetate methyl singlet at δ_H 2.05 (H_3–7') showed a long range correlation with C–2' of the furanose unit, indicating acetylation of the 2' oxygen. The second acetate methyl singlet (δ_H 2.15, H_3–9') correlated only to its carbonyl carbon (C–8'). However, one of the C–5' oxygenated methylene proton signals also correlated to C-8', thereby locating the second acetyl group. HMBC correlations from H–6 to C–2, C–4,

C–5, and C–1', from H–5 to C–4 and C–6, and from H–1' to C–2 confirmed the uracil fragment and its connection to the furanose unit at C–1'. The gross structure of the furanose moiety was confirmed by correlations from H–2'to C–1', C–3'and C–4', from H–3' to C–1'and C–5', and from H–4' to C–3'. The substitution pattern of the aromatic ring was established on the basis of chemical shifts, the *meta* coupling between the two aromatic protons, and HMBC correlations (Figure 3.5), and was located as an acyl substituent of the 3'–oxygen of the furanose ring by correlation of H–3' to the remaining (benzoate) ester carbon C–7".

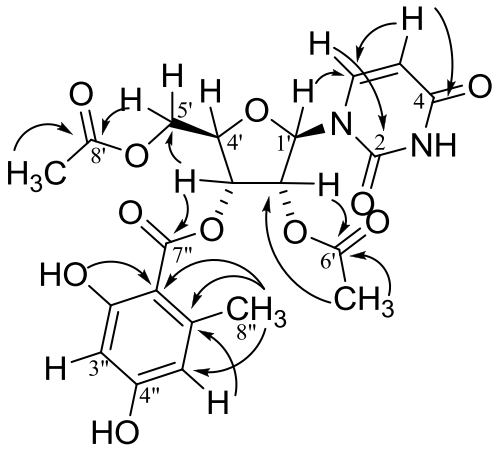

Figure 3.5. Key HMBC Correlations for Kipukasin H (**3.2**).

Table 3.3. NMR Data for Kipukasin H (**3.2**).

Position	δ_H[a] (mult., J_{HH})	δ_C[b]	HMBC[a] (H→C#)
2		149.7	
4		161.9	
5	5.79 (d, 8.1)	103.5	4, 6
6	7.36 (d, 8.1)	139.4	2, 4, 5, 1"
1'	6.04 (d, 6.0)	88.0	2, 6
2'	5.44 (t, 6.0)	72.6	1', 3', 4', 6'
3'	5.58 (dd, 4.0, 6.0)	71.6	1', 5', 7"
4'	4.49 (q, 4.0)	80.4	3'
5'	4.39 (dd, 4.0, 12)	63.3	
	4.45 (dd, 4.0, 12)		8'
6'		169.7	
7'	2.05 (s)	20.5	2', 6'
8'		170.1	
9'	2.15 (s)	20.8	8'
1"		103.5	
2"		166.0	
3"	6.28 (d, 2.6)	101.6	1", 2", 4", 5"
4"		161.2	
5"	6.25 (dd, 0.5, 2.6)	111.9	1", 8"
6"		144.0	
7"		170.2	
8"	2.55 (s)	24.5	1", 5", 6"
2"-OH	11.19		1", 2", 3"

Note: [a]600 MHz. [b]150 MHz.

The gross structure of kipukasin I (**3.3**) was determined by comparison of its ^{1}H NMR and HRESITOFMS data with those of **3.2**. The molecular formula of compound **3.3** was determined by HRESITOFMS to be $C_{19}H_{30}N_2O_8$, indicating one less acetate group than **3.2**, which was confirmed by the presence of only two methyl singlets, compared to the three in the ^{1}H NMR data for **3.2.** The relatively upfield shifts of the C–5' methylene protons at δ_H 3.99 and 4.37, compared to the values for **3.2** at δ_H 4.39 and

4.45, indicated that this position was not acetylated in **3.3**. The location of the benzyl ester moiety was assigned based on the shift of H–3' (δ_H 5.71), which followed the trend of kipukasins A–D (**3.16**–**3.19**) and F–H (**3.21, 3.22, 3.2**), as opposed to kipukasin E (**3.20**) where the benzoyl group was attached to the furanose C–2' oxygen resulting in a relatively upfield shift for this signal to δ_H 4.63.

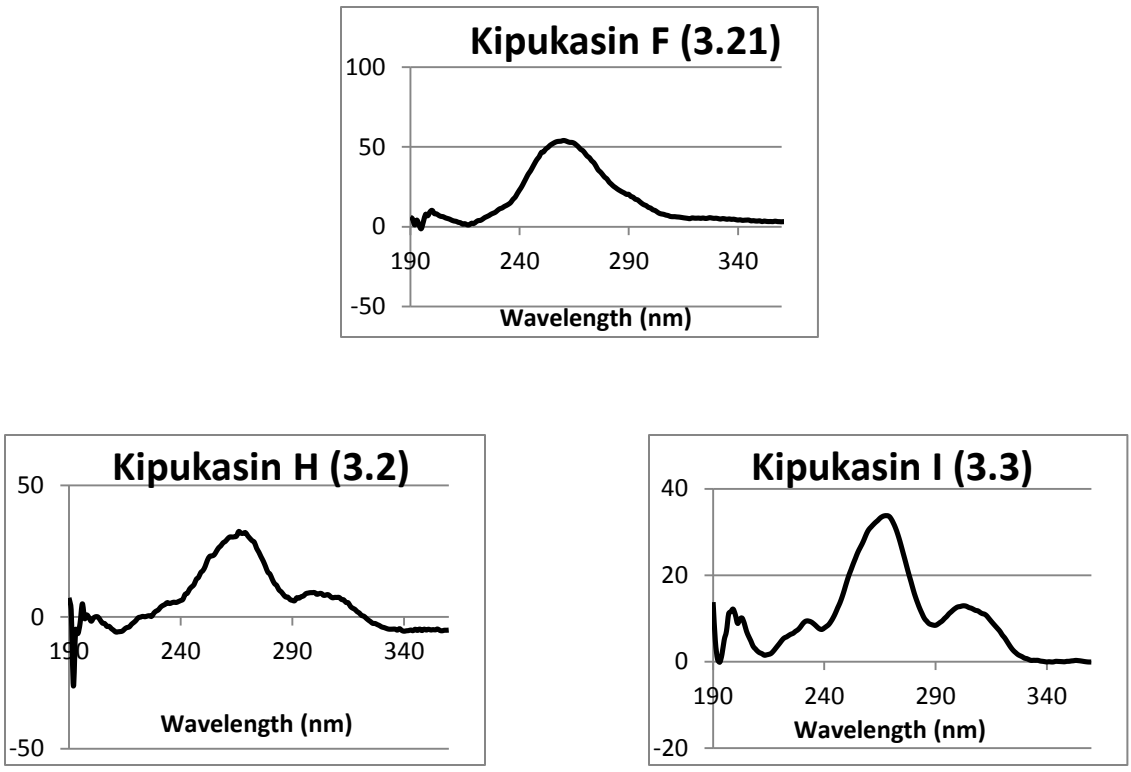

Figure 3.6. ECD Spectra of Kipukasins F (**3.21** top), H (**3.2**, left), and I (**3.3**, right)

The relative configurations of **3.2** and **3.3** were assigned by comparison of the coupling constants of the monosaccharide unit signals to those analogous in **3.16–3.22**. [52] The absolute stereochemistry of the ribose unit in **3.16** was established by comparing ECD spectrum of the hydrolyzed uracil moiety to that of a standard of uracil–1–β–D–ribofuranose.[52] The absolute configurations of kipukasin H (**3.2**) and I (**3.3**) were

determined to match those of kipukasin A–G by comparing their ECD spectra with that of intact kipukasin F (Figure 3.6, above).

The majority of the biological activity initially observed for the extract was accounted for by the high levels of sterigmatocystin present, as kipukasins do not show antiinsectan effects. Compound **3.1** produced an 87% reduction in growth rate in the fall armyworm after four days at 1% by weight application in a minidisk assay.[58] However, a statistically significant reduced growth rate was not observed at 100 ppm in a standard dietary assay.[94] Kipukasins H and I were inactive in standard disk assays against *Staphylococcus aureus* (ATCC 29213), *Enterococcus coli* (ATCC 25922), and *Bacillus subtilis* (ATCC 25922) at 100 µg/disk.

In summary, chemical investigation of this extract yielded three new compounds (**3.1–3.3)**, a new artifact (**3.4**), and nine known compounds (**3.5-3.13**). Elucidation of the absolute configuration of **3.1**, 15-*epi*-oxepinamide E, enabled assignment of the absolute configuration of the literature compound brevianamide L (**3.15**) as well. The relative configuration of **3.1** was determined through analysis of X–ray crystallographic data, while GCMS analysis of the phenylalanine present in the acid hydrolyzate of **3.1** after derivatization to its *N*-TFA-2-butyl ester allowed assignment of the absolute configuration of **3.1**. In this case, X-ray analysis was essential in order to assign the relative configuration because the three stereocenters were insulated from each other, making other methods ineffective. The configuration assigned to **3.1** was supported by comparing the experimental ECD spectrum to the ECD spectrum calculated based on the crystallographic data. Since the experimental and calculated ECD spectra corresponded very well, we employed an analogous method comparing the experimental ECD spectrum to the calculated ECD spectrum to assign the absolute configuration of the related artifact **3.4**.

In addition to new compounds, **3.1** and **3.4**, two new members of the kipukasin family (**3.2** and **3.3**) were also encountered. While kipukasins H and I are simple

analogues of the previously known kipukasins A-G, these nine compounds are the only reported fungal derivatives of the nucleoside uridine. Fungal nucleoside derivatives are relatively rare as secondary metabolites. A search of the online Dictionary of Natural Products revealed that there are only 23 nucleoside derivatives known from fungal species, including the seven previously reported kipukasins. Interestingly, the majority of the non-kipukasin derivatives are simple nucleoside phosphate derivatives, making the kipukasin family even more distinctive.

The discovery of new chemistry within this extract led to further investigation into the fungal source. It was only then determined that the fungal isolate was a representative of a new *Aspergillus* species, now named *Aspergillus puulaauensis*, based on its Hawaiian origins.[81]

CHAPTER 4

CHEMICAL INVESTIGATION OF A *TRICHOTHECIUM CROTOCINIGENUM* ISOLATE

In the course of our ongoing studies of fungicolous and mycoparasitic fungi,[50-52] an isolate of *Trichothecium crotocinigenum* (syn. *Acremonium crotocinigenum*; MYC-2235 = NRRL 62714), identified based on micromorphology, was isolated from the black stromata of a pyrenomycete collected from a dead hardwood branch in Kipuka ki (Volcanoes National Park), Ka'u District, Hawaii. The culture was incubated on rice (2 x 50 g) at 25^{0}C for 30 days and the resulting fermentation mixtures were extracted with EtOAc. The filtered EtOAc solution was evaporated to dryness, yielding approximately one gram of crude extract. Its EtOAc–soluble fermentation extract showed antifungal activity against *F. verticillioides* and *A. flavus*, as well as antiinsectan activity against the fall armyworm,[58] and was therefore chemically investigated.

Chromatographic separation of the acetonitrile–soluble portion of the extract (284 mg) yielded three major metabolites: the new compound **4.1**, cyclo-(L-pipecolinyl-aminocyclopropane-carboxylic acid), and the known compounds 3-deoxotrichothecin (**4.2**) and guangomide A (**4.3**). Compound **4.2** was found to be a member of the trichothecene class of fungal metabolites, and was identified by comparison of ^{1}H NMR data with literature values.[95] Trichothecenes comprise a well–known class of mycotoxins that show a variety of biological activities often including significant cytotoxicity.[96, 97] As suspected, the majority of the observed antiinsectan activity for the extract in this case was due to the amount of 3-deoxotrichothecin encountered, and this was confirmed by minidisk assay.[58] Guangomide A (**4.3**) is a depsipeptide containing a distinctive 2,3-dihydroxy-isovaleric acid unit.[98,99] Guangomide A was identified by HRESITOFMS and

^{1}H NMR analysis without complete purification. Both **4.2** and **4.3** have been previously reported from *Trichothecium* spp. [95,98,99]

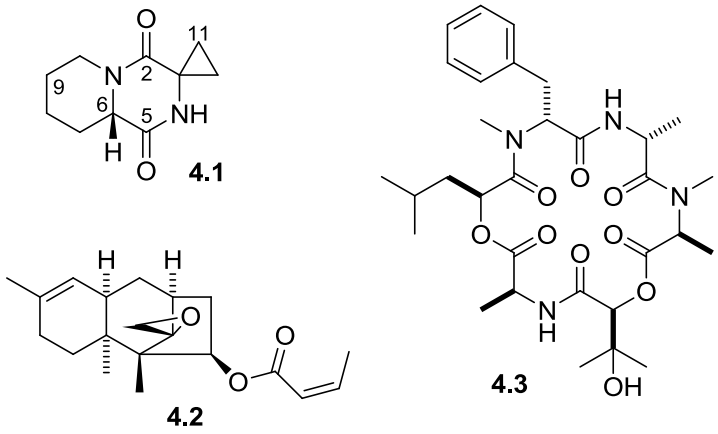

Aside from **4.3**, a number of minor compounds were detected whose ^{1}H NMR spectra contained signals characteristic of peptide/depsipeptide–type metabolites. Trace quantities of two of these compounds (**4.4** and **4.5**) were isolated and tentatively identified as shown by HRESITOFMS and HRESITOFMS-MS analysis, but there was not enough material to provide quality NMR data or enable NMR assignments. Problematic issues encountered with these two compounds, such as possible degradation and difficulties in isolating more material, will be discussed in detail later in this chapter. Briefly, despite scaling up the fermentation of this isolate twice, further samples of **4.4** and **4.5** were not obtained. However, both scale–up extracts (585 mg and 726 mg of acetonitrile partitions) again contained **4.1** and **4.2**. In each scale–up, the signals for peptide/depsipeptide–type metabolites, possibly including **4.4** and **4.5**, were still present, but only in very small quantities that did not allow for isolation of the compounds.

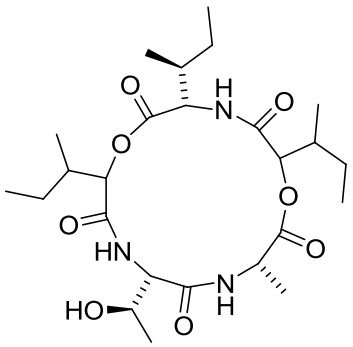

4.4

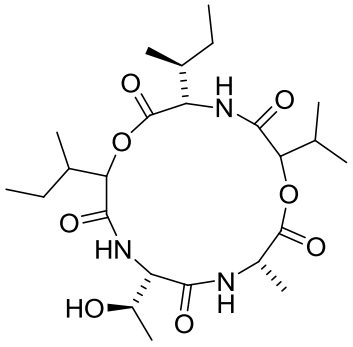

4.5

The other major component (**4.1**) was of immediate interest because its ^{1}H NMR spectrum contained unusually upfield–shifted signal(s) at δ_H 0.89. When $CDCl_3$ was used as the NMR solvent, the signal(s) appeared as a somewhat cryptic, complex two–proton multiplet at δ_H 0.89 (Figure 4.1), which complicated assignment of the corresponding structural feature. In addition, the residual water signal in the spectrum overlapped with and obscured several other signals. In an effort to resolve these issues, NMR data were acquired using methanol-d_4 as the solvent. This process resulted in deconvolution of the upfield signal(s) to a pair of mutually coupled ddd's (Figure 4.1), initially suggestive of a pair of diastereotopic CH_2 protons with vicinal neighbors. The spectrum in methanol-d_4 also lacked much of the overlap previously observed at δ_H 1.2-1.8, encouraging the use of this solvent for further data collection.

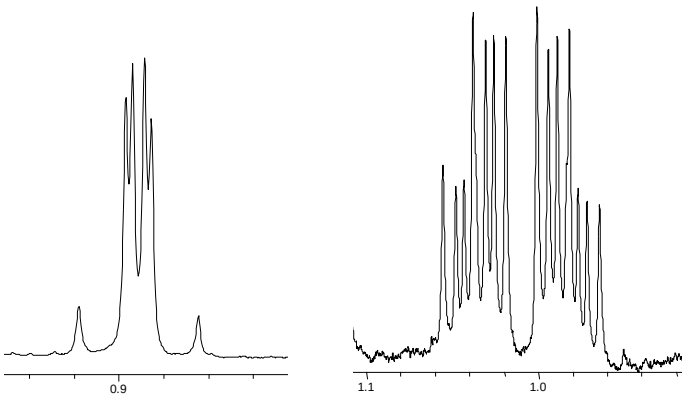

Figure 4.1. Comparison of the Upfield ^{1}H NMR Signals observed for Compound **4.1** in $CDCl_3$ (left) and Methanol-d_4 (right)

Table 4.1. NMR Data for **4.1** in Methanol–d_4

Position	δ_C[b]	δ_H[a] (mult., J_{HH})	HMBC[c] (H→C#)
2	167.5		
3	37.7		
5	169.7		
6	61.1	4.04 (dd; 3.0, 12)	2,5,7,8,10
7	31.9	1.57 (dq; 3.6, 13)	5,6,8
		2.26 (m)	9
8	25.3	1.65 (tt; 3.6, 13)	6,7,9,10
		1.99 (m)	
9	25.7	1.45 (m)	8,10
		1.72 (m)	
10	44.3	2.64 (dt; 3.0, 13)	2,6,8
		4.56 (dm)	6,8
11*	15.8	1.04 (ddd; 4.0, 6.6, 11)	2,3,12
		1.45 (m)	2,3,12
12*	17.2	0.98 (ddd; 4.2, 7.4, 11)	2,3,11
		1.37 (ddd; 4.2, 7.4, 11)	2,3,11

Note: *These position assignments may be interchanged

Interestingly, the HSQC data (Figure 4.2; incorporated into Table 4.1, above) revealed that the upfield proton signals shown in Figure 4.1 correspond to vicinal, not geminal (Figure 4.2), linked to two unusually upfield CH_2 carbons at δ_C 15.8 and 17.2. Moreover, the vicinal coupling constant between these two protons is 11 Hz—larger than the geminal *J*–values observed for each with its geminal partner (6.6 and 7.4 Hz; Table 4.1).

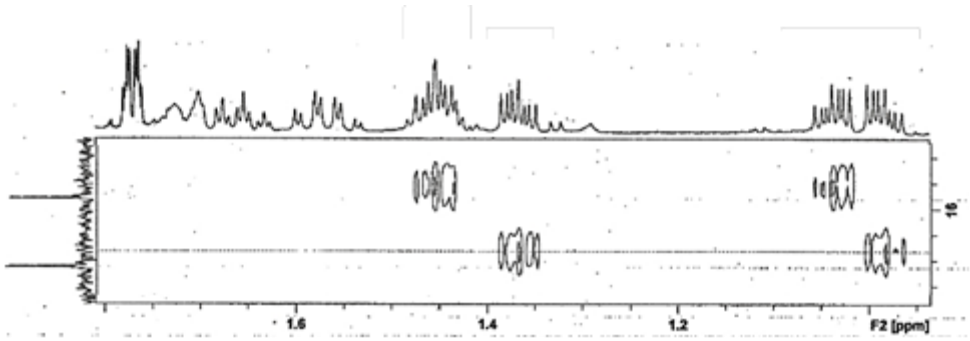

Figure 4.2. Expansion of the Upfield Region of the HSQC Spectrum of **4.1**

HRESITOFMS data (*m/z* 195.1131 $[M+H]^+$, $C_{10}H_{15}N_2O_2$), in conjunction with characteristic shifts of the two carbonyl signals (δ_C 167.5 and 169.7), indicated that **4.1** contained two amide carbonyls. These data also revealed that **4.1** has five unsaturations, three of which must be accounted for by rings, as no other sp^2 carbons were evident. The two upfield CH_2 units showed strong correlations to each other in both the COSY and HMBC spectra. The HMBC data (Table 4.1, Figure 4.3) also revealed that each of these CH_2 signals correlated to a non-protonated sp^3 carbon and an amide carbon. These data and the upfield δ_H– and δ_C–values indicated the presence of a 1,1–disubstituted cyclopropane ring connected to one of the two carbonyls. HMBC correlations for the only methine proton (δ_H 4.04, δ_C 61.1) almost solely enabled the assembly of an acylated pipecolic acid (Pip) unit, as it showed correlations to three other CH_2 units and to both amide carbons. This led to the conclusion that **4.1** is a diketopiperazine containing 1-aminocyclopropane-1-carboxylic acid (Acc) and a Pip units to form a new tricyclic ring system.

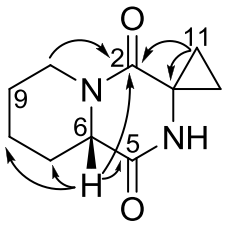

Figure 4.3. Key HMBC Correlations Supporting the Assignment of Structure **4.1**

The upfield shifts of the cyclopropyl CH_2 carbon signals (δ_C 15.8 and 17.2) enabled the use of DEPT as a simple screening tool to help search for analogues containing the Acc unit in other fractions. No such analogous were found, however, this approach did allow **4.1** to be rapidly identified in complex mixtures, including the scale–up fermentation extracts.

The only stereogenic center in **4.1** is contained in the Pip unit. Marfey's method was employed in an effort to assign the absolute configuration.[100,101] A subsample of **4.1** was hydrolyzed to afford a mixture containing Pip. The hydrolyzate was then treated with Marfey's reagent, 1-fluoro-2,4-dinitrophenyl-5-L-alanine amide (FDAA), and the resulting mixture was then subjected to RP-HPLC and chromatographically compared to FDAA–derivatized standards of D– and L–Pip. Co–injection of the standards with the sample derived from **4.1** (Figure 4.4) enabled assignment of the hydrolysis product from **4.1** as L–Pip, requiring the 6*S*– absolute configuration for **4.1**.

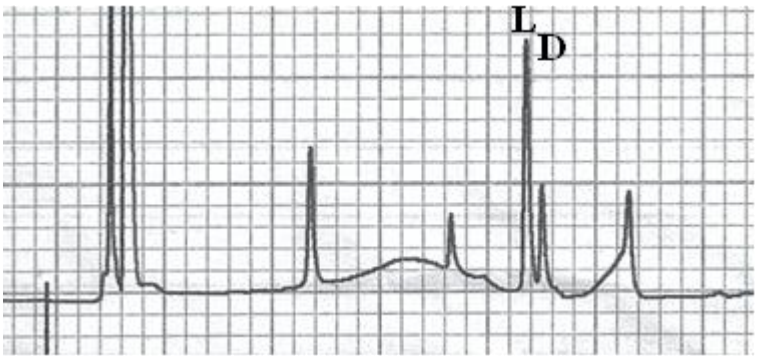

Figure 4.4. Co-injection of FDAA–derivatized D– and L–Pip Standards (1:1) with the Sample Derived from **4.1**

Compound **4.1** was inactive in assays for antifungal, antibacterial, and antiinsectan effects, but the closest known metabolite to **4.1 (**a synthetic proline–containing analogue) reportedly exhibits neuroprotective effects after brain injury.[102]

The Acc unit is rarely encountered as a constituent of natural products, and has not been previously reported as a subunit of a diketopiperazine–type metabolite. The Acc unit has very recently been found as a subunit in fumoquinazolines K – P (from an *Aspergillus* sp.),[103] and has been described previously as a component of a few cyclic and acyclic fungal peptides (serinocyclins A and B, from *Metarhizium anisopliae*, and neoefrapeptins A–N, from *Geotrichum candidum*).[104,105]

The ^{1}H NMR spectrum of **4.4** contained many overlapping signals, however, some structural features could be recognized. The spectrum contained five methyl doublets, two of which were somewhat more downfield (1.28 and 1.59 vs. ~1.00 ppm), one oxygenated methine, and five protons in the peptide α–proton region, as well as two very broad amide signals. At this point, it was assumed that the compound was peptide-like in structure, possibly containing three isoleucine (Ile) units, an alanine (Ala) unit, and a threonine (Thr) moiety. It was thought that the use of a different NMR solvent could aid in resolving the overlapping signals. Therefore, the available sample of **4.4** was

subjected to ^{1}H NMR data collection in different solvents (benzene–d_6, acetone–d_6) in hopes of resolving at least the α–protons to make 2D NMR data collection of maximum use. However, in both of these solvents, a doubling of signals occurred. It was thought that this could be due to a mixture of conformers in solution. Interestingly, reacquiring ^{1}H NMR data in $CDCl_3$, the original solvent used, also showed a doubling of signals, even though the original spectrum had shown only one set of (broad) signals. The temperature of the sample in the NMR instrument was raised from 298K to 308K and 318K in an effort to explore the possibility of a conformational equilibrium. If the temperature is raised to an appropriate level to overcome the conformational energy barrier, interconversion would be rapid, and only one (average) set of signals should be detected by NMR. This variable temperature experiment was performed in $CDCl_3$, but the doubled signals did not coalesce into one set. While it may be that the highest temperature used simply could not overcome the barrier, it was also considered possible that the second set of signals corresponded to a ring–opened hydrolysis product of **4.4**. At this point, MS techniques were employed to attempt to determine more about the structure of **4.4**.

The molecular formula of **4.4** was determined to be $C_{25}H_{43}N_3O_8$ (six unsaturations) on the basis of HRESITOFMS data. This formula would correspond to a cyclic pentadepsipeptide with both ester and amide linkages, rather than a peptide composed of only amide linkages. There are only two pentadepsipeptide natural products comprised of two hydroxy acid (α-HA) units and three amino acid units described in the literature, both of which are from fungal sources,[106,107] and neither has the same elemental composition as **4.4**.

HRESITOFMSMS analysis was performed on the sample using the pseudomolecular ion at *m/z* 514.3132 $[M+H]^+$ as the parent. The resulting data allowed the sequence of the amino acids to be determined and revealed which units were α-HA units. Based on the fragmentation pattern and the original ^{1}H NMR spectrum recorded in

$CDCl_3$, both of the α-HA units were determined to be 2–hydroxy–3–methylpentanoic acid units, also known as isoleucic acid (Ila). While other supporting fragmentation patterns were observed, the most diagnostic pattern started at the parent ion. The first loss was that of the Thr unit (101.0489), resulting in an *m/z* 413.2647 fragment. The Ala unit (71.0367) was lost next and the remaining fragment (*m/z* 342.2280) then further fragmented into a unit with *m/z* 228.1597, which corresponds to a loss of Ila. The remaining ion (*m/z* 228.1597) corresponds to $[Ile + Ila + H]^+$. These data suggested that the order of the units in depsipeptide **4.4** is Thr – Ala – Ila – Ile – Ila, although the directionality of the sequence was uncertain.

At this point, half of the limited sample available (~.4 mg) was hydrolyzed through acid hydrolysis and partitioned between resulting the aqueous acid solution and CH_2Cl_2 to separate the amino acids from the α–hydroxy amino acids. The aqueous partition containing the amino acids was evaporated and then treated with (+)–*S*–2–butanolic HCl, followed by trifluoroacetic anhydride in dichloromethane to form their respective *N*–TFA–*S*–2–butyl esters, which were subsequently compared to similarly derivatized amino acid standards by GCMS. This process enabled assignment of the amino acids present in the hydrolyzate as L–Ala, L–Thr, and L–Ile.

The CH_2Cl_2 partition was evaporated to dryness, dissolved in $CDCl_3$ and analyzed by ^1H NMR. Literature data indicates that the methyl triplet of the *allo*–type Ila isomers appears downfield of the methyl doublet, whereas in the "normal" Ila diastereomeric form, the locations of the two methyls are reversed.[108] The NMR data for the CH_2Cl_2 fraction revealed that both Ila units present in the mixture are *allo*–type. However, an absolute stereochemical assignment could not be made with the material available, as the amount obtained was insufficient to provide valid $[\alpha]_D$ measurements.

At this stage, HSQC and HMBC data were acquired with the remaining sample of **4.4** in acetone–d_6, because this solvent provided the best resolution of signals, even though the doubling was still evident. These data were needed in order to fully determine

the sequence of the five units and to provide position assignments for the NMR signals. Unfortunately, the 2D NMR data obtained were not well enough resolved to provide either. The structure proposed for **4.4** is instead based on a combination of the HRESITOFMSMS data discussed above, together with the literature precedent roseotoxin S (**4.6**), a similar compound previously reported from *Trichothecium roseum*.[106] Roseotoxin S is one of the two natural product pentadepsipeptides described previously in the literature, and its structure differs from that proposed for **4.4** by inclusion of two hydroxyisovaleric acid (Hiv) units instead of two Ila units. Neither the relative nor the absolute configuration of **4.6** was provided in the original report.

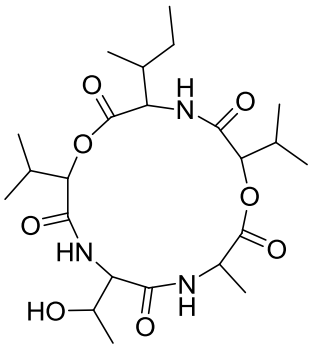

4.6

The ^{1}H NMR data for compound **4.5** also had many overlapping signals when collected using $CDCl_3$, however the signal–to–noise ratio was much worse than that obtained for **4.4** due to the even smaller sample size, and therefore, additional NMR studies were not attempted. HRESITOFMS data revealed a molecular formula of $C_{24}H_{41}N_3O_8$ (six unsaturations), which differs from that of **4.4** by having one less carbon and two fewer hydrogens. It was initially thought that one of the Ila units was simply replaced by a Hiv unit, especially when considering the literature precedent of **4.6**. HRESITOFMSMS data supported this hypothesis, leading to the proposal of structure **4.5** for this metabolite. Briefly, instead of observing fragmentation for a depsipeptide corresponding to Thr – Ala – Ila – Ile – Ila, the data for **4.5** suggested the sequence Thr –

Ala – Hiv – Ile – Ila. It is assumed that the configurations of the amino acids present are analogous to those found in **4.4.**

In summary, investigation of a fungicolous isolate of *Trichothecium crotocinigenum* afforded two known metabolites, 3-deoxotrichothecin (**4.2**) and guangomide A (**4.3**), and a new diketopiperazine (**4.1**) that represents a new tricyclic ring system, and is the first natural diketopiperazine reported to contain a 1-aminocyclopropane-1-carboxylic acid (Acc) unit. While the known compound **4.2** was responsible for the observed activity, literature describing a related, synthetic Acc–containing diketopiperazine suggests that **4.1** may have other interesting bioactivities, but relevant assays were not available for the present study.[103] The structures of new compounds **4.4** and **4.5** were also determined, but because of NMR signal doubling, possible degradation, and small sample sizes, complete assignments could not be made with confidence. It is clear, however, that these two pentadepsipeptides are closely related to the known compound roseotoxin S (**4.6**), and bring the total number of known naturally occurring pentadepsipeptides up to four. Scale–up fermentation was carried out in an effort to obtain additional quantities of **4.4** and **4.5**, but further pure samples could not be obtained despite exhaustive isolation attempts. Each scale–up fermentation extract contained fractions with the characteristic signals for peptide/depsipeptide–type compounds, but the fractions contained so many compounds in such small quantities that efforts to isolate pure samples proved unsuccessful. Ultimately, this result does suggest that there may well be a great deal of additional new chemistry left to be identified from this isolate of *Trichothecium crotocinigenum*, given proper adjustment of culture conditions.

CHAPTER 5

PHOTODEGRADATION AND REGENERATION OF 17A– AND 17B– TRENBOLONE

In 2012, it was estimated that approximately 97% of beef cattle in the U.S. receive hormone supplements.[109] Trenbolone acetate (TbA, **5.1**) is one of six hormonally active licensed growth promoters used in the United States to improve muscle mass and accelerate livestock weight gain.[110,111] TbA is eight to ten times more potent than testosterone in this regard, and is implanted into the animals subcutaneously.[110] Although many studies have explored TbA's safety, for both the animals and meat consumers, little is known about the fate of TbA or its metabolites after excretion by cattle.[110] So far, public concern has mainly focused on the synthetic estrogen and progestin components of oral contraceptives because of their high physiological activity at low doses and their stability in aqueous media.[110] However, the similarity in structure and the potent activity of TbA would seem to warrant similar consideration.

There are three metabolites excreted by TbA–treated livestock; trendione (**5.2**), 17α–trenbolone (**5.4**), and 17β–trenbolone (**5.3**) (Figure 5.1). While 17α–trenbolone is the major metabolite excreted, 17β–trenbolone is by far the more potent endocrine–disrupting metabolite.[109,110,112] When exposed to 50 ng/L of 17β– trenbolone, 100% of the population of zebrafish became phenotypically male, and in populations of flathead minnows effects were seen with concentrations between 10–30 ng/L.[113,114] This concentration is well within the range of concentrations reported in surface waters near animal agriculture operations.[109] In 2001, the stability of 17α– and 17β–trenbolone in liquid manure was tested. The compounds were found to be quite stable with half–lives of 276 and 257 days, respectively.[110] However, in 2008, another study showed that in

non–sterile soil samples only 3–5% of 17α– and 17β–trenbolone remained after 3 days, whereas no significant loss was observed in sterile soil samples, suggesting that the degradation was likely caused by microbes present in the soil.[115] More recent studies suggest that factors other than microbes affect the fate of the excreted metabolites. Specifically, based on a manufacturer's assessment report, photolysis was considered to be an important possible pathway for degradation of the excreted metabolites in the environment.[109] The results of photolysis experiments revealed that 17α– and 17β–trenbolone undergo transformation upon exposure to light, but the phototransformation products could not be identified at the time.

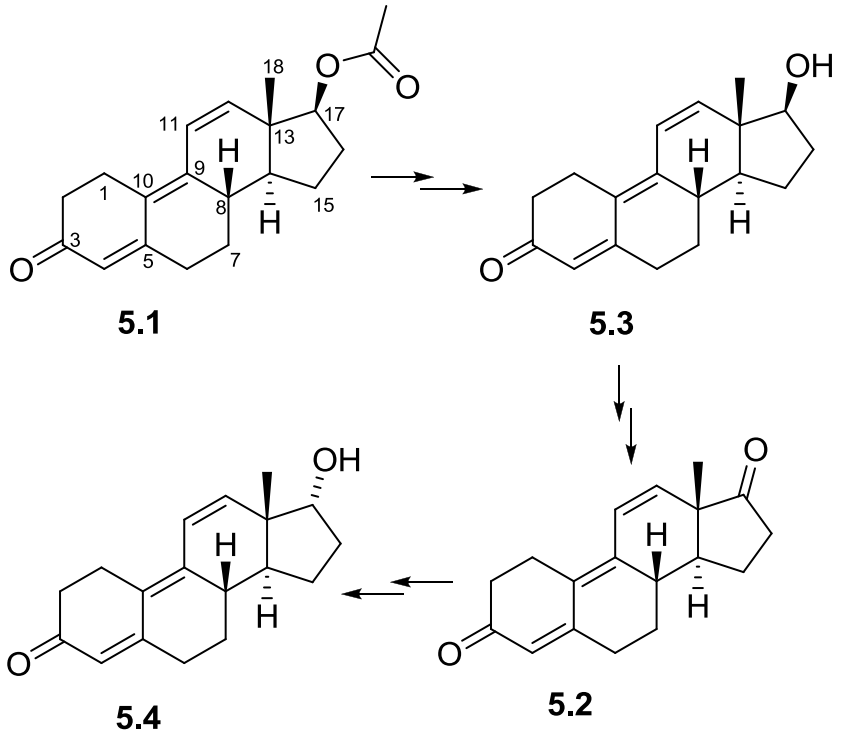

Figure 5.1. Trenbolone Acetate (**5.1**) and its Excreted Metabolites

Given the potency and commercial availability of 17β–trenbolone (**5.3**), it was the first metabolite to be extensively studied to determine the structures of its degradation products. A sample of **5.3** was photolyzed (~10 mg) and subsequently separated into eight fractions by reverse–phase HPLC. Collection of individual peaks afforded four fractions which were found to be pure decomposition products eventually identified as **5.5** (0.7 mg), **5.6** (1.0 mg), **5.7** (2.2 mg), and **5.8** (1.1 mg), through efforts described in detail below, while another fraction consisted of unreacted starting material (**5.3**; 2.1 mg).

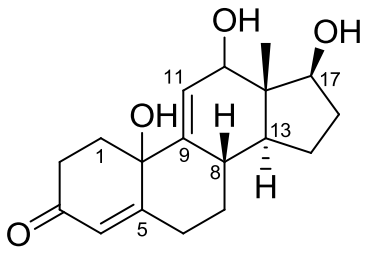

5.5

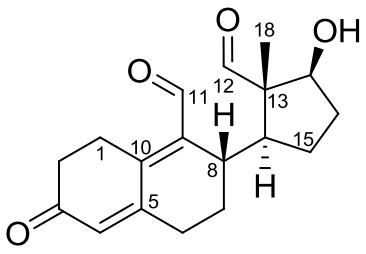

5.6

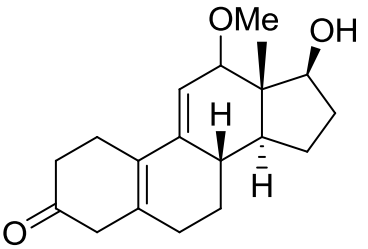

5.8

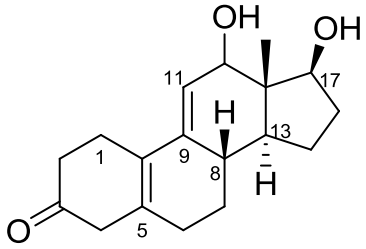

5.7

NMR signal assignments (Table 5.1) were established for a standard of 17β–trenbolone (**5.3**) in order to aid in recognition of changes in the decomposition products encountered. Such assignments had not been previously reported for **5.3** in the literature. Key HMBC and COSY correlations employed in establishing the NMR signal assignments for **5.3** are summarized in Figure 5.2. The ^{1}H NMR signals for the olefinic protons of the A and C rings at δ_H 5.75 (H–4), δ_H 6.49 (H–11), and δ_H 6.54 (H–12)

resolved well and were particularly useful in recognizing structural differences and changes among the decomposition products. The methyl shifts for H_3–18 and those of the oxygenated CHs also proved to be diagnostic when comparing the decomposition products to each other and to 17β–trenbolone.

Table 5.1. NMR Data for 17β–Trenbolone (**5.3**) in CD_3OD

Position	δ_H[a] (mult., J_{HH})	δ_C[b]	HMBC[c] (H→C#)
1	2.80 (ddt, 1.7, 7.2, 17) 2.88 (ddt, 1.7, 7.2, 17)	25.0	2, 3, 5, 9, 10
2	2.43 (t, 7.2)	37.0	1, 3, 4, 10
3		202.0	
4	5.75 (s)	123.2	2, 6, 10
5		160.1	
6	2.61 (m)	32.3	4, 5, 7, 10[e]
7	1.28 (dq, 5.7, 12) 1.93 (dq, 4, 12)	27.8	5, 6, 8, 9
8	2.47 (m)	38.9	6, 9, 10, 15
9		144.4	
10		127.8	
11	6.54 (d, 9.9)	124.2	8,[e] 9, 10, 12, 13
12	6.49 (d, 9.9)	144.2	5,[de] 9, 13, 14, 17, 18
13		46.6	
14	1.46 (m)	48.8	8, 13, 15, 16, 17, 18[e]
15	1.45 (m) 1.70 (m)	23.6	8,[e] 13, 14, 17, 18[de]
16	1.56 (m) 2.09 (m)	30.0	14, 15 13, 14, 17
17	3.81 (dd, 9.0, 8.0)	77.8	12, 13, 15,[e] 16, 18
18	0.90 (s)	13.7	12, 13, 14, 17

Note: [a]500 MHz. [b]150 MHz. [c]600 MHz. [d]Four– or five–bond coupling. [e]Weak correlation.

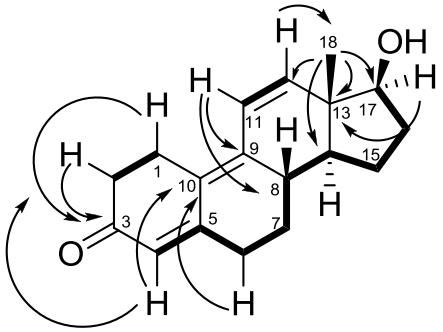

Figure 5.2. Key HMBC (arrows) and COSY (boldface) Correlations for **5.3**

One decomposition product (**5.5**) was identified as a dihydroxylated product by analysis of ^{1}H NMR, HSQC, HMBC, and COSY data (Table 5.2), with key HMBC and COSY correlations shown in Figure 5.3. The addition of two hydroxy groups created two new stereocenters, but the configurations at these centers were not determined. Key features in the ^{1}H NMR spectrum of **5.5** include retention of the olefinic CH alpha to the ketone at δ5.78 (H–4), the appearance of a new sp^{3} oxygenated CH signal as a doublet at δ3.84 (H–12), the absence of the signals for the CH=CH unit in the C–ring of the starting material, and the presence of a different C=CH signal at δ_H 6.02 that was coupled to the new sp^{3} oxygenated CH signal. The methyl singlet (H_3–18) showed an HMBC correlation to the new oxygenated CH (δ_H 3.84, δ_C 69.6; C–12), whose proton, in turn, showed correlations to both olefinic carbons (C–9 and C–11). The C=CH signal at δ_H 6.02 (H–11) showed HMBC correlations to C–8, C–10, and C–13. These results located the oxygenation in the C–ring. The location of the second hydroxy group was determined based on the shift of quaternary sp^{3} carbon C–10 (δ_C 70.8) and HMBC correlations from both H–4 and H–11 to that carbon. These data enabled assignment of the gross structure of **5.5** as shown. This degradation product was found to be stable in methanol at room temperature.

Table 5.2. NMR Data for **5.5** in CD_3OD

Position	δ_H[a] (mult., J_{HH})	δ_C[b]	HMBC[c] (H→C#)
1	2.26 (ddd, 4.0, 8.7, 14) 2.42 (ddd 4.4, 8.7, 14)	33.4	2, 3, 5, 9, 10 2, 3, 5, 10
2	2.47 (ddd, 4.4, 8.7, 13) 2.58 (ddd, 4.0, 8.7, 13)	35.2	3, 10 1, 3, 10
3		201.3	
4	5.78 (d, 1.4)	124.7	2, 6, 10
5		168.2	
6	2.31 (ddd, 3.1, 3.6, 13) 2.87 (m)	31.9	5 4, 5, 7
7 ax 7 eq	1.12 (dq, 3.9, 13) 2.11 (m)	33.4	
8	2.40 (m)	38.2	
9		146.3	
10		70.8	
11	6.02 (dd; 5.7, 2.0)	123.7	8, 10, 13
12	3.84 (d, 5.7)	69.6	9, 11, 14, 18
13		46.3	
14	1.49 (ddd, 7.3, 10, 11)	42	8, 18
15	1.40 (dq, 5.1, 12) 1.80 (m)	24.4	8, 14 14
16	1.58 (m) 2.03 (dddd, 4.0, 5.1, 9.2, 13)	30.0	 13, 17
17	4.26 (t, 9.0)	73.6	13, 18
18	0.75 (s)	10.4	12, 13, 14, 17

Note: [a]500 MHz. [b]150 MHz. [c]600 MHz

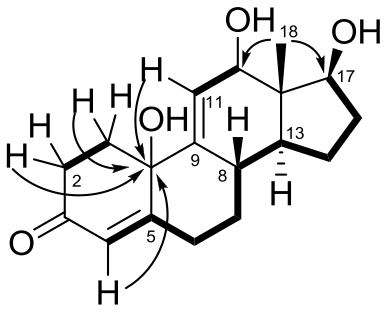

Figure 5.3. Key HMBC (arrows) and COSY (boldface) Correlations for **5.5**

A second decomposition product (**5.6**) was similarly identified by analysis of ^{1}H NMR, HSQC, HMBC, and COSY data (Table 5.4) and determined to be a dialdehyde analogue. Key features include the loss of both signals for the CH=CH unit in the C–ring of 17β–trenbolone and the appearance of two new aldehyde singlets at δ_H 9.13 and 9.99. The locations of the new aldehyde units were assigned by analysis of HMBC correlations (Figure 5.4). The aldehyde signal at δ_H 9.13 (H–12) showed correlations to C–13 and C–18, while the C–12 aldehyde carbon signal correlated with the nearby methyl signal (H_3–18). The second aldehyde signal (δ_H 9.99; H–11) correlated to C–8 and C–9.

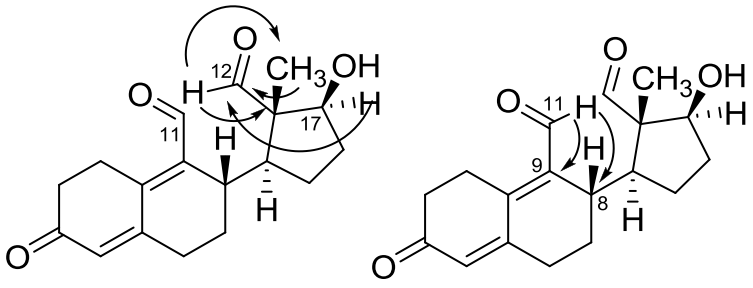

Figure 5.4. Key HMBC Correlations Useful in Locating the Two Aldehyde Units in **5.6**.

Table 5.3. NMR Data for **5.6** in CD_3OD

Position	δ_H[a] (mult., J_{HH})	δ_C[b]	HMBC[c] (H→C#)
1	2.70 (ddd, 6.2, 13, 15) 3.61 (ddd; 3.4, 4.8, 15)	25.1	3, 5, 10
2	2.45 (dq, 0.7, 8) 2.59 (m)	37.3	1, 3, 4 10
3		200.1	
4	6.08 (br s)	130	10
5		156.1	
6	2.60 (m) 2.90 (dddd, 2.0, 5.8, 14, 20)	25.5	
7	1.44 (ddt, 4.0, 6.4, 14) 1.90 (m)	24.4	6, 14
8	3.00 (dt, 4.0, 11)	31.7	6, 9
9		144.7	
10		147.8	
11	9.99 (s)	190.8	8, 9
12	9.13 (s)	207.7	13, 18
13		60.2	
14	2.15 (m)	46.7	16
15	1.61 (m) 1.94 (m)	26.5	16 13
16	1.60 (m) 2.11 (m)	30.0	13, 17
17	4.21 (t, 8.5)	76.6	12, 16
18	1.01 (s)	6	12, 13, 14, 17

Note: [a]500 MHz. [b]150 MHz. [c]600 MHz

This compound degraded further over time to form another product containing only one aldehyde unit (the C–12 aldehyde group remained intact), but the process did not proceed to completion and other minor products were also formed. Therefore, this secondary degradation product was not identified. A compound similar to **5.6** (compound **5.9**) has been reported in the literature as a synthetic oxidation product derived from a synthetically modified trenbolone analogue, **5.9**.[116]

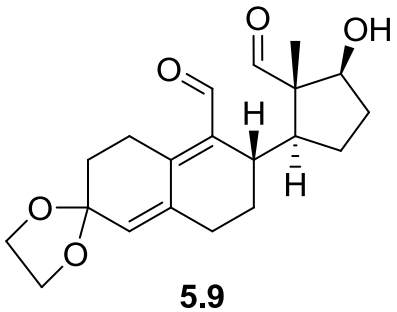

5.9

A third decomposition product (**5.7**) was the major product based on HPLC peak intensity and the amount obtained. This product was identified as a monohydroxylated product (**5.7**) by analysis of ^{1}H NMR, HSQC, HMBC, and COSY data (Table 5.4). Evidence for a change in oxidation of the C–ring was observed in the ^{1}H NMR spectrum of this product, as was the case for **5.5**, but the A–ring olefin CH signal was also absent. The ^{13}C NMR spectrum indicated that the molecule contained only two oxygenated carbons (δ_C 70.3 and δ_C 73.9) ruling out a dihydroxylation analogous to **5.5**. The signal at δ_C 73.9 was determined to correspond to C–17 based on HMBC correlations from H_3–18 and H_2–16; analogous to those observed for 17β–trenbolone itself. The location of hydroxylation at C–12 (δ_C 70.3) was established by HMBC correlations from the corresponding CH proton signal (δ_H 3.89) to carbons 9, 11, 13, 14, and 18, which were analogous to those observed for **5.5**. The shift positions for the non–protonated olefinic carbons C–5, C–9, and C–10 were determined by analysis of HMBC correlations. C–5 was located by correlations from H_2–1, H_2–6, and H_2–7, while C–9 was located based on its correlations to H_2–7 and H–8. The remaining non–protonated olefinic carbon, C–10, was assigned based on its correlations with H_2–1, H_2–2, H_2–6, and H–11. ^{1}H NMR analysis over time revealed that **5.7** gradually degraded to form dialdehyde **5.6**, among other products, upon storage in methanol at room temperature.

Compound **5.8** is a methoxy analogue of **5.7**, and was identified by ^{1}H NMR analysis in comparison with the data for **5.7** (Table 5.4). Minor shifts were seen in a few

of the proton signals, but overall, signal locations and splitting patterns matched those observed in the ^{1}H NMR spectrum of **5.7**. The most notable difference was addition of a three–proton singlet at δ_H 3.47 for the methoxy group. This compound is also unstable in methanol at room temperature, and degrades into multiple products, but there was no indication of aldehyde formation in this instance.

Table 5.4. NMR Data for **5.7** and **5.8** in CD_3OD

	5.7			**5.8**
Position	δ_H[a] (mult., J_{HH})	δ_C[b]	HMBC[c] (H→C#)	δ_H[a] (mult., J_{HH})
1	2.52 (m) 2.75 (m)	26.5	2, 3, 5, 10 3, 5, 10	2.53 (m) 2.77 (m)
2	2.51 (m)	39.3	1, 10	2.53 (m)
3		209.3		
4	2.91 (m)	45.3		2.91 (m)
5		133.8		
6	2.01 (m) 2.27 (m)	31.3	5, 7, 8, 10	2.03 (m) 2.27 (m)
7	1.27 (dq, 5.1, 12) 1.91 (m)	28	6, 8, 9, 14 5, 9	1.24 (dq, 5.3, 12) 1.90 (m)
8	1.94 (m)	39.5	9	1.95 (m)
9		140.5		
10		128.3		
11	5.77 (d, 5.3)	121	8, 10, 12, 13	5.88 (d, 5.4)
12	3.89 (d, 5.3)	70.3	9, 11, 13, 14, 18	3.51 (d, 5.4)
12-OMe				3.47 (s)
13		46.4		
14	1.56 (m)	41.3	8, 12, 13, 18	1.57 (m)
15	1.41 (dq, 5.2, 12) 1.79 (dddd, 4.2, 8.2, 9.6, 12)	24.2	8, 13, 14, 16	1.39 (dq, 5.3, 12) 1.79 (dddd, 4.1, 8.2, 9.6, 12)
16	1.55 (m) 2.02 (m)	29.9	13, 14, 17	1.56 (m) 2.04 (m)
17	4.30 (t, 9.0)	73.9	16	4.27 (t, 9.2)
18	0.71 (s)	10.9	12, 13, 14, 17	0.73 (s)

Note: [a]500 MHz. [b]150 MHz. [c]600 MHz.

Concurrent LC–MS experiments supported the conclusion that **5.7** was the major photodegradation product observed. Another interesting result of the LC–MS experiments was the observation that a small amount of **5.3** reappeared over time when the photodegradation product mixture was stored in the dark. In an attempt to corroborate this result by NMR, an in situ NMR experiment with a saturated D_2O solution of **5.3** was performed with multiple time points: before photolysis, immediately after photolysis, three days later, and eight days later. While the D_2O solution used was saturated with 17β–trenbolone, this only corresponds to approximately 0.25–0.28 mg according to water–solubility data reported in an environmental assessment published in 1988.[117] Due to the limited amount of sample present due to this poor solubility, and the resulting large solvent peak, the NMR data were collected using a presaturation technique. Even though the solubility of both 17α– and 17β–trenbolone is much higher in other solvents, D_2O was used in an effort to keep the results of study as environmentally relevant as possible while still NMR–compatible. During the eight–day span of the experiment, the sample was kept in the NMR tube at room temperature in the dark when not being analyzed.

NMR comparison of the product mixture immediately after photolysis to a standard of **5.3** indicated that the two major products were **5.7** (most prominent) and a new degradation product in which the C–ring double bond remained intact during photolysis. ^{1}H NMR signals for the new "C–ring" product included two doublets at δ_H 6.30 and 6.51. The diagnostic olefinic proton doublets for 17β–trenbolone (in D_2O) are at δ_H 6.55 and δ_H 6.63. After three days at room temperature in the dark, the signals for **5.7** were no longer detectable and signals for other trace components emerged. The signals for the as–yet unidentified "C–ring" decomposition product indicated that it was still a major component, while signals for the parent compound, 17β–trenbolone, were not detectable. After eight days at room temperature in the dark, NMR analysis of the sample did not exhibit any of the diagnostic spectroscopic features of the starting material or the previously encountered photoproducts, which was not indicative of the

regeneration of 17β–trenbolone as had been observed in LC–MS experiments. However, the LC–MS data did indicate that the percentage of starting material regeneration was minimal.

At this point, we undertook an exploration of the similarity between the degradation of 17α–trenbolone (**5.4**) with the results for 17β–trenbolone (**5.3**). Again, complete NMR assignments for **5.4** were not available in the literature, so the corresponding data were collected and assigned using a standard of **5.4** (Table 5.5). The most notable difference between the ^{1}H NMR data for 17α–trenbolone and 17β–trenbolone was the appearance of the oxygenated methine signal (H–17) which occurs as a doublet in **5.4** and a triplet in **5.3** due to the difference in vicinal *J*–values ($J_{H16–H17}$) in the two isomers. Other key differences include the shifts of the C–ring olefinic protons and the methyl group.

Another NMR tube experiment similar to the one described above for **5.3** was performed with a saturated D_2O solution of **5.4**. Unfortunately, the solubility of **5.4** in water is reportedly about ten times lower than that of **5.3**, meaning that only 0.03–0.0315 mg of 17α–trenbolone would be expected in the sample.[117] Comparison of the standard spectrum with data collected immediately after photolysis showed a virtually complete conversion of **5.4** to a single decomposition product. Key changes included shift of the two olefinic proton doublets (H–11 and H–12) from δ_H 6.54 and δ_H 6.66 to δ_H 6.26 and δ_H 6.55, as well as the absence of the H–4 olefinic proton singlet at δ_H 5.68 in the decomposition product. The methyl group also shifted slightly from δ_H 0.83 to δ_H 0.80. After storage at room temperature in the dark for five days, there was a reemergence of the doublets corresponding to 17α–trenbolone (δ_H 6.54 and δ_H 6.66). However, the 17α–trenbolone olefinic singlet at δ_H 5.68 for H–4 did not reappear. This 17α–trenbolone–like product (**5.4'**) was still minor relative to the as–yet unidentified decomposition product.

Table 5.5. NMR Data for 17α–Trenbolone (**5.4**) in CD_3OD

Position	δ_H[a] (mult., J_{HH})	δ_C[b]	HMBC[c] (H→C#)
1	2.82 (ddt, 1.0, 7.8, 16) 2.89 (ddt, 1.0, 7.0, 16)	24.8	2, 3, 5, 9, 10
2	2.44 (t, 7.3)	37.1	1, 3, 4, 9,[de] 10
3		201.7	
4	5.76 (s)	123.1	2, 6, 10
5		159.8	
6	2.64 (m)	32.2	4, 5, 7, 8, 10
7	1.39 (dq, 5.7, 12) 1.98 (m)	28.6	5, 6, 8, 9 5, 9, 14
8	2.46 (m)	38.7	7,[e] 9,[e] 14
9		144.3	
10		127.2	
11	6.59 (d, 10)	125.1	8, 9, 10, 12, 13, 18[d]
12	6.48 (d, 10)	143.8	5,[de] 8,[d] 9, 11, 13, 14, 17, 18
13		49.0	
14	1.95 (m)	47.2	7, 8, 13, 15, 17, 18
5	1.37 (dq, 7.2, 12) 1.84 (dq, 2.1, 9.1)	24.2	13, 14, 16, 17, 18[e] 14, 16
16	1.58 (ddd, 7.2, 9.1, 15) 2.23 (m)	32.9	13, 14, 17 13,[e] 14
17	3.89 (d, 6.0)	78.5	14, 15, 16, 18
18	0.82 (s)	18.5	12, 13, 14, 17

Note: [a]500 MHz. [b]150 MHz. [c]600 MHz. [d]Four–bond. [e]Weak correlation.

Since a photodegradation product analogous to the one obtained in these experiments was not encountered in the original 17β–trenbolone experiment, a series of H_2O and D_2O experiments were performed to compare to the NMR tube experiment results, and to help identify the structure of this potentially environmentally relevant degradation product. Samples of **5.4** were dissolved in either H_2O or D_2O, then photolyzed, and the resulting solution was extracted with dichloromethane. The extraction was done in order to minimize any possible continuing reactions during

processing. Both resulting layers were analyzed. The dichloromethane extract of the photolyzed H_2O–dissolved sample of **5.4** contained three major components: the unidentified degradation product, a monohydroxy compound analogous to **5.7**, and starting material in a 1:1.2:1.6 ratio. The sample also contained trace amounts of a dialdehyde decomposition product, as well as other decomposition products. The sample photoreacted in D_2O contained two major compounds--the unidentified degradation product and starting material in a 6:1 ratio, as well as a plethora of trace compounds, including the **5.7** analogue.

Given that the new decomposition product was formed in aqueous solutions and was therefore of potential environmental relevance, 2D NMR experiments necessary to identify this product were undertaken using the D_2O–reacted, dichloromethane–extracted sample. COSY, HSQC, and HMBC data confirmed that the C– and D– rings and the olefin unit in the B–ring were still intact (Figure 5.4), leading to the conclusion that any difference between **5.4** and the new decomposition product must be associated with the A–ring. Unfortunately, the poor signal–to–noise ratio of the data due to very low water solubility, the lack of resolution of the peaks, and the impurity of the sample precluded complete structure assignment on the basis of these data alone.

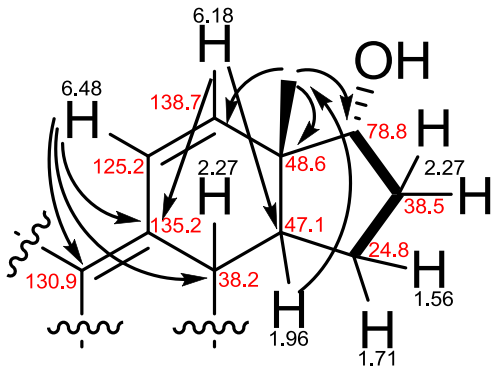

Figure 5.5. Summary of NMR Shift Data and HSQC, HMBC (arrows), and COSY (boldface) Correlations for the as-yet Unidentified Decomposition Product (δ_H in black; δ_C in red)

Another sample of a saturated solution of **5.4** in D_2O was prepared in an NMR tube in an effort to replicate the conditions in which there was complete conversion to the as–yet unidentified decomposition product. This sample was dried and then re–dissolved in CD_3OD in order to foster direct comparison with data from other NMR experiments. The product obtained consisted almost solely of the target degradation product with other trace compounds. However, the signal–to–noise ratio of the ^1H NMR data was clearly not conducive to likely successful 2D data collection. Instead, a small amount was subsampled for HRESITOFMS analysis. The resulting data indicated the presence of a compound with the formula $C_{18}H_{22}D_2O_3$ (*m/*z 313.1755 $[M+Na]^+$ calcd. 313.1747) which indicated that a molecule of D_2O had been added across one of the double bonds. Since the only olefin available, as indicated by the 2D NMR data, was the one in the A–ring, gross structure **5.10** was proposed for the degradation product and its proposed conversion mechanism can be seen in Figure 5.7.

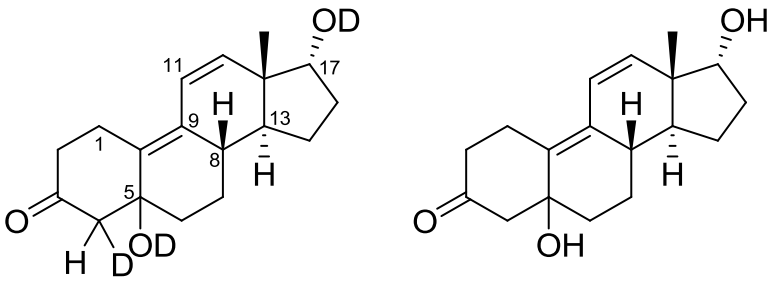

Figure 5.6. Structure of **5.10** Obtained Upon Reaction of **5.4** in D_2O (left) and H_2O (right).

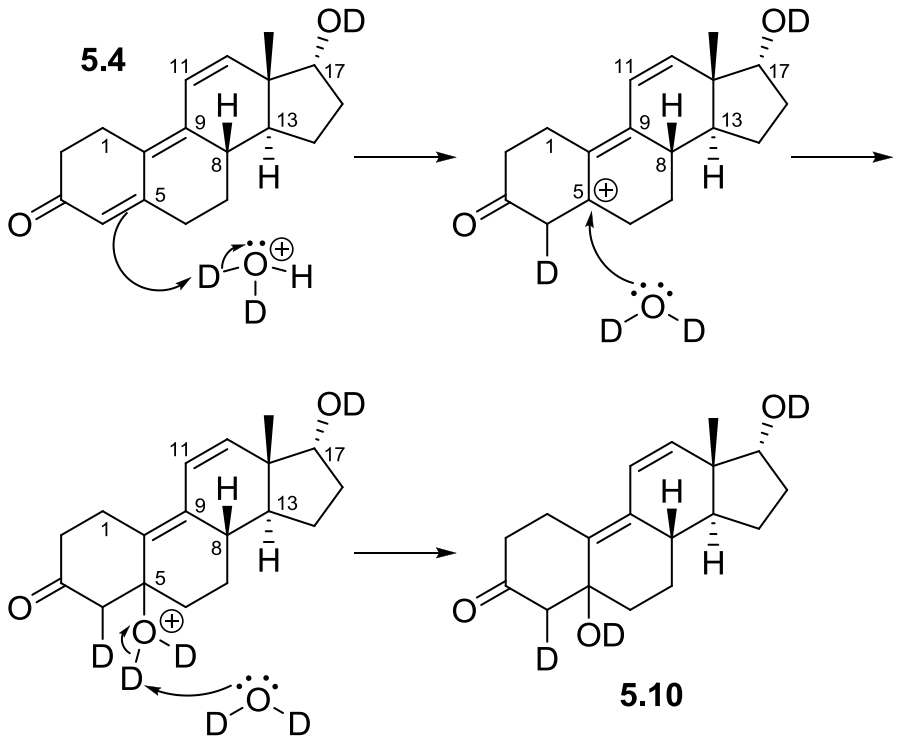

Figure 5.7. Proposed Mechanism for the Conversion of **5.4** to **5.10** in D_2O

As part of an effort to confirm the hypothesis that **5.10** reverts to the starting material **5.4**, the sample was dried and re–dissolved in D_2O and allowed to sit in the dark. The sample was monitored by NMR every few days. After 13 days, the amount of a

17α–trenbolone–like compound (**5.4'**), which lacks the A–ring olefinic ^{1}H NMR signal, exceeded the amount of **5.10**. HRESITOFMS analysis was performed on a subsample of this material. The data suggested that this product has a molecular formula of $C_{18}H_{21}DO_2$ (*m/*z 294.1609 $[M+Na]^+$ calcd. 294.1579). This result, coupled with the NMR data (absence of the singlet at δ_H 5.68) led to the conclusion that **5.4'** is 17α–trenbolone with a deuterium atom incorporated at the 4–position. Such a product would be expected upon the loss of HDO from **5.10** (Figure 5.8). This also supports the conclusion that the location of the oxygenation when D_2O was added across the A–ring olefin was the 5–position.

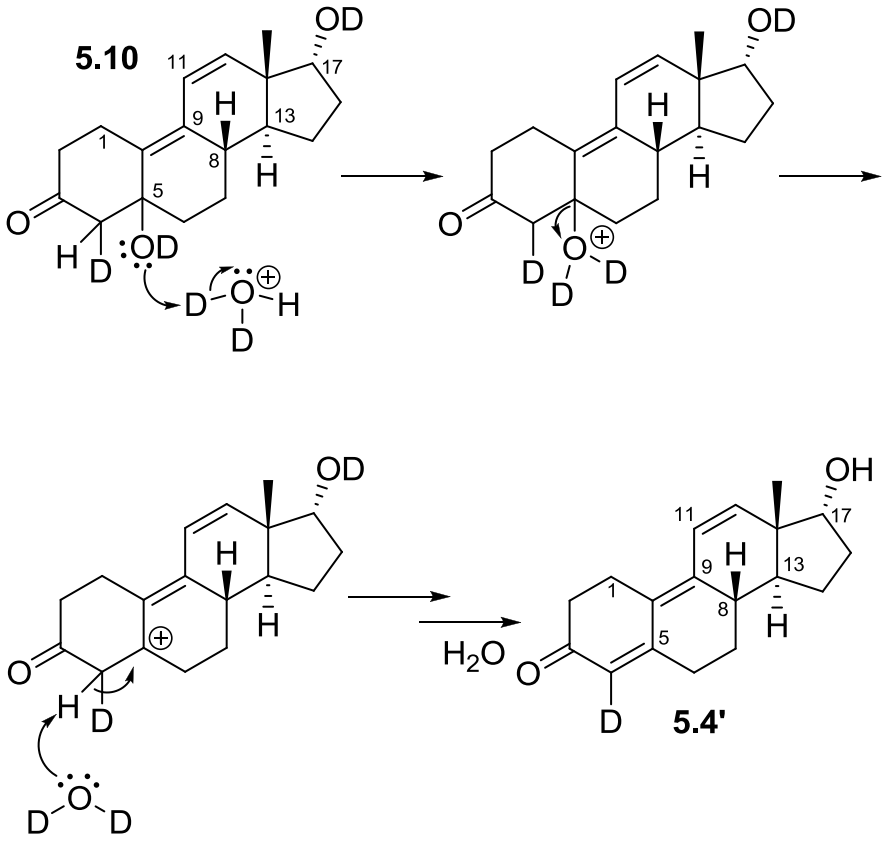

Figure 5.8. Proposed Mechanism for the Reversion of **5.10** to Deuterated 17α–Trenbolone (**5.4'**)

The conversion of **5.10** to **5.4** was also verified by a change in the UV maxima of the two compounds. The λ_{max} of 17α–trenbolone (**5.4**) was determined experimentally to be 347 nm. Estimation through use of the Woodward-Fieser-Scott rules predicted a maximum of 356 nm.[118, 119] The experimental UV spectrum of **5.10** showed a λ_{max} of 246 nm, whereas the predicted maximum was 244. Thus, the difference observed in the UV spectra of **5.4** and **5.10** is fully consistent with the disruption of the extended conjugated system in **5.10** relative to **5.4**.

This project allowed for the identification of the major photodegradation products of the two major excreted metabolites of the widely used growth promoter trenbolone acetate.[120,121] Comparison of the degradation products of 17α– and 17β– trenbolone showed that some analogous products were formed as photoproducts. Each metabolite produced a **5.7** and a **5.10** analogue, each of which retain a steroidal backbone. The effects, potency, and possible environmental impact of these photodegradation products are unknown, and warrant further investigation. However, **5.4** appeared to have a much greater tendency to form the 5-hydroxy analogue (**5.10**), which is now known to at least partially revert back to the starting material over time in the dark. This implies that even though these potent metabolites degrade in the presence of light, they can also regenerate to some degree at night. This is also significant in that it suggests that the environmental persistence of such compounds may be greater than previously thought. Efforts to detect and quantitate such compounds in the field (e.g., in ground waters on and near cattle farms that use TbA) would be important steps in evaluating the true significance of these findings. Other compounds with a steroidal ring system that incorporates a trieneone moiety should perhaps be studied for this phenomenon as well. A SciFinder search yielded 135 compounds that fit this structural classification that are being studied for their biological uses.

CHAPTER 6

SUMMARY AND CONCLUSIONS

This compilation of work involved structural studies of two very different types of samples which were analyzed with very different objectives. One project was directed toward isolation and identification of bioactive secondary metabolites produced by a number of different fungal isolates. The second project involved exploration of the degradation products of the excreted metabolites of trenbolone acetate (TbA), a steroid commonly used to promote growth in beef cattle. While the analytes and objectives studied were very different, the approaches and techniques in both types of work were similar.

The chemical investigation of 15 fungal isolates, eight endophytic fungi and seven from fungicolous/mycoparasitic ecological groups, resulted in the isolation and/or identification of over 30 compounds. Seven of these were determined to be new secondary metabolites, all of which were isolated from fungicolous/mycoparasitic fungi. The majority of the fungicolous/mycoparasitic fungal isolates were collected on the main island of Hawaii. Our lab has previously discovered a variety of new secondary metabolites in other extracts from isolates encountered in this region, which have proven to be a very fruitful source of new natural products chemistry. The endophytic isolates were collected from wheat and corn crops in Illinois, or from Arizona rye crops. While these were often chemically productive, the compounds encountered were all previously known. The vast differences in the locations and the sources of fungal collection and the variety of fungal species studied is reflected in the diversity of compounds encountered. In the majority of the isolates chemically investigated, compounds responsible for the bioactivity observed for the corresponding fermentation extracts were encountered. Unfortunately, in most cases, they were compounds already described in the literature.

Several of the new compounds were simple analogues of known compounds, however, the diketopiperazine cyclo-(L-pipecolinyl-aminocyclopropane-carboxylic acid), **4.1**, represents a new ring system. The absolute configuration of **4.1** was determined by the use of Marfey's method. While **4.1** did not exhibit any activity in the assays available to our group, a synthetic Acc–containing diketopiperazine suggests that **4.1** may have other interesting bioactivities, but relevant assays were not available for the present study.[103] Compounds **4.4** and **4.5** are pentadepsipeptides, each of which contain three amino acid and two hydroxy acid units. Such compounds are rare, with only two examples previously reported from natural sources.[106,107]

Kipukasins H and I (**3.2** and **3.3)** are analogues of the kipukasin class of compounds, but they are unique in the fact that neither contains methoxy groups, a common element of kipukasins A–G.[52] Kipukasin H also contains an acetyl group at the C–5' position, a position where acylation has not been previously reported. The absolute configurations of these two new analogues were verified by comparison of their ECD spectra with that of kipukasin F. Within the same extract, 15-*epi*-oxepinamide E (**3.1**), a stereoisomer of oxepinamide E (**3.14**),[88] and brevianamide L(**3.15**),[89] was also discovered, along with **3.4**, an artifact arising from rearrangement of **3.1**. Compound **3.4** is a stereoisomer of brevianamide O (**3.16**). However, **3.16** was not reported as an artifact, but rather as a separate secondary metabolite. The assignment of the absolute configuration of **3.1**, enabled the absolute configuration of literature compound **3.15** to be assigned as well. Oxepinamide E (**3.14**) has been patented due to its ability to bind to and activate liver X receptors (LXRs), which may signal potential use in the treatment of many diseases, including diabetes, Alzheimer's, and atherosclerosis.[88] Again, relevant assays were not available for the present study of **3.1**. However, this report suggests that additional activity besides the weak antiinsectan activity observed may be present among these compounds.

The study of the photodegradation of 17α–trenbolone (**5.4**) and 17β–trenbolone (**5.3**) yielded very interesting results. While it was previously known that neither **5.3** nor **5.4** are very stable in the environment,[115] it was assumed that they posed no risk, due to their decomposition. However, prior to the work described here, there were no studies of what these potent endocrine disrupting metabolites[109,110,112] were degrading into.[120,121] It was determined in the present study that **5.3** photodegrades to four major components, **5.5–5.8**, three of which still possess the basic steroidal backbone, and may still exhibit bioactivity.[120] Fortunately, from an environmental standpoint, these compounds do continue to degrade into a plethora of further products until there are no distinct ^{1}H NMR signals observable. On the other hand, it was also determined that, while **5.4** similarly photodegrades readily into one major decomposition product (**5.10**), this product can revert back to **5.4** when stored in the dark.[121] This interesting and unprecedented finding suggests that data regarding the environmental fate of TbA may be misleading, and that its persistence may be significantly higher than previously thought. Ultimately, these results provide evidence that the use of TbA in the production of beef can have a larger environmental impact than originally presumed. The main technique in this investigation was NMR. The main reason these decomposition products were not previously identified is likely because the use of NMR analysis is not prevalent in this field, in spite of its power as a spectroscopic technique, due to the complexity of environmental samples. Coincidentally, during the course of this work, an article was published in *Environmental Science and Technology* in which some possible new applications of NMR in this field were discussed.[122] It seems likely that NMR will become more widely utilized in this area in the coming years, as these reports demonstrate that NMR techniques can be applicable in studies with environmental relevance.[120-122]

While progress was made in both areas of focus in this thesis, there are still many related aspects to be studied. For example, trendione, the other excreted metabolite of TbA, should be analyzed in an analogous fashion. There are also many other steroids

used in meat production and pharmaceuticals what would be problematic if present or persistent in the environment, and where studies similar to those described here could be warranted. Also, as mentioned in Chapter four, there are many compounds left to be identified, likely including new chemistry, from the investigated isolate of *Trichothecium crotocinigenum* given proper selection of culture conditions to enhance production of compounds that were very minor in the extracts studied here. There are, of course, many other fungal species that have not been previously investigated that may produce new chemistry as well. It is prudent to continue these types of studies because fungicolous/mycoparasitic fungi have proven to be a particularly productive group of organisms from a chemical standpoint. [50-52,55] Many new natural products are likely to be encountered through further studies of these kinds of fungi.

CHAPTER 7

EXPERIMENTAL

General Experimental Procedures

Solvents and Reagents

Reagent grade solvents were used for partitioning as well as for column chromatography, and HPLC grade solvents were used for HPLC separations employed during the course of this research. All were purchased from Fisher Scientific. Distilled water for HPLC applications was purified using a SYBRON/Barnstead NANOpure system with a pre–treatment cartridge (catalog number D0835), two ultrapure cartridges (D0809), and a 0.2–μm hollow fiber filter (D3750). Reagents and deuterated solvents were purchased either from Sigma–Aldrich Chemical Company or Fisher Scientific.

Weight Measurements

Weights of reagents, crude extracts, and fractions obtained after separation techniques were measured using a Mettler AR 160 balance.

Chromatography

Normal–phase TLC separations were performed using pre–coated plastic sheets (Alltech, 0.25–mm thickness silica gel with fluorescent indicator, 40 x 80 mm), whereas, normal phase preparative TLC separations were done using Analtech Uniplate TLC plates (20x20 cm, 250 μ).

Silica gel column chromatography was carried out using silica gel (63–200–µm particles) from SA Scientific Adsorbents. Sephadex LH–20 (Sigma) was used for performing gel filtration chromatography.

One of the following three Beckman Instruments systems was used for semi–preparative reversed–phase HPLC separations: (**1**) System Gold 127 solvent delivery module with model 166 photodiode array detector, both controlled by System Gold 32 Karat software using an IBM 300PL PC; (**2**) System Gold 127P solvent delivery module with a model 166P variable wavelength UV detector, both controlled with system Gold software (version 5.1); or (**3**) System Gold 127 solvent delivery module with a model 166 variable wavelength UV detector. The three HPLC systems employed Rheodyne model 7725 injectors. These separations were conducted using Alltech Altima C_{18} (5–µm particle size, 10.0 mm x 250 mm) or Alltech Apollo C_{18} (5–µm particle size, 10.0 mm x 250 mm) columns employing a flow rate of 2.0 mL/min unless otherwise noted. Semi–preparative HPLC chromatograms were recorded using a model 1200 Linear chart recorder, and were monitored at selected wavelengths between 210–290 nm.

Spectroscopic Instrumentation

Optical rotations were measured using a Rudolph Research Autopol III automatic polarimeter. Melting points were obtained on a Fisher–Johns micro melting point apparatus, and are uncorrected. UV spectra were recorded using a Varian Cary 100 Bio UV–visible spectrophotometer. Low–resolution EI mass spectra, including those obtained by GC–MS, were acquired at 70 eV on a Finnigan Voyager quadrupole mass spectrometer. Low–resolution ESIMS data, including LC–MSMS data, were obtained

using a ThermoFinnigan LCQ ion trap instrument unless otherwise indicated. High resolution EI and ESI mass spectra were recorded using a Micromass Autospec or QTOF Premier mass spectrometer. Tandem mass spectrometry (MS^n) data were obtained using the Q–TOF instrument. Most ^1H NMR, ^{13}C NMR, and DEPT data were recorded on Bruker AVANCE–500 or DRX–400 spectrometers (5–mm probes) at room temperature. Some ^1H NMR data were recorded on a second Bruker AVANCE–600 spectrometer using a 1.7–mm probe. Homonuclear decoupling experiments were performed on the DRX–400 instrument. All spectrometers used XWINNMR 3.1 or Topspin 1.3 software. The AVANCE–600 operated at ^1H and ^{13}C frequencies of 600.1422 and 150.9203 MHz, respectively and was equipped with a 1.7–mm triple–resonance (^1H, ^{13}C, ^{15}N) inverse microprobe. The AVANCE –500 spectrometer operated at a ^1H frequency of 500.3545 MHz and a ^{13}C frequency of 125.0886 MHz. The DRX–400 spectrometer operated at a ^1H frequency of 400.1355 MHz and a ^{13}C frequency of 100.6230 MHz, and used a 5–mm proton–carbon–fluorine–phosphorous (HCFP) probe. All NMR spectra were recorded in the deuterated equivalents of benzene, chloroform, acetone, methanol, dimethylsulfoxide, acetonitrile, or pyridine, and chemical shifts are reported in ppm downfield from tetramethylsilane (TMS), with the appropriate residual solvent peaks used as internal reference standards (δ_H/δ_C, 7.16/128.1, 7.24/77.0, 2.05/29.8, 3.31/49.0, 2.50/39.5, 1.94/118.3, and 8.74, 7.58, 7.22/150.4, 135.9, 123.9, respectively). HSQC, HMBC, and COSY experiments were conducted on the AVANCE III–600 spectrometer (1.7–mm probe). 1D NMR data were processed using the NUTS program (Acorn NMR Inc., version 5.02). 2D–data were processed using XWINNMR 3.1 on a Silicon Graphics workstation (SGI O2), TopSpin 1.3, or TopSpin 3.0. Five–mm 535–pp and 5–mm 528–

J4–7 NMR sample tubes were purchased from Wilmad Glass Company, and 1.7–mm sample tubes were purchased from Bruker.

General Procedures for NMR Experiments

DEPT Experiment

DEPT experiments were used to establish carbon multiplicities. Data were recorded on the DRX–400 spectrometer using a file size of 16 K and a suitable receiver gain (RG) for a ^{13}C NMR spectrum. The experiment gives CH and CH_3 carbon signals as positive signals, and CH_2 signals as negative signals in the spectrum. Signals for non–protonated carbon signals do not appear. The experimental parameters were set for the DRX–400 instrument (Bruker software, version 3.1) in the program DEPT135. Once the program was loaded, a suitable number of scans was entered and the experiment was started by typing zg.

Homonuclear Decoupling Experiment

Homonuclear decoupling experiments were used to determine which protons in a compound are mutually coupled and/or to help obtain $^{1}H–^{1}H$ coupling constants for individual signals. These experiments were carried out on the DRX–400 spectrometer. A ^{1}H NMR spectrum was first obtained with a suitable number of scans, and saved as a file, entering "1" in the cell labeled as EXPO. The frequencies (O2 values in Hz) of all proton signals to be irradiated were recorded. Different files were created equivalent to the number of protons to be irradiated, and saved with the numbers "2", "3", etc. in the cell labeled EXPO. The decoupling power P24 was set between 50 and 70, usually at 55,

and the frequency to be irradiated (O2 value) was then entered for each EXPO experiment. The number of scans for each experiment was equivalent to the number of scans in EXPO 1. The EXPO 2 file was recalled by typing re 2. The acquisition was started by typing multizg and entering the number of experiments into the dialog box. The resulting data were processed using NUTS software.

Homonuclear COSY Experiment

This two–dimensional NMR technique was used to identify proton spin–systems. COSY experiments were conducted using the AVANCE–600 spectrometer. The procedure began with a well–shimmed proton spectrum that was obtained after carefully tuning the probe. Suitable SW and O2 values were calculated from the proton spectrum. A proton pulse calibration was carried out using the pulse program "zg", from which the parameters P0 (90º pulse), P1 (90º pulse), and P2 (180º pulse) were determined.

For the 5–mm inverse detection probe, the following parameters were set with the COSYPH pulse program: D1 = 4, TD = 2K, NS = 16 (multiples of 16), DS = 16. DW was automatically set, IN0 = 2 x DW, ND0 = 1, parameter mode was set to 2D, SFO1 = SFO2, SW = SW2 = the desired spectrum window of the ^{1}H NMR spectrum, SW 1 = ½ (SW) = center of the desired spectrum window in Hz, SR = SR1 = SR2 = reference for the ^{1}H NMR spectrum (in Hz). With TD1 = 256, acquisition was started by typing zg.

For the 1.7–mm microprobe, the following parameters were set with the COSY pulse program: D1 = 20, NS = multiples of 8, DS = 0, DW was automatically set, IN0 = 2 x DW, ND0 = 1, parameter mode was set to 2D, SFO1 = SFO2, SW = SW2 = the desired ^{1}H NMR spectrum window, O1P = ½ (SW) = center of the desired spectrum window in

Hz. After verifying that SW in F1 was the same as SW in F2 and TD = 256 or 512 in F1, acquisition was started by typing zg. When using the AVANCE III–600 (1.7–mm probe), all parameters were preset for this experiment by the Bruker TopSpin 3.0 software pulse program.

HMQC Experiment

The HMQC experiment was used to provide one–bond proton–carbon correlations. This method relies on indirect detection of ^{13}C nuclei by observing their effect on the more sensitive ^{1}H nuclei to which they are coupled (inverse detection). HMQC experiments were conducted on the AVANCE III–600 spectrometer. The procedure began by tuning the probe followed by obtaining a well–shimmed ^{1}H NMR spectrum. Suitable SW and O2 values were calculated from the ^{1}H NMR spectrum. The proton pulse calibration was carried out using the pulse program "zg," from which the parameters P0 (90° pulse), P1 (90° pulse), and P2 (180° pulse) were determined. The following parameters were set with the pulse program "hmqcgpnd1d": D1 = 4 sec, D2[1/(2xJXH)] = 3.3 msec (if the experiment is optimized for J = 150 Hz), D13 = 3 μsec, DS = 4, NS = 16, TD = 8K. After the acquisition, the commands FT and MC were entered in order to observe signals for protons bound to ^{13}C atoms and to determine signal intensity to predict the number of scans required for the HSQC experiment. The HSQC experiment was then conducted using the pulse program "hmqcgpqf" with the following parameters: DS = 96, TD = 2K, NS = multiple of 8, RG = 16K, TD (F1 dimension) = 256 or 512, SI = 1K, SFO1 (F1 dimension) = 150.92 MHz, ND0 = 2, IN0 = 15 μsec, O2P = 80. The parameter mode was set to 2D and the acquisition was initiated

by typing zg. When using the AVANCE III–600 NMR, all parameters were preset by the Bruker TopSpin 3.0 software pulse program.

HMBC Experiment

Long–range (two– and three–bond) $^{1}H–^{13}C$ correlations were obtained from this type of experiment. The experiment was conducted on the AVANCE–600 spectrometer using a 5–mm inverse detection probe and the pulse program "hmbcgplpndqf". The parameters and procedures were nearly identical to those used for HMQC, with the exception that IN0 = 13 μsec, and O2P = 100. The D6 parameter was used to optimize the experiment for the desired *J*–value. In most cases, a typical value of 8 Hz was used, which corresponds to a D6 value of 60 msec. As with the HMQC parameters and pulse calibrations, the AVANCE III–600 NMR, controlled by Bruker TopSpin 3.0, had many of these parameters preset in the selected program simply named HMBC.

Electronic Circular Dichroism (ECD) Analysis

ECD analysis was carried out on an Olis Cary 17 instrument. Samples analyzed on the ECD instrument were prepared in such a way that the maximum UV absorbance was *ca.* one absorbance unit (AU).

General Procedures for Collection and Refinement of X–Ray Data

Procedures for collection and refinement of X–ray data for individual compounds are included in Appendix B. Crystallographic data have been deposited with the Cambridge Crystallographic Data Centre (CCDC) #996114. Copies of the data can be obtained, free of charge, on application to the Director, CCDC, 12 Union Road, Cambridge CB2 1EZ, UK (fax: +44–(0) 1223–336033 or email: deposit@ccdc.cam.ak.uk).

GCMS Conditions for Amino Acid Derivative Analysis

A Thermo Voyager single–quadrupole mass spectrometer interfaced with a Trace2000 GC equipped with an Agilent Technologies DB–1701 capillary column (30 m x 0.25 mm ID; 0.25 μm film) was used for GCMS analysis. The GC temperature program started at 70°C for one minute, then ramped up at 10°C/min to 280°C and was held there for 18 minutes. Helium was used as the GC carrier gas (1 mL/min flow rate). The GC inlet temperature was set at 280°C. The attached autosampler was set to inject 1 μL for each sample and standard. EIMS data (70 eV) were collected over the mass range 50–700 Da. Thermo's Xcalibur 1.4 software was used for data acquisition and processing.

General Procedures for Isolation of Fungal Species from Wood–Decay Fungal Hosts

Collection of wood–decay fungi was carried out by Dr. Donald T. Wicklow of the Bacterial Foodborne Pathogens and Mycology Research Unit, Agricultural Research Service, National Center for Agricultural Utilization Research (NCAUR), United States Department of Agriculture, in Peoria, Illinois. Samples of wood–decay fungi were returned to the laboratory in Peoria in plastic bags and placed in a freezer (–7 ºC). In order to isolate microfungal colonies, direct plating of filings from the surface of the samples was accomplished by sprinkling a small portion (100–200 mg) of the powders over the surface of each of two plates of dextrose–peptone–yeast extract agar (DPYA) containing streptomycin (25 mg/L) and tetracycline (1.25 mg/L). Plates were incubated in the dark at 25 ºC for five days, and representative cultures were isolated from each colony type showing distinctive morphology on DPYA. After 7–12 days of incubation, tube cultures isolated were segregated into groups of presumptive species and maintained for solid–substrate fermentation and potential identification. All visual identifications, and gene sequencing for taxonomic identification, were performed in Dr. Wicklow's laboratory at the USDA NCAUR.

General Procedures for Solid–Substrate Fermentations

Fermentation of mycoparasitic/fungicolous fungi was conducted in the laboratory of Dr. Donald T. Wicklow of the NCAUR. Fungal strains were cultured on slants of potato dextrose agar (PDA) at 25 ºC for 14 days. Spore inoculum was suspended in

sterile distilled H_2O to give a final spore/cell suspension of 1 x 10^6/mL. Fermentation was carried out in 500–mL Erlenmeyer flasks each containing 50 g of rice (Botan Brand; J.F.C. International). Distilled H_2O (50 mL) was added to each flask and the contents were soaked overnight before autoclaving at 15 lb/in^2 for 30 min. After cooling to room temperature, each was inoculated with 1.0 mL of a selected fungal spore inoculum and incubated at 25 ºC for 15–30 days. After incubation, the fermented substrate was mechanically fragmented and extracted with EtOAc (3 x 50 mL). The combined EtOAc extracts were filtered and concentrated under vacuum to give a crude extract. In cases where additional material was needed, this process was scaled up using the number of flasks expected to give the desired amount of crude extract for a given species.

General Procedures for Antifungal Assays

Antifungal assays against *Aspergillus flavus* (NRRL 6541) and *Fusarium verticillioides* (NRRL 25457) were conducted in the laboratory of Dr. Donald T. Wicklow of the NCAUR. A portion of the EtOAc extract of each solid–substrate fermentation culture (approximately 6 mg) was redissolved in EtOAc. One–mg and 0.5–mg equivalents of extractable residue were pipetted onto individual analytical grade filter paper disks (12.5 mm diameter), which were then placed in individual Petri dish lids and dried for 30 min in a laminar flow hood. After each disk was allowed to dry, up to four disks were placed equidistant from one another on the surface of freshly poured and solidified PDA that was seeded with a spore suspension of *A. flavus* conidia to give a

final spore suspension of 1 x 10^2 cells per mL. These bioassay plates were incubated at 25 ºC for four days and examined for inhibition of *A. flavus* at two and four days as indicated by the presence of a clear or mottled zone around the disk, which is evidence of the inhibition of germination and a measure of fungistatic activity. An analogous procedure was employed for the assay against *F. verticillioides*. Solvent used for extract transfer was used as a negative control. Positive control disks were not used for testing of crude extracts, but were used for later testing of pure compounds. Antifungal assays against *Candida albicans* (ATCC 14053) were conducted in our own laboratory. *C. albicans* test plates were prepared as needed. One *C. albicans* pellet (BioMerieux) was dissolved in 1 mL of sterile H_2O, and 250 μL of the inoculum suspension was transferred to warm agar and mixed thoroughly by gentle swirling. The agar was poured into Petri plates (100 x 15 mm; 5 mL each) which were stored in the refrigerator at 4 ºC. In conducting the disk diffusion assay, each filter paper disk (6.25–mm in diameter) was impregnated with the sample to be tested (typically 100 or 200 µg/disk). After evaporation of the solvent, the disk was placed on the agar surface and incubated at room temperature for 24–72 h. Activity was reported by measuring the diameter (in mm) of the inhibition zone around each disk. Stock solutions of the control antifungal agents filipin or nystatin (Sigma Chemical Co.) at 25 μg/disk were used as positive controls.

General Procedures for Antiinsectan Assays

Antiinsectan assays were developed and conducted by Dr. Patrick F. Dowd, also of the NCAUR. Selection of crude extracts for chemical investigation in search of

antiinsectan metabolites was based on bioactivity against the fall armyworm (*Spodoptera frugiperda*).[58]

Spodoptera frugiperda

S. frugiperda larvae were maintained on a standard pinto bean diet, consisting of the following ingredients: 120 g dried pinto beans, 43 g wheat germ, 28 g brewer's yeast, 8 g Vanderzant's vitamin mix, 2.8 g ascorbic acid, 1.75 g methylparaben, 0.9 g sorbic acid, 12 g sugar, 2 mL formaldehyde (39%), 1.5 mL propionic–phosphoric acid solution (4.2% phosphoric acid), and 550 mL of H_2O. For screening purposes, crude extracts were incorporated into the diet at levels of at least 200 ppm. Column fractions and pure compounds were tested at levels of up to 1000 ppm or more (wet weight). The samples were added in 125 μL of acetone to test tubes (100 x 16 mm) containing 5–mL aliquots of molten diet (60 ºC). The mixture was then blended with a vortex mixer for 20 seconds. The diets were dispensed into Petri plates, allowed to cool to room temperature, and placed in a fume hood for *ca.* 20 min to remove residual solvent. The diet was cut into equal blocks (*ca.* 250 mg). Each block was placed into a single well of a 24–well immunoassay plate, and then a single neonate *S. frugiperda* larva was added to each well. To prevent desiccation of the diet, the plate was covered by a sheet of Parafilm, a sheet of cardboard, and a plastic cover. The cover was secured by two rubber bands. Bioassays were conducted at 27 ºC for seven days at 40% humidity with a 14:10 (light:dark) photoperiod. The insects were inspected at two, four, and seven days for mortality, and seven–day survivors were weighed. A solvent blank was used as a control. Each sample was tested on a total of 40 neonate larvae. Antiinsectan activity was measured by

comparison of the test larval weights relative to those of controls. Data were reported as percent reduction in weight gain relative to controls. Percent mortality was recorded in cases where mortality was also observed.

General Procedures for Antibacterial Assays

Bacillus subtilis

In assays using *Bacillus subtilis* (ATCC 6051), one *B. subtilis* pellet (BioMerieux), was dissolved in 1 mL of sterile H_2O, and 250 μL of the inoculum suspension was transferred to warm Penassay seed agar (Difco) and mixed thoroughly by gentle swirling. The agar was poured into Petri plates (100 x 15 mm; 5 mL each) which were stored in the refrigerator at 4 ºC. The antibiotic agent gentamycin (Sigma Chemical Co.) was used as a positive control at a level of 25 μg/disk.

Staphylococcus aureus

In assays using *Staphylococcus aureus* (ATCC 29213) pellets (BioMerieux), one pellet was dissolved in 1 mL of sterile H_2O, and 250 μL of the inoculum suspension was transferred to warm agar and mixed thoroughly by gentle swirling. The agar was poured into Petri plates (100 x 15 mm; 5 mL each) which were stored in the refrigerator at 4 ºC. The antibiotic gentamycin (Sigma Chemical Co.) was again used as a positive control at 25 μg/disk.

Escherichia coli

In assays using *Escherichia coli* (ATCC 25922) pellets (BioMerieux), one pellet was dissolved in 1 mL of sterile H_2O, and 250 μL of the inoculum suspension was transferred to warm agar and mixed thoroughly by gentle swirling. The agar was poured into Petri plates (100 x 15 mm; 5 mL each) which were stored in the refrigerator at 4 ºC. The gentamycin (Sigma Chemical Co.) was used as a positive control at 25 μg/disk.

In conducting all of the above disk diffusion assays, the filter paper disks (6.25–mm in diameter) were impregnated with the sample to be tested (200 µg/disk). After evaporation of the solvent, the disk was placed on the agar surface of a *B. subtilis*, *S. aureus*, or *E. coli* petri plate, and the plate was then incubated at room temperature for 24–48 hr. The antimicrobial activity of the sample was reported by measuring the diameter (in mm) of the inhibition zone around the disk in which no growth of the test organism was observed.

Procedures for Isolation and Characterization of Metabolites from an isolate of *Aspergillus puulaauensis* (MYC–2152 = NRRL 62124)

Fungal Material. An isolate of *Aspergillus* sp. (MYC–2152 = NRRL 62124) was obtained from a basidioma of an *Inonotus* sp. found on a dead soapberry tree in a forest in Kipuka ki (Volcanoes National Park) in the Ka'u District of Hawaii. Sequencing studies later showed that this isolate is a representative of a previously undescribed species of *Aspergillus* Section Versicolores (GenBank Accession No. JN093265), now named *Aspergillus puulaauensis* (Trichocomaceae).[81] The culture was incubated on rice (2 x 50g) at 25^{0}C for 30 days and the resulting fermentation mixtures

were extracted with EtOAc. The filtered EtOAc solution was evaporated to dryness, yielding 590 mg of crude extract.

Isolation. The crude extract was partitioned between MeCN and hexanes (1:1), yielding the expected layers as well as a precipitate, which was later identified as sterigmatocystin. The MeCN–soluble portion produced more precipitate when exposed to $CDCl_3$ and MeOH, yielding a combined total of 292 mg of sterigmatocystin (**3.5**),[123] which was identified by spectroscopic comparison with an authentic standard. The remainder of the MeCN fraction (218 mg) was chromatographed on a Si gel column eluting with a hexanes/EtOAc/MeOH gradient yielding 15 fractions. Fraction four (50 mg) contained additional sterigmatocystin. Compound **3.1** was the major component of fractions five, six, and seven (5.3 mg, 28 mg, and 11 mg, respectively). Fraction six contained a 10:1 ratio of **3.1** with diastereomer oxepinamide E (**3.14**), however, additional purification was not initially needed to assign the structure of **3.1**. A portion of fraction five (3.5 mg of 5.3 mg) was subjected to RP–HPLC hexanes/EtOAc/MeOH gradient yielding 15 fractions, one of which was **3.4** (0.8 mg). Fraction eight (7.5 mg) was further separated using RP–HPLC (isocratic 40% MeCN in H_2O for 15 min, 40–100% over 15 min, ending with a 100% MeCN wash) yielding notoamide K (**3.12**; 0.7 mg),[85] notoamide D (**3.9**; 0.7 mg),[86] and 6,8–di–O–methylnidurufin (**3.6**; 0.3 mg).[82] Fractions nine (19 mg) and eleven (14 mg) also were further separated using RP–HPLC (isocratic 50% MeCN in H_2O for 15 min, 50–100% over 15 min, ending with a 100% MeCN wash). Separation of fraction 9 yielded kipukasin I (**3.2**; 1.6 mg), kipukasin H (**3.3**; 3.5 mg), avrainvillamide (**3.8**; 1.3 mg),[84] stephacidin A (**3.13**; 1.9 mg),[124] notoamide F (**3.11**; 0.8 mg),[85] and notoamide E (**3.10**; 0.6 mg).[87] Fraction 11 yielded kipukasin I (**3.2**; 1.7 mg), aspergamide A (**3.7**; 2.5 mg),[83] avrainvillamide (**3.8**; 1.9 mg),[84] notoamide F (**3.10**; 0.4 mg),[85] and notoamide E (**3.11**; 0.2 mg).[87] All known compounds

encountered were identified by comparison of ^{1}H NMR, HRESIMS, and ECD (when applicable) data to those reported in the literature.

X-ray Crystallographic Analysis of 15–*epi*–Oxepinamide E (3.1). A thin yellow orange plate, obtained from a mixture of $CHCl_3/CH_3OH$, (0.18 x 0.12 x 0.025 mm) was mounted with paratone oil on a nylon loop attached to a stainless steel pin mounted in a Nonius goniometer head. 45918 data for **3.1** were collected with an Nonius KappaCCD diffractometer at 220K (cold N_2 gas stream). The HKL 2000 suite was used for data reduction: 4525 reflections, 2652 >2sigma(I), R(sym)=0.125. The structure was solved and refined using the Shelxtl suite. Final refinement values: R_1=0.115, wR_2=0.298, goof=1.05.

Energy Minimization and ECD Calculations. Structures were minimized by performing an equilibrium geometry calculation using the Merck Molecular Mechanics Force Field (MMFF) in Spartan '10. Monte Carlo conformer distribution was performed using Semi Empirical AM1 calculations in Spartan '10. Initial structures were fully optimized using the 6-31G(d) basis set[64, 66] combined with the M06-2X functional[67] followed by frequency calculations at the same level of theory using Gaussian 09 Rev. B.01. Absence of imaginary frequencies confirmed that all conformers were minima on the potential energy surface. No symmetry constraints were used during the optimization.

Time-dependent density functional calculations (TDDFT) were performed to calculate ECD spectra at the optimized geometry using the same basis set and functional. A total of 40 excited states were calculated and only singlet excited states were considered. Both gas-phase and solution-phase calculations were performed using methanol solvent and the PCM solvation model.[68] Gaussian 09 Rev. B.01 was used in all calculations.[71] To visualize the spectra, SpecDis software (version 1.53; by Dr. Torsten Bruhn) was used.[72]

15–*epi*–Oxepinamide E (3.1): yellow–orange needles; $[\alpha]_D$ +12 (*c* 0.12, acetone); $[\alpha]_D$ +129 (*c* 0.25, $CHCl_3$); UV (MeOH) λ_{max} 330 nm (log ε 3.6), NMR data, see Table 3.1; HRESITOFMS *m/z* 394.1758 $[M+H]^+$ (calcd. for $C_{22}H_{24}N_3O_4$, 394.1766), 416.1582 $[M+Na]^+$ (calcd for $C_{22}H_{23}N_3O_4Na$, 416.1586).

Artifact Arising from 15–*epi*–Oxepinamide E (3.4): Light yellow powder; $[\alpha]_D$ –84 (*c* 0.05, acetone); NMR data, see Table 3.2

Kipukasin H (3.2): off–white film; $[\alpha]_D$ –54 (*c* 0.11, MeOH); UV (MeOH) λ_{max} 213 (log ε 4.6), 266 (4.4), 302 nm (3.7); NMR data, see Table 3.3; HRESITOFMS *m/z* 501.1110 $[M+Na]^+$ (calcd for $C_{21}H_{22}N_2O_{11}Na$, 501.1121)

Kipukasin I (3.3): white powder; $[\alpha]_D$ –99 (*c* 0.05, MeOH); UV (MeOH) λ_{max} 213 (log ε 4.7), 266 (4.6), 302 nm (2.9); ^1H NMR (CD_3OD, 400 MHz) δ 8.05 (d, *J* = 8.1 Hz, H–6), 6.26 (dd, *J* = 2.4, 0.7 Hz, H–3" or 5"); 6.23 (d, *J* = 6.7 Hz, H–1'), 6.19 (dd, *J* = 2.4, 0.3 Hz, H–3" or 5"), 5.76 (d, *J* = 8.1 Hz, H–5), 5.71 (dd, *J* = 5.7, 2.7 Hz, H–3'), 5.58 (d, *J* = 6.7, 5.7 Hz, H–2'), 4.39 (q, *J* = 2.7 Hz, H–4'), 3.88 (d, *J* = 2.7 Hz, H_2–5'), 2.57 (s, H_3–8"), 2.01 (s, H_3–7'). HRESITOFMS *m/z* 437.1161 $[M+H]^+$ (calcd for $C_{18}H_{31}N_2O_{10}$, 437.1196)

Chiral Amino Acid Analysis of the Phe Unit in 3.1. A sample of **3.1** (0.7 mg) was dissolved in 0.5 mL 6N HCl and heated at 110 °C for 24 h in a vacuum–sealed

hydrolysis tube. The mixture was then cooled and dried directly under air flow. The resulting hydrolyzate of **3.1** was dissolved in ~ 0.5 mL of (+)–*S*–2–butanolic HCl (0.5 mL (+)–*S*–2–butanol + 17.5 µL acetyl chloride) and heated at 110 °C for 30 mins in a vacuum–sealed hydrolysis tube. After evaporation, resulting residue was dissolved in 0.5 mL CH_2Cl_2 and 250 µL of trifluoroacetic anhydride (TFAA) and then heated at 150 °C for 5 min. This solution was cooled, dried to near completion under air, diluted with CH_2Cl_2, and subjected to GCMS analysis.

Derivatives of standard amino acids (1.0 mg each) were prepared in a manner analogous to that as described above for the peptide hydrolyzate. Retention times of each of the trifluoroacetyl (+)–*S*–2–butyl esters of the amino acids were: D–Phe (t_R = 14.46) and L–Phe (t_R = 14.53). Comparison of the retention times and MS data, as well as co–injection of the TFA(+)–*S*–2–butyl ester derivatives of the standards with the derivative mixture prepared from the hydrolyzate of compound **3.1** allowed identification of the amino acid moiety in the compound as D–Phe.

Procedures for Isolation and Characterization of Metabolites from an Isolate of *Trichothecium crotocinigenum* (MYC–2235)

Fungal Material. An isolate of *Trichothecium crotocinigenum* (syn. *Acremonium crotocinigenum*; MYC–2235 = NRRL 62714) was obtained from the black stromata of a pyrenomycete collected from a dead hardwood branch in Kipuka ki (Volcanoes National Park), Ka'u District, Hawaii. This isolate was initially identified based on micromorphology, and sequencing studies later confirmed this identification (GenBank

Accession No. KF430640). Initially, *T. crotocinigenum* was grown on 2 x 50 g of autoclaved rice for 30 days at 25 °C. The resulting culture material was then extracted with EtOAc, affording approximately 1 g of crude material upon evaporation of the solvent. The first scale–up was grown on 6 x 50 g of autoclaved rice for 30 days at 25 °C, resulting in about 1.4 g of EtOAc extract. The second scale–up was grown on 20 x 50 g of autoclaved rice for 30 days at 25 °C, resulting in about 1.7 g of EtOAc extract.

Isolation. The initial crude EtOAc extract was partitioned between MeCN and hexanes (1:1). The MeCN–soluble portion (284 mg) was subjected to Si gel column chromatography eluting with a hexanes/EtOAc/MeOH gradient yielding 15 fractions. Fractions 4 and 5 (10.5 mg, 7.6 mg) were identified as 3–deoxotrichothecin (**4.2**).[95] The major component of fraction 12 (5.6 mg) was identified as guangomide A (**4.3**)[98, 99] without further separation. These two known compounds were identified by comparison of ^{1}H NMR data to those reported in the literature. Fractions 13 and 14 (6.0 mg and 12.4 mg, respectively) were each further fractionated through the use of RP– HPLC (isocratic 20% MeCN in H_2O for 20 min, 20–100% over 10 min, ending with a 100% MeCN wash). Compound **4.1** was found in HPLC subfractions from both fractions 13 and 14, totaling 4.7 mg. Separation of fraction 13 also yielded **4.4** and **4.5** (1.0 mg and 0.6 mg). The other subfractions from fractions 13 and 14 contained mixtures of compounds that exhibited peptide/depsipeptide–type ^{1}H NMR signals (similar to those of **4.4** and **4.5**) in submilligram quantities.

Compound 4.1: off–white oil; $[\alpha]_D$ +9.2 (*c* 0.14, MeOH); UV (MeOH) λ_{max} 213 (log ε 4.7), 266 (4.6), 302 nm (2.9); NMR data, see Table 4.1; HRESITOFMS *m/z* 195.1131 $[M+H]^+$ (calcd for $C_{10}H_{15}N_2O_2$, 195.1134)

Compound 4.4: off–white oil; HRESITOFMS *m/z* 514.3132 $[M+H]^+$ (calcd. for $C_{25}H_{44}N_3O_8$, 514.3128), HRESITOFMSMS data, see Appendix Figure A29. Due to lack of sample and signal doubling/degradation, no NMR signals were assigned, however, spectra can be viewed in the Appendix (Figures A26–A28).

Compound 4.5: off–white oil; HRESITOFMS *m/z* 522.2802 $[M+Na]^+$ (calcd for $C_{24}H_{41}N_3O_8Na$, 522.2791), HRESITOFMSMS data, see Appendix Figure A31. Due to lack of sample and signal doubling/degradation, no NMR signals were assigned, however, spectra can be viewed in the Appendix (Figure A32).

Chiral Amino Acid Analysis of the Pip Unit in 4.1. A sample of **4.1** (0.5 mg) was hydrolyzed in 0.5 mL of 6N HCl in a sealed hydrolysis tube *in vacuo* at 110 °C for 24 h, then cooled in an ice bath, and dried to completion under an air stream. The hydrolyzate was dissolved in 1 mL H_2O, and solutions of 1M $NaHCO_3$ (40 μL) and 1% 1–fluoro–2,4–dinitrophenyl–5–L–alanine amide (FDAA) in acetone (40 μL) were added. The reaction mixture was heated to 40 °C for 1 h. After cooling the resulting mixture and adding MeCN (due to solvent evaporation), the sample was subjected to RP–HPLC on a 5–μm C_{18} column (10 x 250 mm) at a flow rate of 2 mL/min with UV detection at 340 nm (solvent A = 10mM NaOAc, solvent B = MeCN, 10–40% B over 30 min). FDAA derivatives of D– and L–Pip standards were prepared and analyzed in the same way. A reaction blank was also prepared (no sample or standard) in the same manner in order help identify any residual HPLC peaks resulting from the reagents themselves. The retention times for FDAA–derivatized D–Pip and L–Pip were 11.13 and 10.6 min, respectively. The product from **4.1** co–eluted with the L–isomer.

Chiral Amino Acid Analysis of 4.4. A sample of **4.4** (0.5 mg) was dissolved in 0.5 mL 6N HCl and heated at 110 °C for 24 h in a vacuum–sealed hydrolysis tube. The

mixture was then cooled and partitioned with CH_2Cl_2. Both partitions were dried down directly under air flow. The CH_2Cl_2 portion was dissolved in $CDCl_3$ and analyzed by ^1H NMR in order to determine if the Ila units present were *allo*–, "normal," or a mixture of stereoisomer types. Comparison to literature data[108] suggested that both Ila units were *allo*–type, since the methyl triplet (δ_H 0.95) appeared downfield of the methyl doublet (δ_H 0.86).

The resulting aqueous portion of the hydrolyzate of **4.4** was dissolved in ~ 0.2 mL of (+)–*S*–2–butanolic HCl (0.2 mL (+)–*S*–2–butanol + 17.5 µL acetyl chloride) and heated at 110 °C for 30 mins in a vacuum–sealed hydrolysis tube. After evaporation, resulting residue was dissolved in 0.5 mL CH_2Cl_2 and 250 µL of trifluoroacetic anhydride and heated at 150 °C for 5 min. This solution was cooled, dried to near completion under air, diluted with CH_2Cl_2 and subjected to GCMS analysis.

Derivatives of standard amino acids (0.5 mg each) were prepared in a manner analogous to that as described above for the peptide hydrolyzate. Retention times of each of the trifluoroacetyl (+)–*S*–2–butyl esters of the amino acids were: D–Ala (t_R = 10.52) and L–Ala (t_R = 10.62); D–Thr (t_R = 12.04), L–Thr (t_R = 12.09), D–*allo*–Thr (t_R = 12.91), L–*allo*–Thr (t_R = 13.00); D –Ile (t_R = 12.72), L –Ile (t_R = 12.84), D–*allo*–Ile (t_R = 12.59), L–*allo*–Ile (t_R = 12.67). Comparison of the retention times and MS data, as well as co–injection of the TFA(+)–*S*–2–butyl ester derivatives of the standards with the trifluoroacetyl (+)–*S*–2–butyl ester derivative mixture prepared from the hydrolyzate of compound **4.4** allowed identification of the amino acid components in **4.4** as L–Ala, L–Thr, and L–Ile.

Procedures for Isolation and Characterization of Metabolites from 17α–Trenbolone and 17β–Trenbolone[120, 121]

This work was performed in collaboration with Professor David M. Cwiertny, Department of Civil and Environmental Engineering and Department of Chemical and Biochemical Engineering, University of Iowa, and his then graduate student, Dr. Shen Qu.

Materials (Provided by the Cwiertny Lab). 17α–Trenbolone (17α–hydroxyestra–4,9,11–trien–3–one) was obtained from BDG Synthesis (Lower Hut, NZ). 17β–Trenbolone (17β–hydroxyestra–4,9,11–trien–3–one) was obtained from Sigma Aldrich (St. Louis, MO). Solid–phase extraction was employed using 6–mL C–18 solid–phase extraction cartridges (Restek, Bellefonte, PA). Stock solutions (2–10 mg/L) of each of the steroid analytes were prepared in silanized volumetric glassware, then serially diluted to create working standards. Deionized water was obtained from a Milli–Q system (Millipore, Billerica, MA, USA).

Light Source and Photoreactor Details. Most laboratory photoreactor experiments used a commercially available 450 W Xenon arc lamp (Newport Corporation) and a water–jacketed borosilicate photoreactor. A small number of experiments requiring larger sample volumes utilized a Suntest CPS+ solar simulator. A limited number of experiments also utilized natural sunlight. These photoreactor experiments were conducted by Dr. Shen Qu.

Degradation of 17β–Trenbolone (5.3). Sample preparation was performed by Dr. Shen Qu. A Suntest solar simulator was used to irradiate in parallel several (five) 100 mL solutions of 100 μM of **5.3** in borosilicate glass beakers. The cumulative mass of **5.3**

in all systems was ~14 mg. After 4 h of irradiation (sufficient for 98+% transformation of 17β–trenbolone parent), the entire contents of each beaker was extracted onto preconditioned C–18 SPE cartridges that were subsequently eluted with 2 mL of methanol. These methanol extracts from each photoreactor were then combined into one 10 mL solution used in NMR analysis. Prior to analysis, this solution was further concentrated under N_2 to reduce the methanol volume to 200 μL, freeze–dried to evaporate residual methanol, and then redissolved in a known volume of methanol prior to sample fractionation.

Isolation and Identification of Products from Degradation of 17β–Trenbolone (5.3). The sample was separated into eight fractions by reversed–phase HPLC (Grace Apollo 5–μm C_{18} column; 10 x 250 mm; 25–72% MeCN–H_2O over 13 minutes, 72–100% over 2 minutes, and isocratic 100% MeCN for 5 minutes at a flow rate of 2 mL/min). Four of these fractions were found to be pure decomposition products **5.5** (0.7 mg), **5.6** (1.0 mg), **5.7** (2.2 mg), and **5.8** (1.1 mg), while another consisted of unreacted starting material (**5.3**; 2.1 mg). The structures of these products were assigned independently by analysis of 1D and 2D NMR data, including ^{1}H NMR, COSY, HSQC, and HMBC experiments. Due to degradation of the samples over time, $[\alpha]_D$ values were not recorded, nor were MS data collected.

17β–Trenbolone (5.3): white powder. ^{1}H NMR, COSY, HSQC, and HMBC NMR data, see Table 5.1 and Figure 5.2

17α–Trenbolone (5.4): colorless oil. ^{1}H NMR, COSY, HSQC, and HMBC NMR data, see Table 5.5; UV (by LC–DAD) λ_{max} 350

10,12,17–Trihydroxy–estra–4,9(11)–dien–3–one (5.5): colorless oil. ^{1}H NMR, COSY, HSQC, and HMBC NMR data, see Table 5.2 and Figure 5.3

11,12–Dialdehyde Product of 17β–Trenbolone (5.6): colorless oil. ^{1}H NMR, HSQC, and HMBC NMR data, see Table 5.3 and Figure 5.4

12,17–Dihydroxy–estra–5(10),9(11)–dien–3–one (5.7): colorless oil. ^{1}H NMR, HSQC, and HMBC NMR data, see Table 5.4

17–Hydroxy–12–methoxy–estra–5(10),9(11)–dien–3–one (5.8): colorless oil. ^{1}H NMR data, see Table 5.4

NMR Support for Product–to–Parent Reversion. In an effort to monitor a complete reversion cycle (i.e., photolysis and dehydration) via NMR, separate samples of **5.3** and **5.4** were subjected to photodegradation in D_2O (pH 7), and ^{1}H NMR data were collected before degradation, immediately after irradiation, and every few days thereafter while the sample was kept in the dark. The NMR tube experiment involving **5.3** showed that two major products, **5.7** and a new unidentified decomposition product, were produced. After monitoring the sample for eight days, there were no remaining spectroscopic features diagnostic for the starting material or the previously encountered photoproducts. However, the NMR study of **5.4** showed a complete conversion to **5.10**, which then converted to **5.4'** in the dark. The experiment was repeated in H_2O to determine whether **5.10** was produced under environmentally relevant conditions.

Compound 5.10: HRESITOFMS *m/z* 313.1755 $[M+Na]^+$ calcd. for $C_{18}H_{22}D_2O_3Na$, 313.1749); UV (by LC–DAD) λ_{max} 245; partial NMR data, Figure 5.5

Compound 5.4': HRESITOFMS *m*/*z* 294.1609 $[M+Na]^+$ (calcd. for $C_{18}H_{21}DO_2Na$, 294.1580).

APPENDIX A

Selected NMR and Mass Spectra

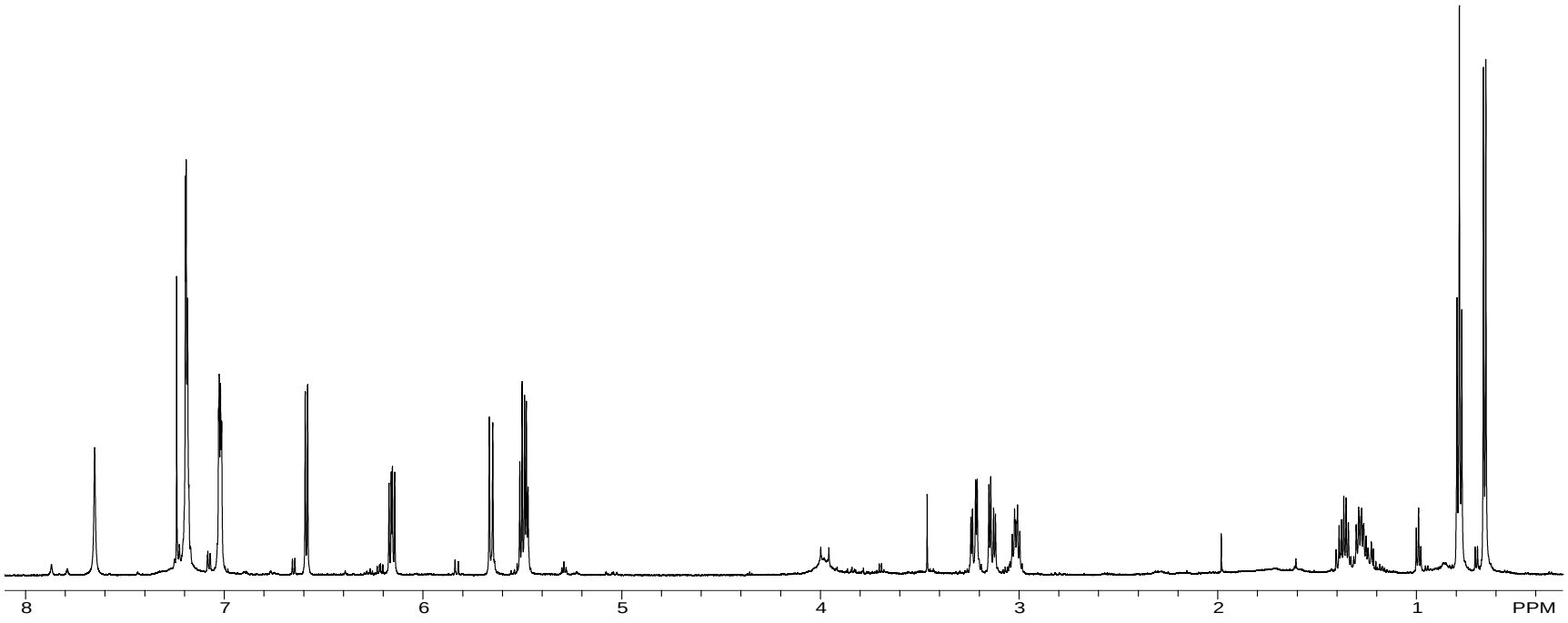

Figure A1. ^{1}H NMR Spectrum of 15–*epi*–Oxepinamide E (**3.1**; $CDCl_3$, 600 MHz)

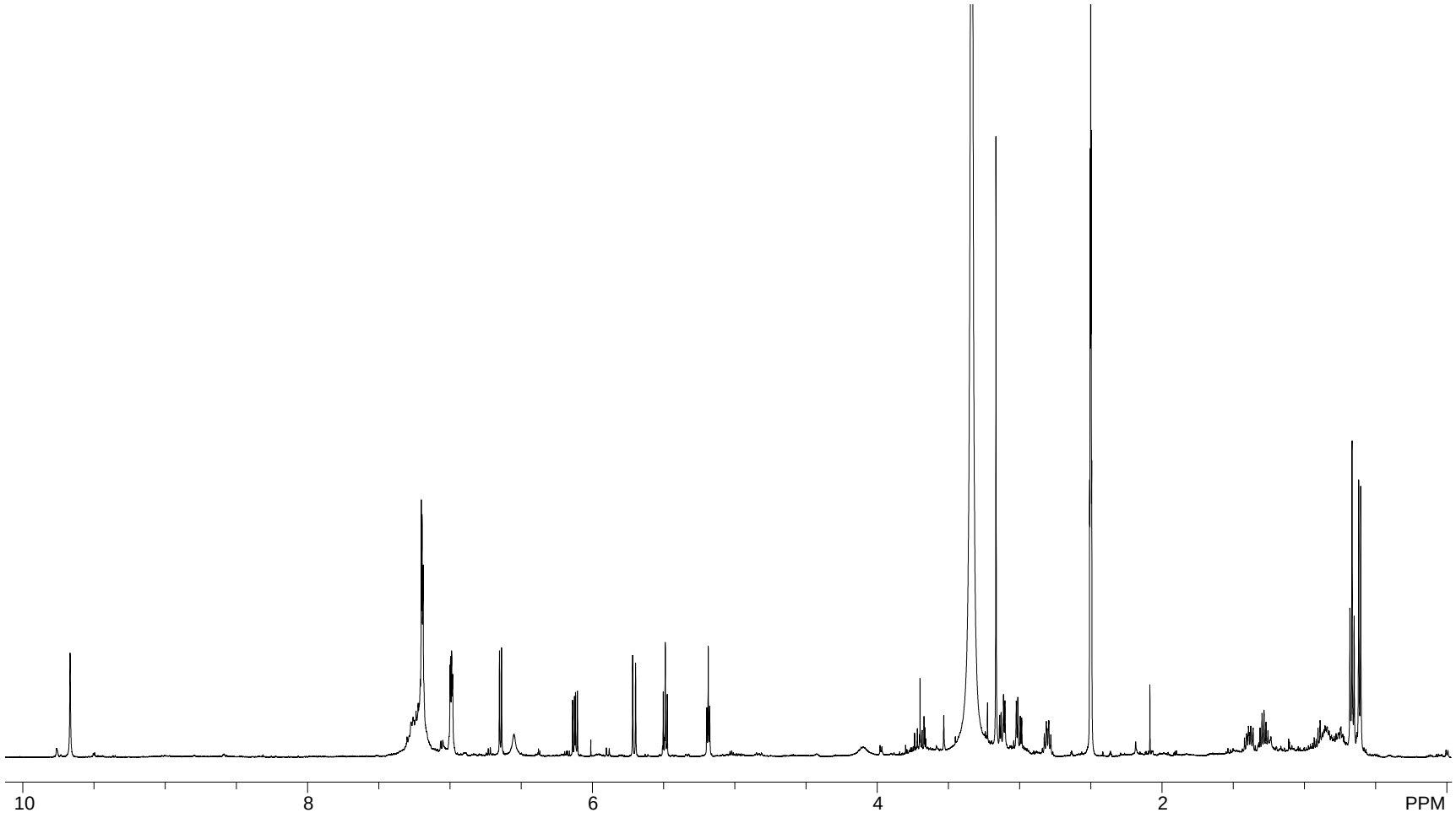

Figure A2. ^{1}H NMR Spectrum of 15–*epi*–Oxepinamide E (**3.1;** 500 MHz, DMSO–d_6)

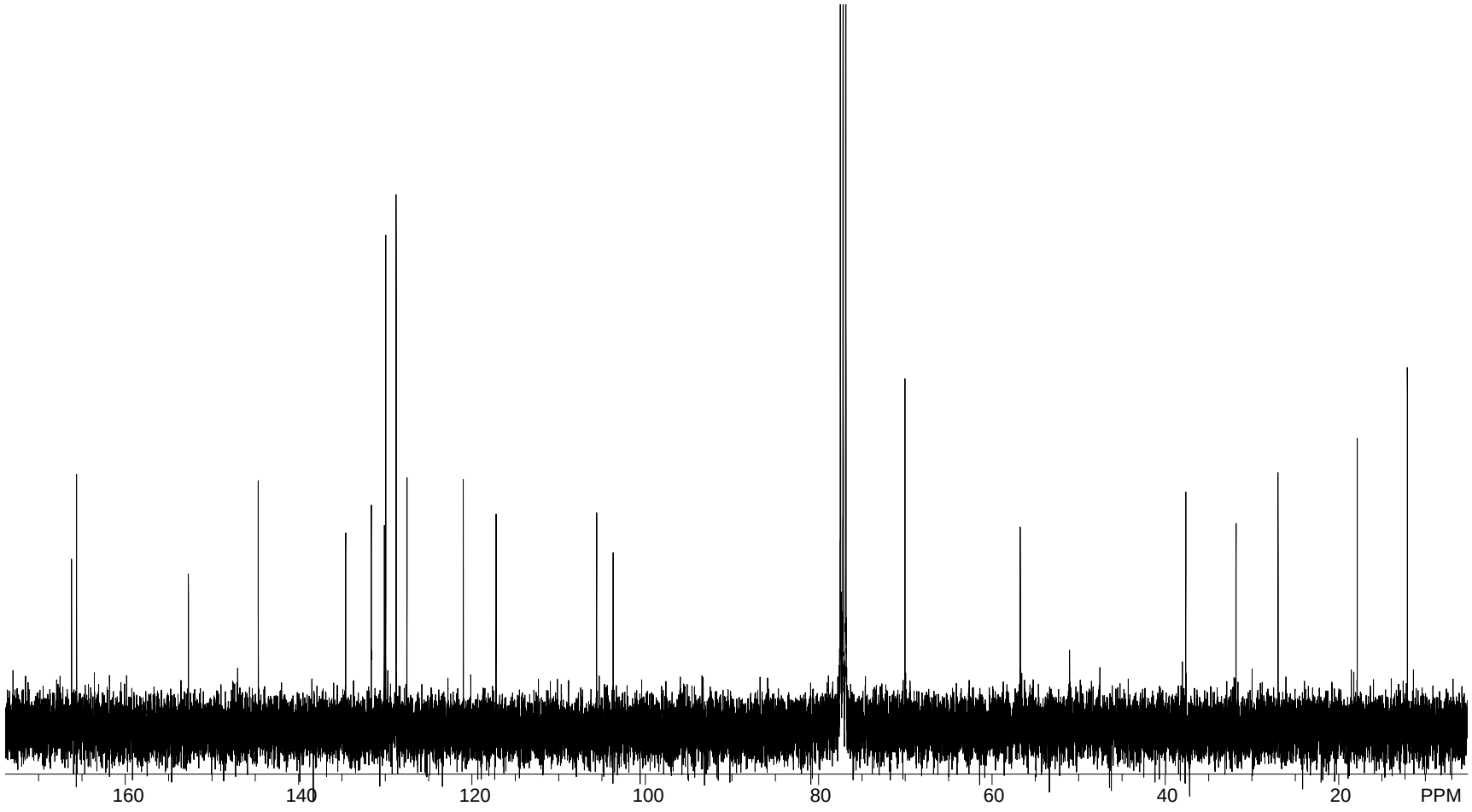

Figure A3. ^{13}C NMR Spectrum of 15–*epi*–Oxepinamide E (**3.1**; $CDCl_3$, 100 MHz)

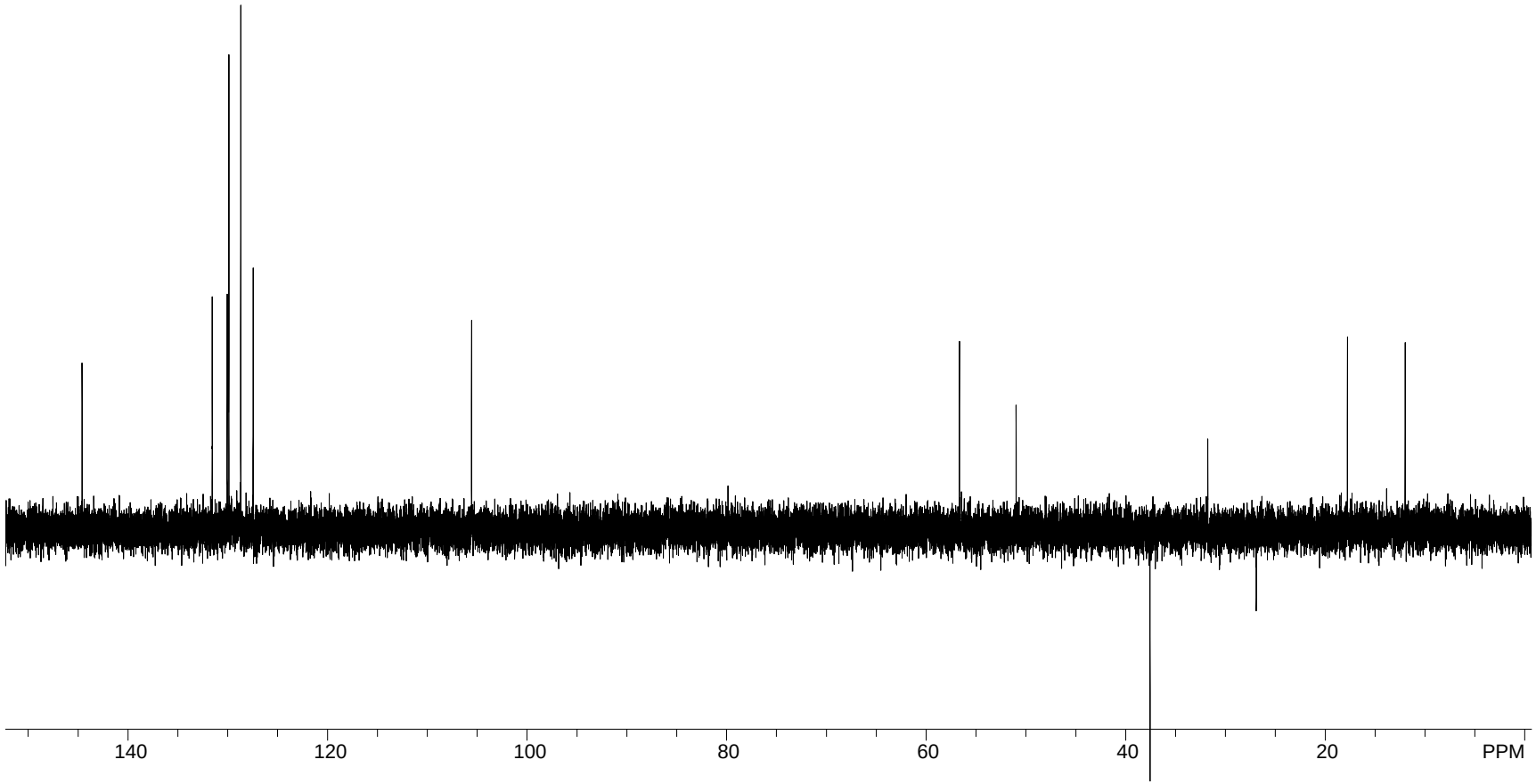

Figure A4. DEPT Spectrum of 15–*epi*–Oxepinamide E (**3.1**; $CDCl_3$, 100 MHz)

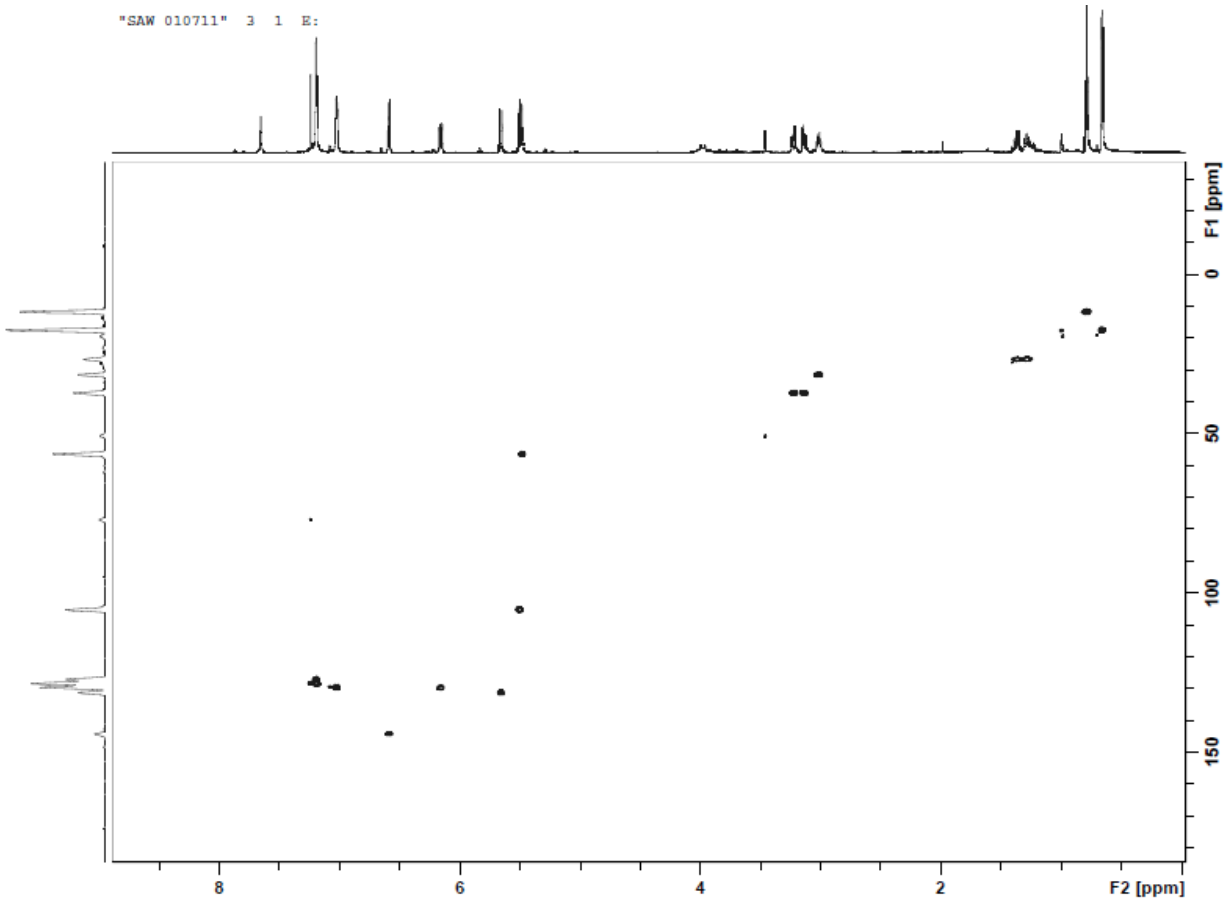

Figure A5. HSQC Spectrum of 15–*epi*–Oxepinamide E (**3.1**; $CDCl_3$, 600 MHz)

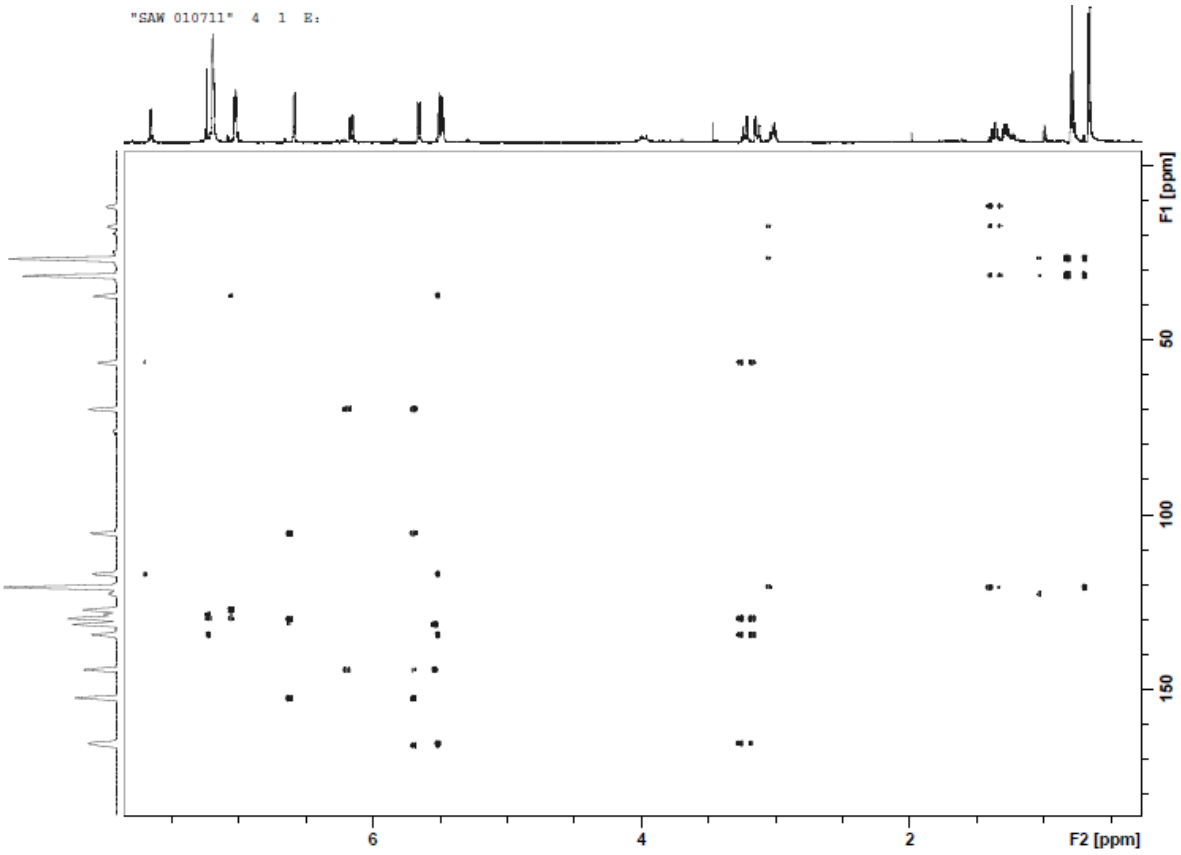

Figure A6. HMBC Spectrum of 15–*epi*–Oxepinamide E (**3.1**; $CDCl_3$, 600 MHz)

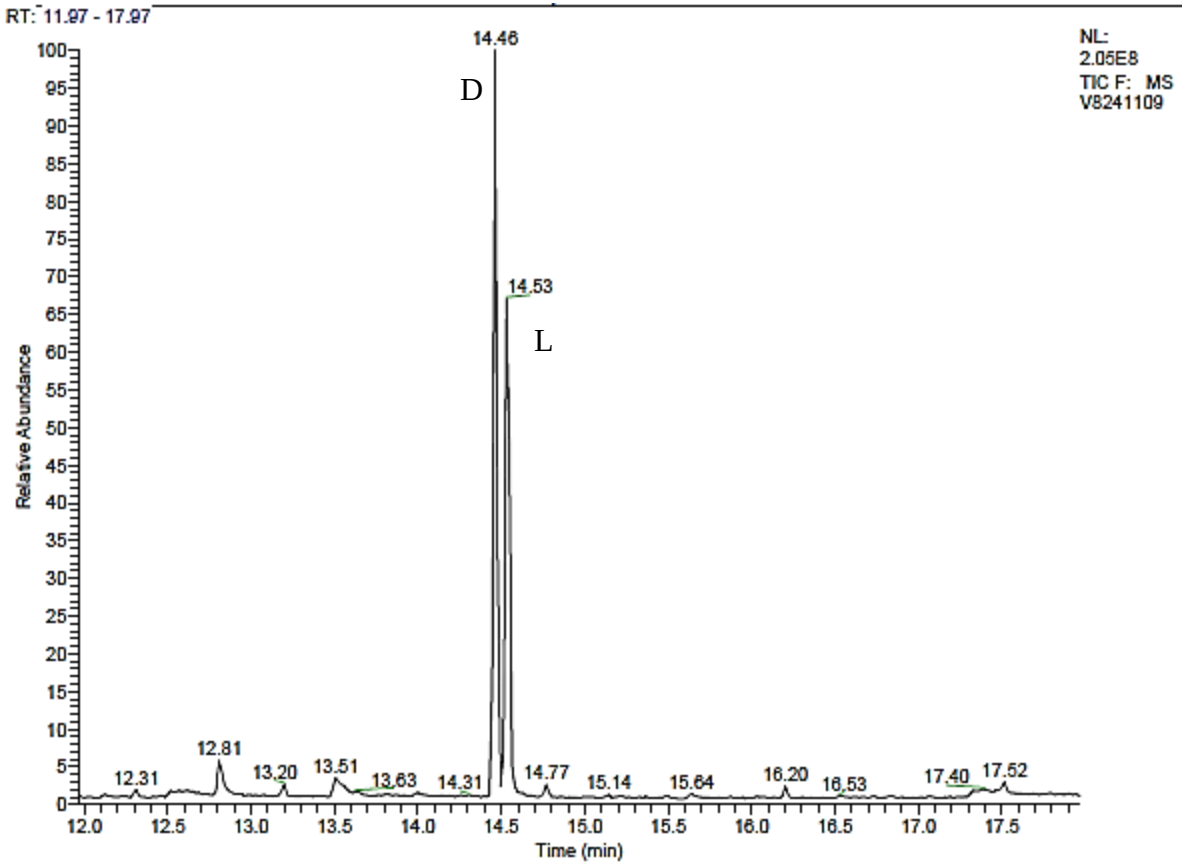

Figure A7. Co-injection of the TFA(+)–*S*–2–butyl Ester Derivatives of the D– and L–Standards (1:1) with the Derivative Mixture Prepared from the Hydrolyzate of Compound **3.1**

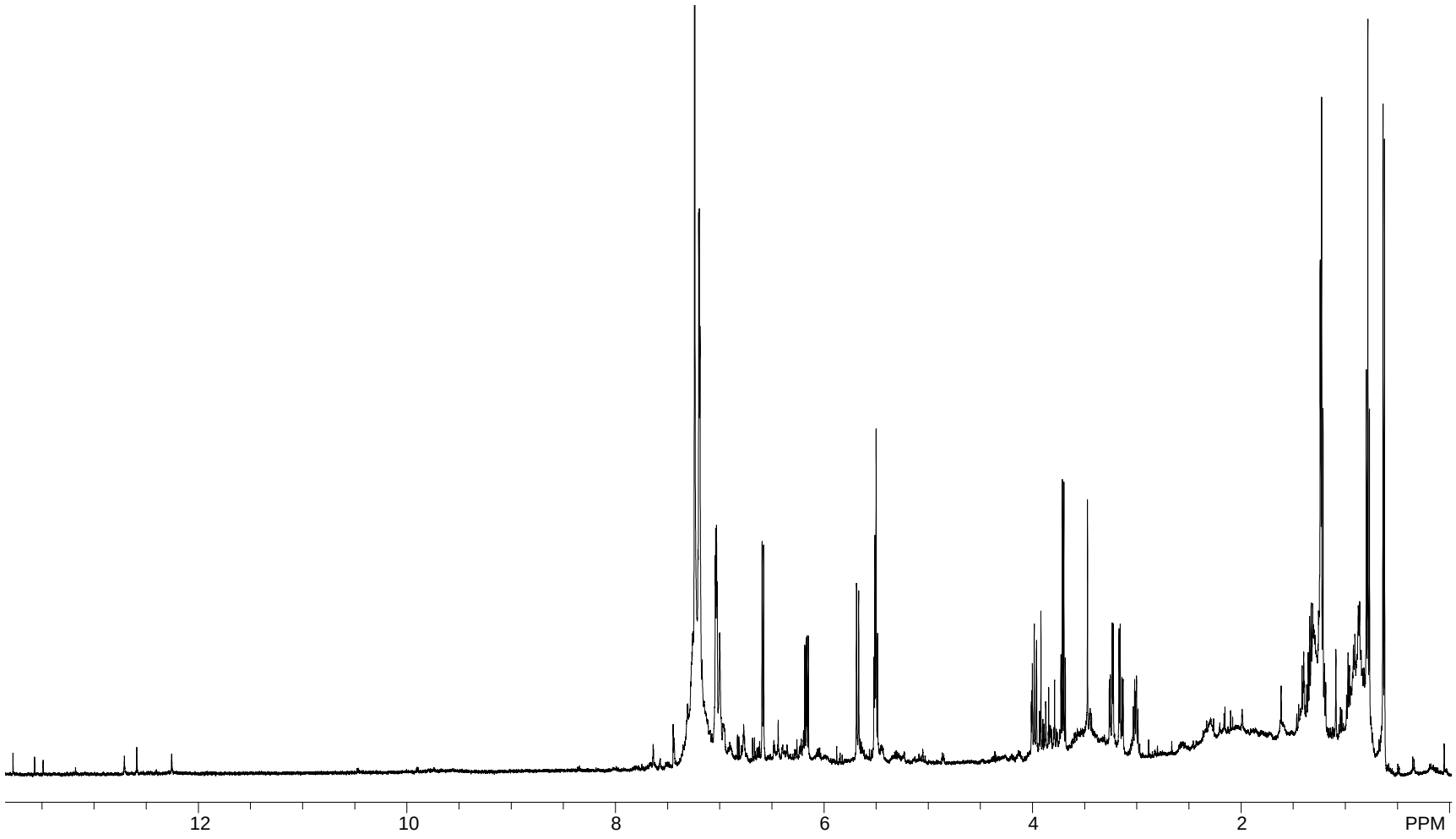

Figure A8. ^{1}H NMR Spectrum of Fraction 5 of the MYC–2152 Extract Before HPLC ($CDCl_3$, 500 MHz)

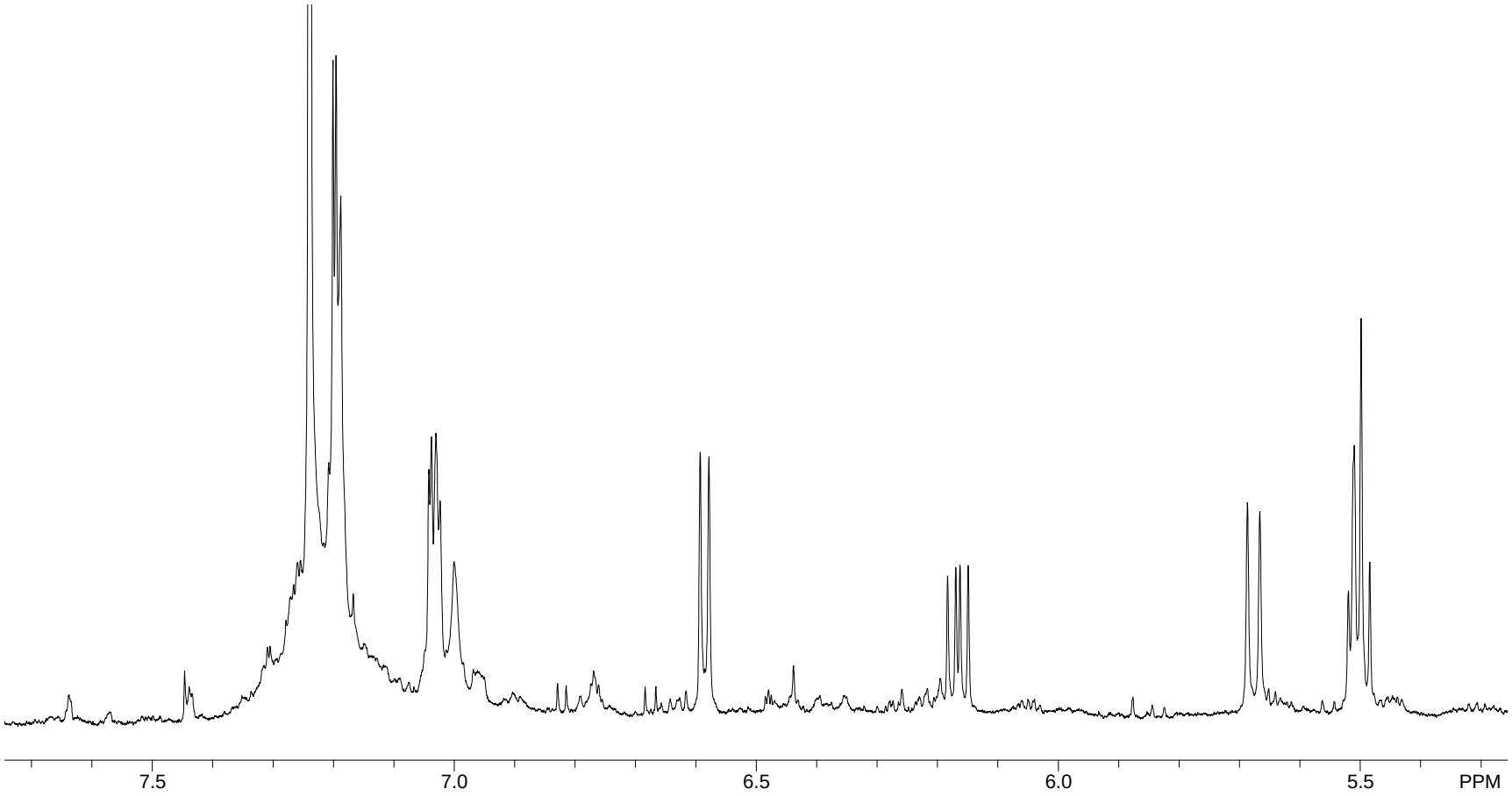

Figure A9. ^{1}H NMR Spectrum of Fraction 5 of the MYC–2152 Extract Before HPLC; Expansion of the Downfield Region ($CDCl_3$, 500 MHz)

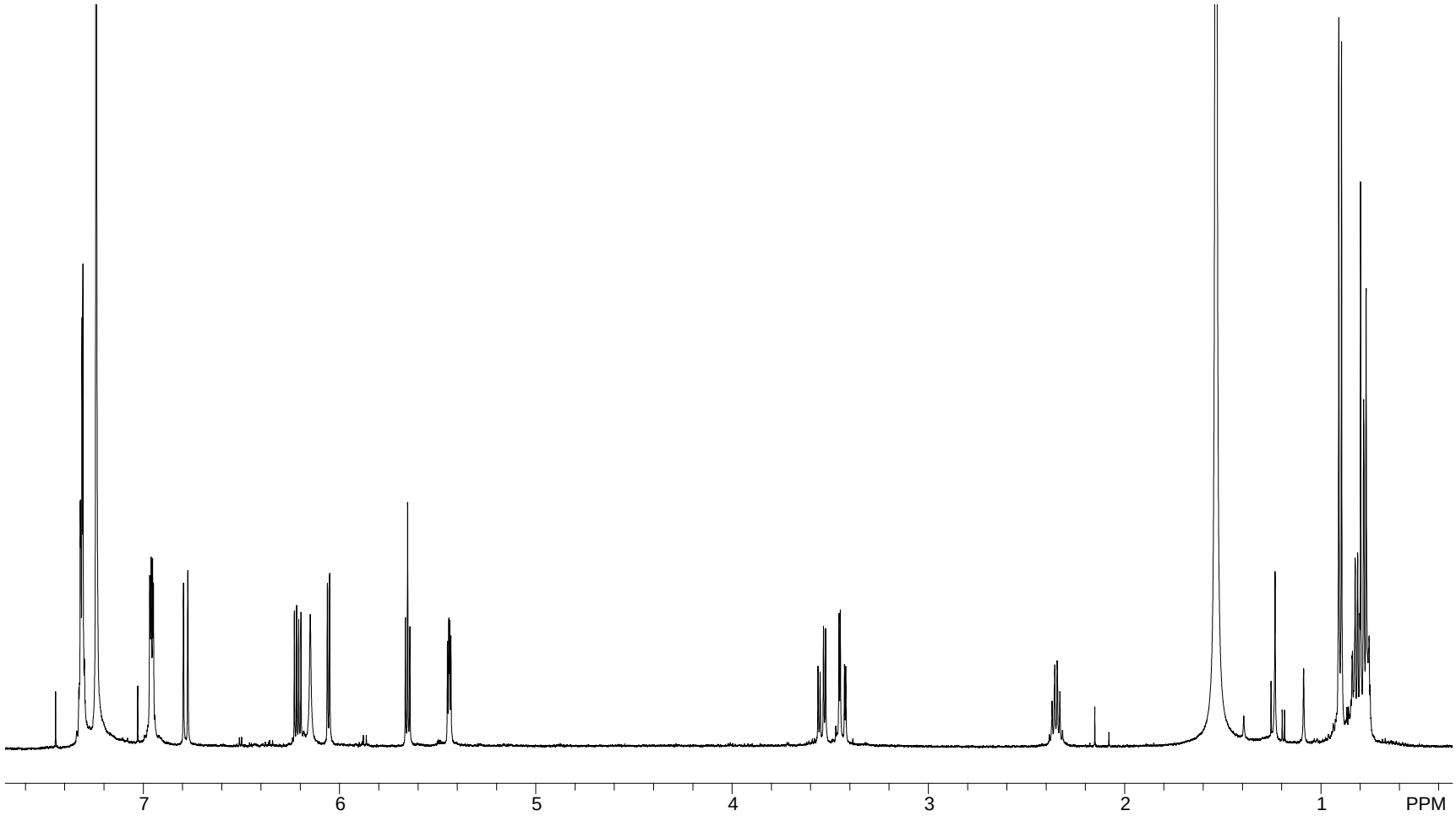

Figure A10. ^{1}H NMR Spectrum of Artifact **3.4** ($CDCl_3$, 500 MHz)

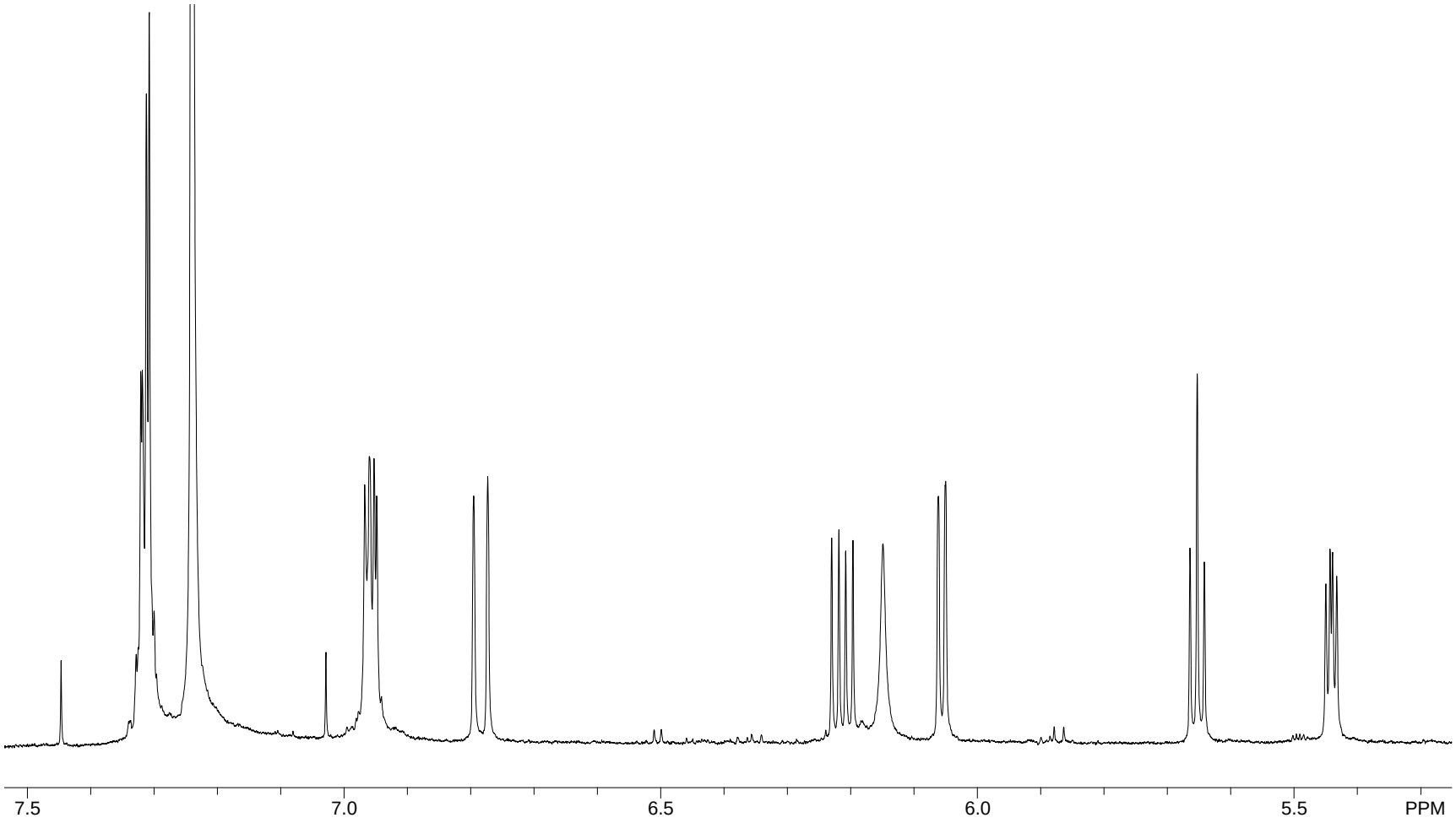

Figure A11. ^{1}H NMR Spectrum of **3.4**; Expansion of the Downfield Region ($CDCl_3$, 500 MHz)

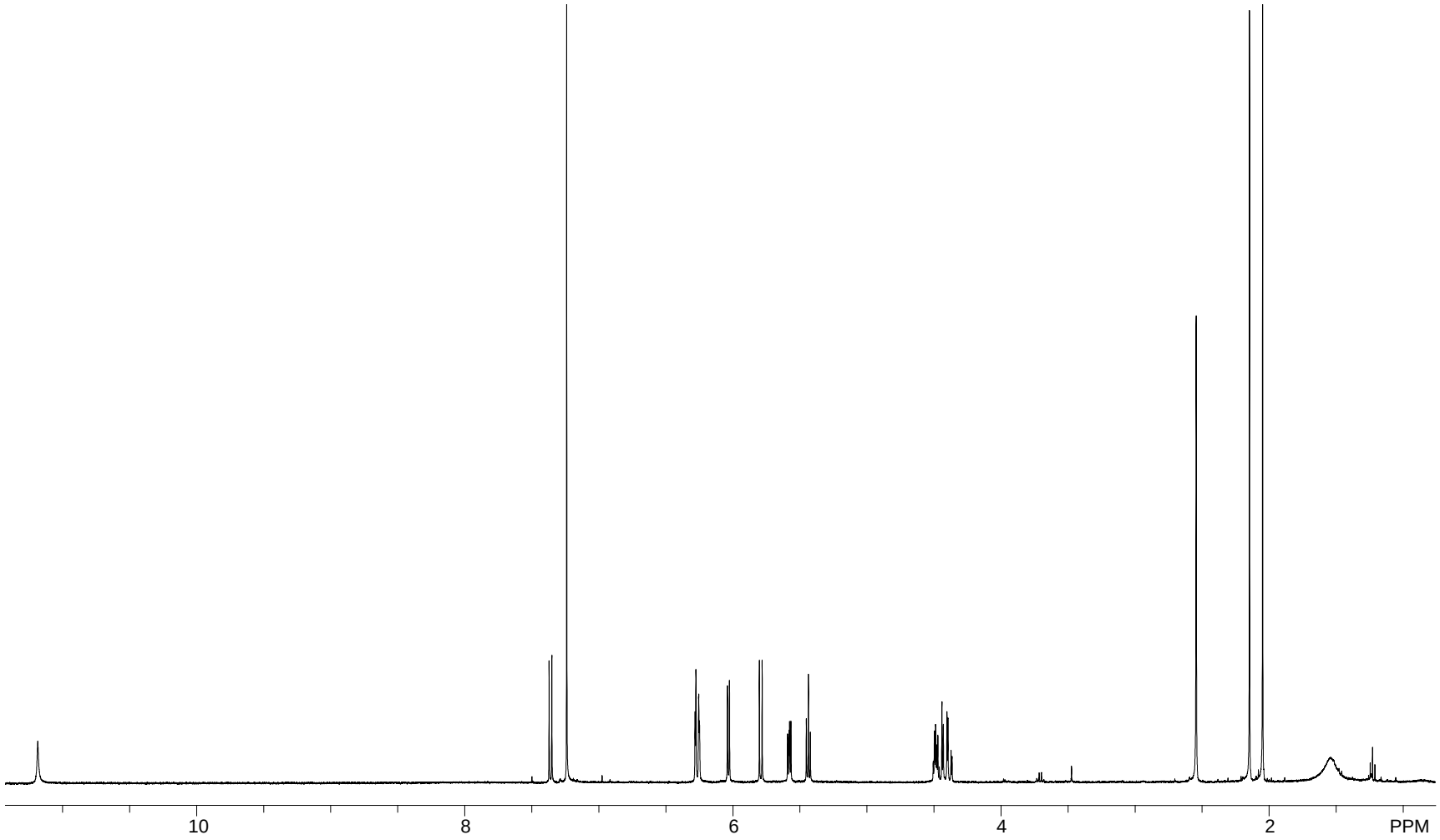

Figure A12. ^{1}H NMR Spectrum of Kipukasin H (**3.2**; $CDCl_3$, 400 MHz)

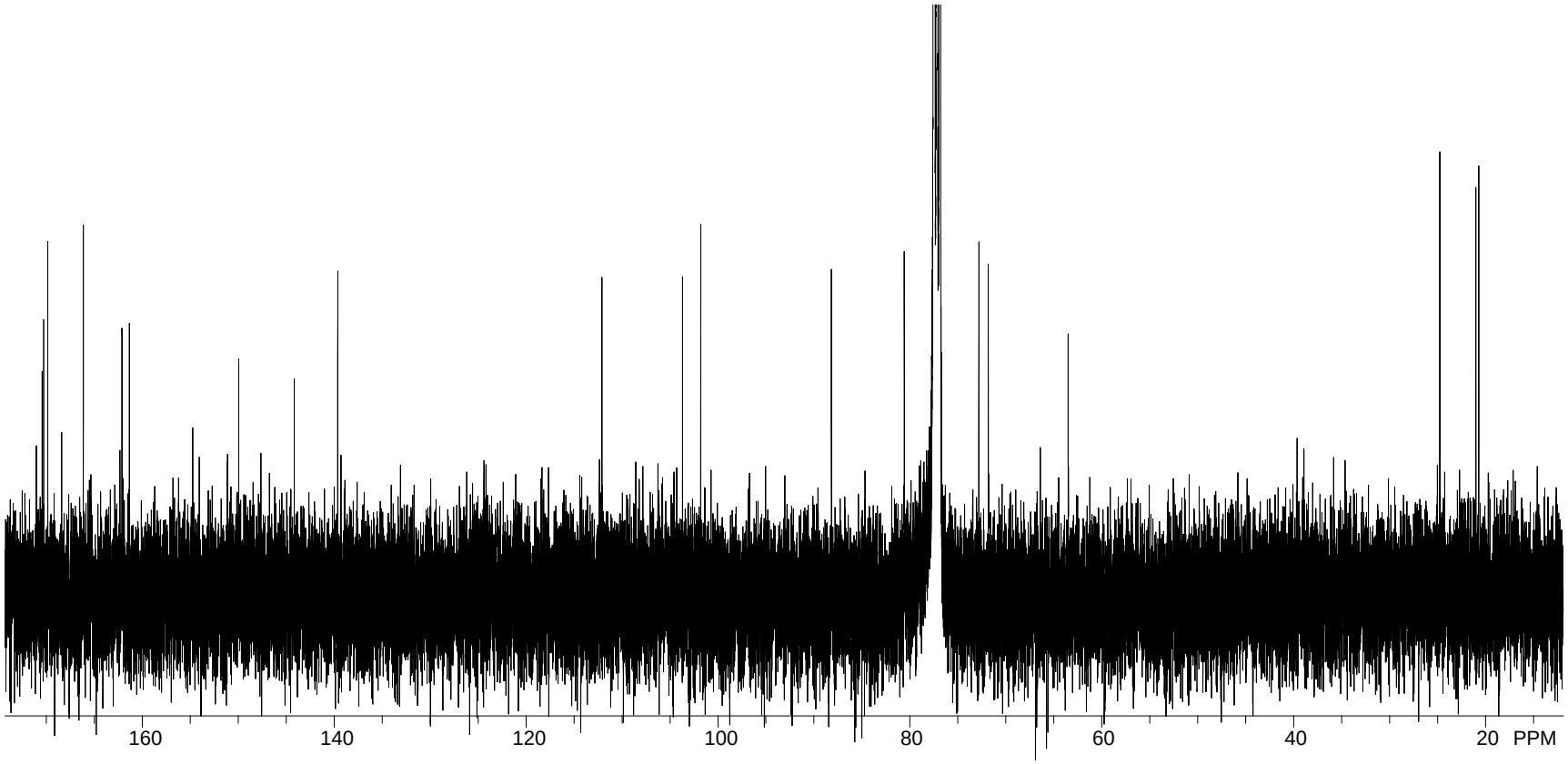

Figure A13. ^{13}C NMR Spectrum of Kipukasin H (**3.2**; $CDCl_3$, 100 MHz)

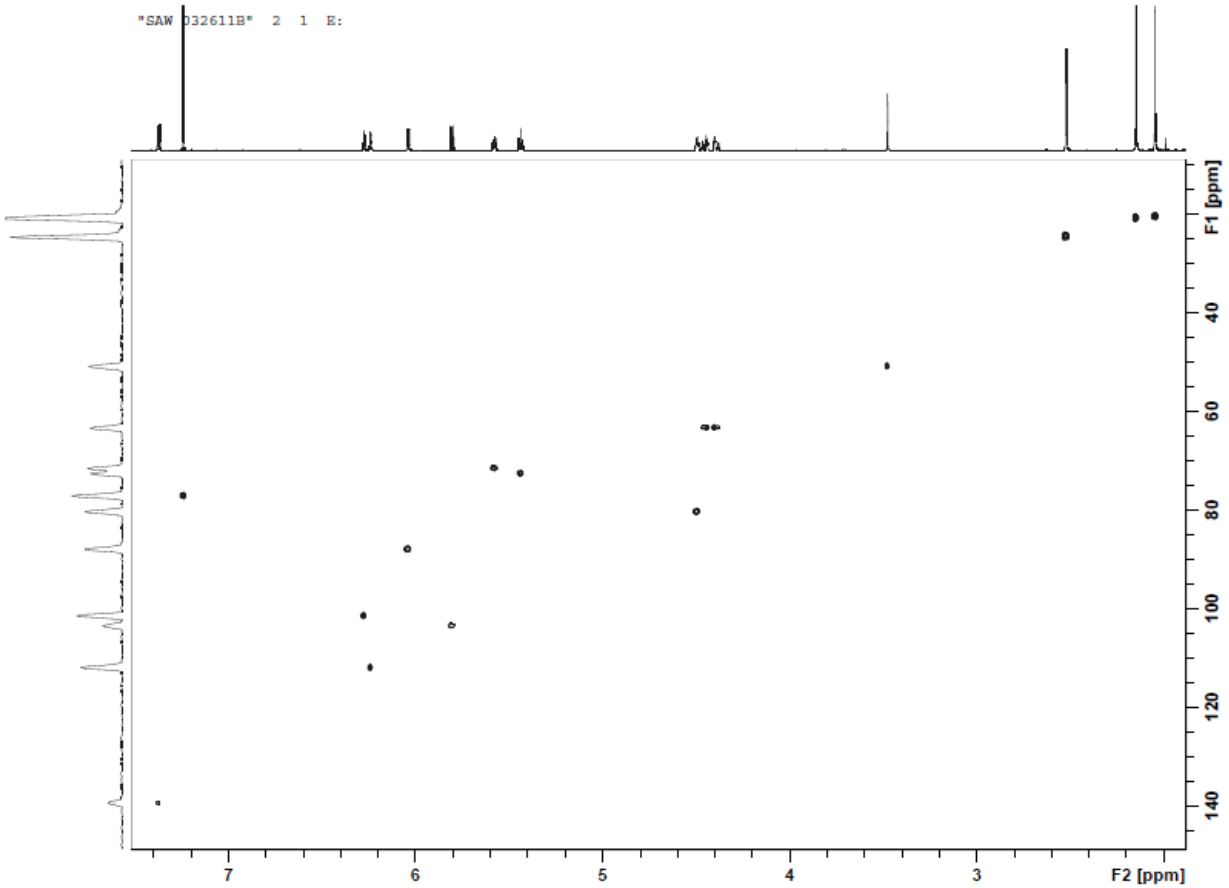

Figure A14. HSQC NMR Spectrum of Kipukasin H (**3.2**; $CDCl_3$, 600 MHz)

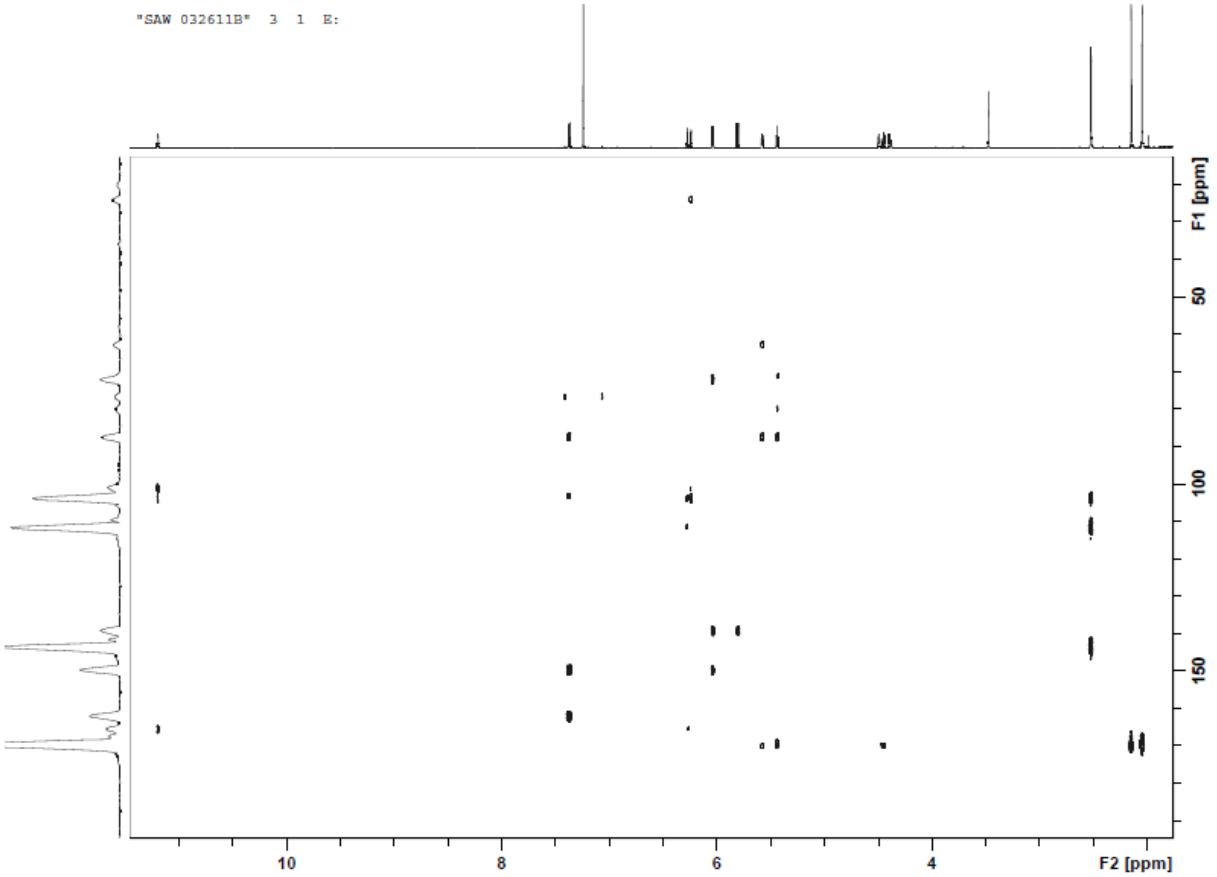

Figure A15. HMBC NMR Spectrum of Kipukasin H (**3.2**; $CDCl_3$, 600 MHz)

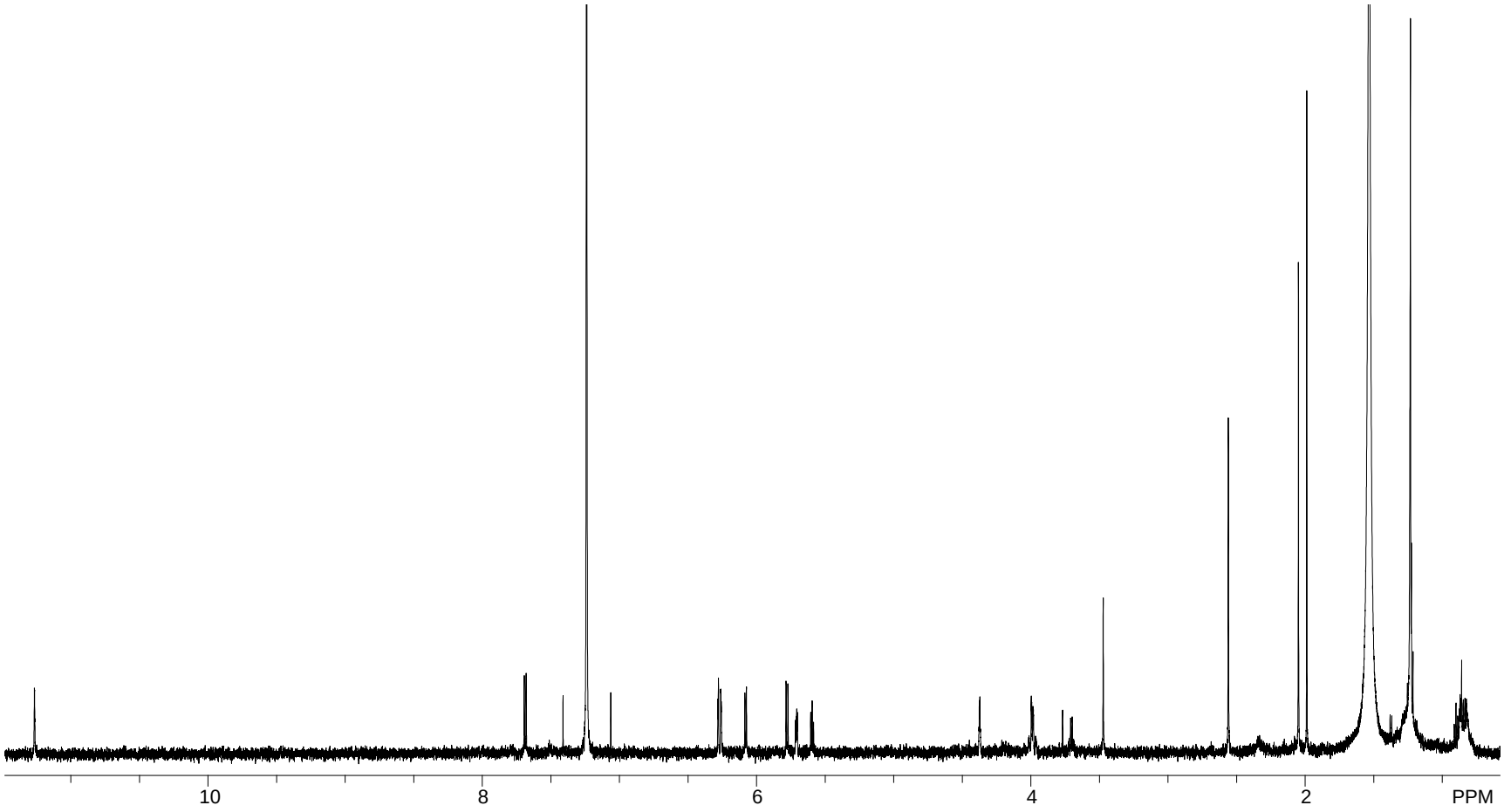

Figure A16. ^{1}H NMR Spectrum of Kipukasin I (**3.3**; $CDCl_3$, 600 MHz)

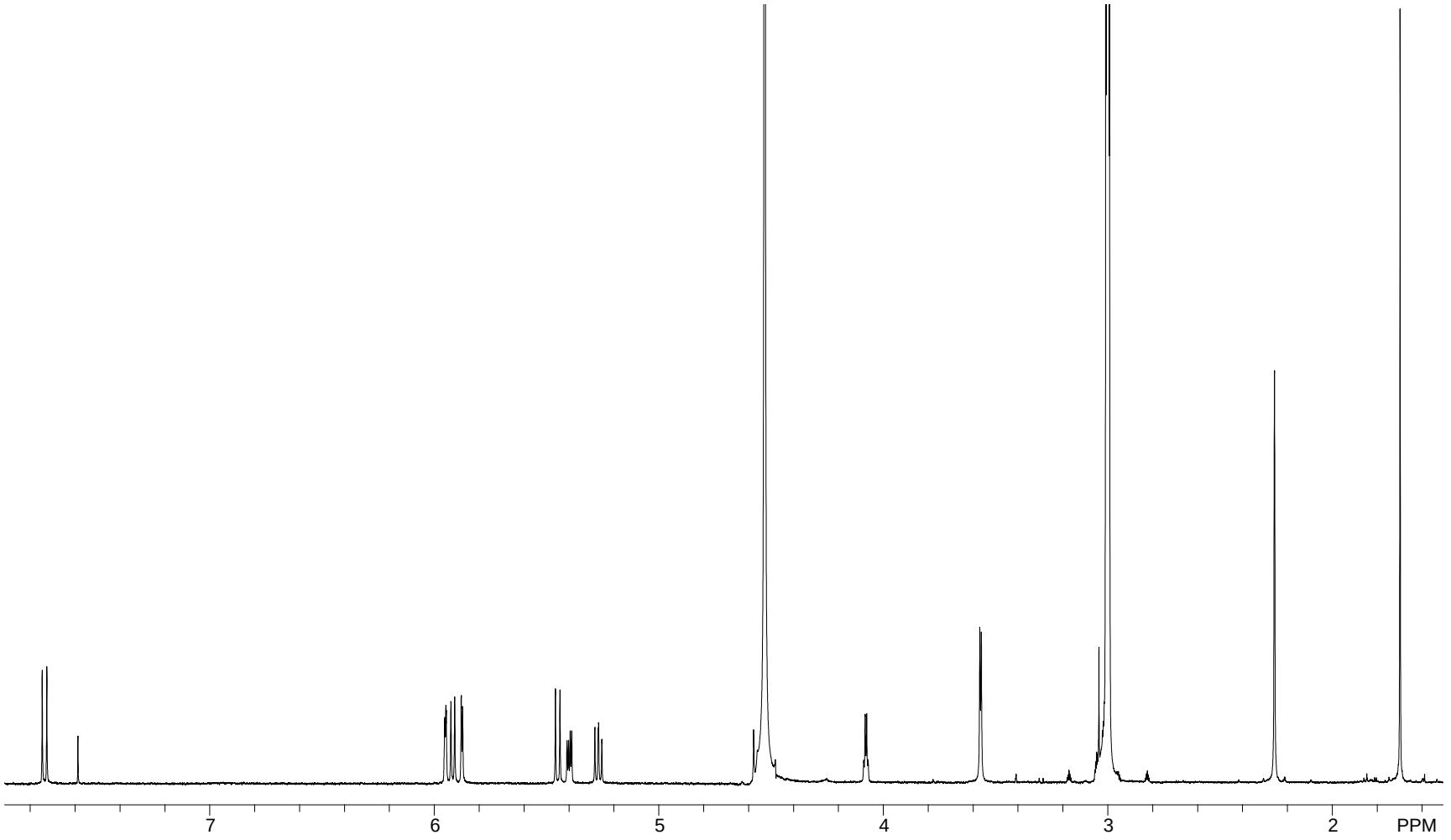

Figure A17. ^{1}H NMR Spectrum of Kipukasin I (**3.3**; CD_3OD, 400 MHz)

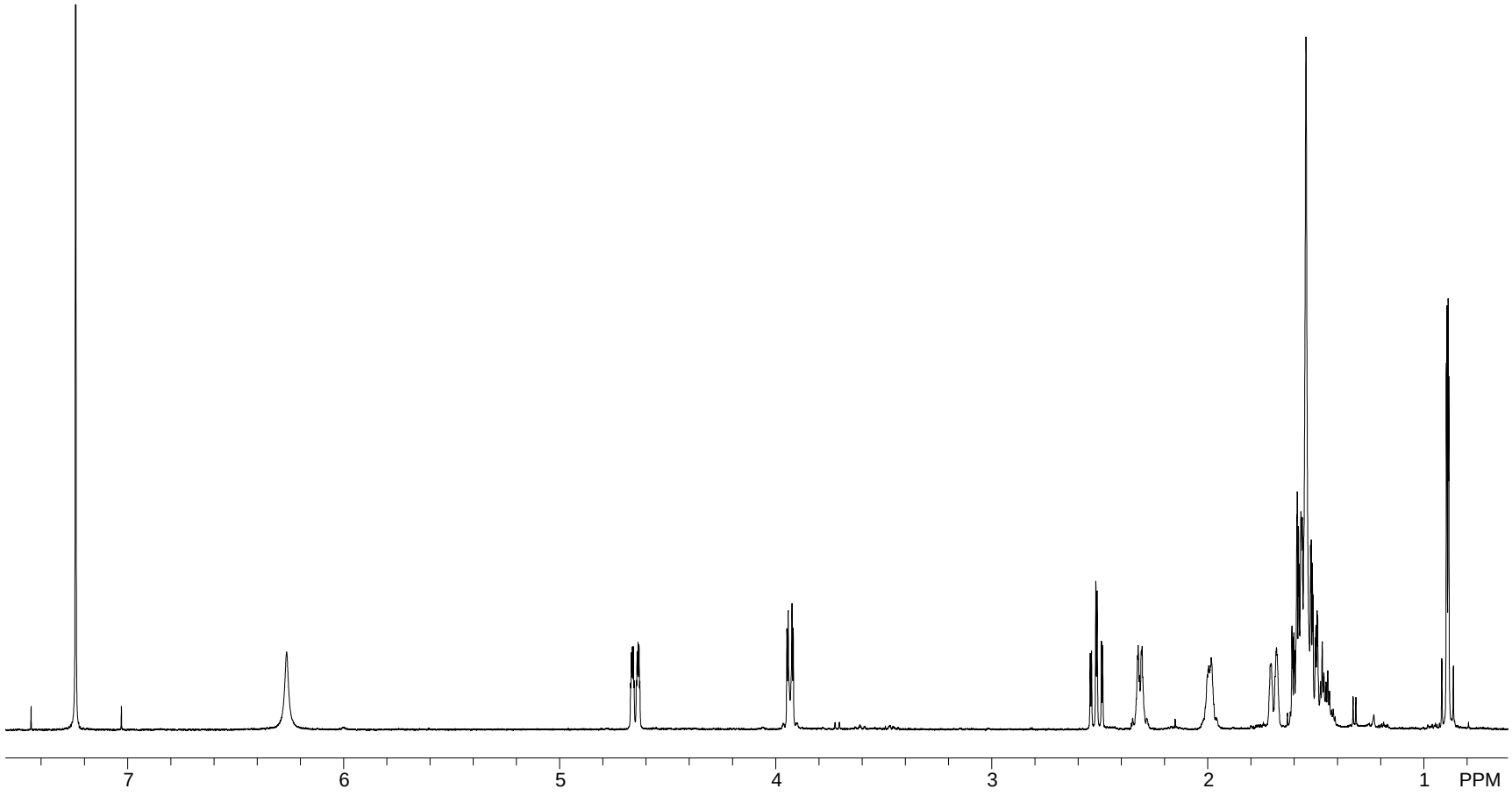

Figure A18. ^{1}H NMR Spectrum of Cyclo-(L-pipecolinyl-aminocyclopropane-carboxylic acid) (**4.1**; $CDCl_3$, 500 MHz)

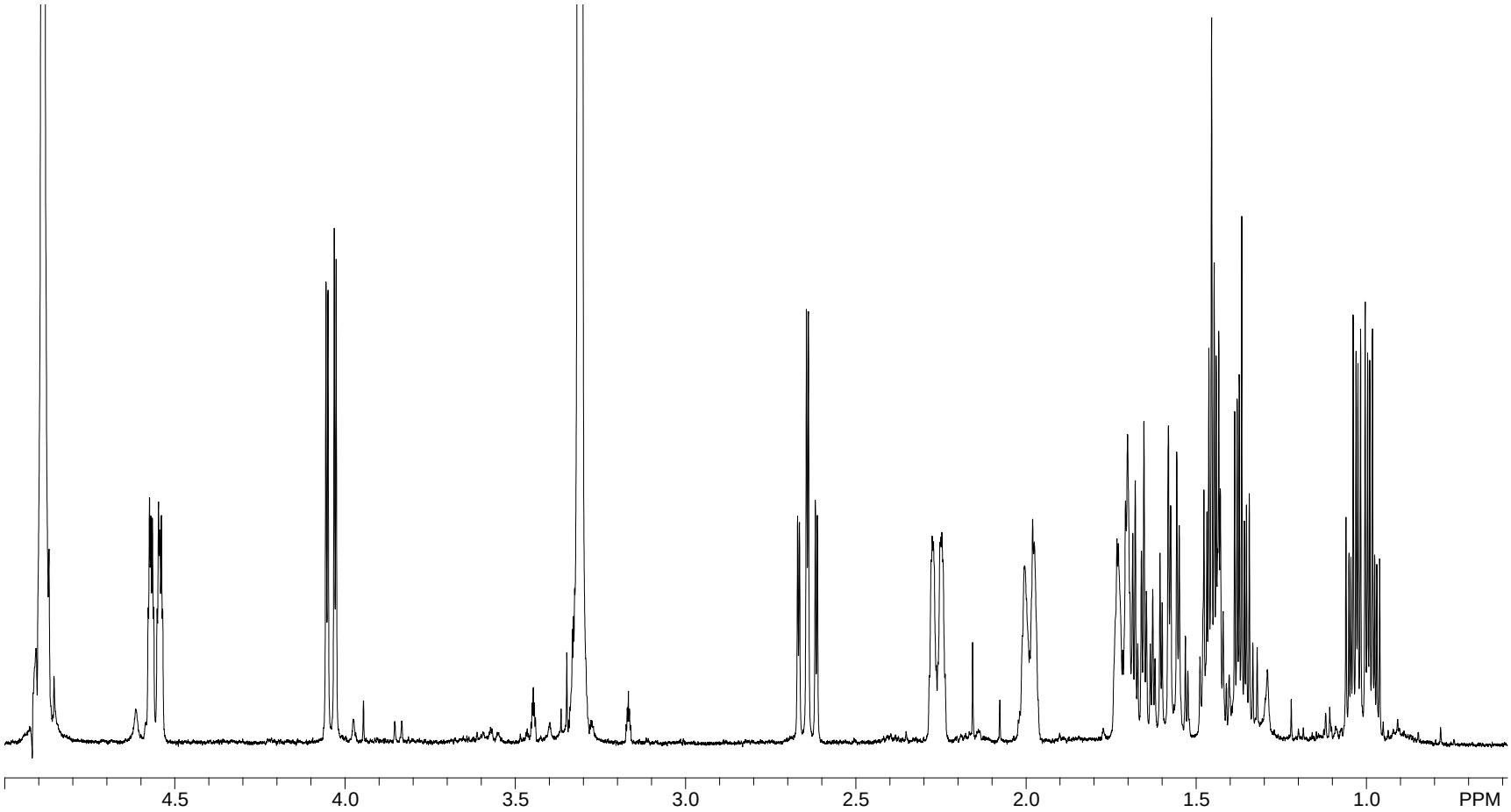

Figure A19. ^{1}H NMR Spectrum of Cyclo-(L-pipecolinyl-aminocyclopropane-carboxylic acid) (**4.1**; CD_3OD, 500 MHz)

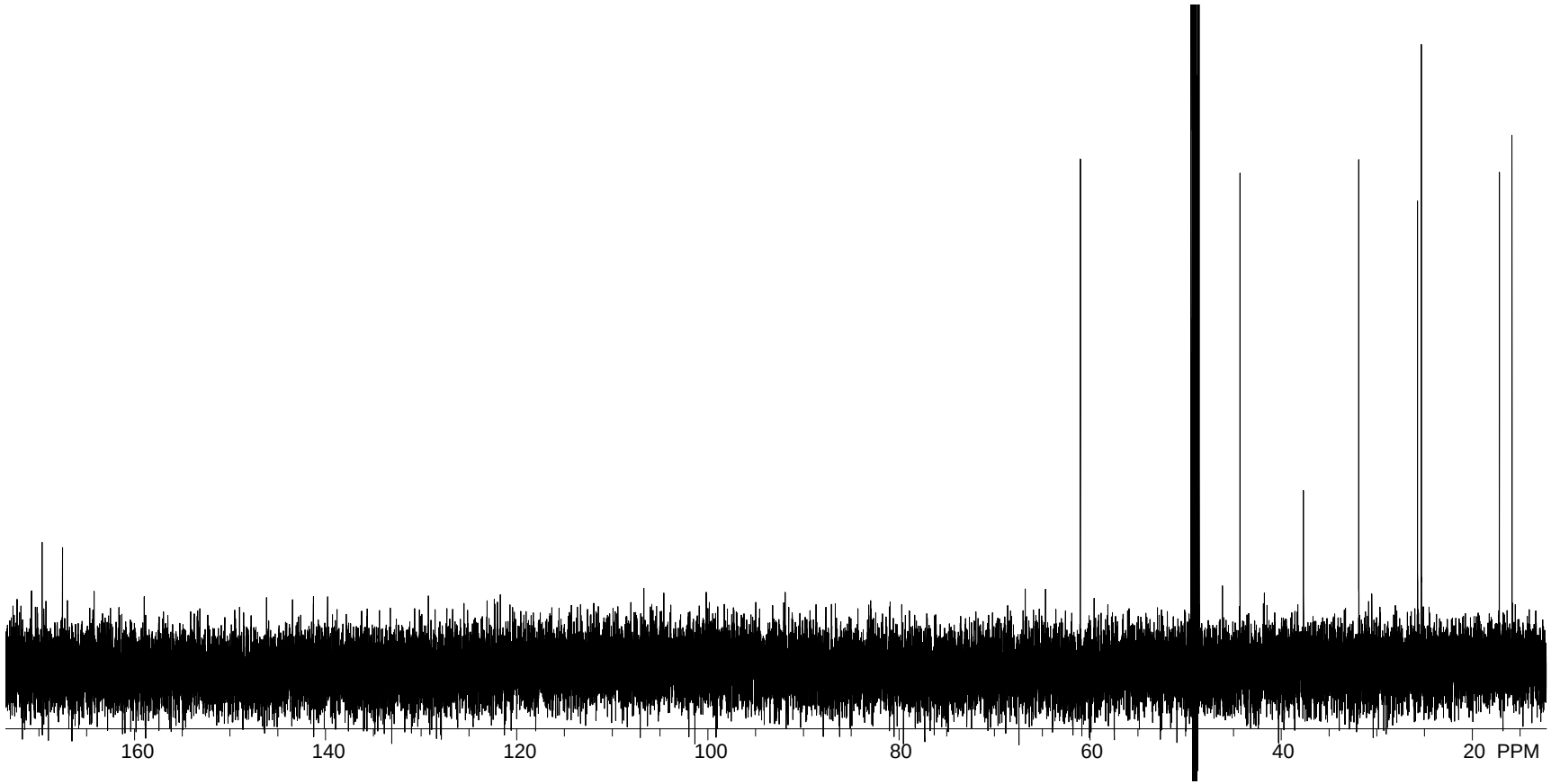

Figure A20. ^{13}C NMR Spectrum of Cyclo-(L-pipecolinyl-aminocyclopropane-carboxylic acid) (**4.1**; CD_3OD, 150 MHz)

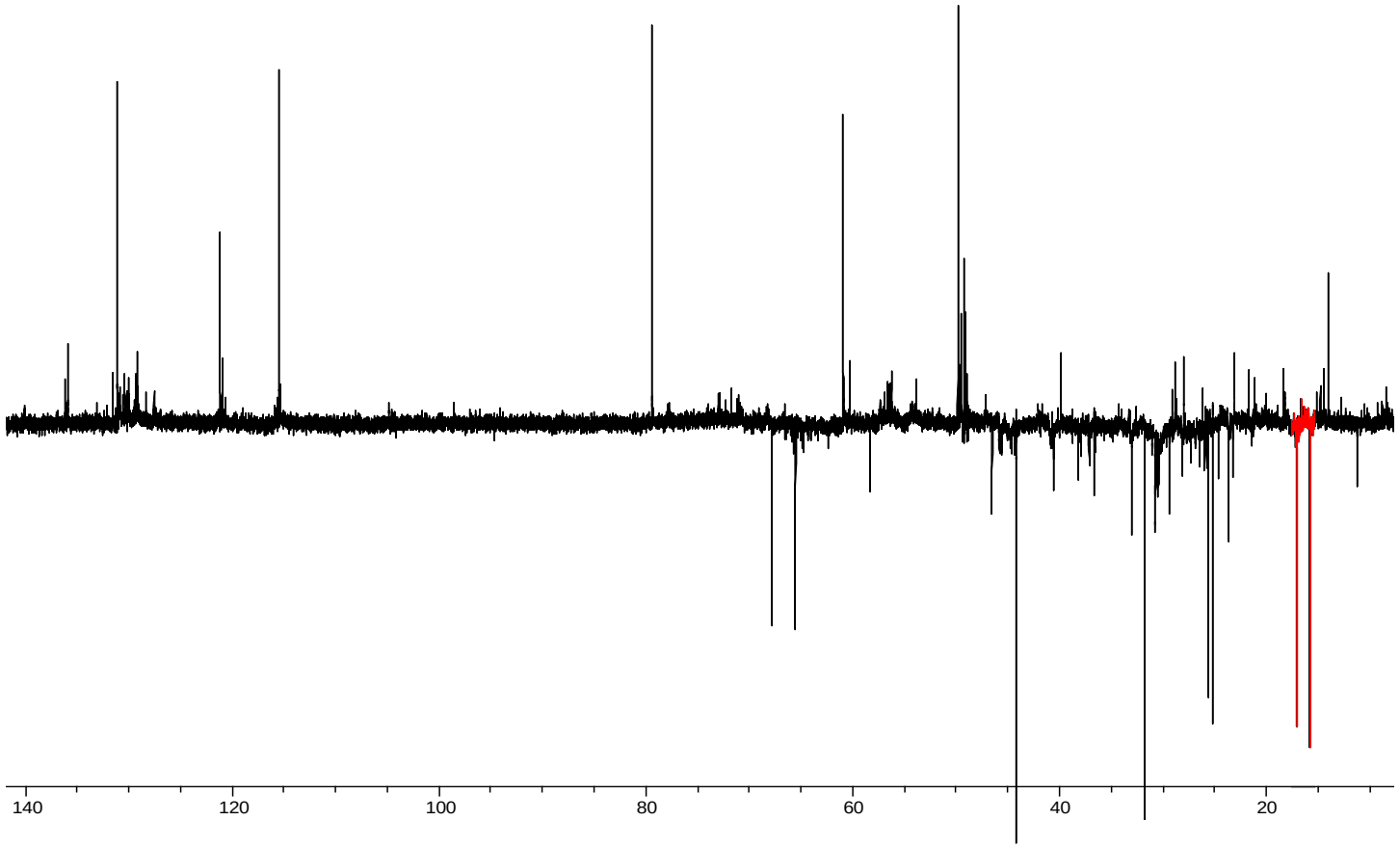

Figure A21. DEPT NMR Spectrum of Crude Extract of *Trichothecium crotocinigenum* (NRRL 62714) with Diagnostic CH_2 Signals from **4.1** Overlaid in Red (CD_3OD, 100 MHz)

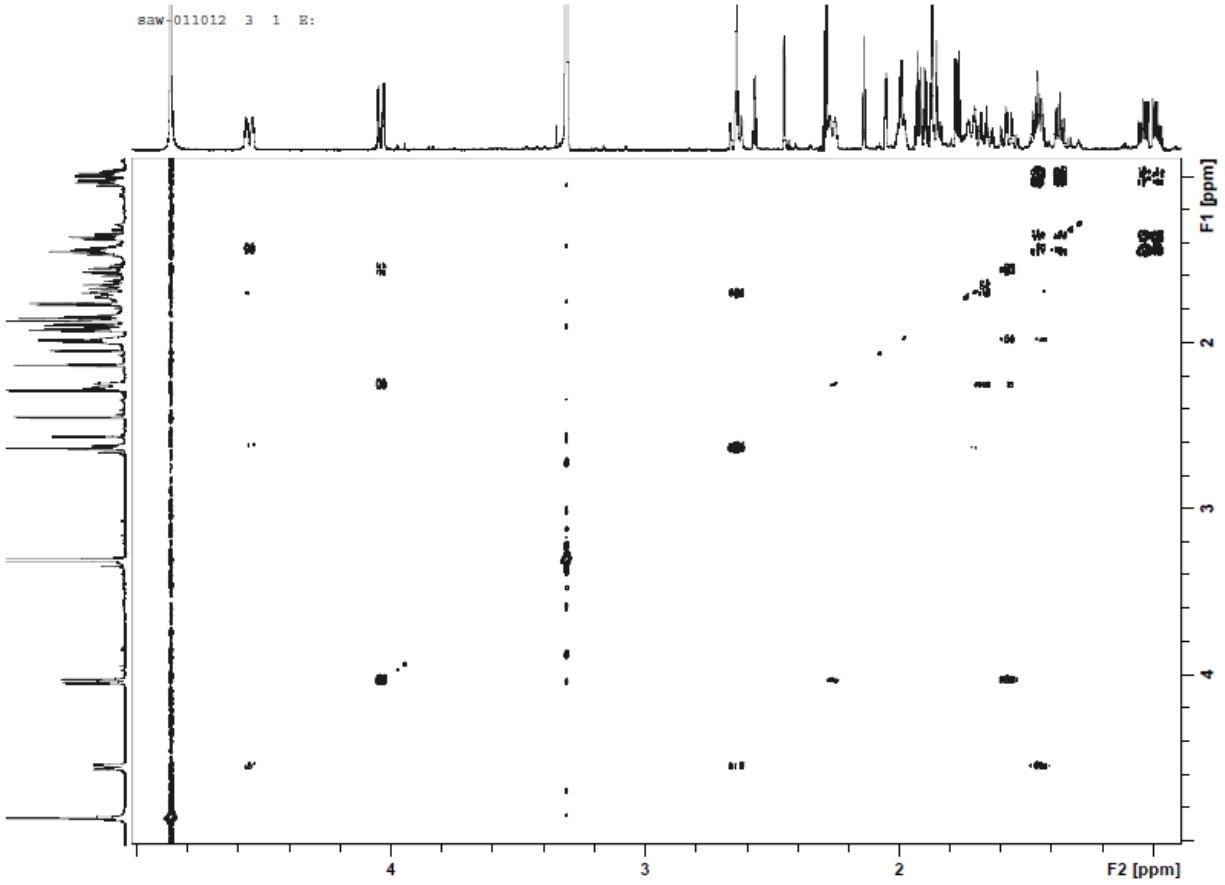

Figure A22. COSY NMR Spectrum of Cyclo-(L-pipecolinyl-aminocyclopropane-carboxylic acid) (**4.1**; CD_3OD, 600 MHz)

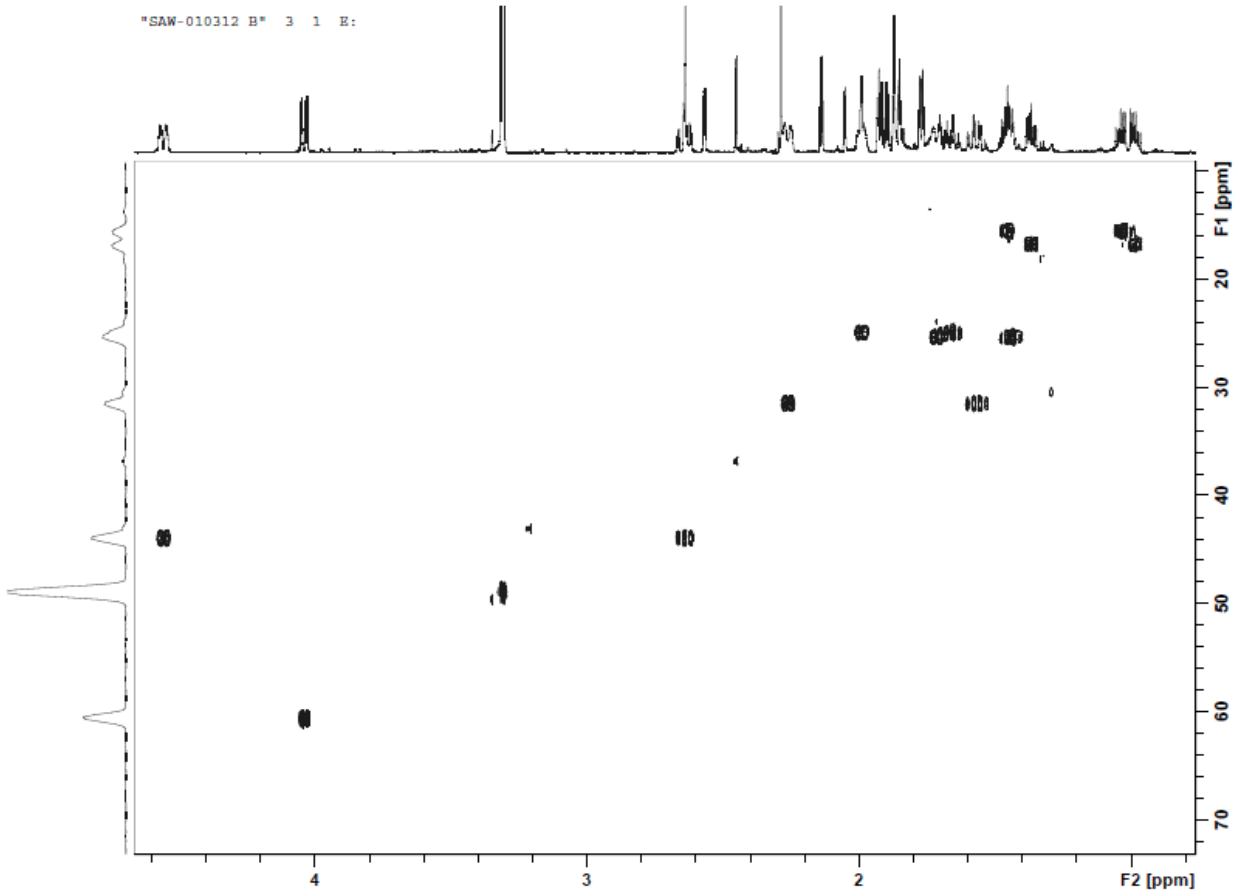

Figure A23. HSQC NMR Spectrum of Cyclo-(L-pipecolinyl-aminocyclopropane-carboxylic acid) (**4.1**; CD_3OD, 600 MHz)

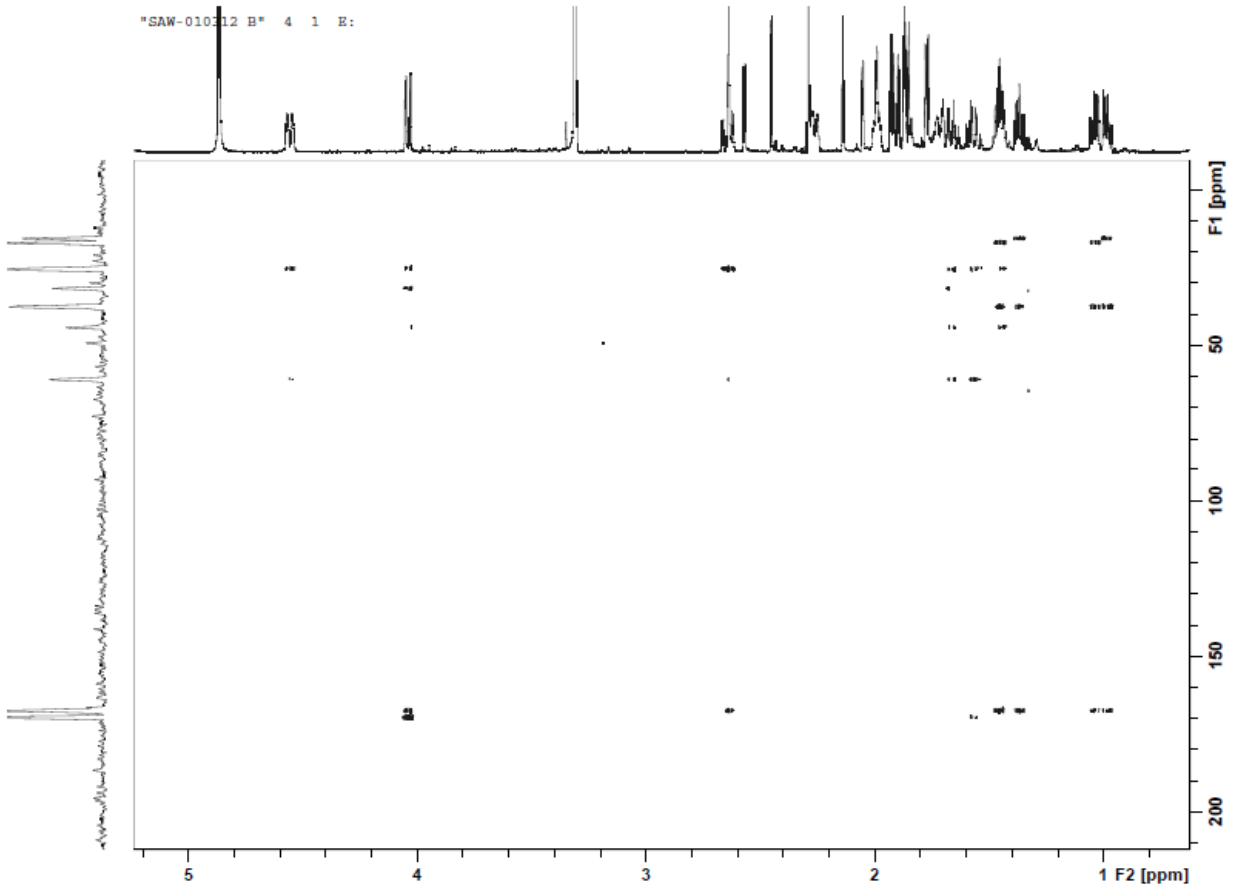

Figure A24. HMBC NMR Spectrum of Cyclo-(L-pipecolinyl-aminocyclopropane-carboxylic acid) (**4.1**; CD_3OD, 600 MHz)

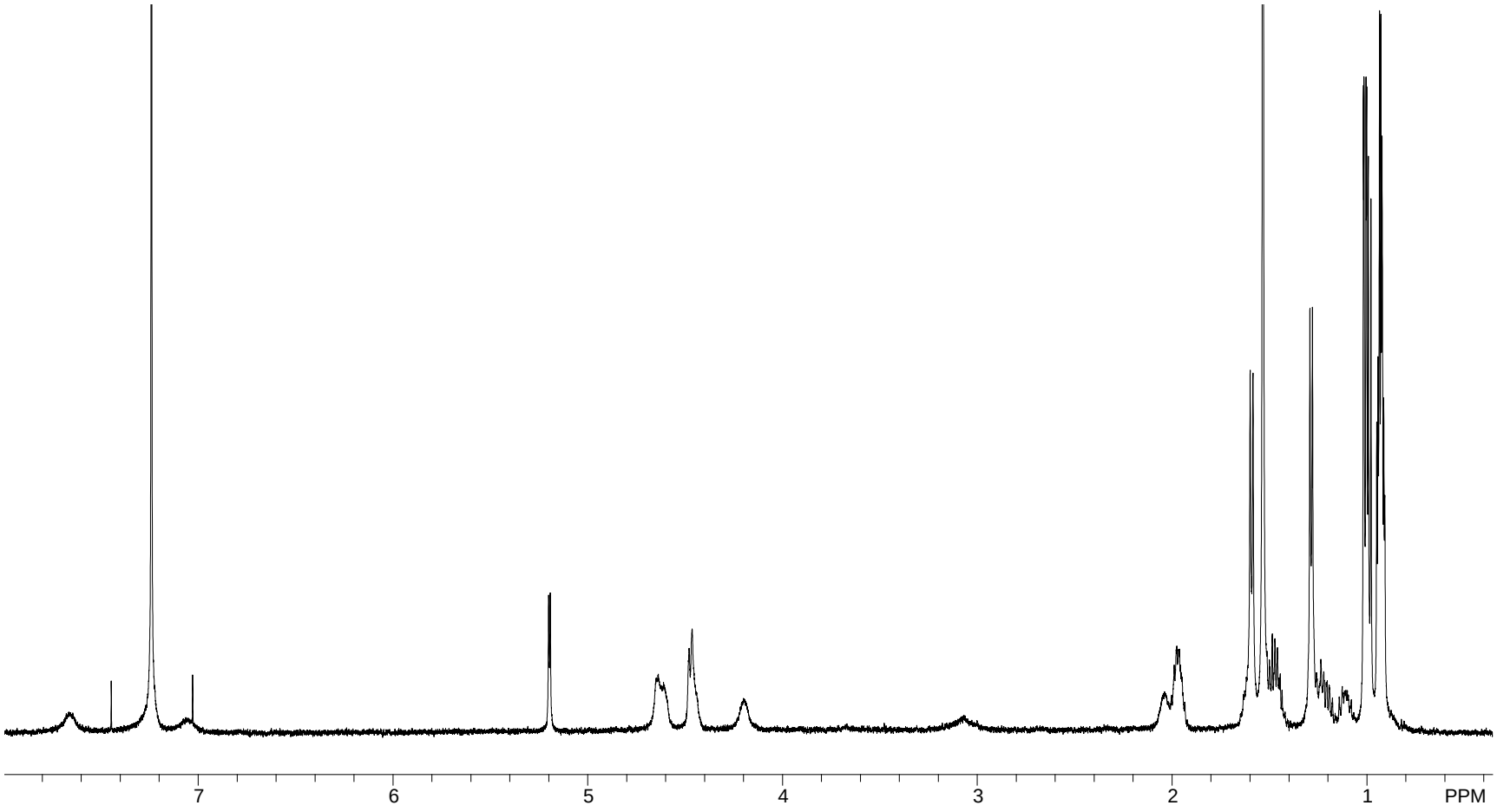

Figure A25. ^{1}H NMR Spectrum of Pentadepsipeptide **4.4** ($CDCl_3$, 500 MHz)

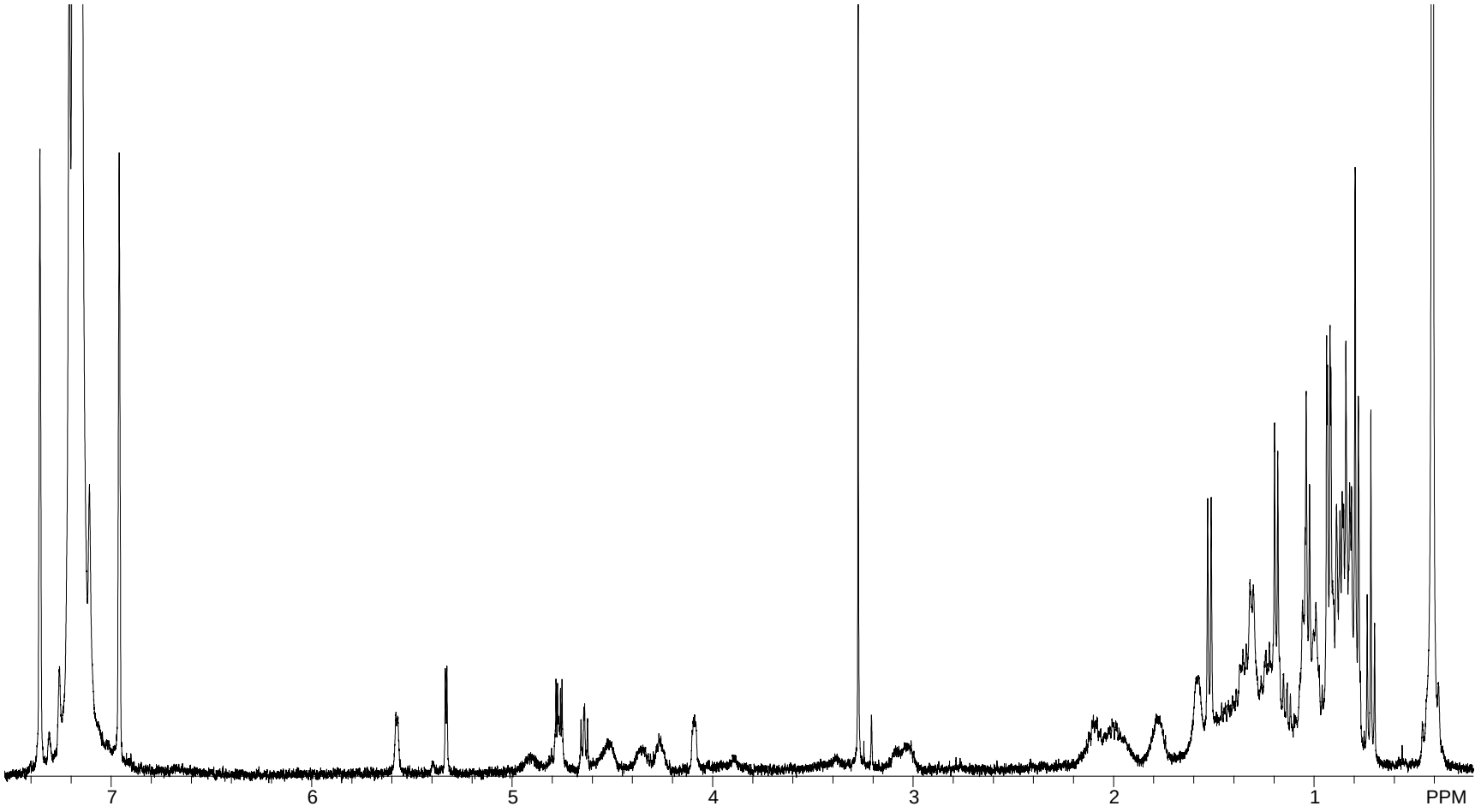

Figure A26. ^{1}H NMR Spectrum of Pentadepsipeptide **4.4** (Benzene–d_6, 500 MHz)

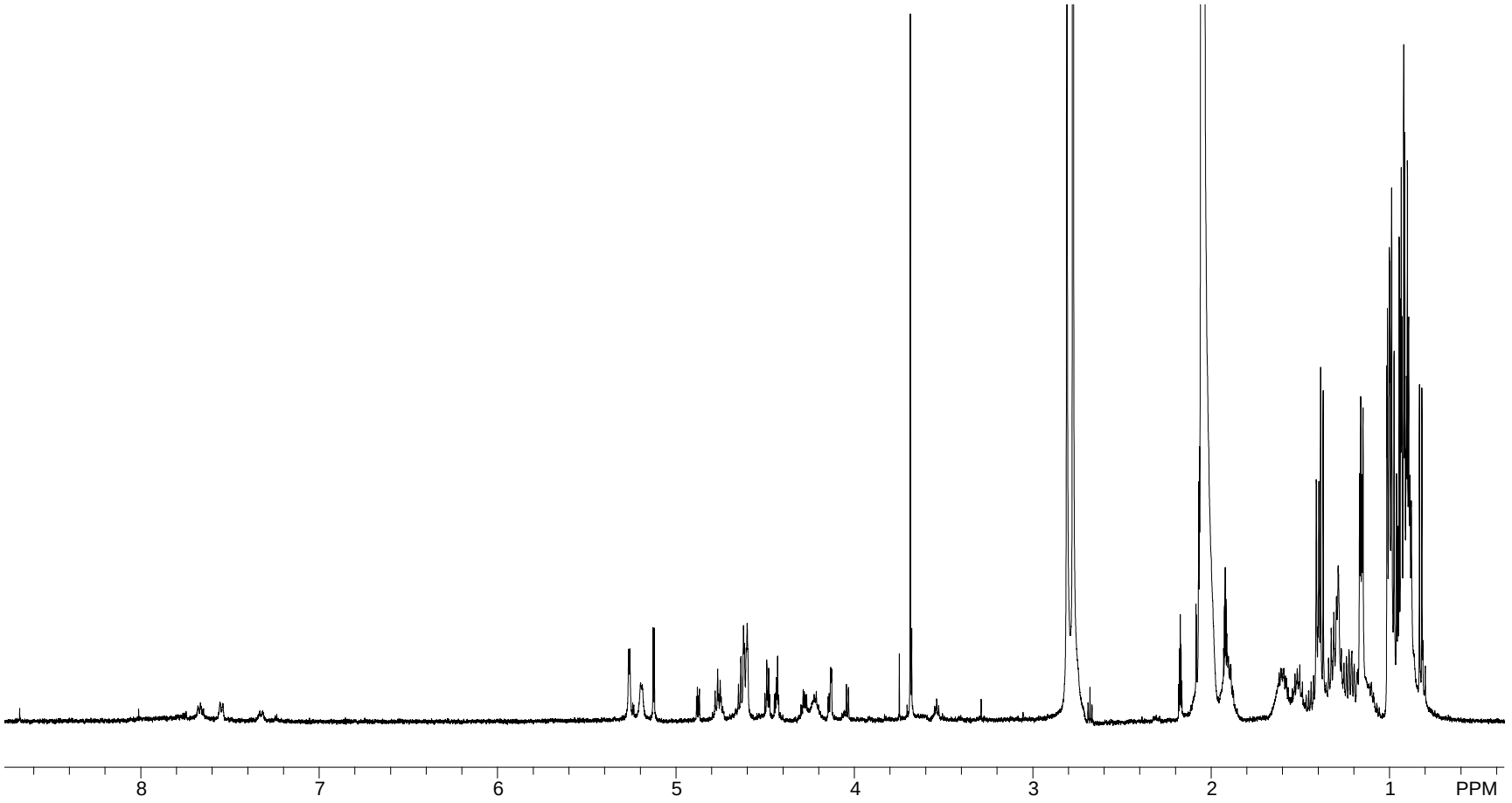

Figure A27. ^{1}H NMR Spectrum of Pentadepsipeptide **4.4** (Acetone–d_6, 500 MHz)

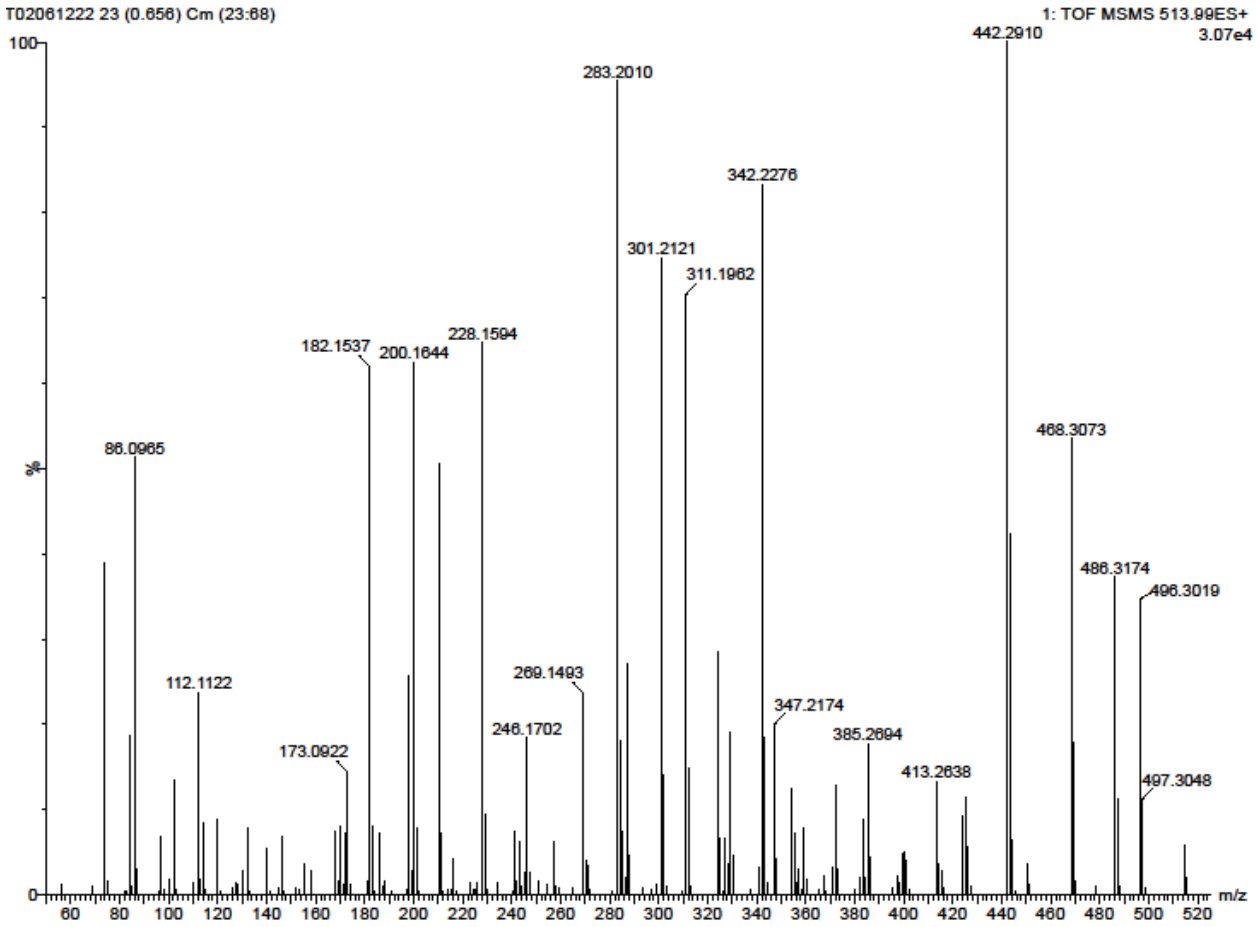

Figure A28. HRESITOFMSMS Data for Pentadepsipeptide **4.4**

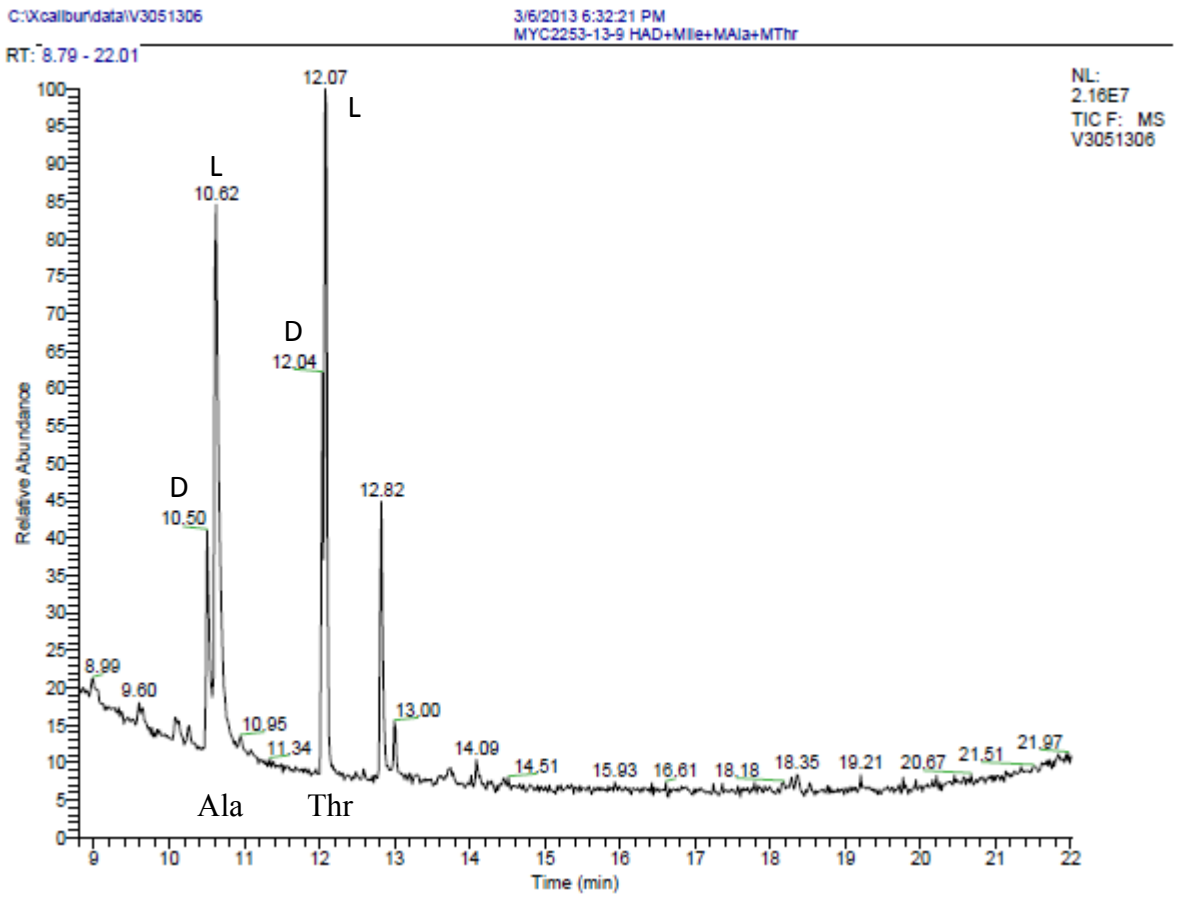

Figure A29. Chromatogram of the Co-injection of Derivatized Hydrolyzate from Pentadepsipeptide **4.4** with the D– and L–Standards of Ala and Thr

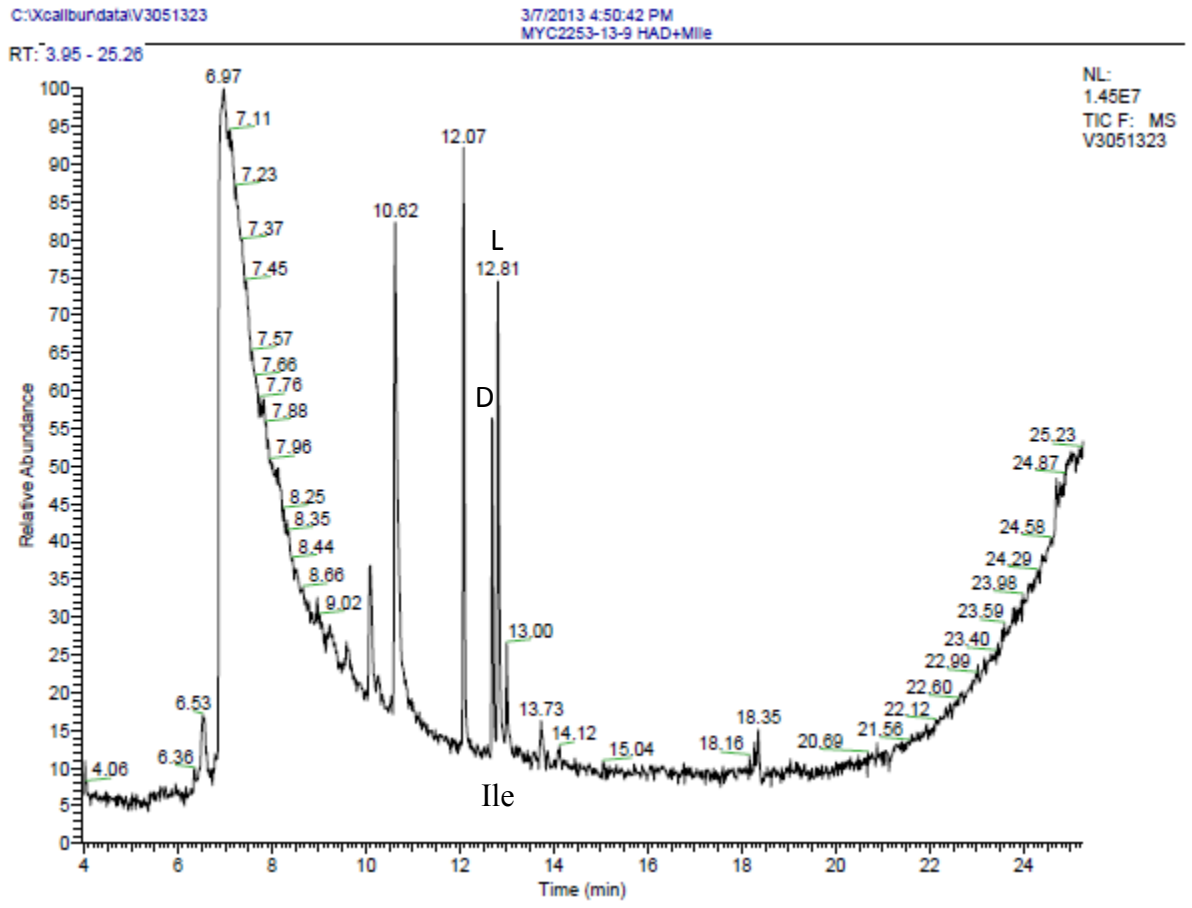

Figure A30. Chromatogram of the Co-injection of Derivatized Hydrolyzate from Pentadepsipeptide **4.4** with the D– and L–Standards of Ile

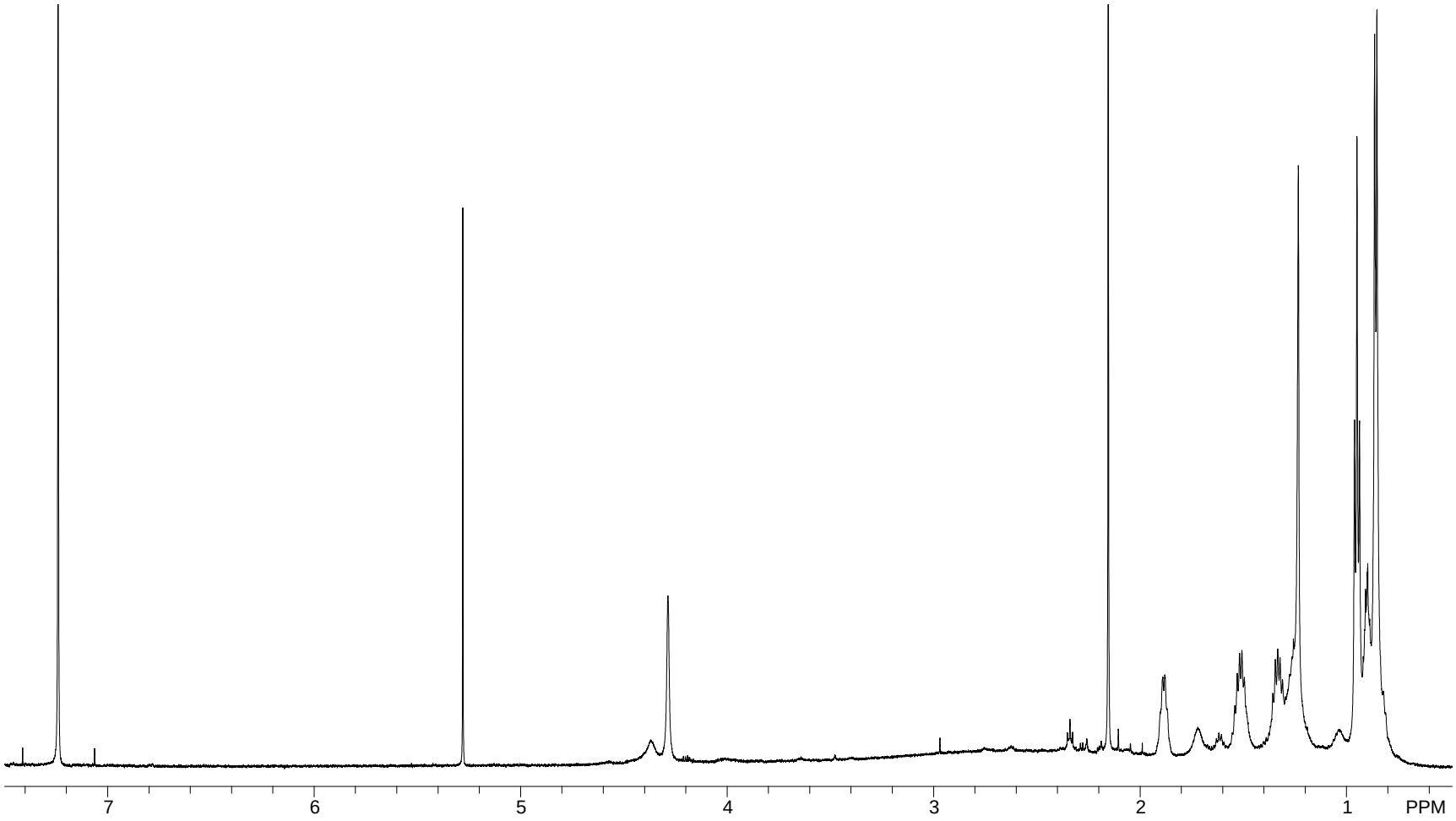

Figure A31. ^{1}H NMR Spectrum of the CH_2Cl_2 partition of the Hydrolyzate of **4.5** ($CDCl_3$, 500 MHz)

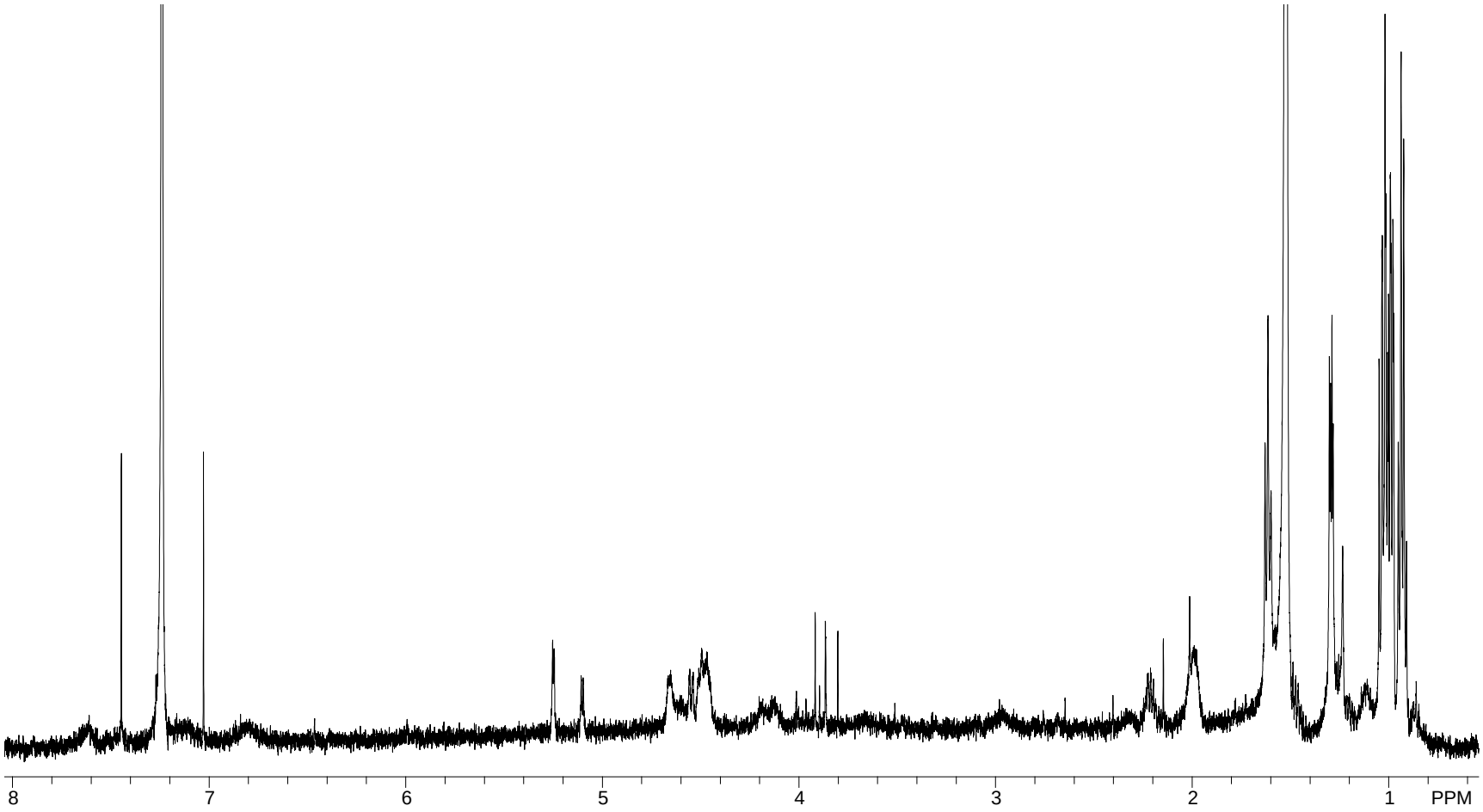

Figure A32. ^{1}H NMR Spectrum of Pentadepsipeptide **4.5** ($CDCl_3$, 500 MHz)

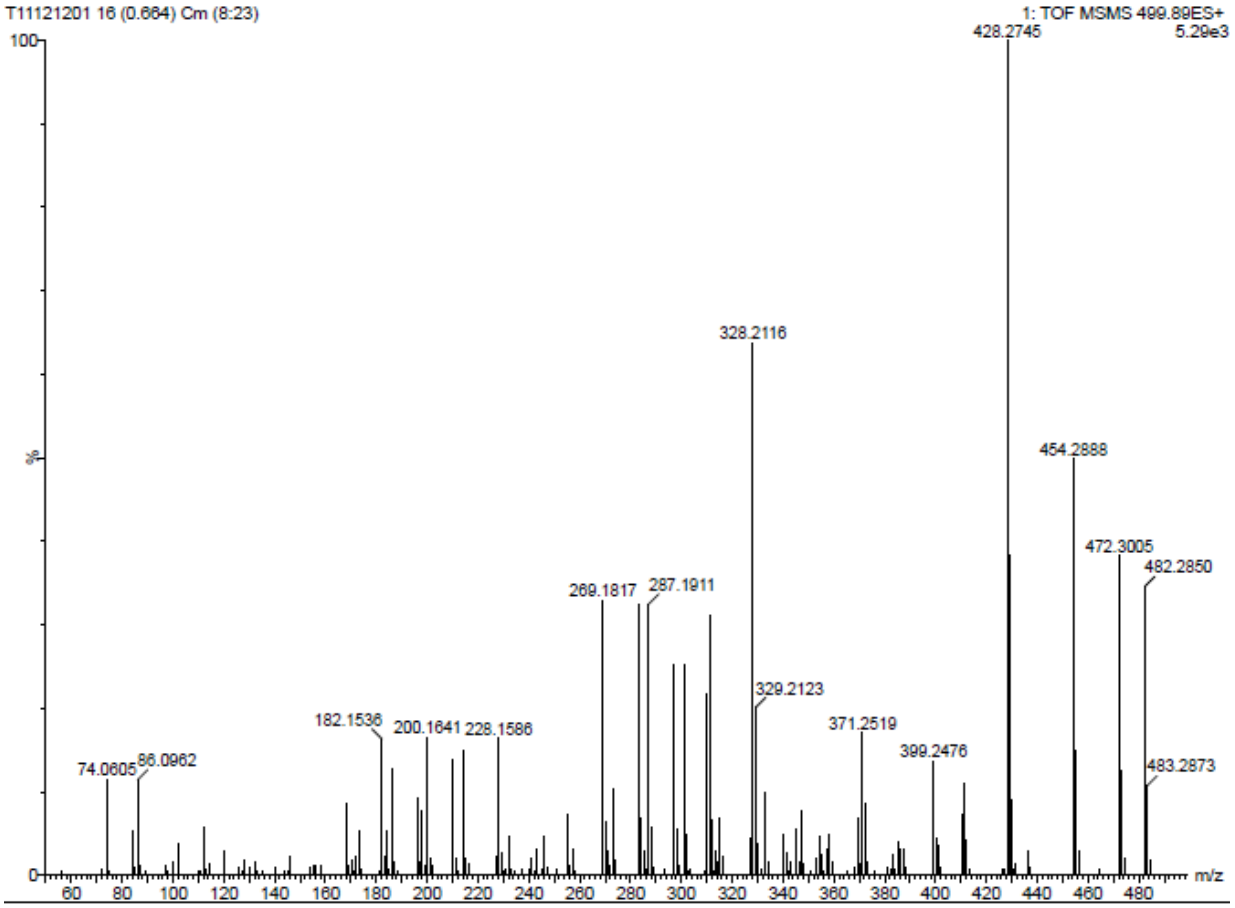

Figure A33. HRESITOFMSMS Data for Pentadepsipeptide **4.5**

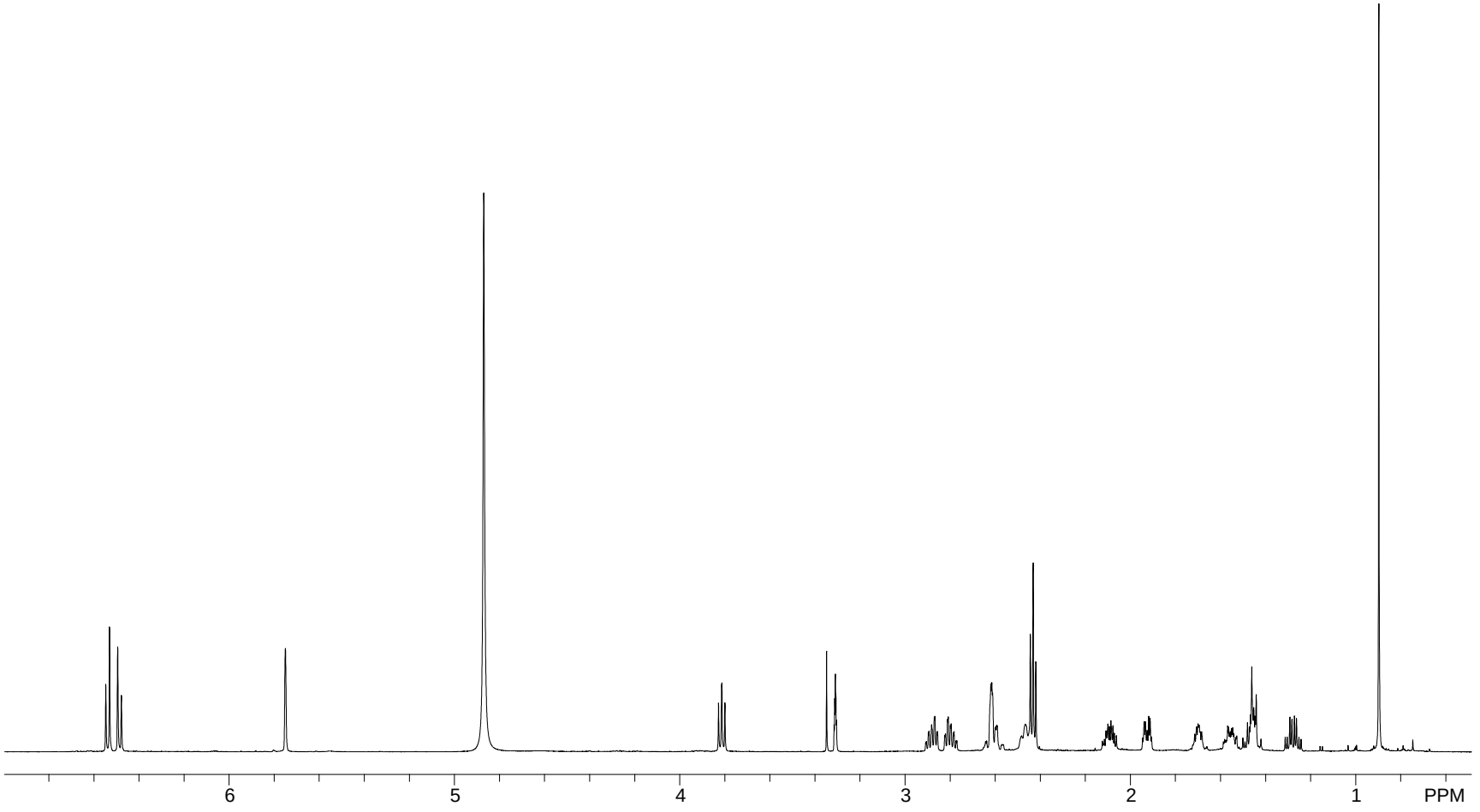

Figure A34. ^{1}H NMR Spectrum of β–Trenbolone (**5.4**; CD_3OD, 600 MHz)

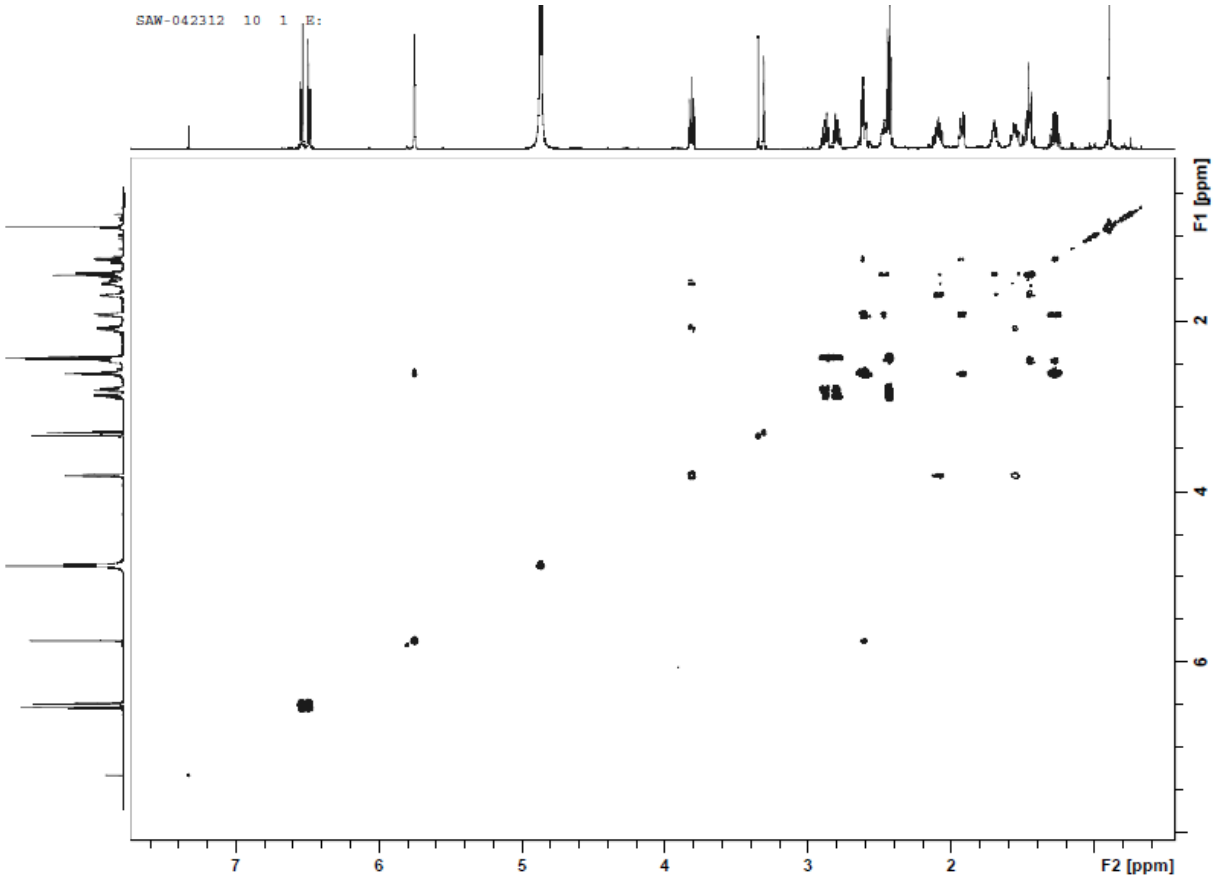

Figure A35. COSY NMR Spectrum of β–Trenbolone (**5.4**; CD_3OD, 600 MHz)

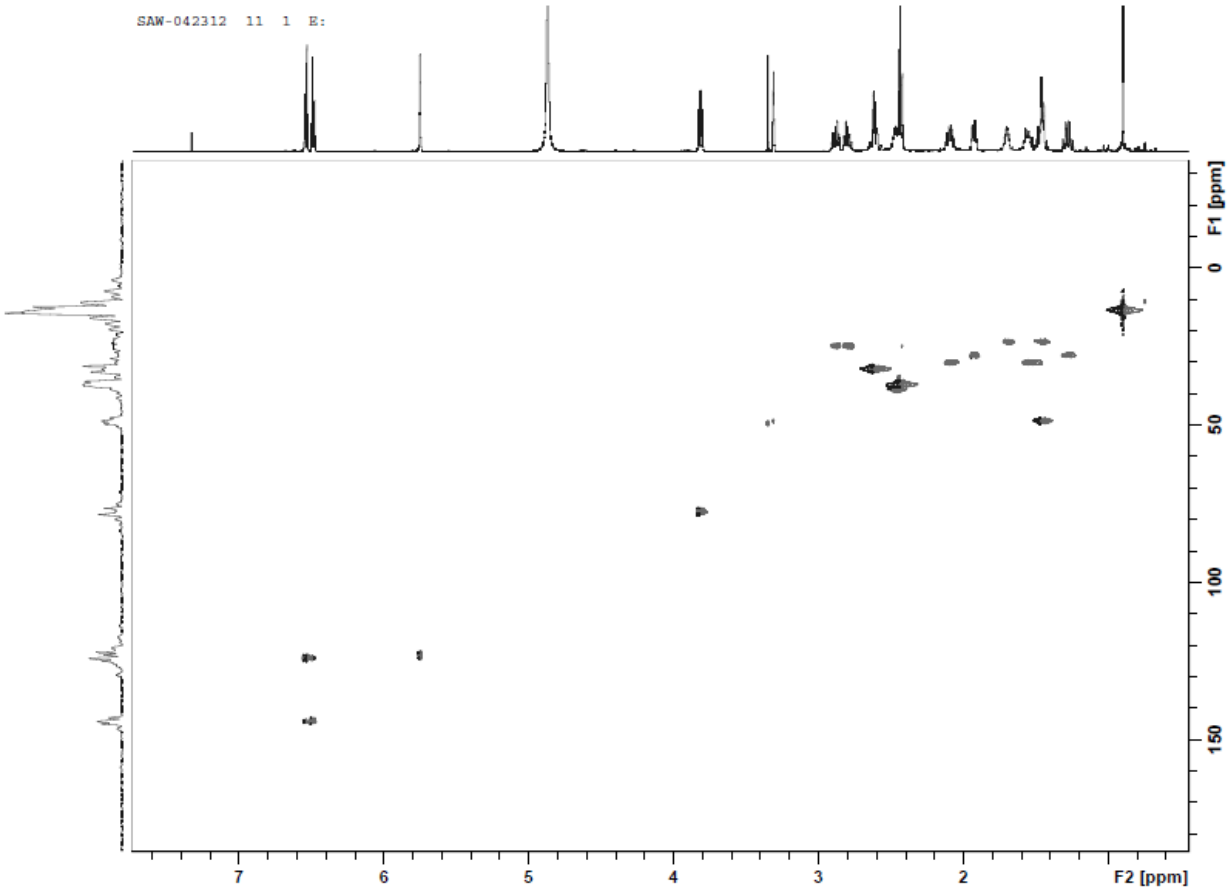

Figure A36. HSQC NMR Spectrum of β–Trenbolone (**5.4**; CD_3OD, 600 MHz)

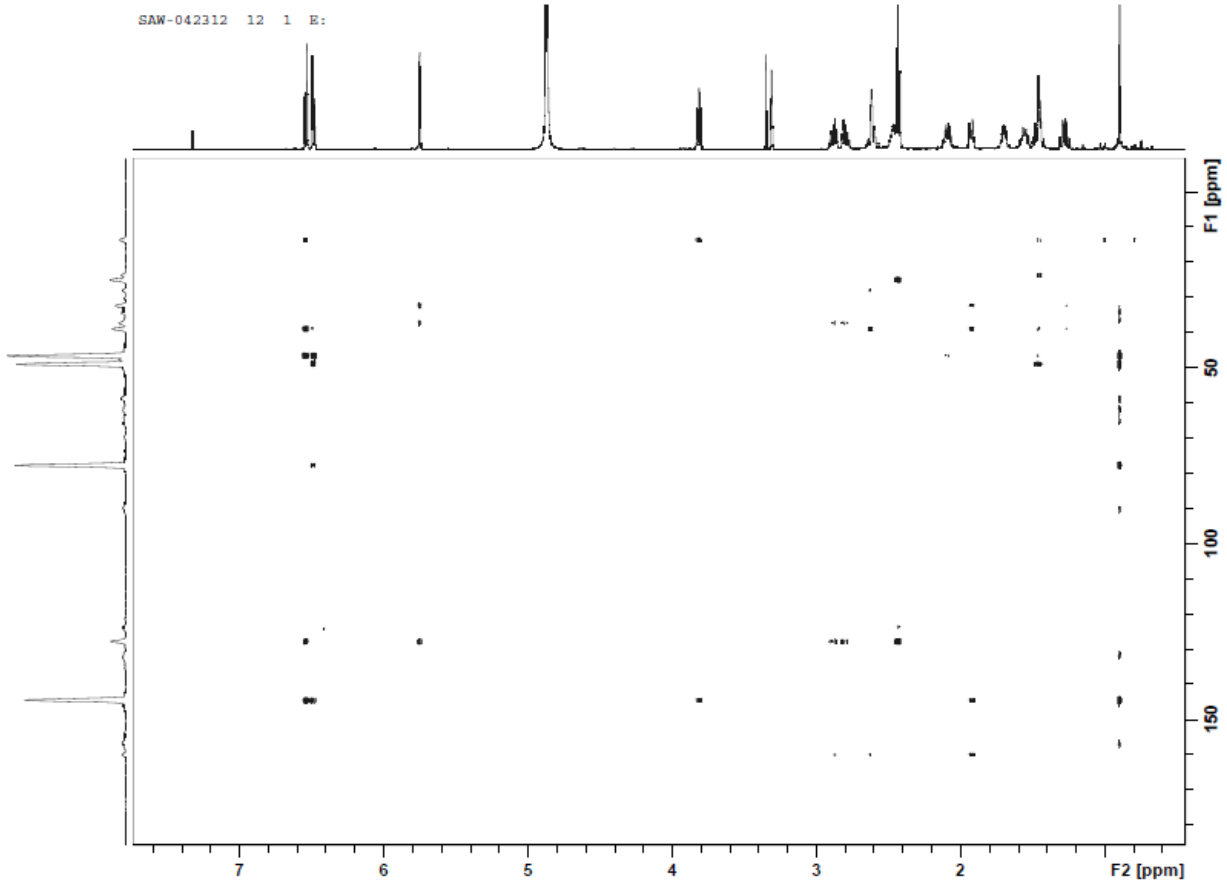

Figure A37. HMBC NMR Spectrum of β–Trenbolone (**5.4**; CD_3OD, 600 MHz)

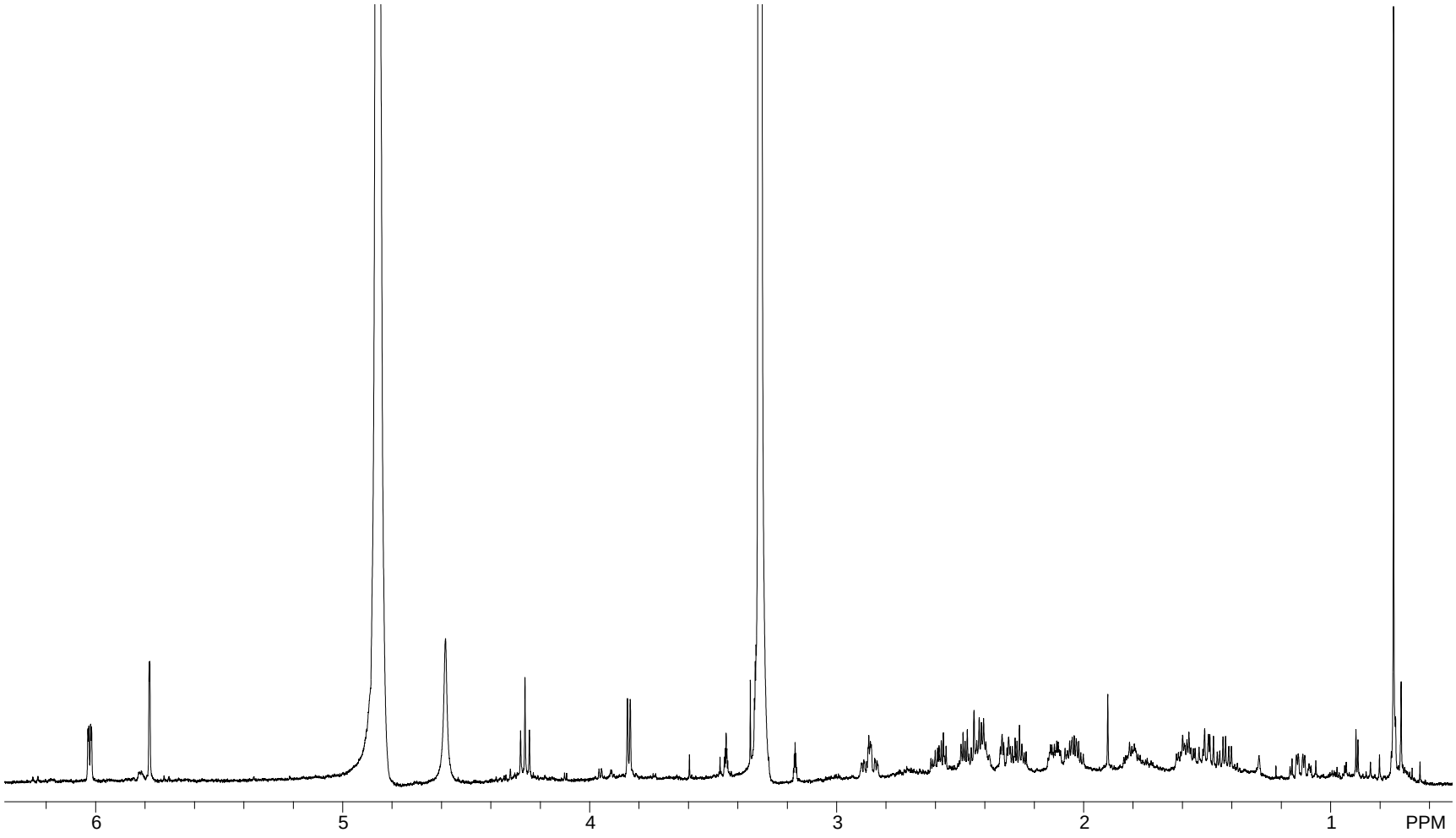

Figure A38. ^{1}H NMR Spectrum of **5.5** (CD_3OD, 500 MHz)

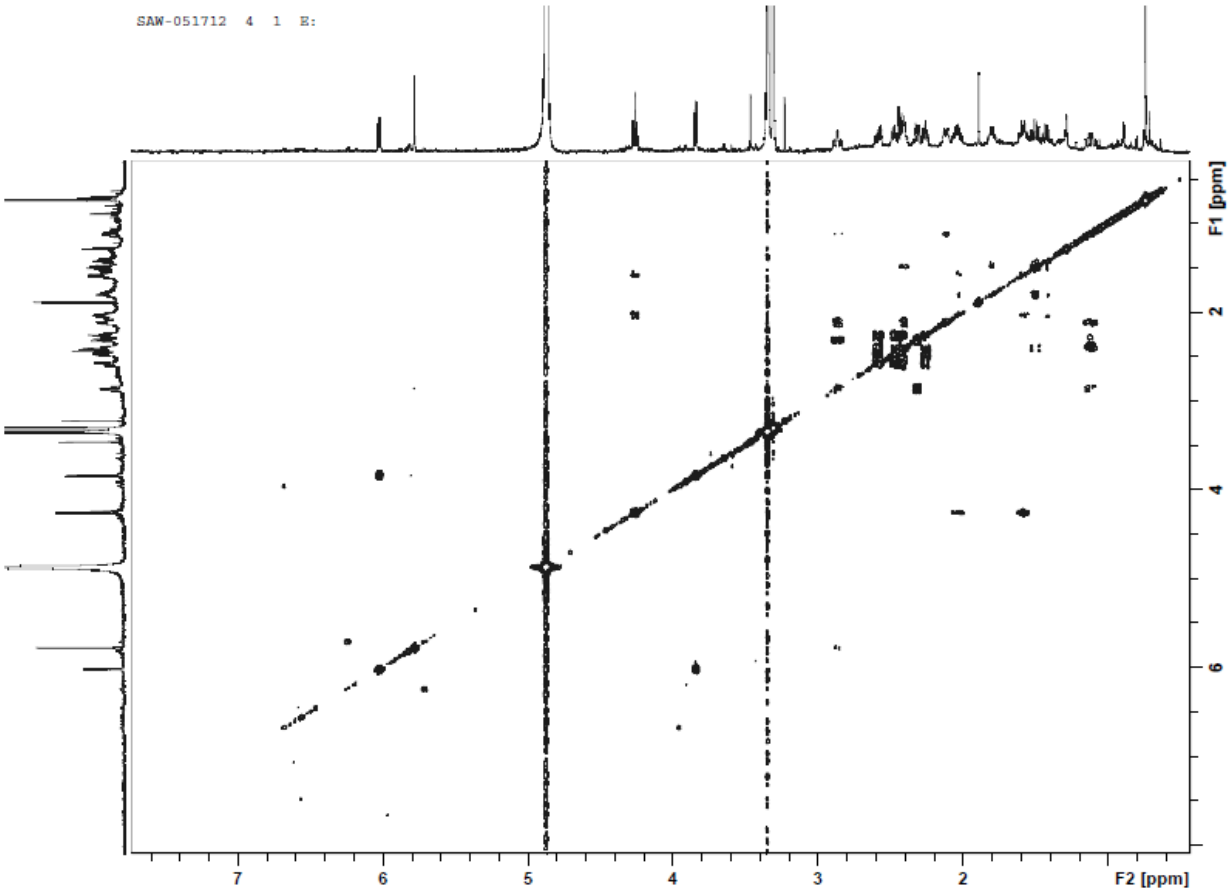

Figure A39. COSY NMR Spectrum of **5.5** (CD_3OD, 600 MHz)

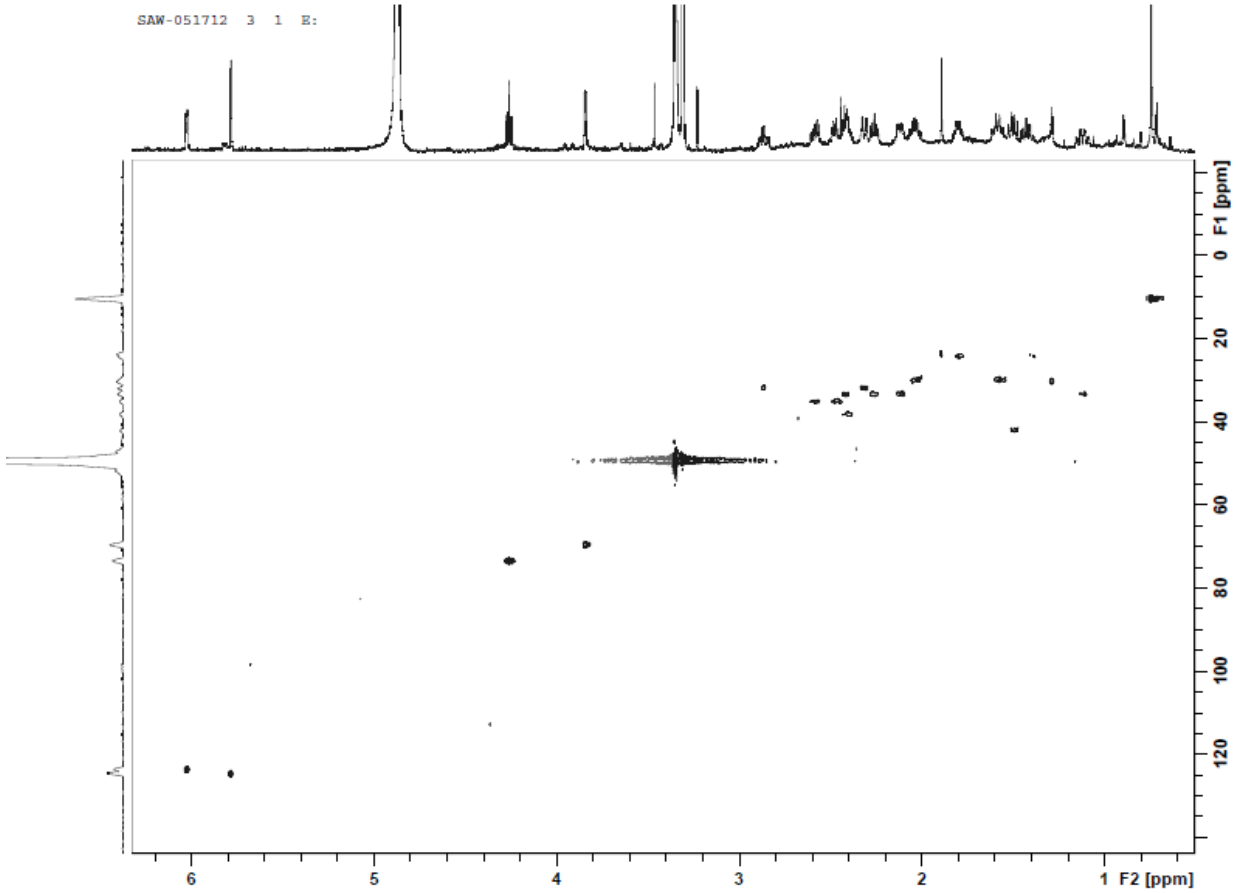

Figure A40. HSQC NMR Spectrum of **5.5** (CD_3OD, 600 MHz)

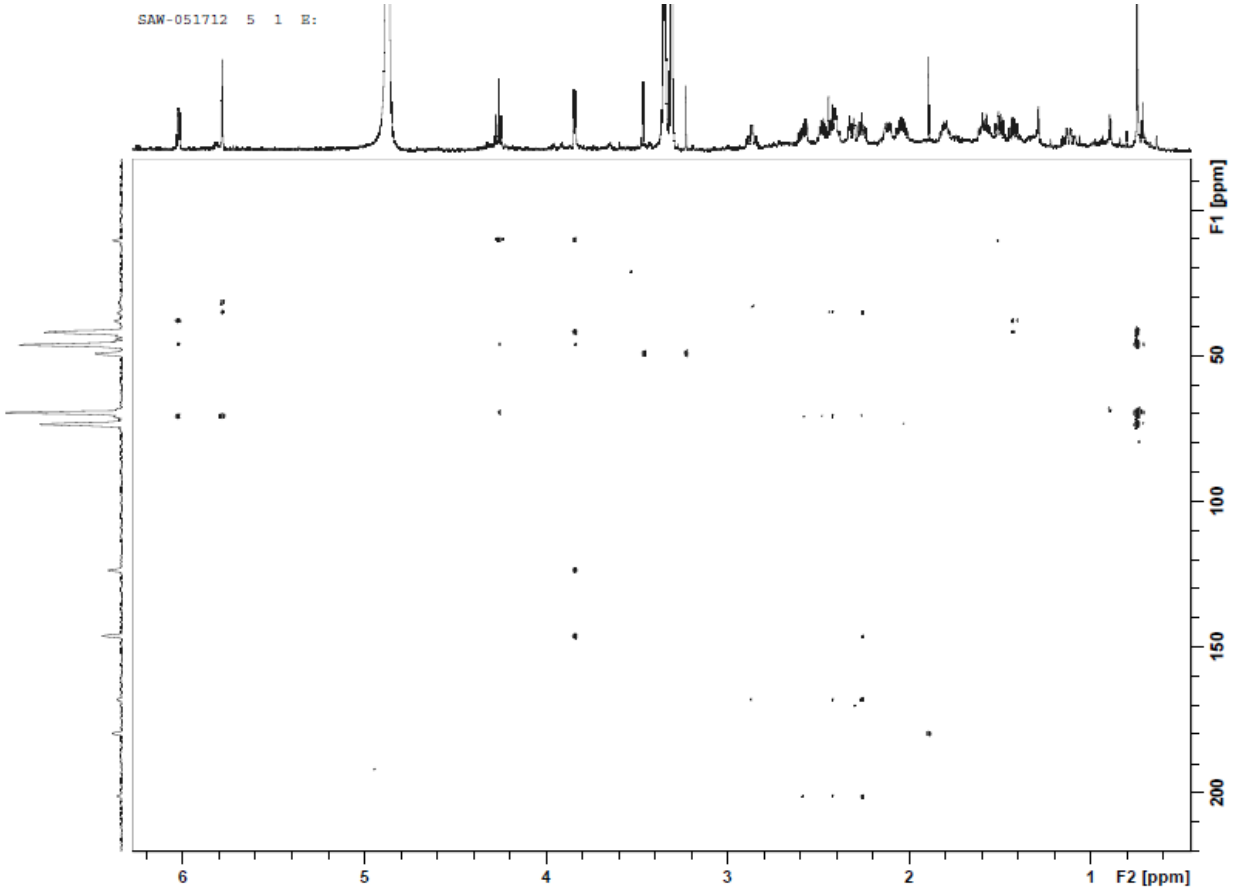

Figure A41. HMBC NMR Spectrum of **5.5** (CD_3OD, 600 MHz)

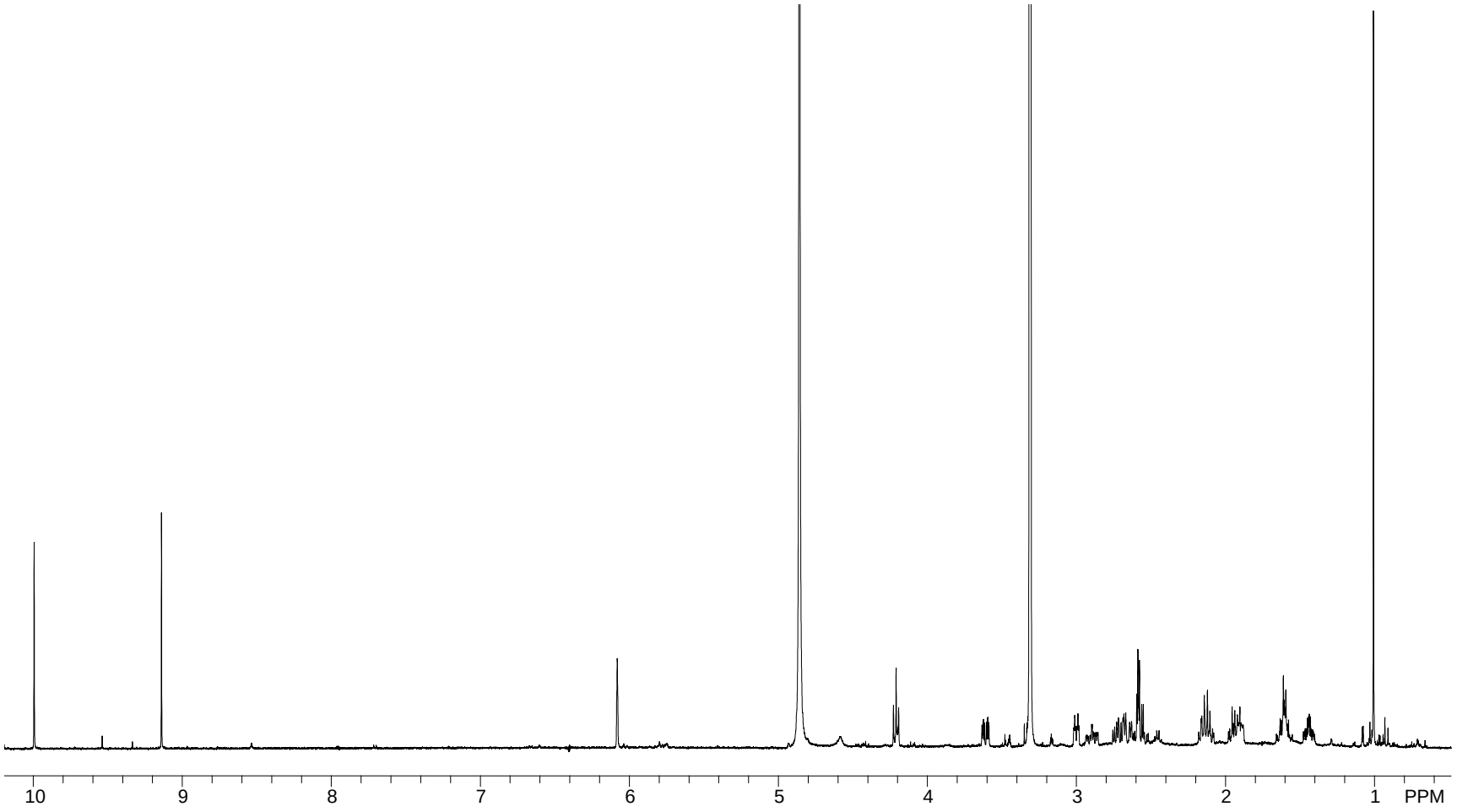

Figure A42. ^{1}H NMR Spectrum of **5.6** Before 2D NMR Data Collection (CD_3OD, 500 MHz)

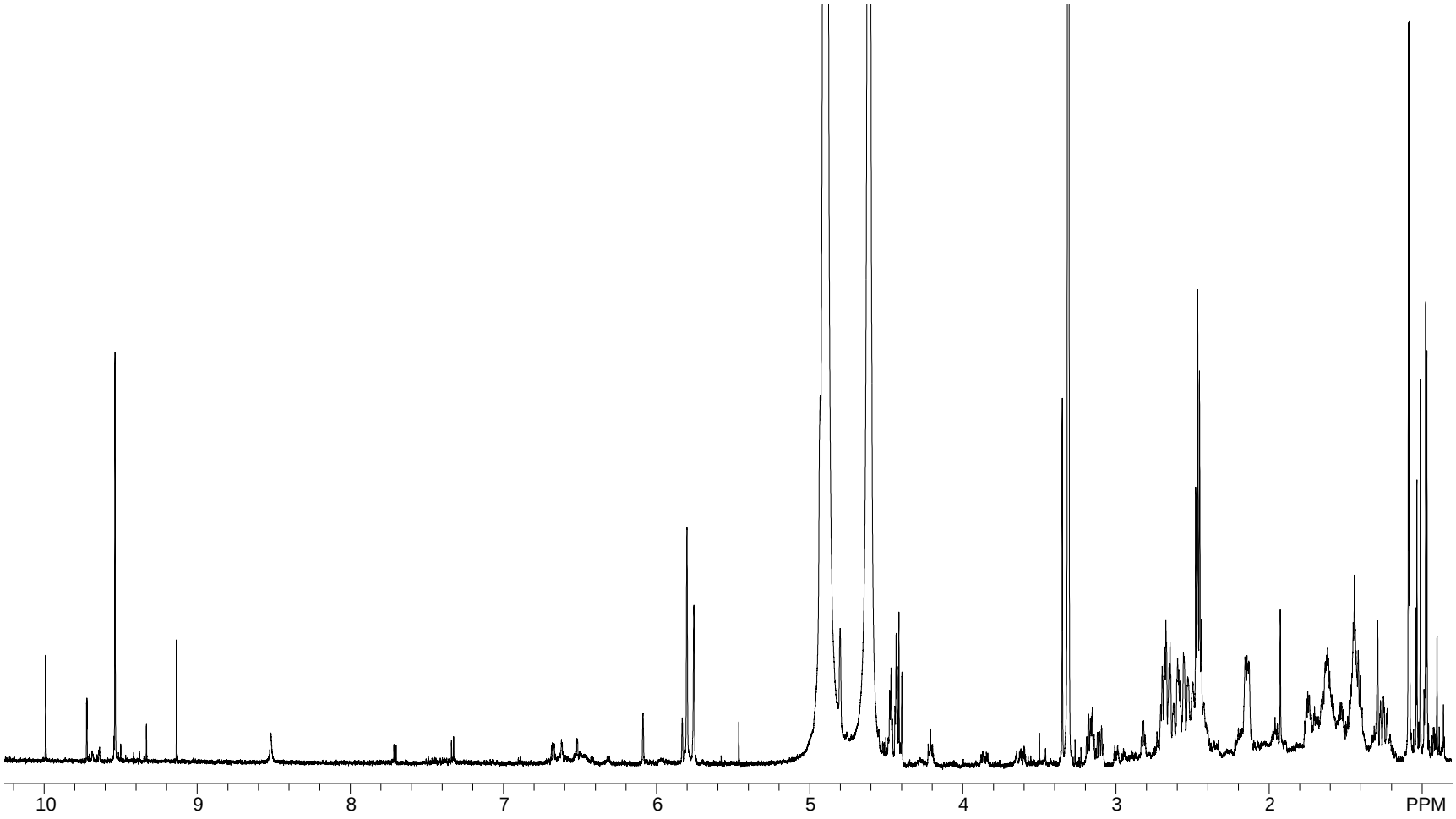

Figure A43. ^{1}H NMR Spectrum of **5.6** After 2D NMR Data Collection (CD_3OD, 600 MHz)

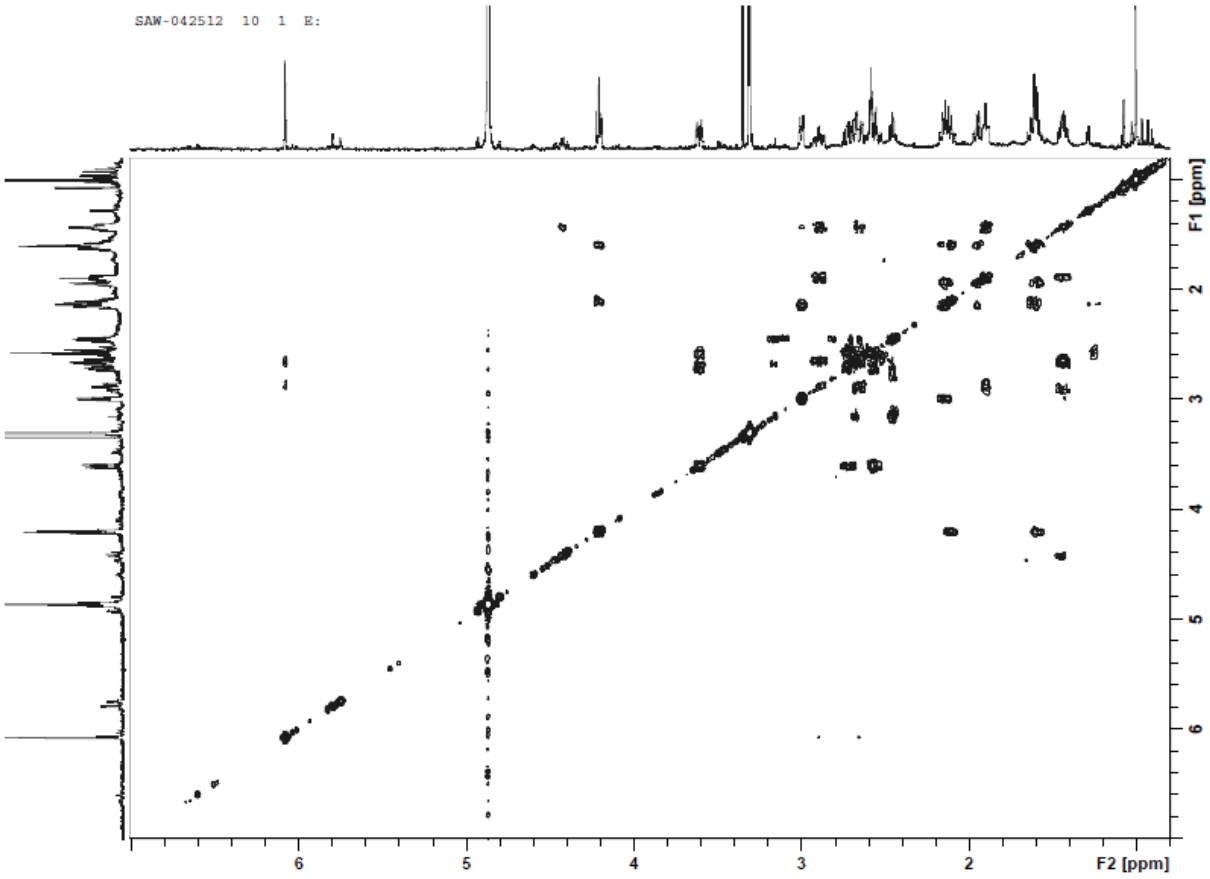

Figure A44. COSY NMR Spectrum of **5.6** (CD_3OD, 600 MHz)

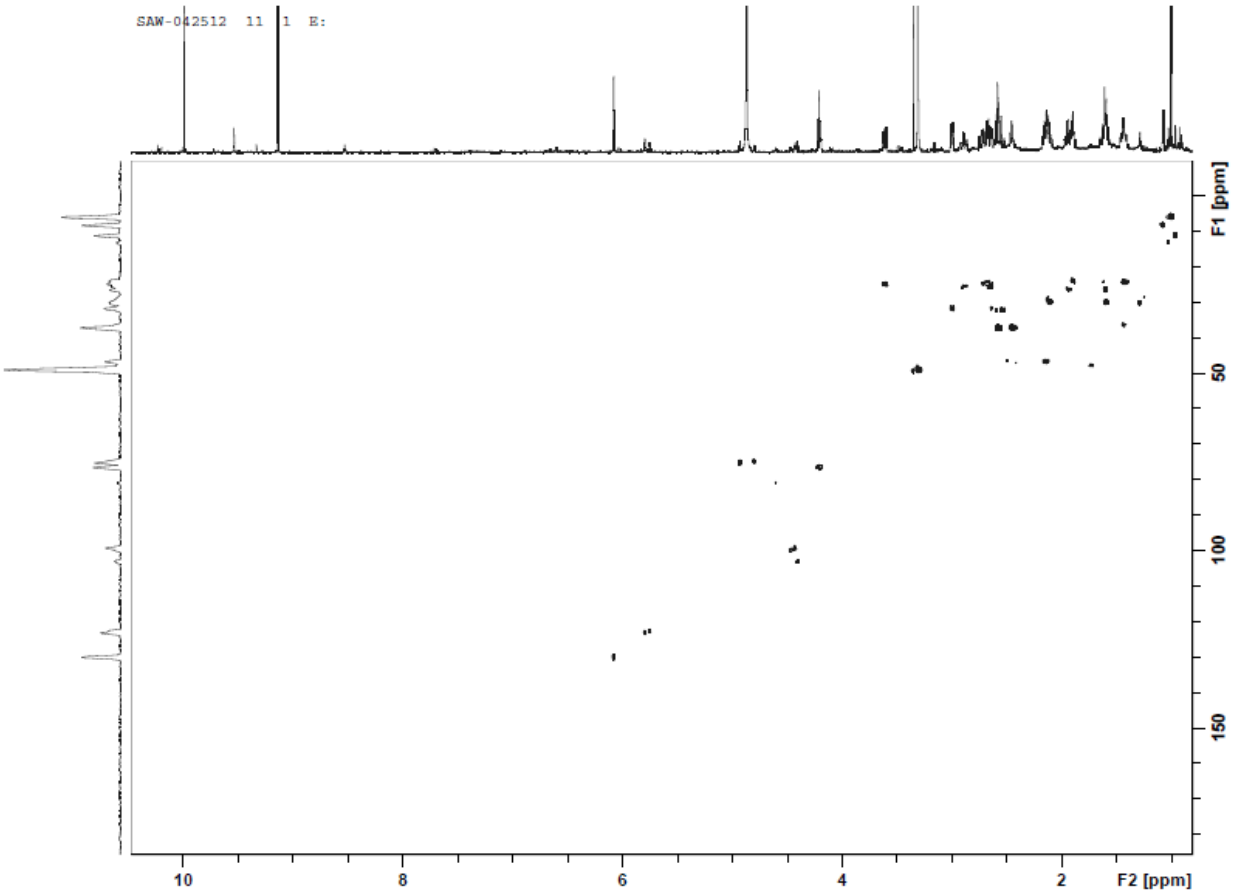

Figure A45. HSQC NMR Spectrum of **5.6** Acquired using Standard Parameters (CD_3OD, 600 MHz)

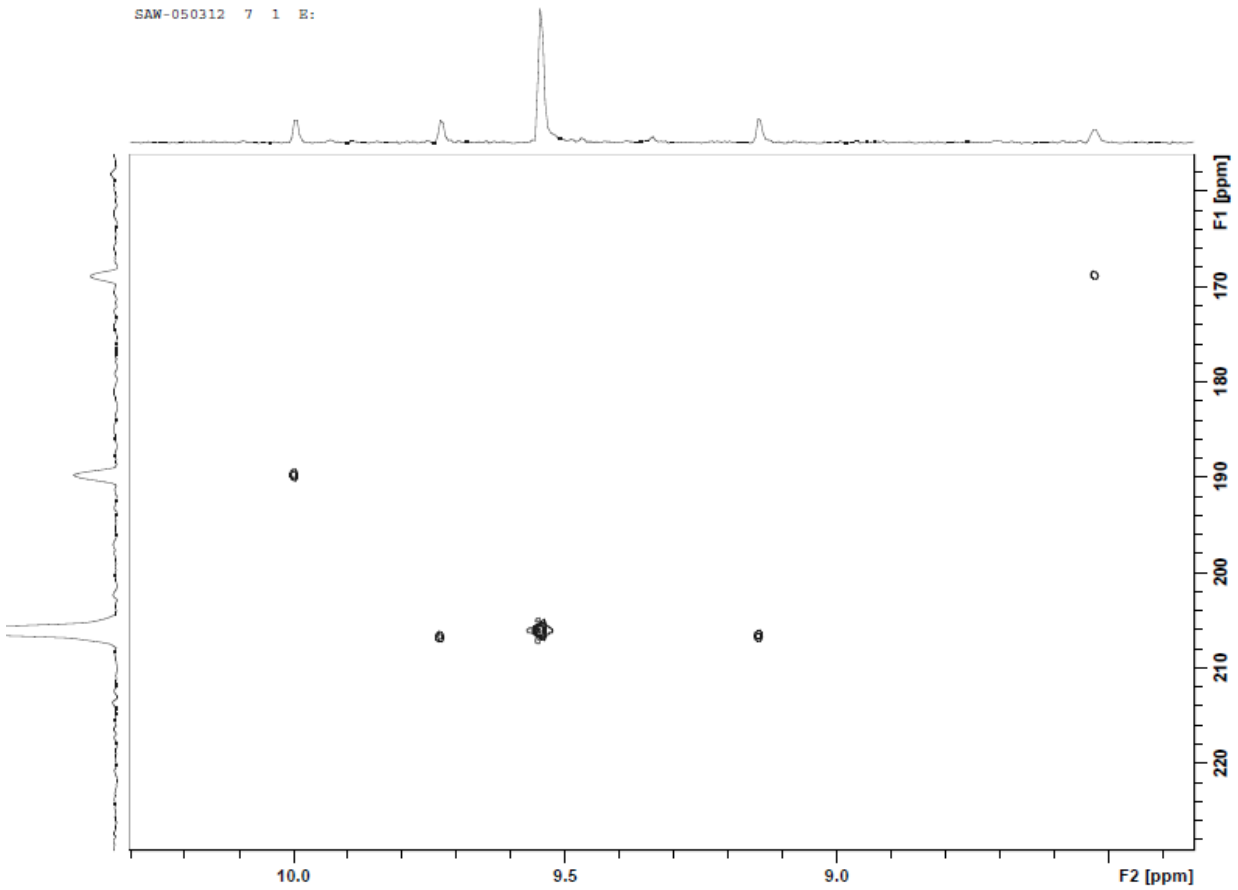

Figure A46. HSQC NMR Spectrum of **5.6** with Parameters Optimized for Aldehyde $^{1}J_{CH}$ of 170 Hz (CD_3OD, 600 MHz)

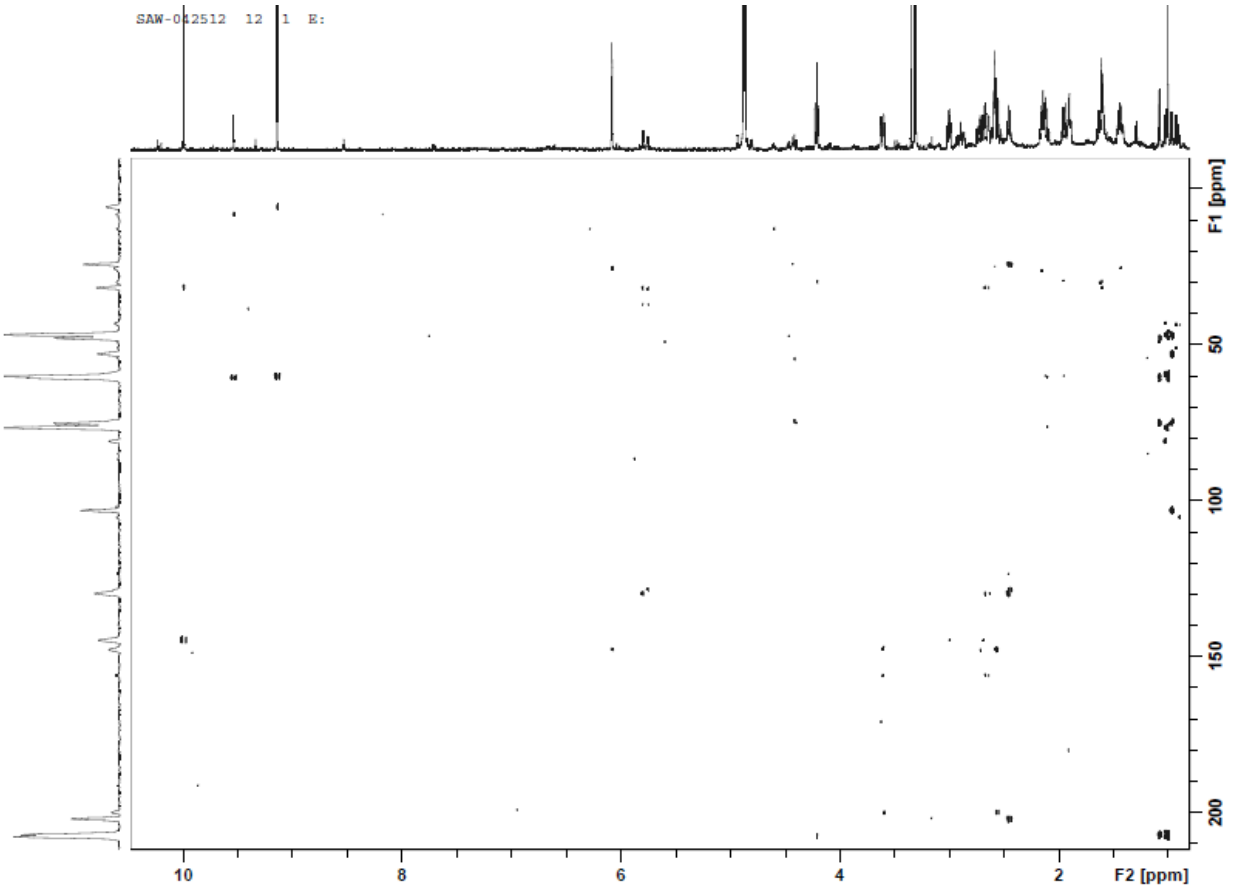

Figure A47. HMBC NMR Spectrum of **4.6** (CD_3OD, 600 MHz)

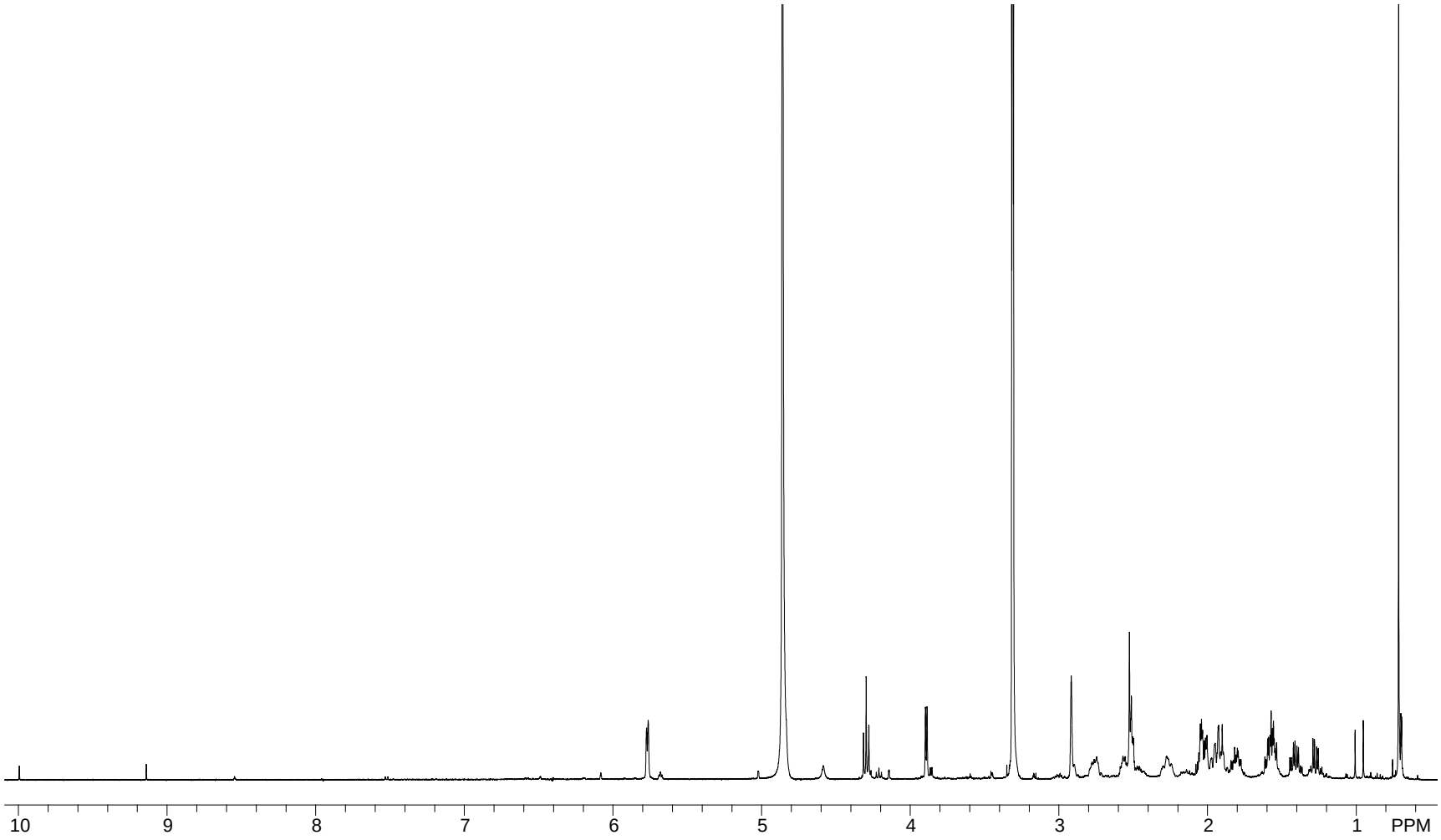

Figure A48. Original ^{1}H NMR Spectrum of **5.7** (CD_3OD, 500 MHz)

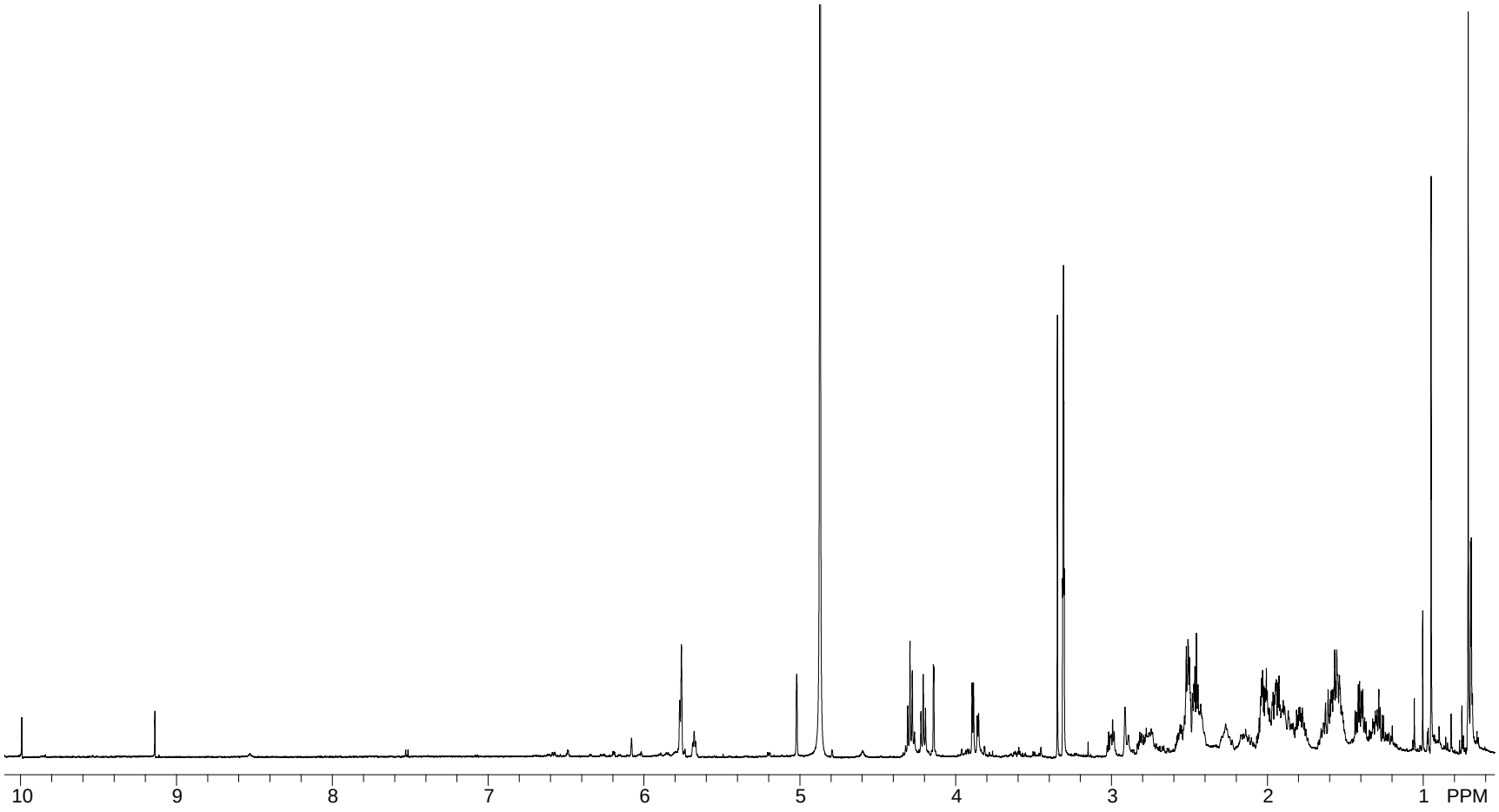

Figure A49. ^{1}H NMR Spectrum of **5.7** Before 2D NMR Data Collection (CD_3OD, 600 MHz)

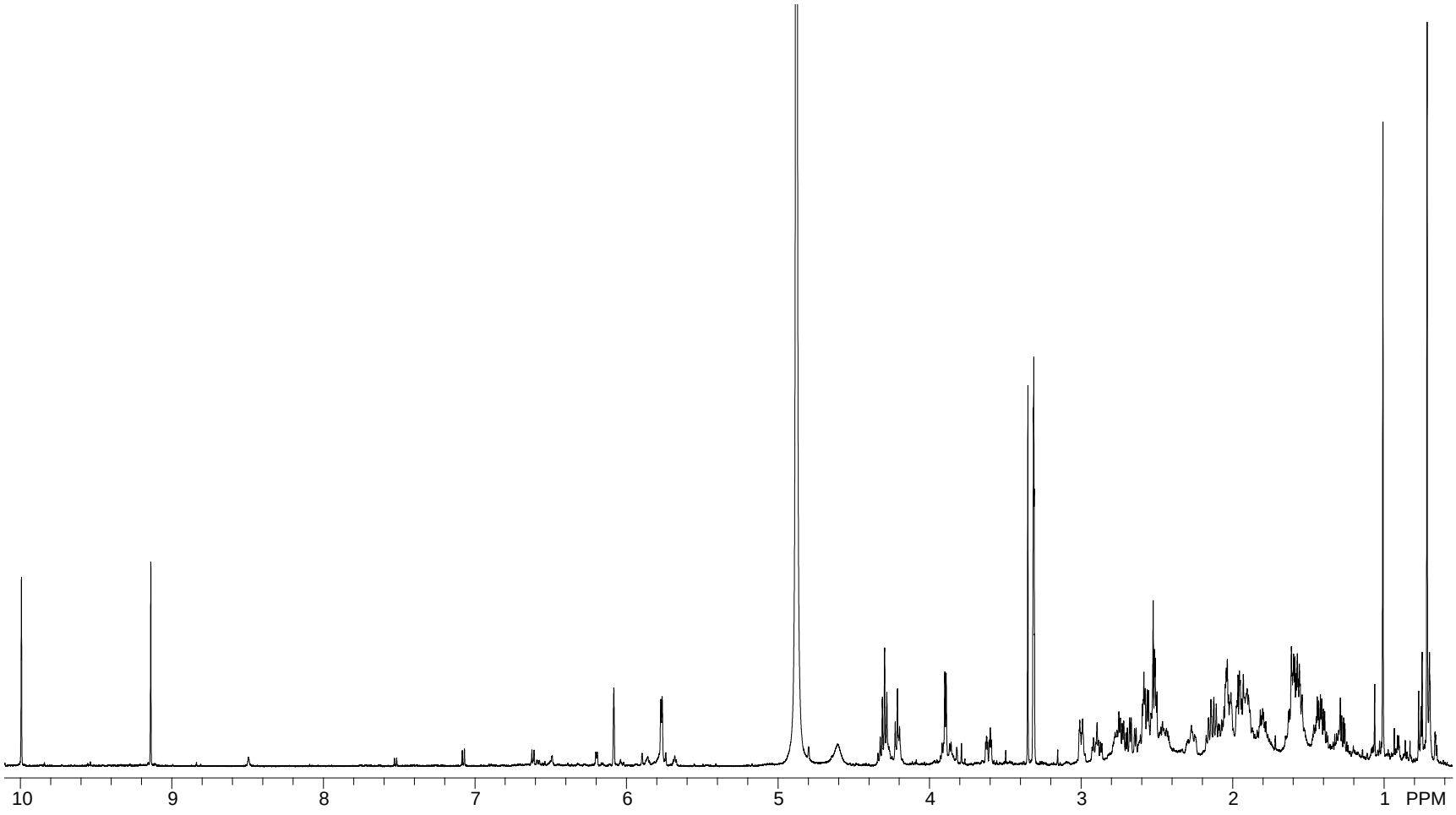

Figure A50. ^{1}H NMR Spectrum of **5.7** After 2D NMR Data Collection (CD_3OD, 600 MHz)

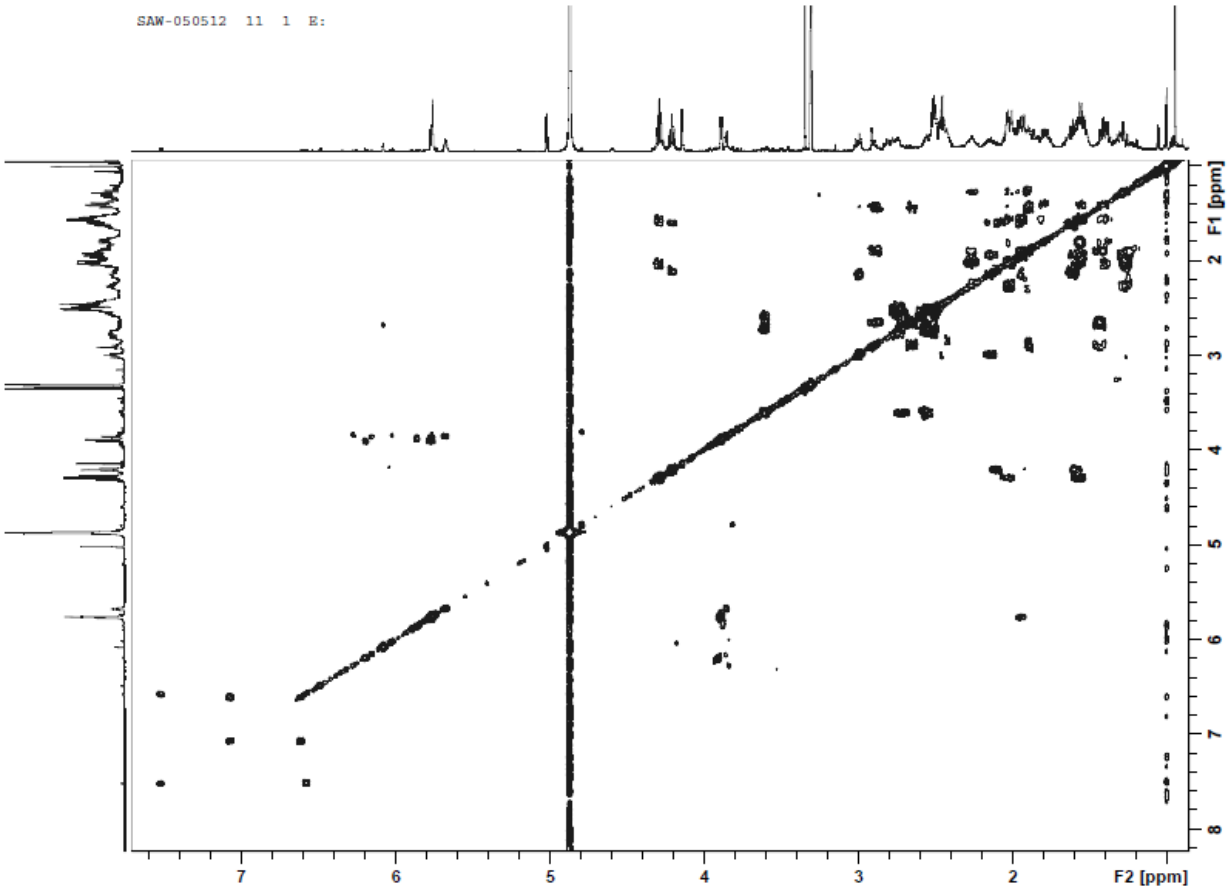

Figure A51. COSY NMR Spectrum of **5.7** (CD_3OD, 600 MHz)

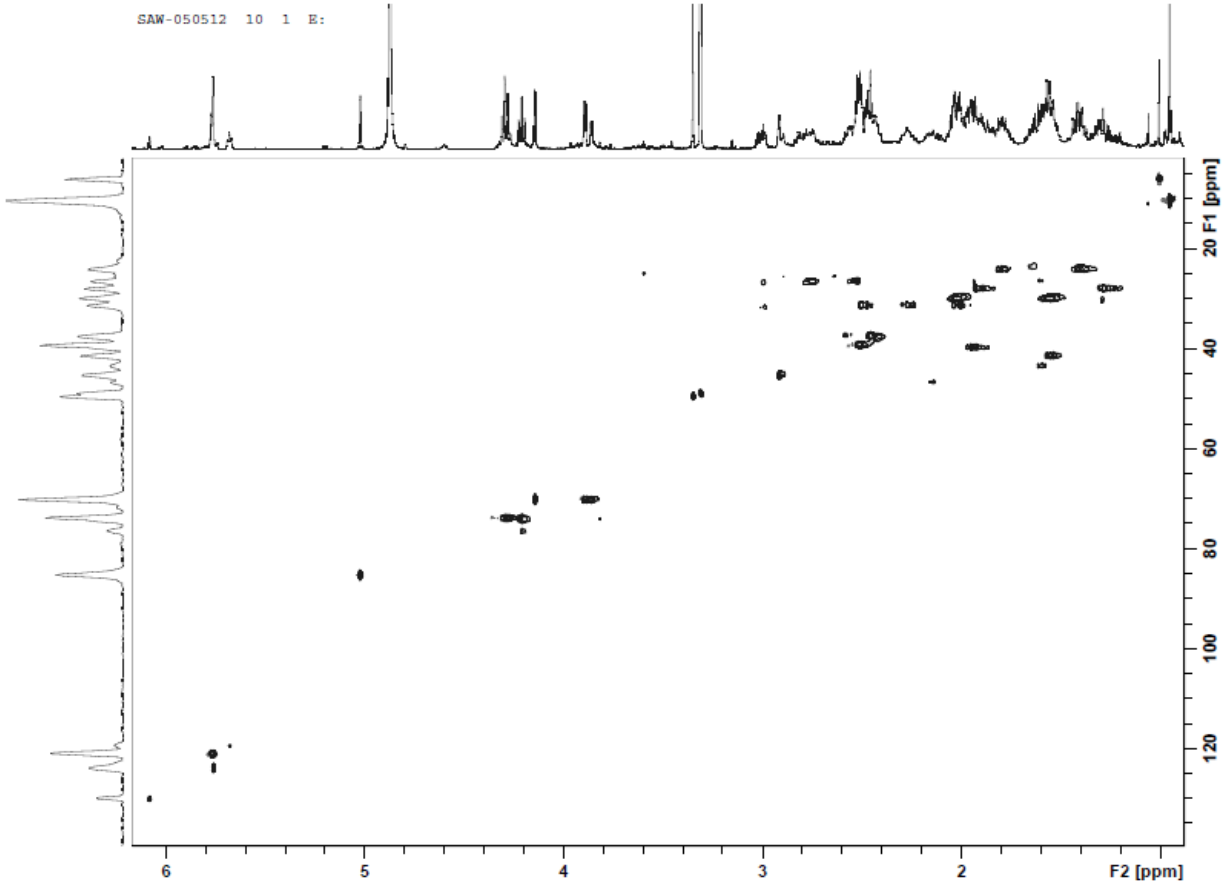

Figure A52. HSQC NMR Spectrum of **5.7** (CD_3OD, 600 MHz)

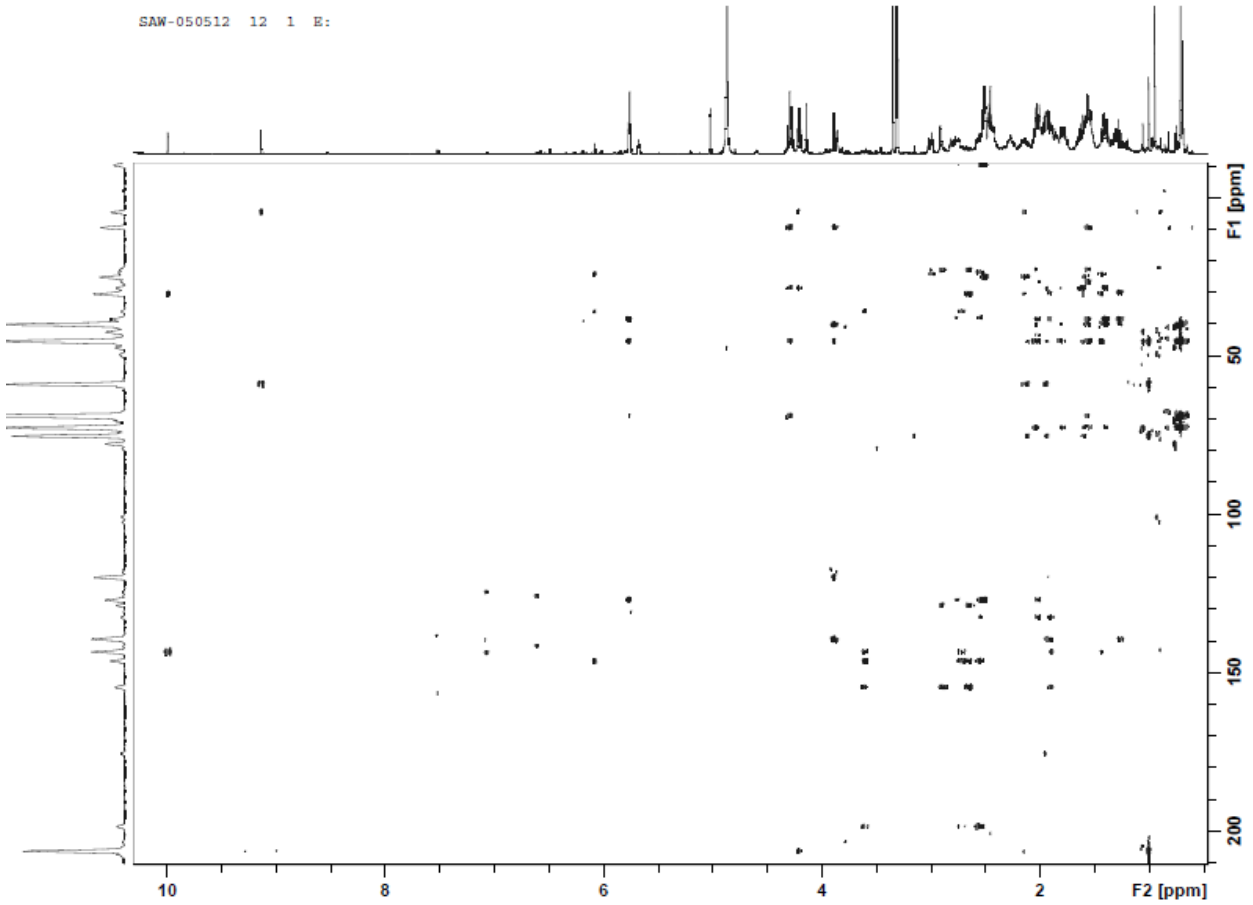

Figure A53. HMBC NMR Spectrum of **5.7** (CD_3OD, 600 MHz)

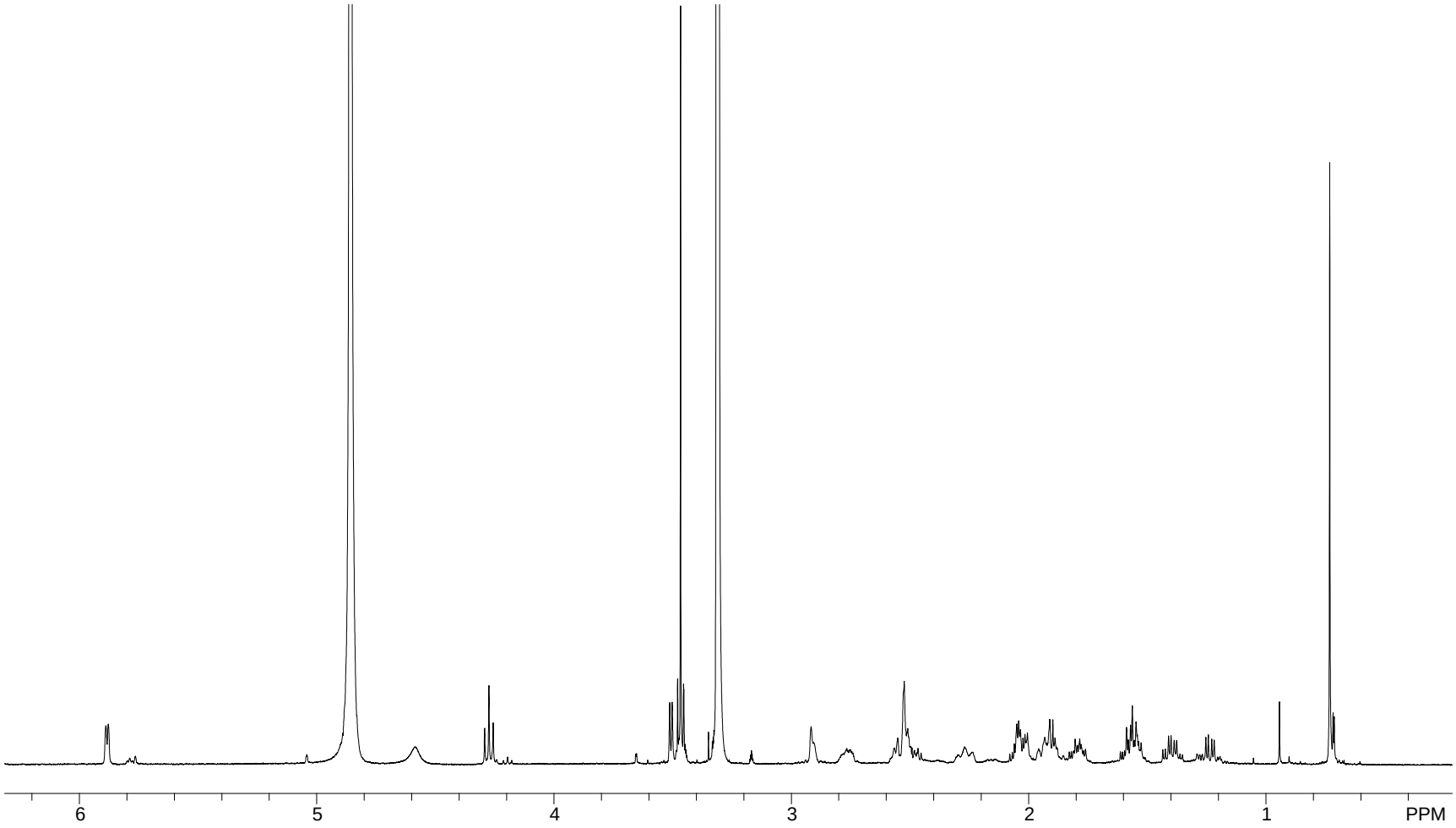

Figure A54. ^{1}H NMR Spectrum of **5.8** (CD_3OD, 500 MHz)

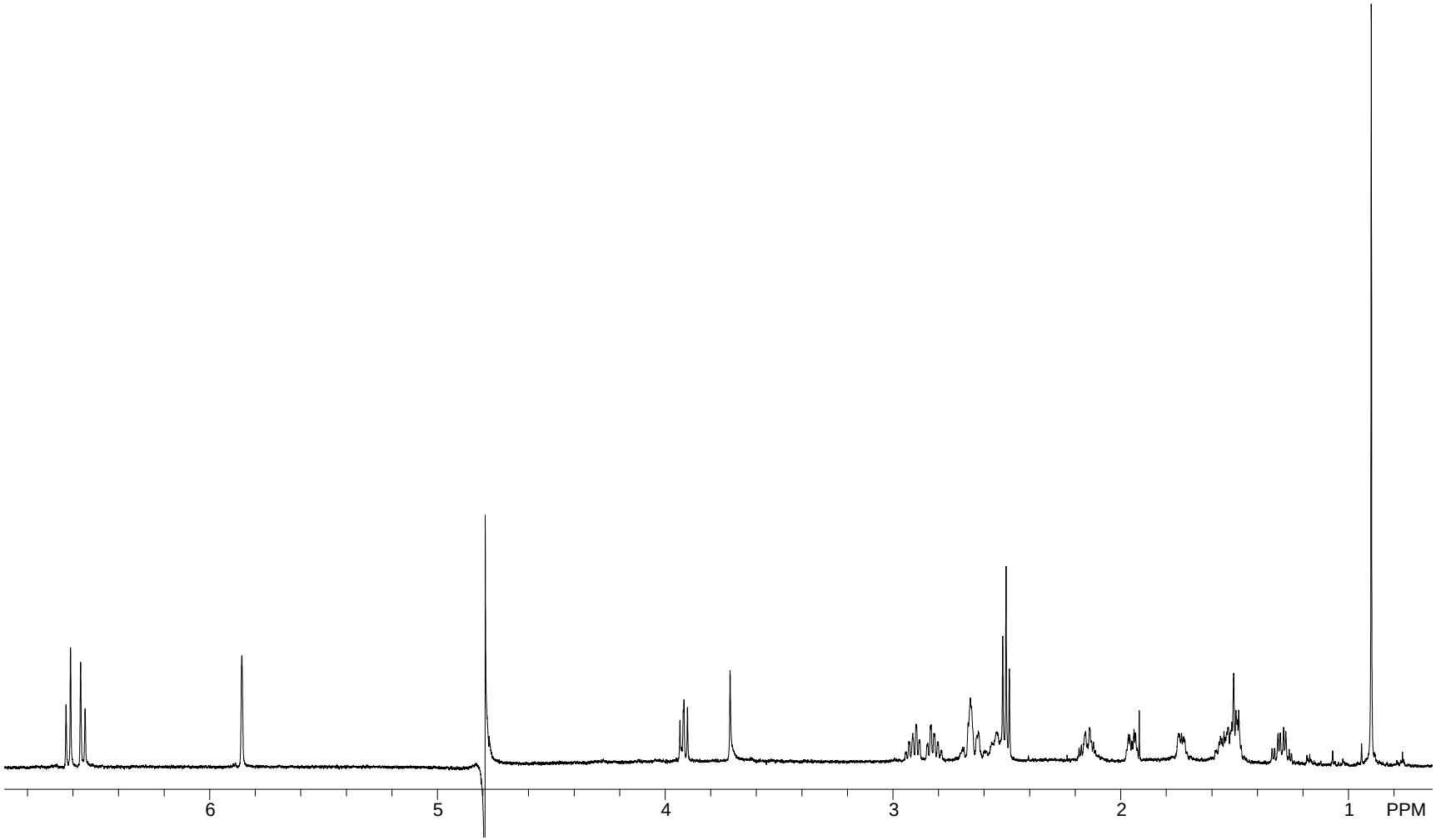

Figure A55. ^{1}H NMR Spectrum of β–Trenbolone (**5.3**); NMR Tube Experiment, Before Photolysis (D_2O, 500 MHz)

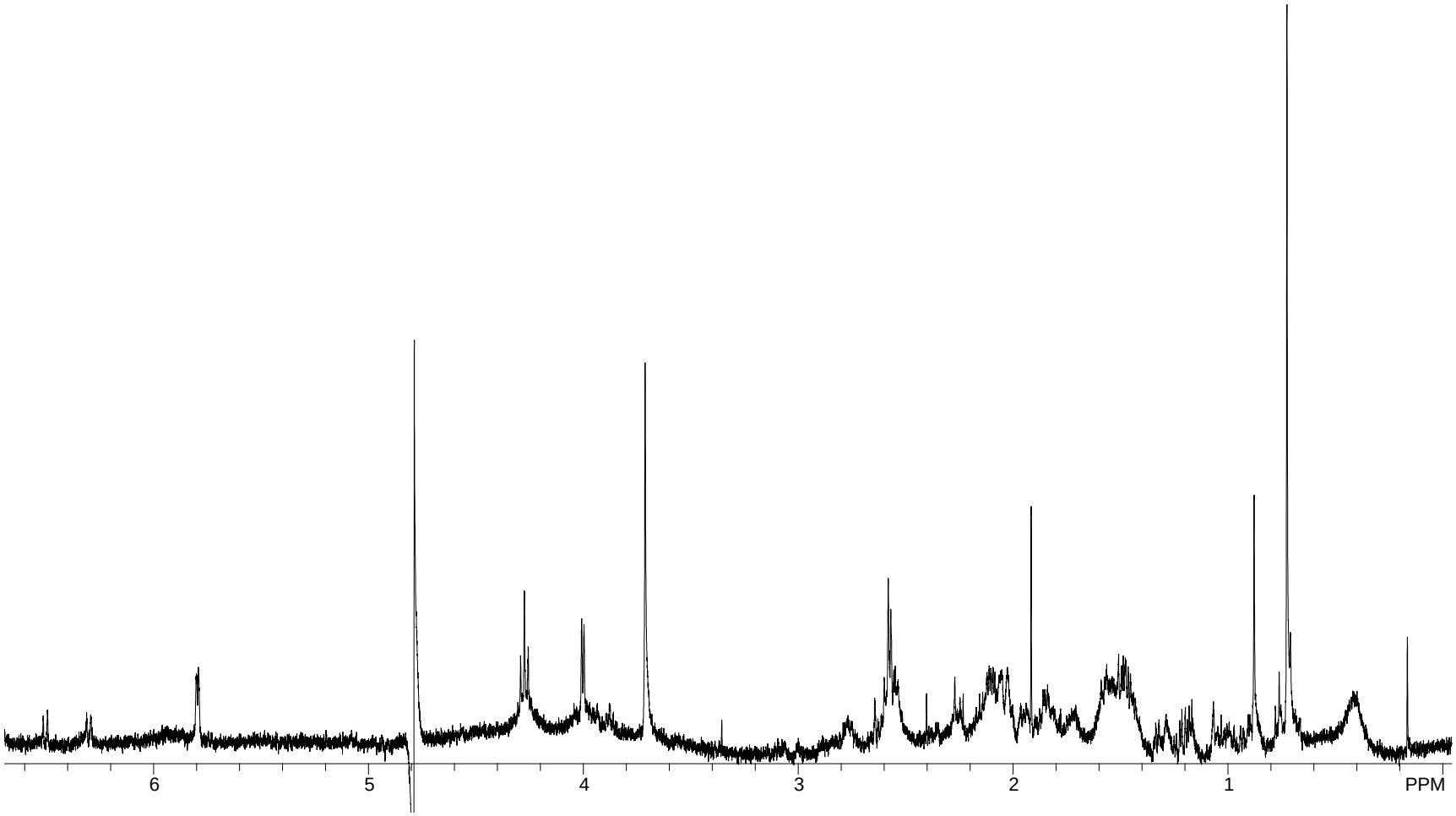

Figure A56. ^{1}H NMR Spectrum of β–Trenbolone (**5.3**); NMR Tube Experiment, Immediately After Photolysis (D_2O, 500 MHz)

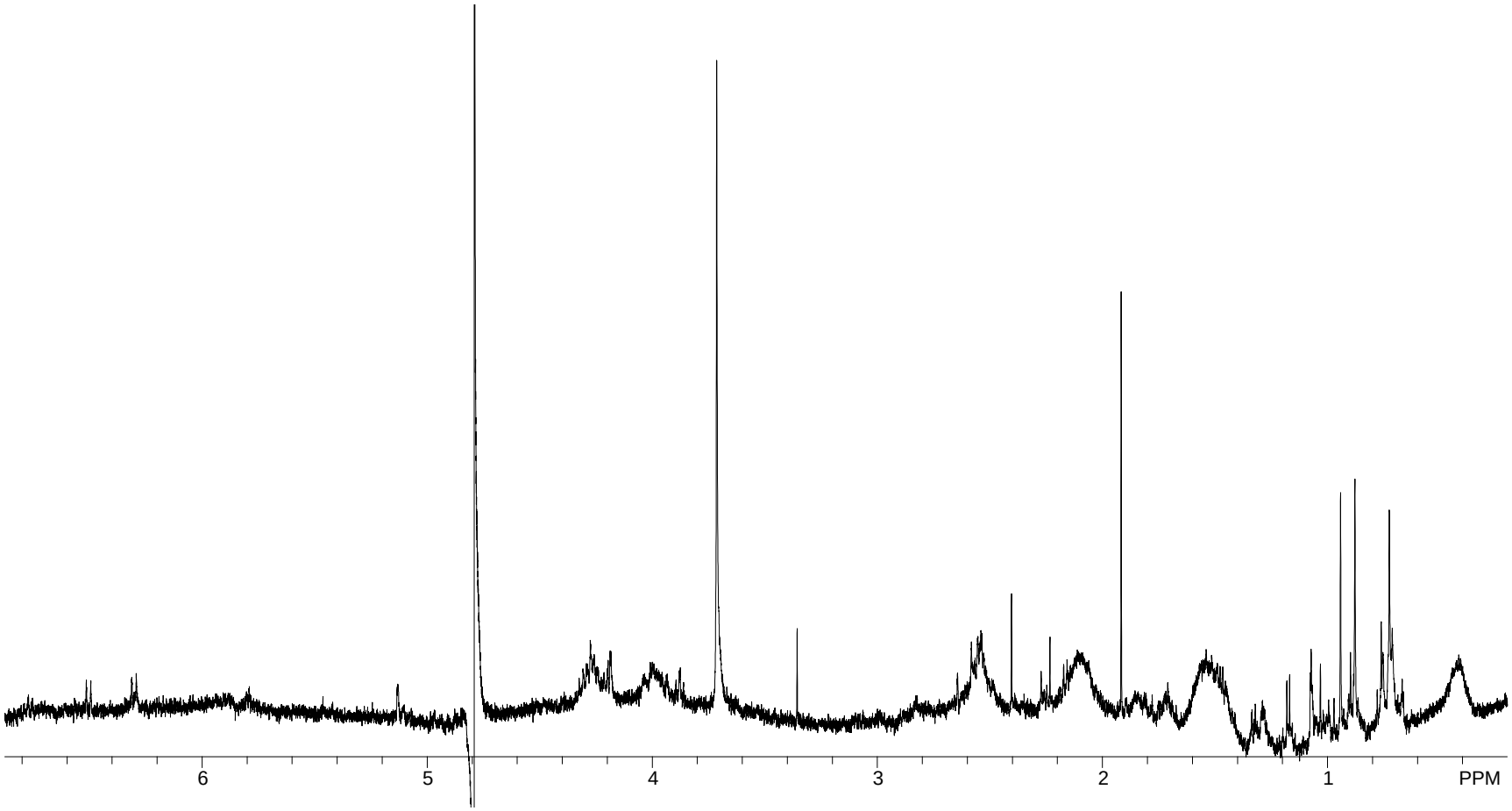

Figure A57. ^{1}H NMR Spectrum of β–Trenbolone (**5.3**); NMR Tube Experiment, Three Days After Photolysis (D_2O, 500 MHz)

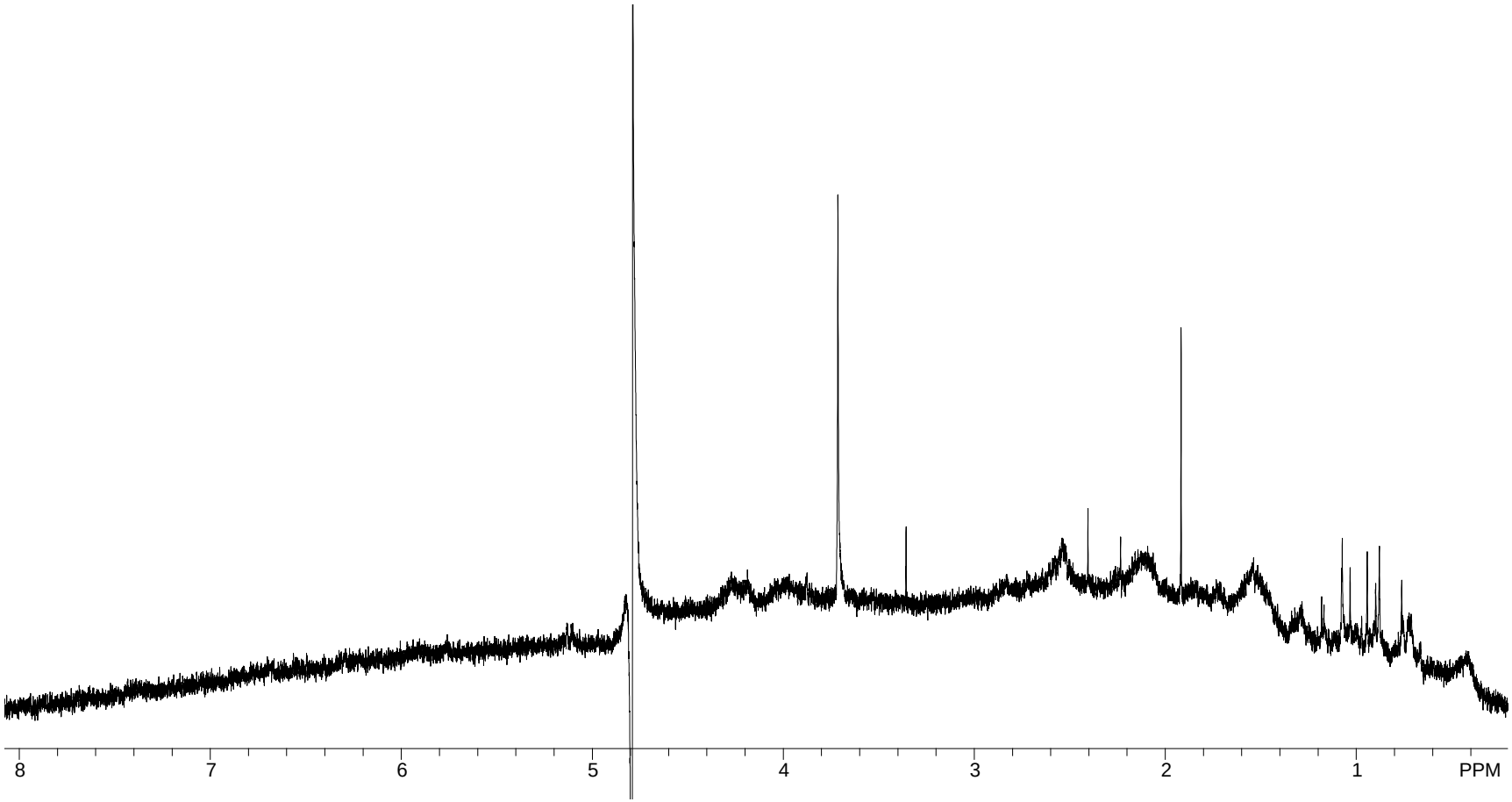

Figure A58. ^{1}H NMR Spectrum of β–Trenbolone (**5.3**); NMR Tube Experiment, Eight Days After Photolysis (D_2O, 500 MHz)

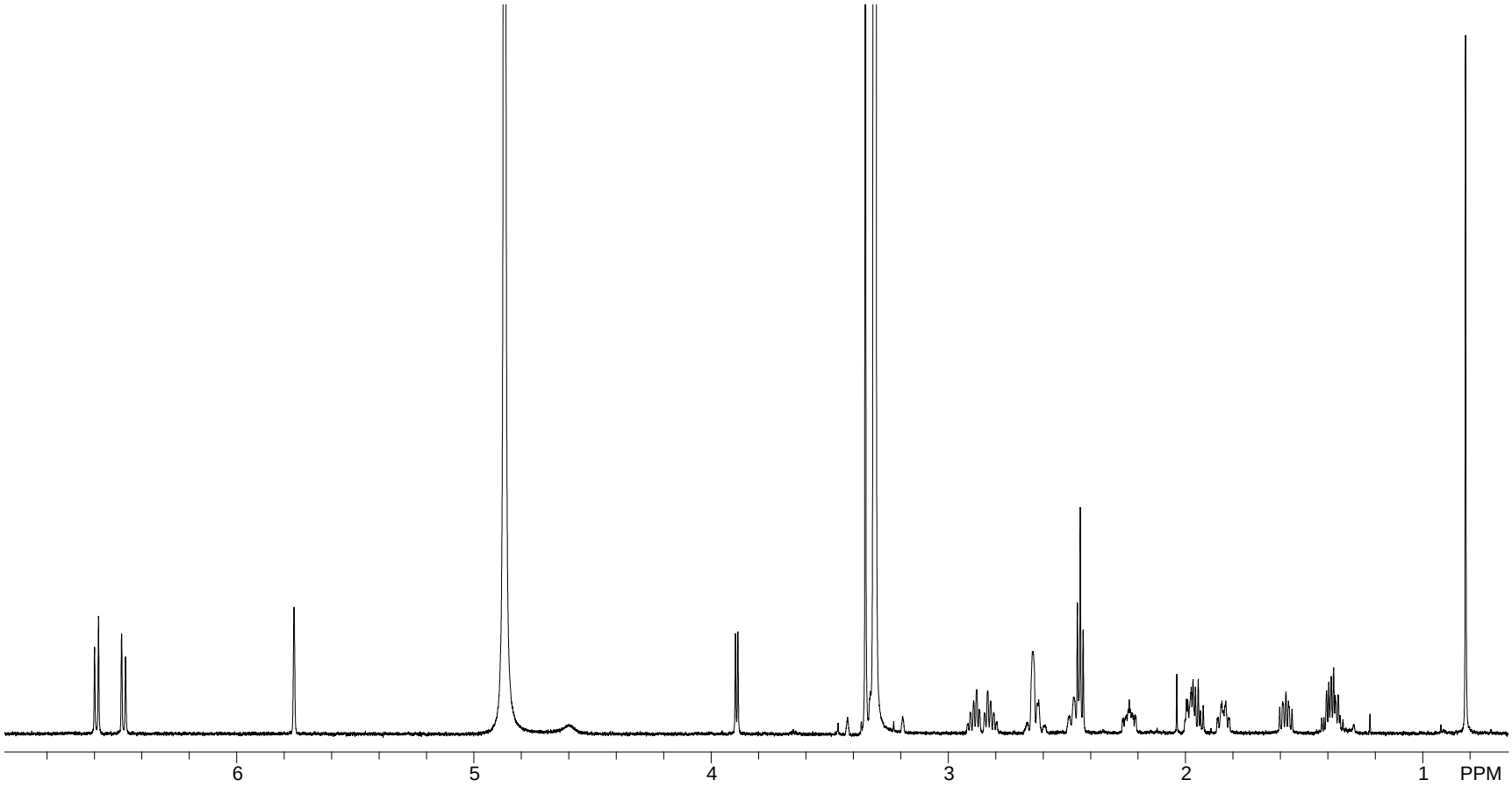

Figure A59. ^{1}H NMR Spectrum of α–Trenbolone (**5.4**; CD_3OD, 600 MHz)

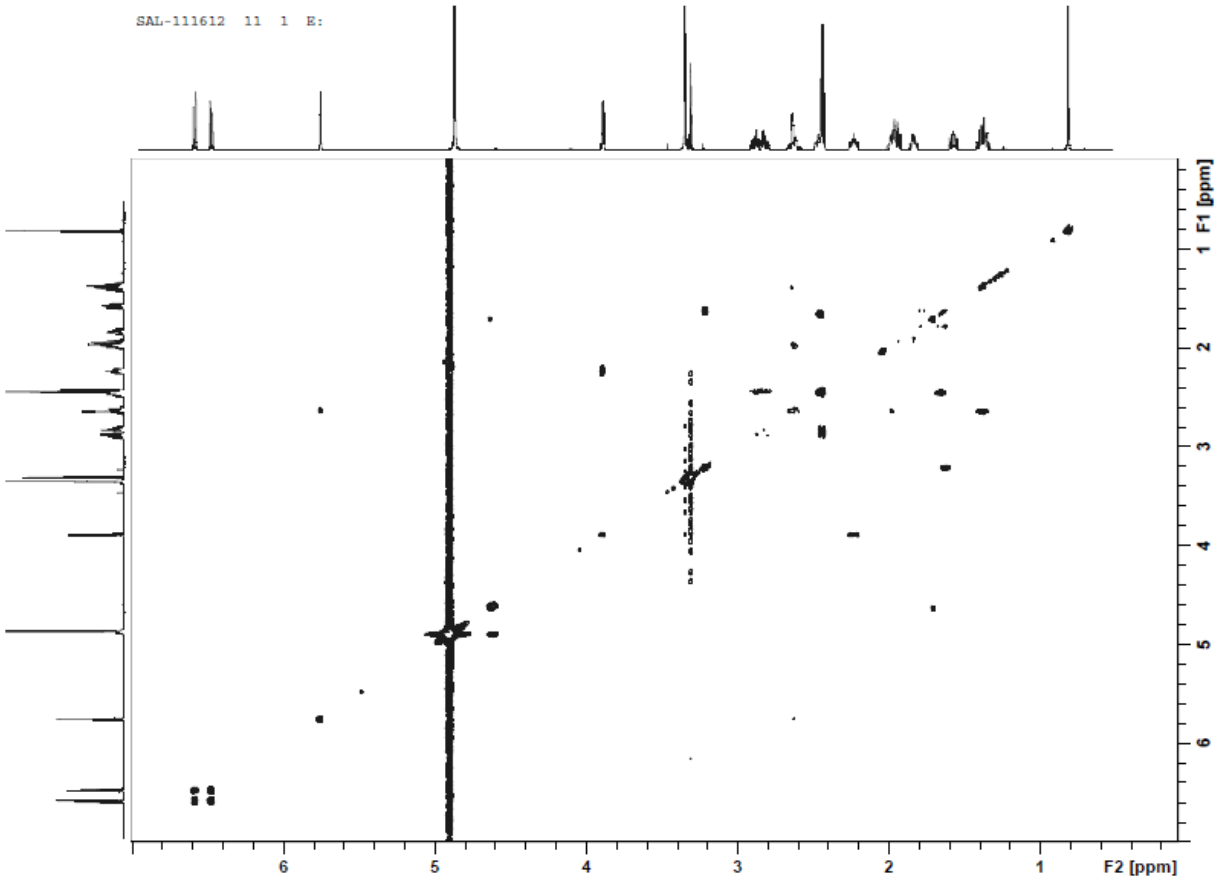

Figure A60. COSY NMR Spectrum of α–Trenbolone (**5.4**; CD_3OD, 600 MHz)

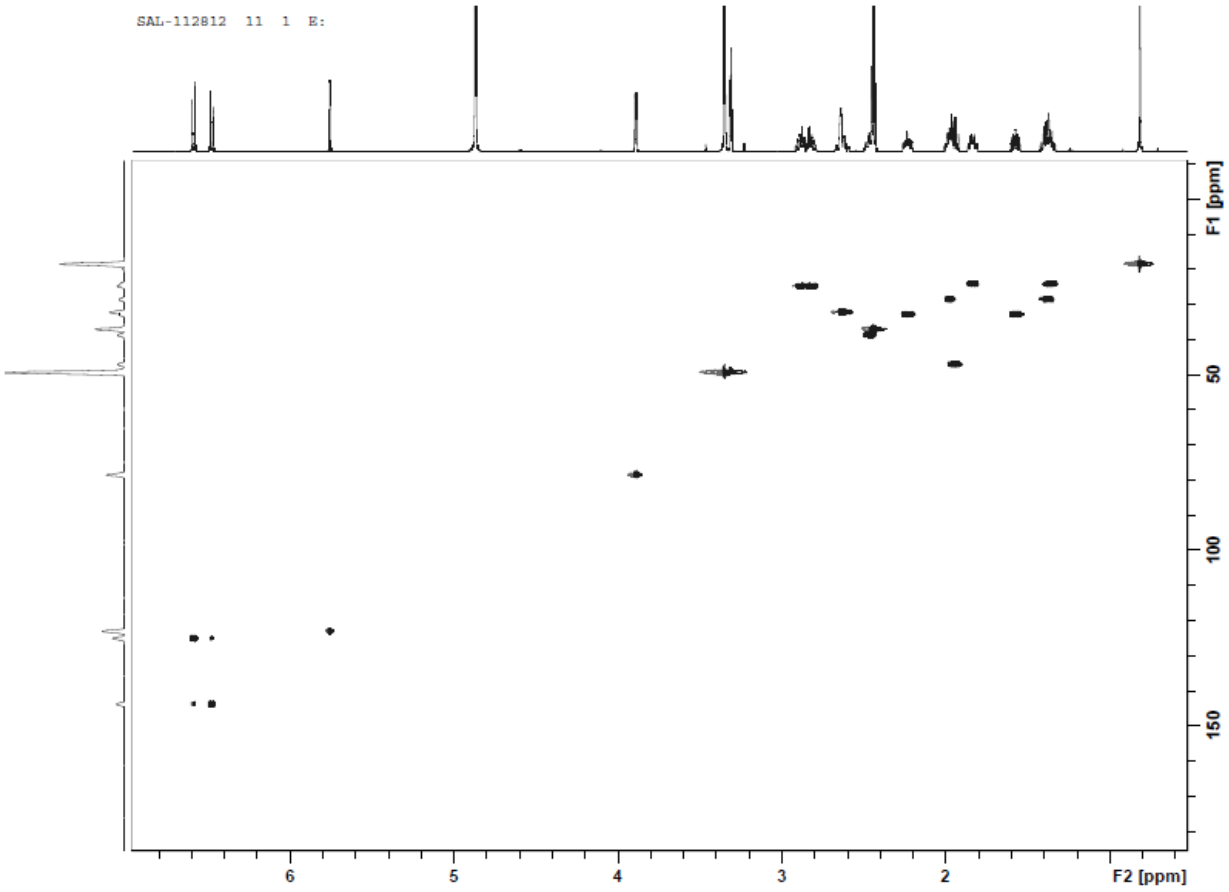

Figure A61. HSQC NMR Spectrum of α–Trenbolone (**5.4**; CD_3OD, 600 MHz)

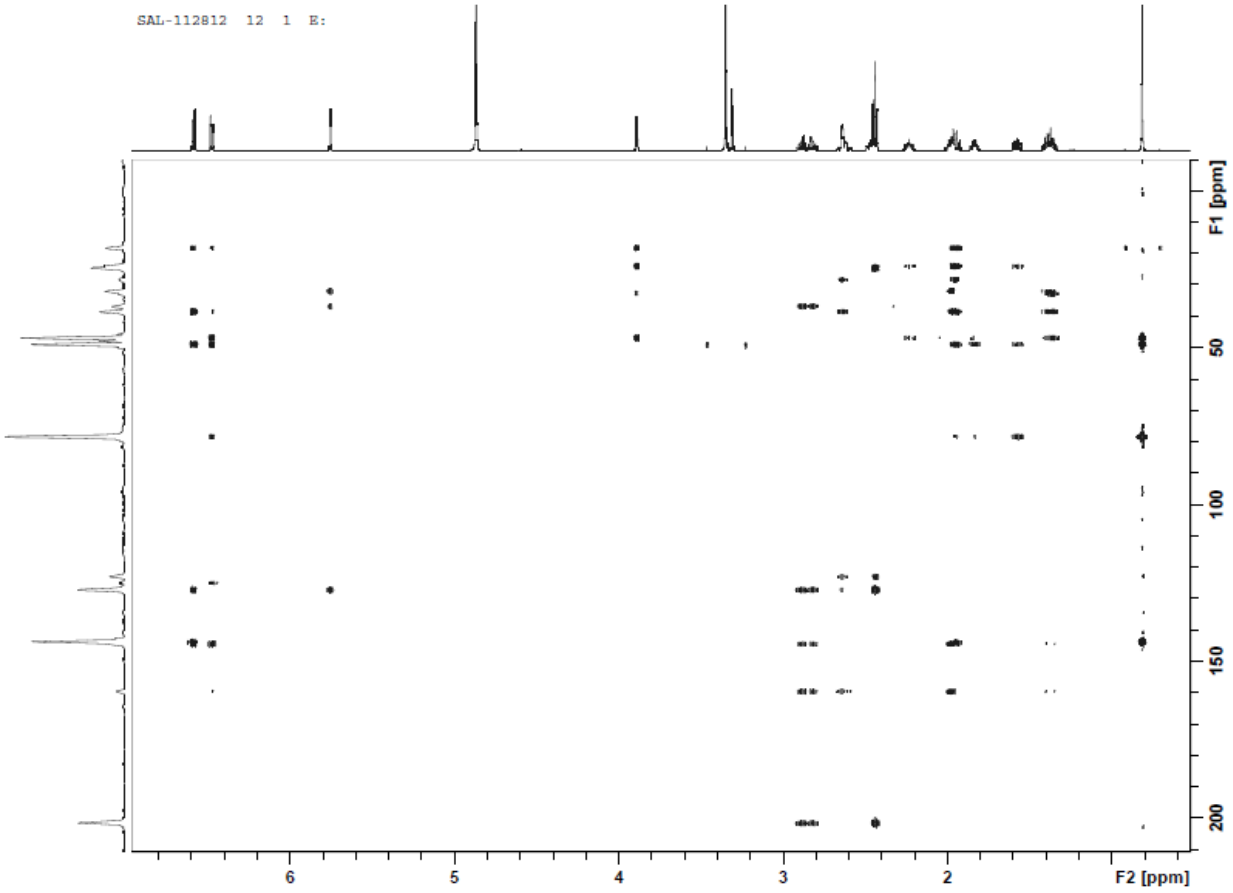

Figure A62. HMBC NMR Spectrum of α–Trenbolone (**5.4**; CD_3OD, 600 MHz)

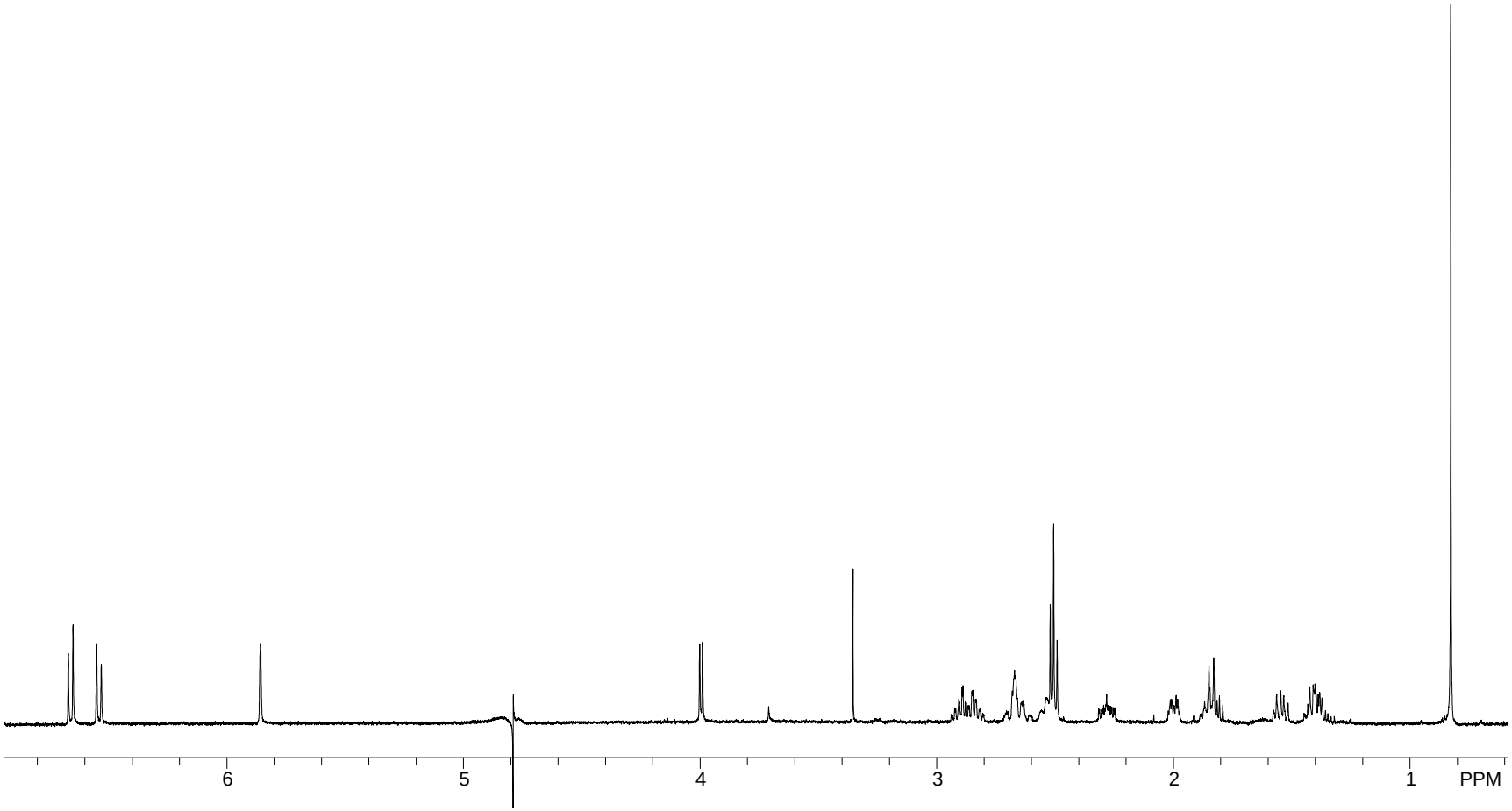

Figure A63. ^{1}H NMR Spectrum of α–Trenbolone (**5.4**); NMR Tube Experiment, Before Photolysis (D_2O, 500 MHz)

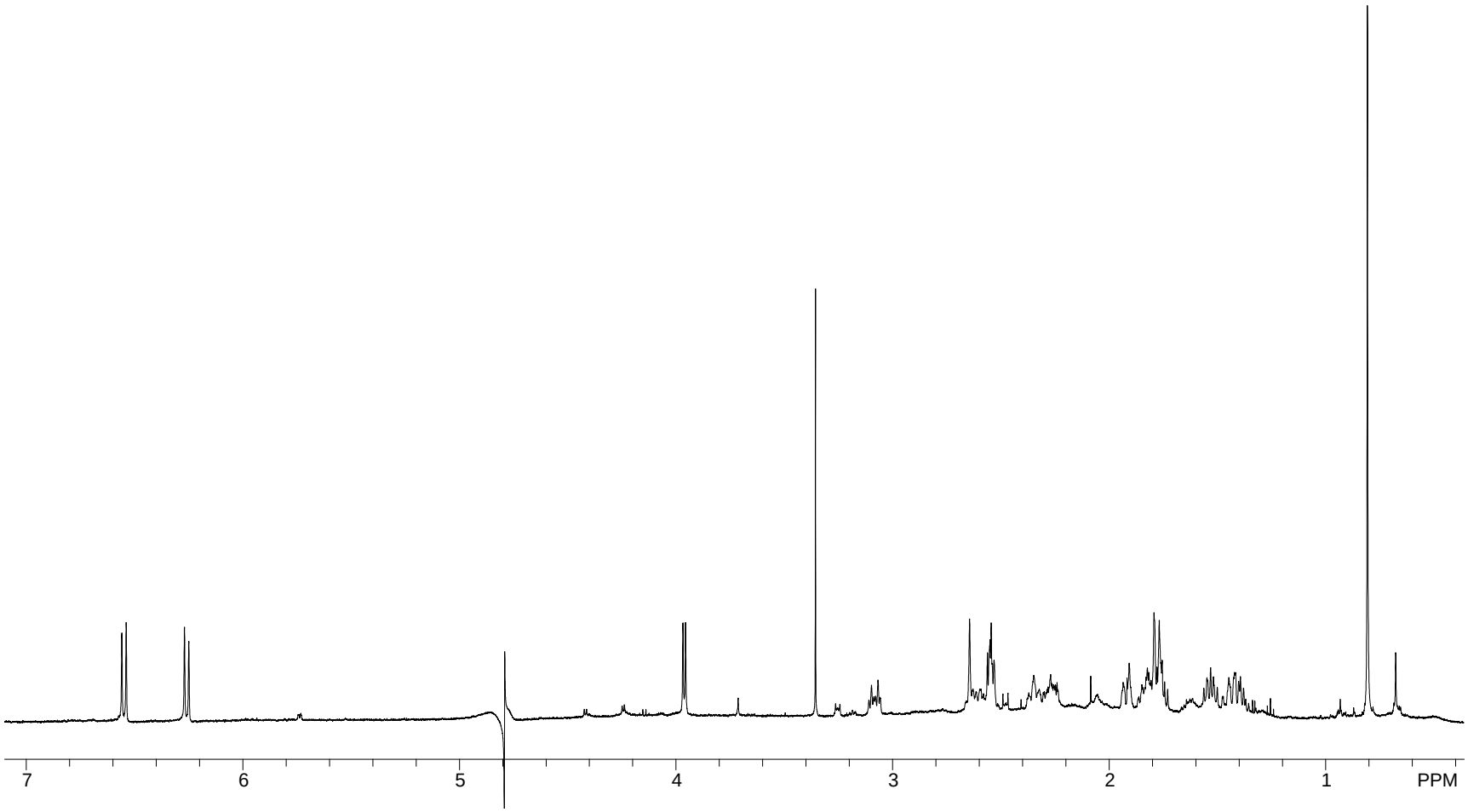

Figure A64. ^{1}H NMR Spectrum of α–Trenbolone (**5.4**); NMR Tube Experiment, Immediately After Photolysis (D_2O, 500 MHz)

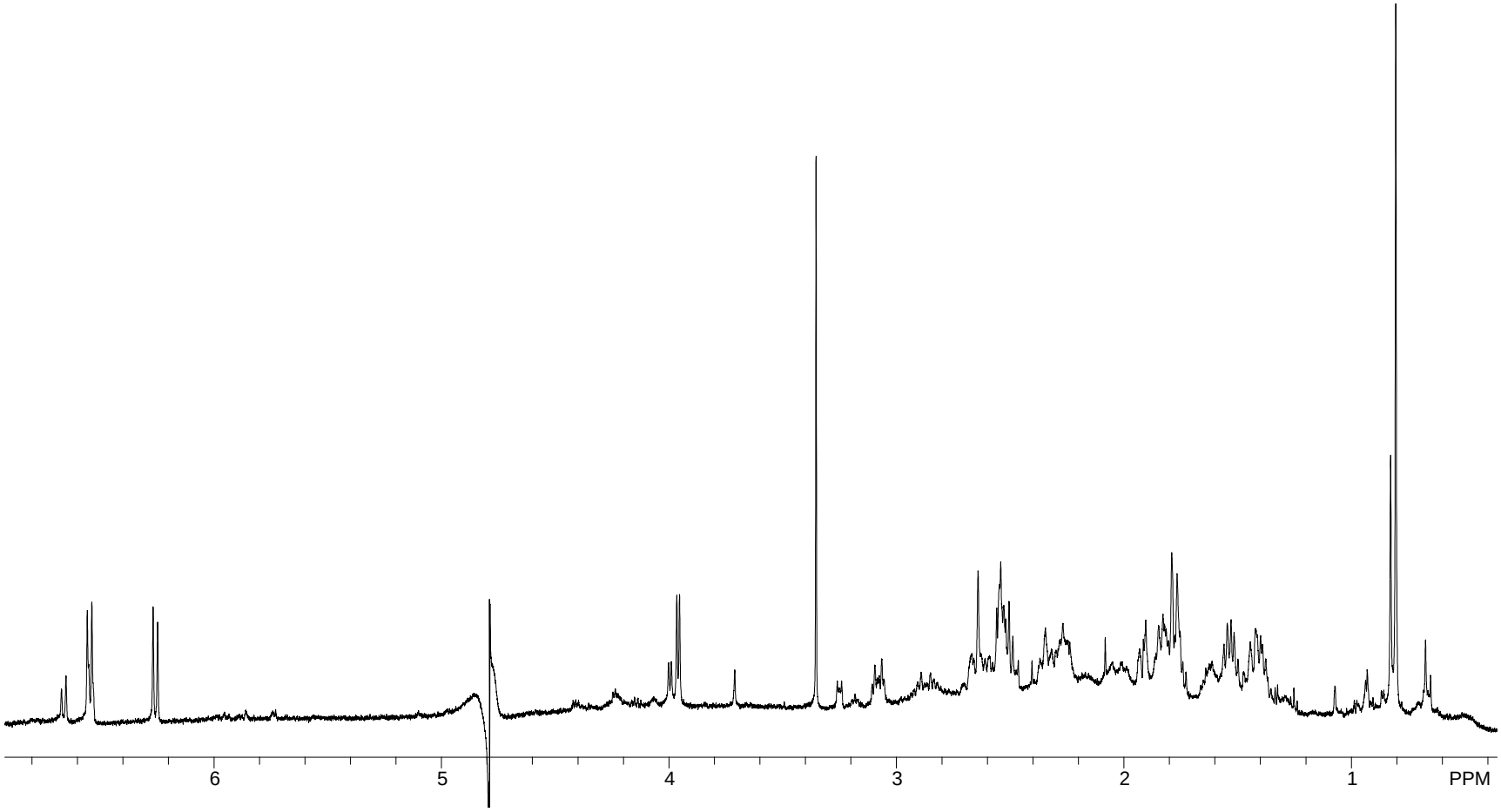

Figure A65. ^{1}H NMR Spectrum of α–Trenbolone (**5.4**); NMR Tube Experiment, Five Days After Photolysis (D_2O, 500 MHz)

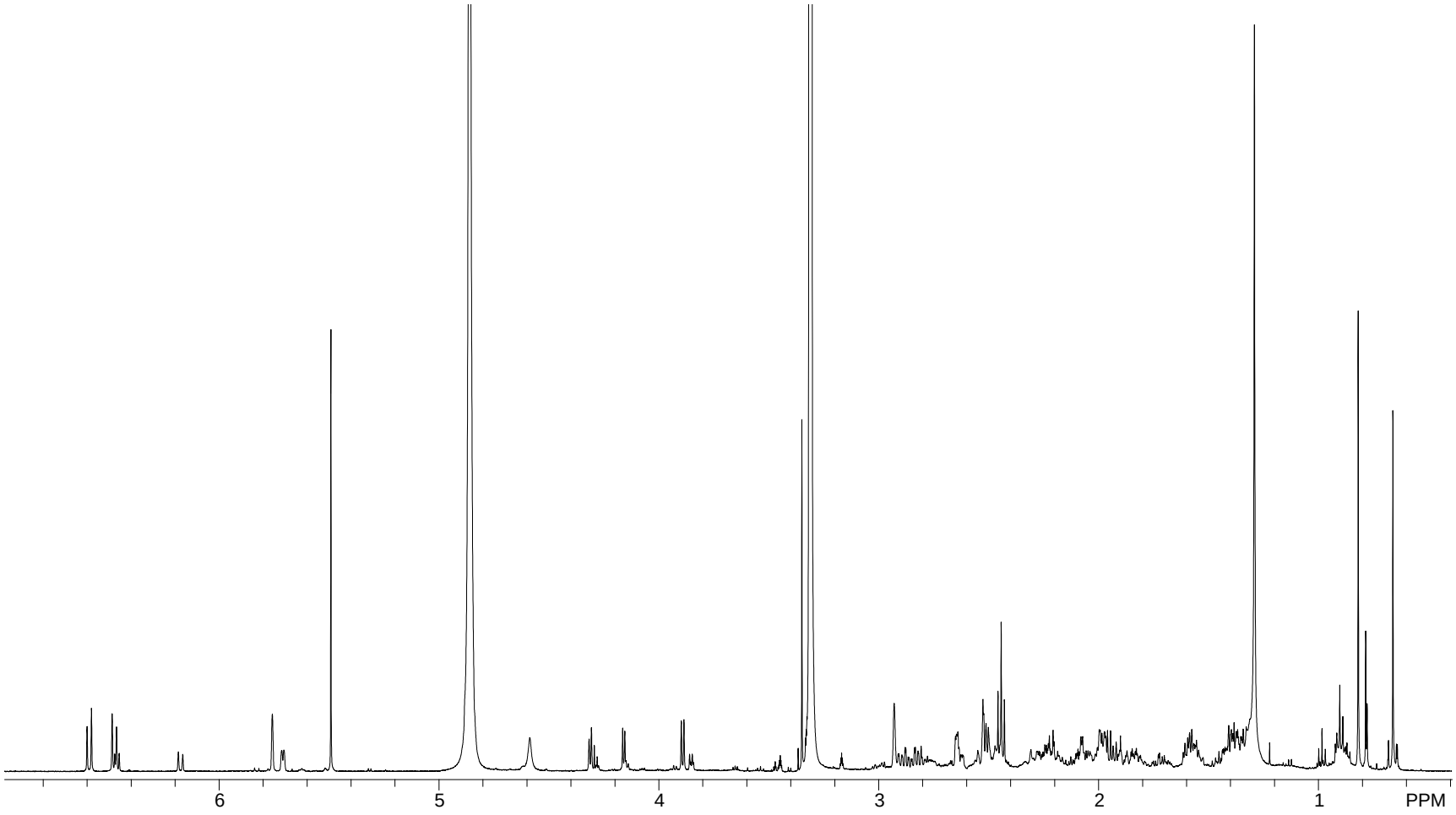

Figure A66. ^{1}H NMR Spectrum of α–Trenbolone (**5.4**) After Photolysis in H_2O, and Extraction with CH_2Cl_2 (CD_3OD, 500 MHz)

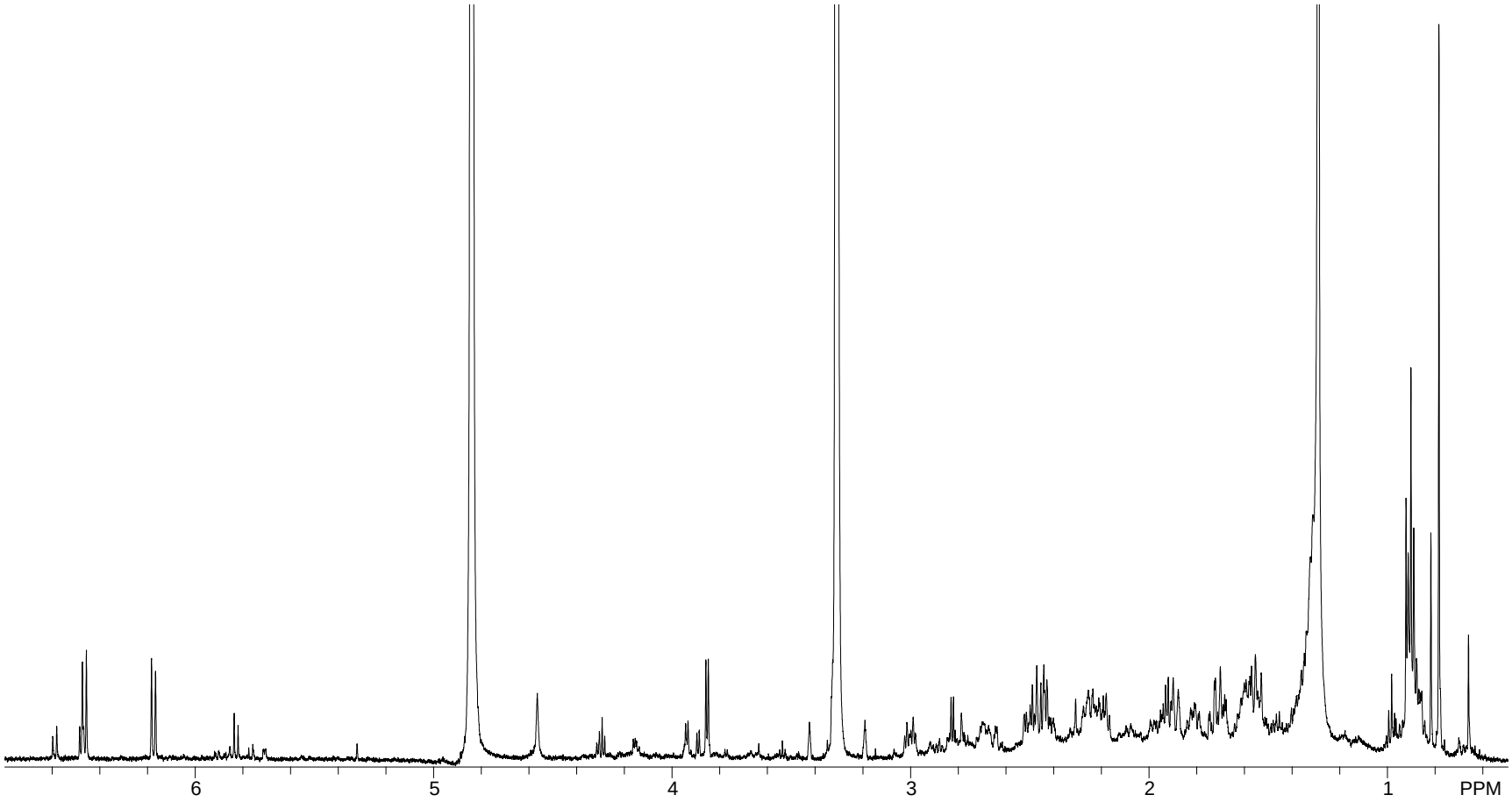

Figure A67. ^{1}H NMR Spectrum of α–Trenbolone (**5.4**) After Photolysis in D_2O, and Extraction with CH_2Cl_2 (CD_3OD, 500 MHz)

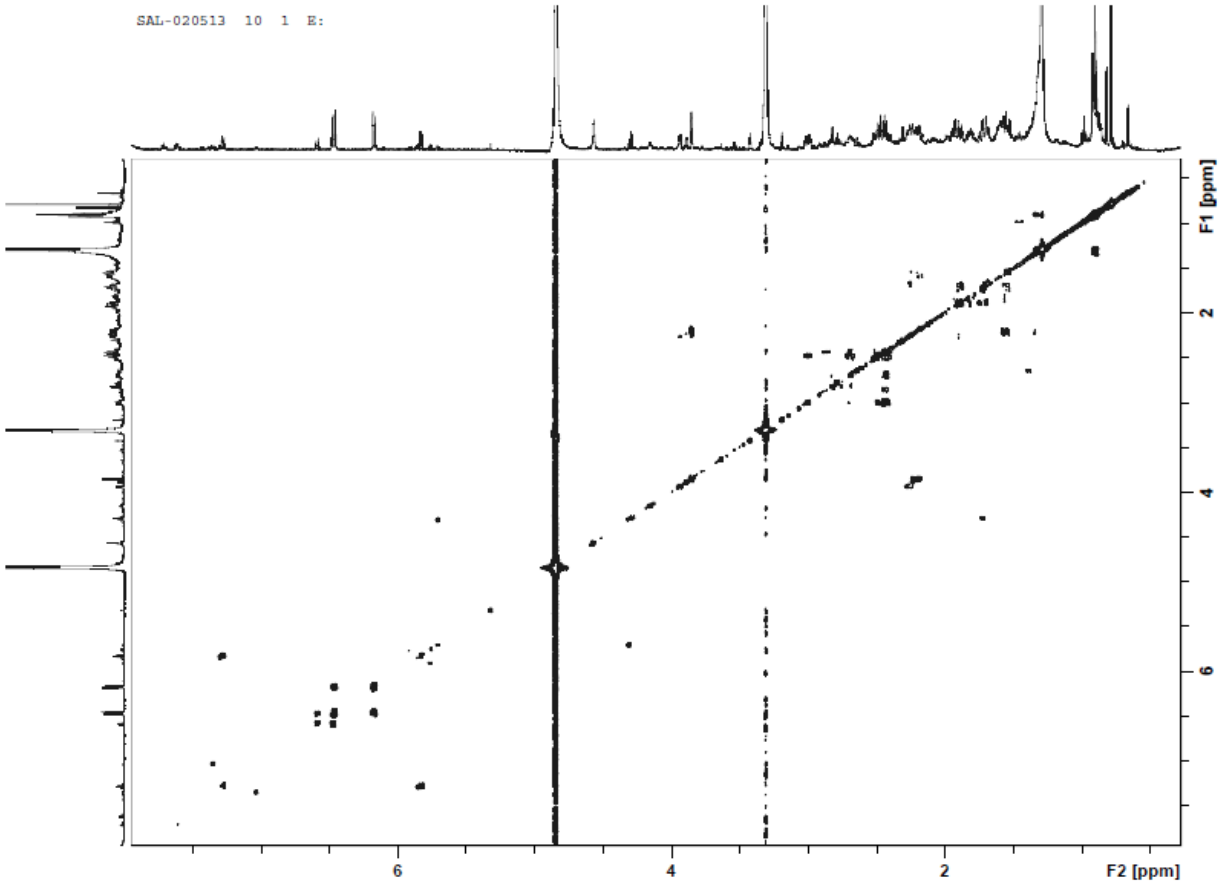

Figure A68. COSY NMR Spectrum of α–Trenbolone (**5.4**) After Photolysis in D_2O, and Extraction with CH_2Cl_2 (CD_3OD, 600 MHz)

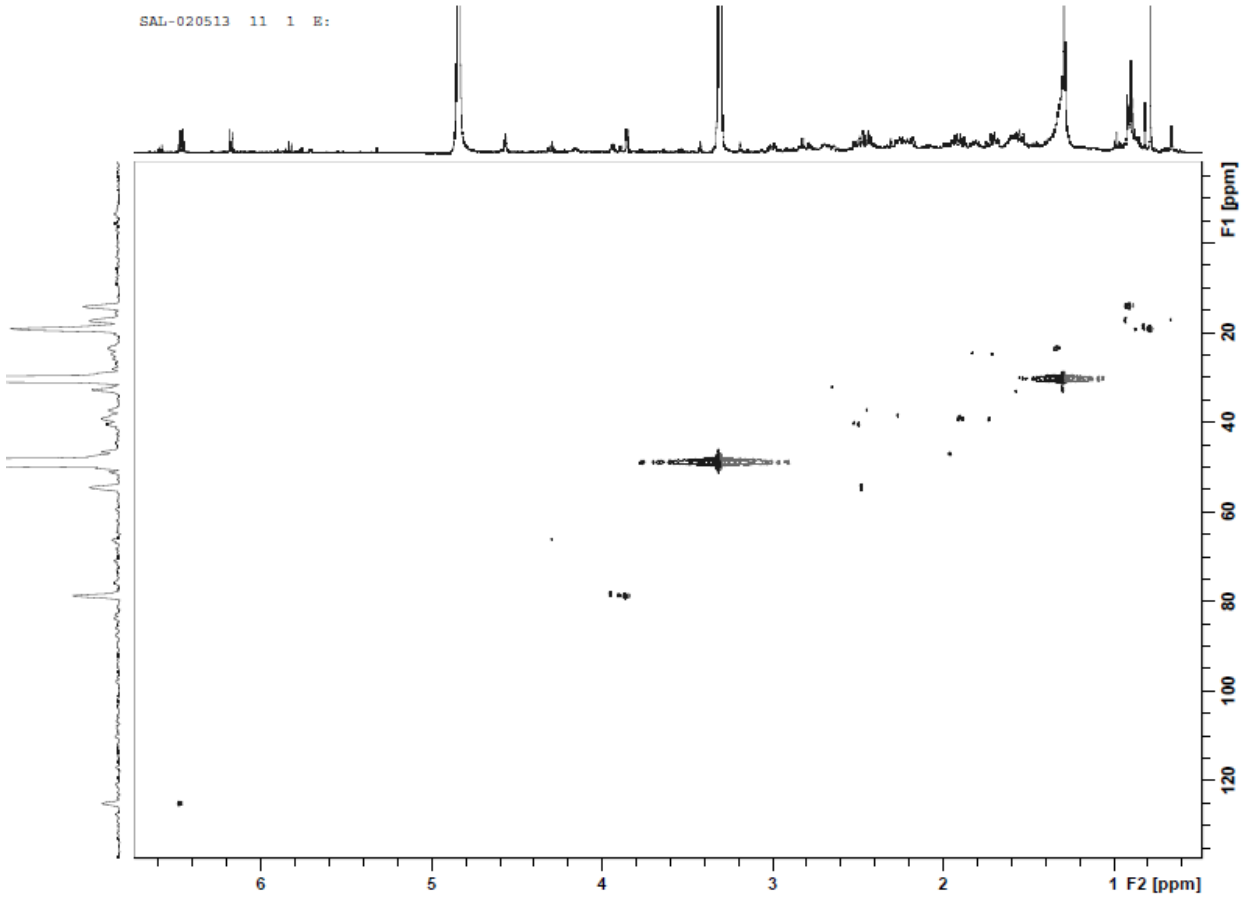

Figure A69. HSQC NMR Spectrum of α–Trenbolone (**5.4**) After Photolysis in D_2O, and Extraction with CH_2Cl_2 (CD_3OD, 600 MHz)

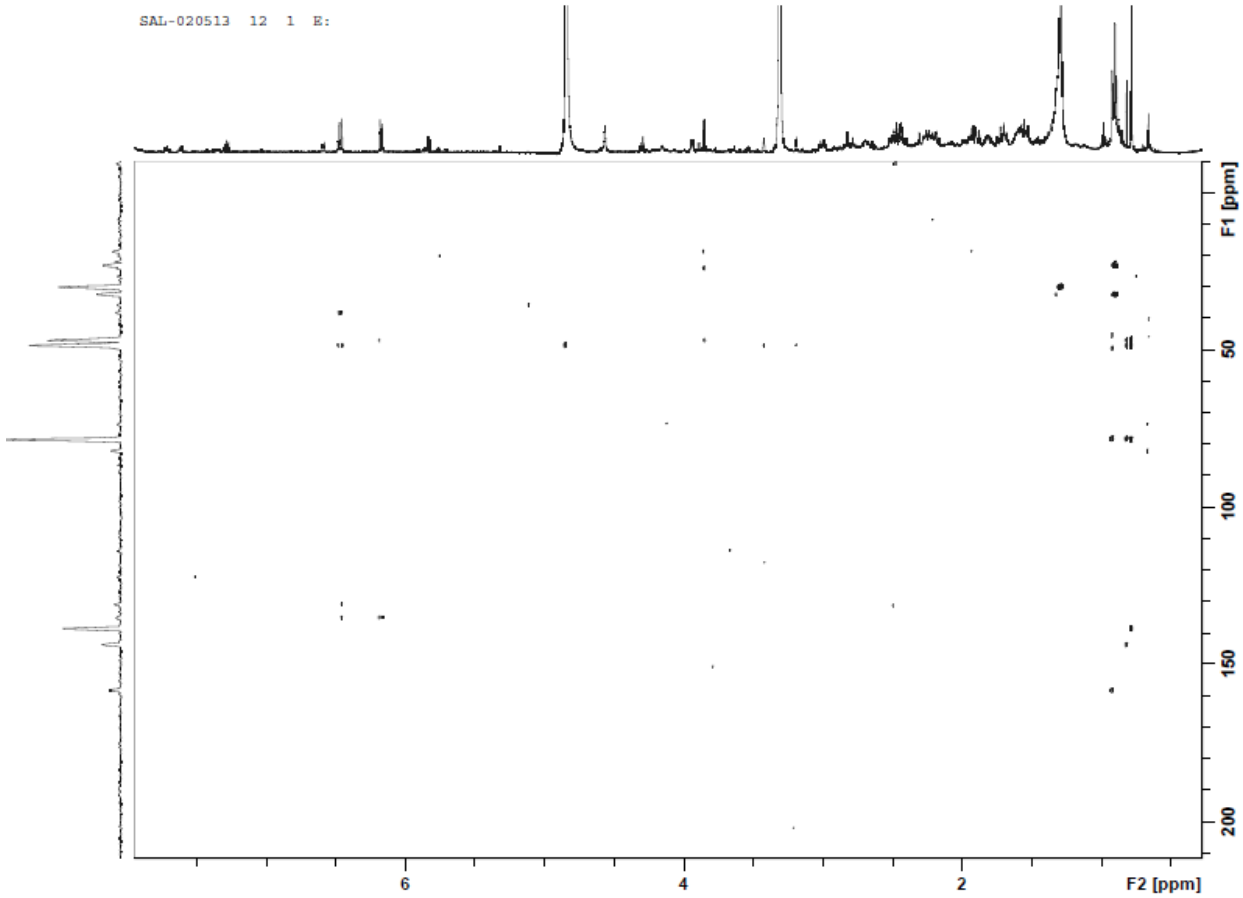

Figure A70. HMBC NMR Spectrum of α–Trenbolone (**5.4**) After Photolysis in D_2O, and Extraction with CH_2Cl_2 (CD_3OD, 600 MHz)

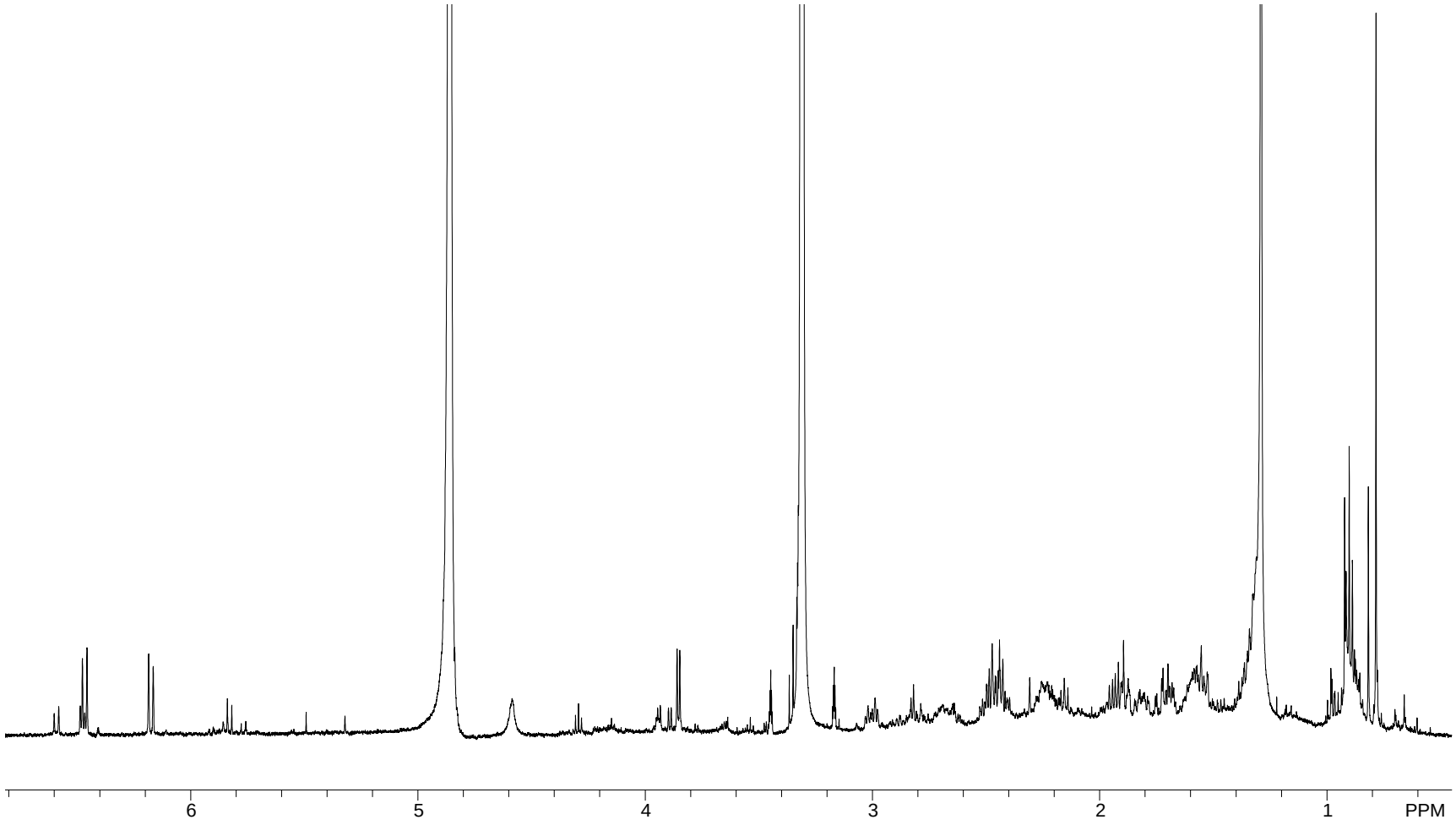

Figure A71. ^{1}H NMR Spectrum of α–Trenbolone (**5.4**) After Photolysis in D_2O, Extraction with CH_2Cl_2, Dried and Stored in the Dark, After 23 Days (CD_3OD, 500 MHz)

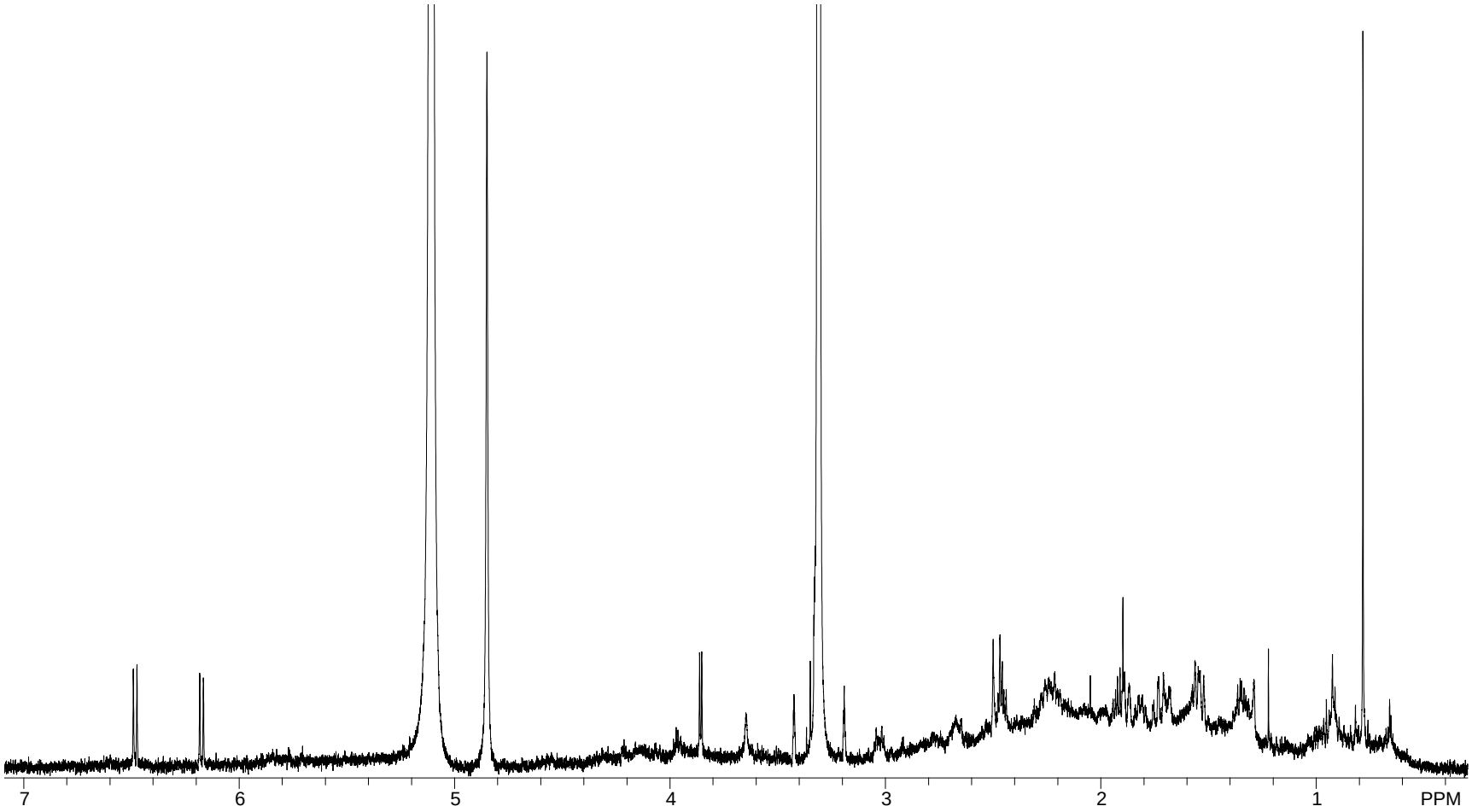

Figure A72. ^{1}H NMR Spectrum of α–Trenbolone (**5.4**) After Photolysis in D_2O, Dried, and Dissolved in CD_3OD (500 MHz)

APPENDIX B

X–Ray Crystallographic Data of 15-*epi*-oxepinamide E

(GLO11_6)

Table B1. Crystal Data and Structure Refinement for Glo11_6.

Identification code	Glo11_6
Empirical formula	C22.48 H22.48 Cl1.45 N3 O4
Formula weight	450.13
Temperature	220(2) K
Wavelength	0.71073 A
Crystal system, space group	Orthorhombic, P 21 21 2
Unit cell dimensions	a = 16.2855(16) A alpha = 90 deg. b = 19.469(2) A beta = 90 deg. c = 15.3159(15) A gamma = 90 deg.
Volume	4856.1(8) A^3
Z, Calculated density	8, 1.231 Mg/m^3
Absorption coefficient	0.238 mm^-1
F(000)	1880
Crystal size	0.18 x 0.12 x 0.03 mm
Theta range for data collection	2.94 to 20.00 deg.
Limiting indices	-15<=h<=15, -18<=k<=18, -14<=l<=14
Reflections collected / unique	45918 / 4525 [R(int) = 0.1271]
Completeness to theta = 20.00	99.5 %
Absorption correction	Semi-empirical from equivalents
Max. and min. transmission	0.9941 and 0.9584
Refinement method	Full-matrix least-squares on F^2
Data / restraints / parameters	4525 / 20 / 449
Goodness-of-fit on F^2	1.045
Final R indices [I>2sigma(I)]	R1 = 0.1152, wR2 = 0.2984
R indices (all data)	R1 = 0.1858, wR2 = 0.3537
Absolute structure parameter	0.0(4)
Largest diff. peak and hole	0.417 and -0.324 e.A^-3

Table B2. Atomic Coordinates (x 10^4) and Equivalent Isotropic Displacement Parameters (A^2 x 10^3) for Glo11_6. U(eq) is Defined as One Third of the Trace of the Orthogonalized Uij Tensor.

x	y	z	U(eq)	
C(1)	7180(12)	4698(9)	8043(9)	81(6)
O(1)	7037(9)	5259(5)	7743(6)	102(5)
N(2)	7426(10)	4139(6)	7577(7)	89(5)
C(3)	7606(9)	3468(7)	7885(9)	58(4)
C(4)	7580(9)	3348(8)	8751(10)	68(4)
N(5)	7834(7)	2724(6)	9093(8)	70(3)
C(6)	7873(10)	2632(8)	9917(10)	75(5)
O(7)	8242(8)	2053(5)	10146(6)	92(4)
C(8)	8004(17)	1690(8)	10882(14)	106(8)
C(9)	7388(18)	1768(10)	11423(11)	107(8)
C(10)	6780(14)	2284(9)	11457(11)	97(6)
C(11)	6910(12)	2907(8)	11062(9)	85(6)
C(12)	7667(10)	3150(7)	10589(10)	63(4)
O(12)	8339(7)	3211(4)	11163(6)	82(3)
C(13)	7485(11)	3837(7)	10232(8)	72(5)
O(13)	7328(8)	4349(4)	10707(6)	90(4)
N(14)	7379(7)	3914(6)	9339(7)	64(3)
C(15)	7042(10)	4575(7)	9032(9)	65(4)
C(16)	6106(14)	4577(7)	9137(9)	98(8)
C(1')	5642(12)	4041(9)	8682(12)	91(6)
C(2')	5330(12)	4064(11)	7825(12)	93(6)
C(3')	4923(13)	3515(13)	7425(12)	99(6)
C(4')	4768(14)	2900(13)	7846(16)	113(7)
C(5')	5052(16)	2848(10)	8647(18)	124(7)
C(6')	5436(12)	3413(13)	9064(13)	112(7)
C(17)	7781(10)	2903(8)	7230(10)	69(4)
C(18)	8568(14)	3042(9)	6786(11)	106(7)
C(19)	9316(19)	3031(10)	7402(17)	160(10)
C(20)	7107(12)	2868(9)	6581(11)	100(6)
C(1A)	7282(12)	-783(8)	6931(9)	74(5)
O(1A)	7047(8)	-1376(5)	7209(5)	87(4)
N(2A)	7599(9)	-340(5)	7444(6)	73(4)
C(3A)	7851(10)	298(8)	7124(10)	69(4)
C(4A)	7832(9)	436(7)	6264(9)	57(4)
N(5A)	8175(7)	1066(6)	5956(8)	65(3)
C(6A)	8198(10)	1149(6)	5133(9)	69(5)
O(7A)	8609(9)	1735(5)	4904(6)	98(4)
C(8A)	8400(16)	2154(10)	4228(14)	95(6)
C(9A)	7800(20)	2144(11)	3750(15)	114(8)
C(10A)	7112(19)	1662(14)	3740(12)	128(9)
C(11A)	7147(14)	1016(9)	4062(11)	104(6)
C(12A)	7911(10)	696(7)	4444(10)	68(4)

Table B2. Continued

O(12A)	8546(7)	617(5)	3821(6)	84(3)
C(13A)	7642(9)	4(6)	4823(8)	51(4)
O(13A)	7469(7)	-473(5)	4310(5)	67(3)
N(14A)	7549(6)	-57(5)	5669(7)	49(3)
C(15A)	7096(9)	-645(7)	6015(9)	57(4)
C(16A)	6153(13)	-498(7)	5929(8)	120(8)
C(17A)	8196(12)	807(10)	7837(13)	101(6)
C(20A)	7570(15)	962(9)	8492(10)	123(8)
C(18A)	8996(14)	531(10)	8208(12)	122(8)
C(19A)	9523(14)	961(12)	8826(13)	137(8)
C(1"A)	5910(12)	0(7)	6621(10)	71(8)
C(2"A)	5961(11)	699(7)	6439(10)	71
C(3"A)	5642(12)	1174(6)	7024(11)	71
C(4"A)	5272(12)	952(8)	7792(11)	71
C(5"A)	5222(11)	254(9)	7974(9)	71
C(6"A)	5541(12)	-222(7)	7388(10)	71
C(1'A)	5697(17)	-175(9)	5179(13)	128(14)
C(2'A)	5456(19)	-588(11)	4485(14)	128
C(3'A)	5110(20)	-294(17)	3744(12)	128
C(4'A)	5010(20)	414(17)	3696(14)	128
C(5'A)	5250(19)	827(12)	4390(17)	128
C(6'A)	5594(17)	533(9)	5132(16)	128
C(99)	9729(6)	8474(6)	5897(7)	71(8)
Cl(1)	9165(9)	8489(6)	6870(7)	149(6)
Cl(2)	9642(13)	9270(7)	5374(10)	252(11)
Cl(3)	9346(11)	7829(7)	5214(8)	187(8)
C(99')	9035(7)	8314(7)	5420(10)	160(40)
Cl(1')	9005(19)	8403(10)	6556(10)	125(10)
Cl(2')	9467(9)	9052(6)	4957(9)	59(4)
Cl(3')	9631(11)	7598(6)	5146(10)	64(5)
Cl(4)	5850(30)	10(20)	1380(30)	74(15)
C(98)	4990(20)	-375(19)	900(20)	74
Cl(5)	4400(30)	250(30)	370(40)	150(20)
Cl(6)	5300(30)	-990(20)	140(30)	84(14)
Cl(4')	5930(30)	300(30)	1500(30)	83(16)
C(98')	5370(30)	-450(30)	1290(20)	83
Cl(5')	4320(30)	-270(40)	1360(50)	150(40)
Cl(6')	5610(40)	-750(30)	240(30)	120(20)

Table B3. Bond Lengths [A] and Angles [deg] for Glo11_6.

C(1)-O(1)	1.208(16)
C(1)-N(2)	1.361(18)
C(1)-C(15)	1.55(2)
N(2)-C(3)	1.419(17)
N(2)-H(2)	0.8700
C(3)-C(4)	1.347(18)
C(3)-C(17)	1.51(2)
C(4)-N(5)	1.387(17)
C(4)-N(14)	1.459(17)
N(5)-C(6)	1.275(17)
C(6)-O(7)	1.326(18)
C(6)-C(12)	1.48(2)
O(7)-C(8)	1.39(2)
C(8)-C(9)	1.31(3)
C(8)-H(8)	0.9400
C(9)-C(10)	1.41(3)
C(9)-H(9)	0.9400
C(10)-C(11)	1.37(2)
C(10)-H(10)	0.9400
C(11)-C(12)	1.51(2)
C(11)-H(11)	0.9400
C(12)-O(12)	1.409(17)
C(12)-C(13)	1.474(18)
O(12)-H(12)	0.8300
C(13)-O(13)	1.262(14)
C(13)-N(14)	1.387(16)
N(14)-C(15)	1.476(17)
C(15)-C(16)	1.53(2)
C(15)-H(15)	0.9900
C(16)-C(1')	1.47(2)
C(16)-H(16A)	0.9800
C(16)-H(16B)	0.9800
C(1')-C(6')	1.40(3)
C(1')-C(2')	1.41(2)
C(2')-C(3')	1.40(2)
C(2')-H(2')	0.9400
C(3')-C(4')	1.38(3)
C(3')-H(3')	0.9400
C(4')-C(5')	1.32(3)
C(4')-H(4')	0.9400
C(5')-C(6')	1.42(3)
C(5')-H(5')	0.9400
C(6')-H(6')	0.9400
C(17)-C(18)	1.48(2)
C(17)-C(20)	1.48(2)
C(17)-H(17)	0.9900
C(18)-C(19)	1.54(3)
C(18)-H(18A)	0.9800
C(18)-H(18B)	0.9800
C(19)-H(19A)	0.9700
C(19)-H(19B)	0.9700
C(19)-H(19C)	0.9700

Table B3. Continued

C(20)-H(20A)	0.9700
C(20)-H(20B)	0.9700
C(20)-H(20C)	0.9700
C(1A)-N(2A)	1.276(17)
C(1A)-O(1A)	1.289(16)
C(1A)-C(15A)	1.460(19)
N(2A)-C(3A)	1.397(17)
N(2A)-H(2A)	0.8700
C(3A)-C(4A)	1.344(18)
C(3A)-C(17A)	1.58(2)
C(4A)-N(14A)	1.401(15)
C(4A)-N(5A)	1.428(17)
N(5A)-C(6A)	1.271(16)
C(6A)-O(7A)	1.368(16)
C(6A)-C(12A)	1.453(19)
O(7A)-C(8A)	1.36(2)
C(8A)-C(9A)	1.22(3)
C(8A)-H(8A)	0.9400
C(9A)-C(10A)	1.46(3)
C(9A)-H(9A)	0.9400
C(10A)-C(11A)	1.35(3)
C(10A)-H(10A)	0.9400
C(11A)-C(12A)	1.51(2)
C(11A)-H(11A)	0.9400
C(12A)-O(12A)	1.415(17)
C(12A)-C(13A)	1.532(18)
O(12A)-H(12A)	0.8300
C(13A)-O(13A)	1.248(13)
C(13A)-N(14A)	1.310(14)
N(14A)-C(15A)	1.461(16)
C(15A)-C(16A)	1.57(2)
C(15A)-H(15A)	0.9900
C(16A)-C(1"A)	1.489(9)
C(16A)-C(1'A)	1.505(9)
C(17A)-C(20A)	1.46(2)
C(17A)-C(18A)	1.52(3)
C(17A)-H(17A)	0.9900
C(20A)-H(20D)	0.9700
C(20A)-H(20E)	0.9700
C(20A)-H(20F)	0.9700
C(18A)-C(19A)	1.53(2)
C(18A)-H(18C)	0.9800
C(18A)-H(18D)	0.9800
C(19A)-H(19D)	0.9700
C(19A)-H(19E)	0.9700
C(19A)-H(19F)	0.9700
C(1"A)-C(2"A)	1.3900
C(1"A)-C(6"A)	1.3900
C(2"A)-C(3"A)	1.3900
C(2"A)-H(2"A)	0.9400
C(3"A)-C(4"A)	1.3900
C(3"A)-H(3"A)	0.9400
C(4"A)-C(5"A)	1.3900
C(4"A)-H(4"A)	0.9400
C(5"A)-C(6"A)	1.3900

Table B3. Continued

C(5"A)-H(5"A)	0.9400
C(6"A)-H(6"A)	0.9400
C(1'A)-C(2'A)	1.3900
C(1'A)-C(6'A)	1.3900
C(2'A)-C(3'A)	1.3900
C(2'A)-H(2'A)	0.9400
C(3'A)-C(4'A)	1.3900
C(3'A)-H(3'A)	0.9400
C(4'A)-C(5'A)	1.3900
C(4'A)-H(4'A)	0.9400
C(5'A)-C(6'A)	1.3900
C(5'A)-H(5'A)	0.9400
C(6'A)-H(6'A)	0.9400
C(99)-Cl(1)	1.7499
C(99)-Cl(2)	1.7500
C(99)-Cl(3)	1.7500
C(99)-H(99)	0.9800
Cl(3)-H(99')	1.6391
C(99')-Cl(1')	1.7499
C(99')-Cl(2')	1.7499
C(99')-Cl(3')	1.7500
C(99')-H(99')	0.9800
Cl(4)-C(98)	1.7499
Cl(4)-H(98')	1.7577
C(98)-Cl(6)	1.7500
C(98)-Cl(5)	1.7500
C(98)-H(98)	0.9800
C(98)-H(98')	1.7322
Cl(4')-C(98')	1.7500
C(98')-Cl(5')	1.7499
C(98')-Cl(6')	1.7500
C(98')-H(98)	1.2022
C(98')-H(98')	0.9800
Cl(5')-H(98)	0.8296

O(1)-C(1)-N(2)	125.5(12)
O(1)-C(1)-C(15)	118.9(13)
N(2)-C(1)-C(15)	115.5(13)
C(1)-N(2)-C(3)	128.5(12)
C(1)-N(2)-H(2)	115.8
C(3)-N(2)-H(2)	115.8
C(4)-C(3)-N(2)	118.6(13)
C(4)-C(3)-C(17)	122.2(13)
N(2)-C(3)-C(17)	119.1(12)
C(3)-C(4)-N(5)	121.0(14)
C(3)-C(4)-N(14)	119.0(13)
N(5)-C(4)-N(14)	119.6(12)
C(6)-N(5)-C(4)	120.8(13)
N(5)-C(6)-O(7)	113.8(14)
N(5)-C(6)-C(12)	125.5(15)
O(7)-C(6)-C(12)	119.9(13)
C(6)-O(7)-C(8)	121.5(15)
C(9)-C(8)-O(7)	132.0(17)
C(9)-C(8)-H(8)	114.0
O(7)-C(8)-H(8)	114.0

Table B3. Continued

C(8)-C(9)-C(10)	130.1(16)
C(8)-C(9)-H(9)	114.9
C(10)-C(9)-H(9)	114.9
C(11)-C(10)-C(9)	120.2(19)
C(11)-C(10)-H(10)	119.9
C(9)-C(10)-H(10)	119.9
C(10)-C(11)-C(12)	128.1(17)
C(10)-C(11)-H(11)	116.0
C(12)-C(11)-H(11)	116.0
O(12)-C(12)-C(13)	108.2(12)
O(12)-C(12)-C(6)	108.3(12)
C(13)-C(12)-C(6)	113.9(13)
O(12)-C(12)-C(11)	111.2(12)
C(13)-C(12)-C(11)	107.4(14)
C(6)-C(12)-C(11)	107.8(12)
C(12)-O(12)-H(12)	109.5
O(13)-C(13)-N(14)	117.3(11)
O(13)-C(13)-C(12)	123.0(11)
N(14)-C(13)-C(12)	119.2(12)
C(13)-N(14)-C(4)	120.0(11)
C(13)-N(14)-C(15)	117.0(11)
C(4)-N(14)-C(15)	123.0(11)
N(14)-C(15)-C(16)	109.8(12)
N(14)-C(15)-C(1)	113.1(12)
C(16)-C(15)-C(1)	104.3(13)
N(14)-C(15)-H(15)	109.8
C(16)-C(15)-H(15)	109.8
C(1)-C(15)-H(15)	109.8
C(1')-C(16)-C(15)	117.4(14)
C(1')-C(16)-H(16A)	108.0
C(15)-C(16)-H(16A)	108.0
C(1')-C(16)-H(16B)	108.0
C(15)-C(16)-H(16B)	108.0
H(16A)-C(16)-H(16B)	107.2
C(6')-C(1')-C(2')	109.4(19)
C(6')-C(1')-C(16)	123.2(17)
C(2')-C(1')-C(16)	127.4(17)
C(3')-C(2')-C(1')	123.7(19)
C(3')-C(2')-H(2')	118.1
C(1')-C(2')-H(2')	118.1
C(4')-C(3')-C(2')	123.0(18)
C(4')-C(3')-H(3')	118.5
C(2')-C(3')-H(3')	118.5
C(5')-C(4')-C(3')	116(2)
C(5')-C(4')-H(4')	122.1
C(3')-C(4')-H(4')	122.1
C(4')-C(5')-C(6')	121(2)
C(4')-C(5')-H(5')	119.5
C(6')-C(5')-H(5')	119.5
C(5')-C(6')-C(1')	126.6(19)
C(5')-C(6')-H(6')	116.7
C(1')-C(6')-H(6')	116.7
C(18)-C(17)-C(20)	110.0(14)
C(18)-C(17)-C(3)	109.6(13)
C(20)-C(17)-C(3)	109.8(13)

Table B3. Continued

C(18)-C(17)-H(17)	109.1
C(20)-C(17)-H(17)	109.1
C(3)-C(17)-H(17)	109.1
C(17)-C(18)-C(19)	113.6(16)
C(17)-C(18)-H(18A)	108.8
C(19)-C(18)-H(18A)	108.8
C(17)-C(18)-H(18B)	108.8
C(19)-C(18)-H(18B)	108.8
H(18A)-C(18)-H(18B)	107.7
C(18)-C(19)-H(19A)	109.5
C(18)-C(19)-H(19B)	109.5
H(19A)-C(19)-H(19B)	109.5
C(18)-C(19)-H(19C)	109.5
H(19A)-C(19)-H(19C)	109.5
H(19B)-C(19)-H(19C)	109.5
C(17)-C(20)-H(20A)	109.5
C(17)-C(20)-H(20B)	109.5
H(20A)-C(20)-H(20B)	109.5
C(17)-C(20)-H(20C)	109.5
H(20A)-C(20)-H(20C)	109.5
H(20B)-C(20)-H(20C)	109.5
N(2A)-C(1A)-O(1A)	121.5(12)
N(2A)-C(1A)-C(15A)	123.5(13)
O(1A)-C(1A)-C(15A)	114.9(13)
C(1A)-N(2A)-C(3A)	120.3(12)
C(1A)-N(2A)-H(2A)	119.9
C(3A)-N(2A)-H(2A)	119.9
C(4A)-C(3A)-N(2A)	120.9(13)
C(4A)-C(3A)-C(17A)	124.1(15)
N(2A)-C(3A)-C(17A)	114.9(13)
C(3A)-C(4A)-N(14A)	120.5(13)
C(3A)-C(4A)-N(5A)	119.1(13)
N(14A)-C(4A)-N(5A)	120.1(11)
C(6A)-N(5A)-C(4A)	116.7(12)
N(5A)-C(6A)-O(7A)	112.1(12)
N(5A)-C(6A)-C(12A)	129.3(13)
O(7A)-C(6A)-C(12A)	118.5(12)
C(8A)-O(7A)-C(6A)	124.9(15)
C(9A)-C(8A)-O(7A)	130(2)
C(9A)-C(8A)-H(8A)	114.8
O(7A)-C(8A)-H(8A)	114.8
C(8A)-C(9A)-C(10A)	129(2)
C(8A)-C(9A)-H(9A)	115.5
C(10A)-C(9A)-H(9A)	115.5
C(11A)-C(10A)-C(9A)	124(2)
C(11A)-C(10A)-H(10A)	117.9
C(9A)-C(10A)-H(10A)	117.9
C(10A)-C(11A)-C(12A)	124(2)
C(10A)-C(11A)-H(11A)	118.0
C(12A)-C(11A)-H(11A)	118.0
O(12A)-C(12A)-C(6A)	108.7(13)
O(12A)-C(12A)-C(11A)	112.7(13)
C(6A)-C(12A)-C(11A)	107.3(13)
O(12A)-C(12A)-C(13A)	111.6(12)
C(6A)-C(12A)-C(13A)	110.6(12)

Table B3. Continued

C(11A)-C(12A)-C(13A)	105.9(13)
C(12A)-O(12A)-H(12A)	109.5
O(13A)-C(13A)-N(14A)	122.0(11)
O(13A)-C(13A)-C(12A)	118.7(11)
N(14A)-C(13A)-C(12A)	119.1(12)
C(13A)-N(14A)-C(4A)	123.0(11)
C(13A)-N(14A)-C(15A)	119.1(11)
C(4A)-N(14A)-C(15A)	117.8(10)
C(1A)-C(15A)-N(14A)	112.8(12)
C(1A)-C(15A)-C(16A)	108.5(12)
N(14A)-C(15A)-C(16A)	108.8(11)
C(1A)-C(15A)-H(15A)	108.9
N(14A)-C(15A)-H(15A)	108.9
C(16A)-C(15A)-H(15A)	108.9
C(1"A)-C(16A)-C(1'A)	98.1(13)
C(1"A)-C(16A)-C(15A)	108.6(14)
C(1'A)-C(16A)-C(15A)	128.5(17)
C(20A)-C(17A)-C(18A)	114.5(18)
C(20A)-C(17A)-C(3A)	110.9(15)
C(18A)-C(17A)-C(3A)	110.0(15)
C(20A)-C(17A)-H(17A)	107.0
C(18A)-C(17A)-H(17A)	107.0
C(3A)-C(17A)-H(17A)	107.0
C(17A)-C(20A)-H(20D)	109.5
C(17A)-C(20A)-H(20E)	109.5
H(20D)-C(20A)-H(20E)	109.5
C(17A)-C(20A)-H(20F)	109.5
H(20D)-C(20A)-H(20F)	109.5
H(20E)-C(20A)-H(20F)	109.5
C(17A)-C(18A)-C(19A)	121.3(19)
C(17A)-C(18A)-H(18C)	107.0
C(19A)-C(18A)-H(18C)	107.0
C(17A)-C(18A)-H(18D)	107.0
C(19A)-C(18A)-H(18D)	107.0
H(18C)-C(18A)-H(18D)	106.7
C(18A)-C(19A)-H(19D)	109.5
C(18A)-C(19A)-H(19E)	109.5
H(19D)-C(19A)-H(19E)	109.5
C(18A)-C(19A)-H(19F)	109.5
H(19D)-C(19A)-H(19F)	109.5
H(19E)-C(19A)-H(19F)	109.5
C(2"A)-C(1"A)-C(6"A)	120.0
C(2"A)-C(1"A)-C(16A)	118.6(7)
C(6"A)-C(1"A)-C(16A)	120.9(7)
C(3"A)-C(2"A)-C(1"A)	120.0
C(3"A)-C(2"A)-H(2"A)	120.0
C(1"A)-C(2"A)-H(2"A)	120.0
C(2"A)-C(3"A)-C(4"A)	120.0
C(2"A)-C(3"A)-H(3"A)	120.0
C(4"A)-C(3"A)-H(3"A)	120.0
C(5"A)-C(4"A)-C(3"A)	120.0
C(5"A)-C(4"A)-H(4"A)	120.0
C(3"A)-C(4"A)-H(4"A)	120.0
C(6"A)-C(5"A)-C(4"A)	120.0
C(6"A)-C(5"A)-H(5"A)	120.0

Table B3. Continued

C(4"A)-C(5"A)-H(5"A)	120.0
C(5"A)-C(6"A)-C(1"A)	120.0
C(5"A)-C(6"A)-H(6"A)	120.0
C(1"A)-C(6"A)-H(6"A)	120.0
C(2'A)-C(1'A)-C(6'A)	120.0
C(2'A)-C(1'A)-C(16A)	118.8(8)
C(6'A)-C(1'A)-C(16A)	120.9(8)
C(3'A)-C(2'A)-C(1'A)	120.0
C(3'A)-C(2'A)-H(2'A)	120.0
C(1'A)-C(2'A)-H(2'A)	120.0
C(2'A)-C(3'A)-C(4'A)	120.0
C(2'A)-C(3'A)-H(3'A)	120.0
C(4'A)-C(3'A)-H(3'A)	120.0
C(5'A)-C(4'A)-C(3'A)	120.0
C(5'A)-C(4'A)-H(4'A)	120.0
C(3'A)-C(4'A)-H(4'A)	120.0
C(4'A)-C(5'A)-C(6'A)	120.0
C(4'A)-C(5'A)-H(5'A)	120.0
C(6'A)-C(5'A)-H(5'A)	120.0
C(5'A)-C(6'A)-C(1'A)	120.0
C(5'A)-C(6'A)-H(6'A)	120.0
C(1'A)-C(6'A)-H(6'A)	120.0
Cl(1)-C(99)-Cl(2)	109.5
Cl(1)-C(99)-Cl(3)	109.5
Cl(2)-C(99)-Cl(3)	109.5
Cl(1')-C(99')-Cl(2')	109.5
Cl(1')-C(99')-Cl(3')	109.5
Cl(2')-C(99')-Cl(3')	109.5
Cl(1')-C(99')-H(99')	109.5
Cl(2')-C(99')-H(99')	109.5
Cl(3')-C(99')-H(99')	109.5
Cl(4)-C(98)-Cl(6)	109.5
Cl(4)-C(98)-Cl(5)	109.5
Cl(6)-C(98)-Cl(5)	109.5
Cl(5')-C(98')-Cl(4')	109.5
Cl(5')-C(98')-Cl(6')	109.5
Cl(4')-C(98')-Cl(6')	109.5

Table B4. Anisotropic Displacement Parameters (A^2 x 10^3) for Glo11_6. The Anisotropic Displacement Factor Exponent Takes the Form: -2 pi^2 [h^2 a^{*2} U11 + ... + 2 h k a* b* U12]

	U11	U22	U33	U23	U13	U12
C(1)	159(17)	55(11)	29(8)	-16(9)	-1(9)	31(11)
O(1)	241(15)	29(6)	38(6)	22(5)	15(7)	23(7)
N(2)	182(15)	47(8)	36(7)	6(6)	-7(8)	1(9)
O(7)	207(13)	35(5)	36(6)	-11(5)	-6(7)	21(7)
C(8)	220(30)	49(11)	52(12)	4(11)	-41(15)	23(13)
C(9)	230(30)	58(13)	32(10)	27(9)	3(14)	-19(16)
C(10)	165(19)	53(11)	73(12)	22(10)	-3(12)	16(13)
C(11)	145(17)	62(11)	48(9)	-17(9)	-30(10)	25(11)
O(12)	138(10)	53(6)	55(6)	-6(5)	2(7)	15(6)
C(13)	160(16)	37(8)	17(7)	8(7)	-7(9)	2(9)
O(13)	206(13)	37(5)	29(5)	-11(5)	-20(7)	27(7)
C(16)	230(30)	21(8)	43(9)	13(7)	-30(12)	11(11)
C(1')	131(16)	60(12)	81(14)	32(11)	7(12)	21(12)
C(2')	115(16)	94(14)	70(13)	-1(11)	-7(11)	46(12)
C(3')	102(15)	122(17)	73(13)	-38(15)	-13(11)	12(14)
C(4')	126(19)	120(20)	96(18)	11(15)	-12(14)	-4(14)
C(5')	180(20)	73(14)	117(18)	12(14)	-3(18)	-9(15)
C(6')	113(17)	136(19)	88(14)	-16(16)	-28(12)	11(15)
C(18)	180(20)	81(12)	59(11)	-20(10)	-33(14)	34(13)
C(19)	230(30)	90(15)	160(20)	-41(16)	-20(20)	22(18)
C(20)	128(16)	99(13)	72(11)	-29(10)	8(12)	22(12)
C(1A)	141(16)	51(10)	29(8)	-3(8)	12(9)	-25(10)
O(1A)	166(11)	59(7)	35(5)	-7(5)	23(6)	-7(7)
N(2A)	182(14)	21(6)	17(5)	-3(5)	-1(7)	-24(7)
C(6A)	134(15)	26(8)	48(9)	12(7)	-27(9)	-24(9)
O(7A)	197(13)	57(7)	40(6)	6(6)	-4(7)	-31(8)
C(8A)	140(20)	73(13)	77(14)	16(13)	17(14)	1(13)
C(9A)	200(30)	65(13)	74(15)	8(11)	-22(16)	-11(18)
C(10A)	200(30)	116(18)	69(13)	-24(14)	-31(15)	70(20)
C(11A)	157(19)	65(12)	89(13)	14(11)	-9(13)	-2(12)
O(12A)	128(10)	66(6)	59(6)	-22(5)	43(7)	-29(6)
C(13A)	86(11)	31(7)	35(8)	5(7)	-7(8)	-9(8)
O(13A)	109(9)	65(6)	28(5)	1(5)	2(5)	-14(6)
C(16A)	180(20)	124(16)	59(11)	22(11)	-19(12)	-31(15)
C(20A)	230(20)	88(12)	49(10)	-10(9)	50(13)	-69(15)
C(18A)	180(20)	115(16)	74(13)	2(12)	-16(14)	-32(15)
C(19A)	160(20)	148(19)	103(15)	-22(15)	-25(15)	-9(17)

Table B5. Hydrogen Coordinates (x 10^4) and Isotropic Displacement Parameters (A^2 x10^3) for Glo11_6.

	x	y	z	U(eq)
H(2)	7480	4201	7018	106
H(8)	8349	1319	11019	127
H(9)	7344	1428	11856	128
H(10)	6283	2200	11752	117
H(11)	6472	3221	11089	102
H(12)	8223	3485	11559	123
H(15)	7285	4957	9371	79
H(16A)	5981	4542	9762	118
H(16B)	5901	5024	8938	118
H(2')	5400	4470	7503	112
H(3')	4747	3567	6845	119
H(4')	4478	2541	7575	135
H(5')	4999	2430	8948	149
H(6')	5565	3360	9658	135
H(17)	7819	2459	7541	83
H(18A)	8538	3494	6504	128
H(18B)	8649	2698	6327	128
H(19A)	9811	3128	7072	240
H(19B)	9362	2581	7671	240
H(19C)	9246	3376	7853	240
H(20A)	7235	2521	6147	150
H(20B)	7047	3311	6298	150
H(20C)	6599	2748	6874	150
H(2A)	7659	-436	7995	88
H(8A)	8777	2507	4111	114
H(9A)	7778	2495	3329	137
H(10A)	6613	1811	3495	154
H(11A)	6666	750	4046	125
H(12A)	8387	361	3422	127
H(15A)	7233	-1056	5665	68
H(17A)	8327	1243	7535	121
H(20D)	7702	1393	8777	184
H(20E)	7555	597	8923	184
H(20F)	7038	999	8212	184
H(18C)	9344	407	7710	147
H(18D)	8865	103	8514	147
H(19D)	10074	773	8848	206
H(19E)	9284	954	9406	206
H(19F)	9546	1431	8616	206
H(2"A)	6211	849	5920	85
H(3"A)	5676	1646	6901	85
H(4"A)	5056	1273	8188	85
H(5"A)	4971	103	8493	85
H(6"A)	5506	-694	7511	85
H(2'A)	5526	-1067	4517	153
H(3'A)	4949	-573	3274	153

Table B5. Continued

H(4'A)	4777	613	3195	153
H(5'A)	5181	1306	4358	153
H(6'A)	5757	813	5601	153
H(99)	10307	8382	6028	187
H(99')	8476	8252	5197	64
H(98)	4656	-595	1357	84
H(98')	5515	-806	1716	116

Table B6. Torsion Angles [deg] for Glo11_6.

O(1)-C(1)-N(2)-C(3)	179.9(18)
C(15)-C(1)-N(2)-C(3)	-3(3)
C(1)-N(2)-C(3)-C(4)	-4(3)
C(1)-N(2)-C(3)-C(17)	173.4(17)
N(2)-C(3)-C(4)-N(5)	-173.1(13)
C(17)-C(3)-C(4)-N(5)	10(2)
N(2)-C(3)-C(4)-N(14)	-1(2)
C(17)-C(3)-C(4)-N(14)	-177.9(13)
C(3)-C(4)-N(5)-C(6)	174.1(15)
N(14)-C(4)-N(5)-C(6)	2(2)
C(4)-N(5)-C(6)-O(7)	-170.2(13)
C(4)-N(5)-C(6)-C(12)	0(2)
N(5)-C(6)-O(7)-C(8)	-146.5(15)
C(12)-C(6)-O(7)-C(8)	43(2)
C(6)-O(7)-C(8)-C(9)	7(3)
O(7)-C(8)-C(9)-C(10)	-4(4)
C(8)-C(9)-C(10)-C(11)	-21(3)
C(9)-C(10)-C(11)-C(12)	-2(3)
N(5)-C(6)-C(12)-O(12)	-126.7(17)
O(7)-C(6)-C(12)-O(12)	42.9(19)
N(5)-C(6)-C(12)-C(13)	-6(2)
O(7)-C(6)-C(12)-C(13)	163.3(15)
N(5)-C(6)-C(12)-C(11)	112.8(17)
O(7)-C(6)-C(12)-C(11)	-77.6(18)
C(10)-C(11)-C(12)-O(12)	-65.4(19)
C(10)-C(11)-C(12)-C(13)	176.4(15)
C(10)-C(11)-C(12)-C(6)	53(2)
O(12)-C(12)-C(13)-O(13)	-57(2)
C(6)-C(12)-C(13)-O(13)	-177.2(16)
C(11)-C(12)-C(13)-O(13)	64(2)
O(12)-C(12)-C(13)-N(14)	131.6(15)
C(6)-C(12)-C(13)-N(14)	11(2)
C(11)-C(12)-C(13)-N(14)	-108.3(16)
O(13)-C(13)-N(14)-C(4)	177.7(14)
C(12)-C(13)-N(14)-C(4)	-10(2)
O(13)-C(13)-N(14)-C(15)	-4(2)
C(12)-C(13)-N(14)-C(15)	168.4(14)
C(3)-C(4)-N(14)-C(13)	-169.0(14)
N(5)-C(4)-N(14)-C(13)	4(2)
C(3)-C(4)-N(14)-C(15)	13(2)
N(5)-C(4)-N(14)-C(15)	-174.9(13)
C(13)-N(14)-C(15)-C(16)	-80.7(16)
C(4)-N(14)-C(15)-C(16)	97.7(15)
C(13)-N(14)-C(15)-C(1)	163.2(14)
C(4)-N(14)-C(15)-C(1)	-18(2)
O(1)-C(1)-C(15)-N(14)	-169.6(16)
N(2)-C(1)-C(15)-N(14)	13(2)
O(1)-C(1)-C(15)-C(16)	71(2)
N(2)-C(1)-C(15)-C(16)	-106.2(17)

Table B6. Continued

N(14)-C(15)-C(16)-C(1')	-58.7(16)
C(1)-C(15)-C(16)-C(1')	62.7(16)
C(15)-C(16)-C(1')-C(6')	92(2)
C(15)-C(16)-C(1')-C(2')	-88(2)
C(6')-C(1')-C(2')-C(3')	-3(2)
C(16)-C(1')-C(2')-C(3')	177.1(19)
C(1')-C(2')-C(3')-C(4')	2(3)
C(2')-C(3')-C(4')-C(5')	-2(3)
C(3')-C(4')-C(5')-C(6')	5(3)
C(4')-C(5')-C(6')-C(1')	-7(4)
C(2')-C(1')-C(6')-C(5')	6(3)
C(16)-C(1')-C(6')-C(5')	-174(2)
C(4)-C(3)-C(17)-C(18)	-114.7(17)
N(2)-C(3)-C(17)-C(18)	68.1(18)
C(4)-C(3)-C(17)-C(20)	124.3(17)
N(2)-C(3)-C(17)-C(20)	-52.8(19)
C(20)-C(17)-C(18)-C(19)	-175.4(15)
C(3)-C(17)-C(18)-C(19)	63.8(18)
O(1A)-C(1A)-N(2A)-C(3A)	179.8(15)
C(15A)-C(1A)-N(2A)-C(3A)	-5(3)
C(1A)-N(2A)-C(3A)-C(4A)	-6(2)
C(1A)-N(2A)-C(3A)-C(17A)	177.4(15)
N(2A)-C(3A)-C(4A)-N(14A)	1(2)
C(17A)-C(3A)-C(4A)-N(14A)	177.1(14)
N(2A)-C(3A)-C(4A)-N(5A)	-173.4(13)
C(17A)-C(3A)-C(4A)-N(5A)	3(2)
C(3A)-C(4A)-N(5A)-C(6A)	174.8(15)
N(14A)-C(4A)-N(5A)-C(6A)	0.8(19)
C(4A)-N(5A)-C(6A)-O(7A)	-174.1(13)
C(4A)-N(5A)-C(6A)-C(12A)	1(2)
N(5A)-C(6A)-O(7A)-C(8A)	-143.2(15)
C(12A)-C(6A)-O(7A)-C(8A)	41(2)
C(6A)-O(7A)-C(8A)-C(9A)	7(3)
O(7A)-C(8A)-C(9A)-C(10A)	-1(4)
C(8A)-C(9A)-C(10A)-C(11A)	-23(4)
C(9A)-C(10A)-C(11A)-C(12A)	-2(3)
N(5A)-C(6A)-C(12A)-O(12A)	-130.1(18)
O(7A)-C(6A)-C(12A)-O(12A)	44.7(19)
N(5A)-C(6A)-C(12A)-C(11A)	107.7(19)
O(7A)-C(6A)-C(12A)-C(11A)	-77.5(18)
N(5A)-C(6A)-C(12A)-C(13A)	-7(2)
O(7A)-C(6A)-C(12A)-C(13A)	167.5(14)
C(10A)-C(11A)-C(12A)-O(12A)	-65(2)
C(10A)-C(11A)-C(12A)-C(6A)	55(2)
C(10A)-C(11A)-C(12A)-C(13A)	173.2(17)
O(12A)-C(12A)-C(13A)-O(13A)	-50.5(18)
C(6A)-C(12A)-C(13A)-O(13A)	-171.7(13)
C(11A)-C(12A)-C(13A)-O(13A)	72.4(17)
O(12A)-C(12A)-C(13A)-N(14A)	133.7(14)
C(6A)-C(12A)-C(13A)-N(14A)	13(2)
C(11A)-C(12A)-C(13A)-N(14A)	-103.3(15)
O(13A)-C(13A)-N(14A)-C(4A)	171.9(12)
C(12A)-C(13A)-N(14A)-C(4A)	-13(2)
O(13A)-C(13A)-N(14A)-C(15A)	-11(2)
C(12A)-C(13A)-N(14A)-C(15A)	164.2(12)

Table B6. Continued

C(3A)-C(4A)-N(14A)-C(13A)	-168.4(15)
N(5A)-C(4A)-N(14A)-C(13A)	5.5(19)
C(3A)-C(4A)-N(14A)-C(15A)	14.8(19)
N(5A)-C(4A)-N(14A)-C(15A)	-171.2(12)
N(2A)-C(1A)-C(15A)-N(14A)	20(2)
O(1A)-C(1A)-C(15A)-N(14A)	-165.2(13)
N(2A)-C(1A)-C(15A)-C(16A)	-100.9(19)
O(1A)-C(1A)-C(15A)-C(16A)	74.3(18)
C(13A)-N(14A)-C(15A)-C(1A)	159.6(13)
C(4A)-N(14A)-C(15A)-C(1A)	-23.5(17)
C(13A)-N(14A)-C(15A)-C(16A)	-80.0(15)
C(4A)-N(14A)-C(15A)-C(16A)	96.9(13)
C(1A)-C(15A)-C(16A)-C(1"A)	47.3(14)
N(14A)-C(15A)-C(16A)-C(1"A)	-75.7(12)
C(1A)-C(15A)-C(16A)-C(1'A)	164.5(12)
N(14A)-C(15A)-C(16A)-C(1'A)	41.5(17)
C(4A)-C(3A)-C(17A)-C(20A)	122.4(19)
N(2A)-C(3A)-C(17A)-C(20A)	-61(2)
C(4A)-C(3A)-C(17A)-C(18A)	-109.9(19)
N(2A)-C(3A)-C(17A)-C(18A)	66.7(19)
C(20A)-C(17A)-C(18A)-C(19A)	-62(2)
C(3A)-C(17A)-C(18A)-C(19A)	172.1(17)
C(1'A)-C(16A)-C(1"A)-C(2"A)	-46.4(19)
C(15A)-C(16A)-C(1"A)-C(2"A)	88.9(14)
C(1'A)-C(16A)-C(1"A)-C(6"A)	125.2(15)
C(15A)-C(16A)-C(1"A)-C(6"A)	-99.4(14)
C(6"A)-C(1"A)-C(2"A)-C(3"A)	0.0
C(16A)-C(1"A)-C(2"A)-C(3"A)	171.7(18)
C(1"A)-C(2"A)-C(3"A)-C(4"A)	0.0
C(2"A)-C(3"A)-C(4"A)-C(5"A)	0.0
C(3"A)-C(4"A)-C(5"A)-C(6"A)	0.0
C(4"A)-C(5"A)-C(6"A)-C(1"A)	0.0
C(2"A)-C(1"A)-C(6"A)-C(5"A)	0.0
C(16A)-C(1"A)-C(6"A)-C(5"A)	-171.5(18)
C(1"A)-C(16A)-C(1'A)-C(2'A)	-153.8(17)
C(15A)-C(16A)-C(1'A)-C(2'A)	85(2)
C(1"A)-C(16A)-C(1'A)-C(6'A)	33(2)
C(15A)-C(16A)-C(1'A)-C(6'A)	-89(2)
C(6'A)-C(1'A)-C(2'A)-C(3'A)	0.0
C(16A)-C(1'A)-C(2'A)-C(3'A)	-173(3)
C(1'A)-C(2'A)-C(3'A)-C(4'A)	0.0
C(2'A)-C(3'A)-C(4'A)-C(5'A)	0.0
C(3'A)-C(4'A)-C(5'A)-C(6'A)	0.0
C(4'A)-C(5'A)-C(6'A)-C(1'A)	0.0
C(2'A)-C(1'A)-C(6'A)-C(5'A)	0.0
C(16A)-C(1'A)-C(6'A)-C(5'A)	173(3)

Table B7. Hydrogen Bonds for Glo11_6 [A and deg.].

D-H...A	d(D-H)	d(H...A)	d(D...A)	<(DHA)
O(12)-H(12)...O(1a)#1	0.83	1.96	2.695(13)	148
O(12a)-H(12a)...O(1)#2	0.83	1.92	2.670(14)	149

Symmetry transformations used to generate equivalent atoms:
#1 -x+3/2,y+1/2,-z+2 #2 -x+3/2,y-1/2,-z+1

REFERENCES

1. Queiroz, E. F.; Hostettmann, K.; Wolfender, J. Modern Approaches in the Search for New Active Compounds from Crude Extracts of Natural Sources. In *Plant Bioactives and Drug Discovery;* John Wiley & Sons, Inc.: 2012; pp 43-80.

2. Gloer, J. B. Applications of Fungal Ecology in the Search for New Bioactive Natural Products. In *The Mycota; Vol. IV;* Kubicek, C. P., Druzhinina, I. S., Eds.; Springer–Verlag: New York, 2007; Vol. IV, pp 257-283.

3. Newman, D. J.; Cragg, G. M. *J. Nat. Prod.* **2007**, *70*, 461-477.

4. Cragg, G. M.; Grothaus, P. G.; Newman, D. J. *J. Nat. Prod.* **2014**, *77*, 703-723.

5. Mueller, G. M.; Schmit, J. P. *Biodervers. Conserv.* **2007**, *16*, 1-5.

6. Brenton, R. C.; Reynolds, W. F. *Nat. Prod. Rep.* **2013**, *30*, 501-524.

7. Crews, P.; Rodriguez, J.; Marcel, J. Mass Spectrometry: Core Techniques and Ionization Processess. In *Organic Structure Analysis;* Oxford University Press: New York, 2010; Vol. Second Edition, pp 273-324.

8. Smyth, M. S.; Martin, J. H. *Mol. Path.* **2000**, *50*, 8-14.

9. Crews, P.; Rodriguez, J.; Jaspars, M. Using Spectroscopic and Analytical Data in Organic Structure Analysis. In *Organic Structure Analysis;* Oxford Press: New York, 2010; Vol. Second Edition, pp 1-20.

10. Reynolds, W. F.; Enriquez, R. G. *J. Nat. Prod.* **2002**, *65*, 221-244.

11. Wynants, C.; Hallenga, K.; Van Binst, G.; Michel, A.; Zanin, J. *J. Magn. Reson.* **1984**, *57*, 93-98.

12. Kessler, H.; Griesenger, C.; Zarbock, J.; Loosli, H. R. *J. Magn. Reson.* **1984**, *57*, 331-336.

13. Reynolds, W. F.; Enriquez, R. G.; Escobar, L. I.; Lozoya, X. *Can. J. Chem.* **1984**, *62*, 2421-2425.

14. Patt, S. L.; Shoolery, J. N. *J. Magn. Reson.* **1982**, *46*, 535-539.

15. Morris, G. A.; Freeman, R. *J. Am. Chem. Soc.* **1979**, *101*, 760-761.

16. Doddrell, D. M.; Pegg, D. T.; Bendall, M. R. *J. Magn. Reson.* **1982**, *48*, 323-327.

17. Bigler, P.; Kümmerle, R.; Bermel, W. *Magn. Reson. Chem.* **2007**, *45*, 469-472.

18. Bax, A.; Freeman, R. *J. Magn. Reson.* **1981**, *44*, 542-561.

19. Hurd, R. E. *J. Magn. Reson.* **1990**, *87*, 422-428.

20. Piantini, U.; Sorensen, O. W.; Ernst, R. R. *J. Am. Chem. Soc.* **1982**, *104*, 6800-6801.

21. Davis, D. G.; Bax, A. *J. Am. Chem. Soc.* **1985**, *107*, 7197-7198.

22. Boyer, R.; Johnson, R.; Krishnamurthy, K. *J. Magn. Reson.* **2003**, *165*, 253-259.

23. Hu, H.; Krishnamurthy, K. *Magn. Reson. Chem.* **2008**, *46*, 683-689.

24. Willker, W.; Liebfrits, D.; Kerresebaum, R.; Bermel, W. *Magn. Reson. Chem.* **1993**, *31*, 287-292.

25. Krishnamurthy, V. V.; Russell, D. J.; Hadden, C. E.; Martin, G. E. *J. Magn. Reson.* **2000**, *146*, 232-239.

26. Nyberg, N. T.; Duus, J. O.; Sorensen, O. W. *J. Am. Chem. Soc.* **2005**, *127*, 6154-6155.

27. Furrer, J. Chapter 6 - Recent Developments in HMBC Studies. In *Annual Reports on NMR Spectroscopy;* Academic Press: 2011; Vol. 74, pp 293-354.

28. Ellis, G. A.; Wyche, T. O.; Fry, C. G.; Braun, D. R.; Bugni, T. S. *Mar. drugs* **2014**, *12*, 1013-1022.

29. Karplus, M. A. *J. Am. Chem. Soc.* **1963**, *85*, 2870-2871.

30. Hansnoot, C. A. G.; Deleeuw, F. A. A. M.; Altona, C. *Tetrahedron* **1980**, *36*, 2783-2792.

31. Macura, S.; Huang, Y.; Suter, D.; Ernst, R. R. *J. Magn. Reson.* **1981**, *43*, 259-281.

32. Bax, A.; Davis, D. G. *J. Magn. Reson.* **1985**, *63*, 207-213.

33. Hoye, T. R.; Jeffery, C. S.; Shao, F. *Nat. Protoc.* **2007**, *2*, 2451-2458.

34. Shanda, P.; Kupce, E.; Brutscher, B. *J. Biomol. NMR* **2005**, *33*, 199-211.

35. Kupce, E.; Freeman, R. *Magn. Reson. Chem.* **2007**, *45*, 2-4.

36. Furrer, J. *Chem. Commun.* **2010**, *46*, 3396-3398.

37. Gurevich, A. Z.; Barkushov, I. L.; Aresniev, A. S.; Bystrov, V. F. *J. Magn. Reson. Chem.* **1984**, *56*, 471-478.

38. Kupce, E.; Freeman, R. *J. Am. Chem. Soc.* **2008**, *130*, 10788-10792.

39. Hoch, J. C.; Maciejewski, M. W.; Mobli, M.; Schuyler, A. D.; Stern, A. S. *Acc. Chem. Res.* **2014**, *47*, 708-717.

40. Mobli, M.; Maciejwski, M. W.; Schuyler, A. D.; Stern, A. S.; Hoch, J. C. *Phys. Chem. Chem. Phys* **2012**, *14*, 10835-10843.

41. Elyashberg, M.; Williams, A. J.; Blinov, K. *Nat. Prod. Rep.* **2010**, *27*, 1296-1328.

42. Ibraheim, Z. Z.; Abdel-Mageed, W. M.; Dai, H.; Guo, H.; Zhang, L.; Jaspars, M. *Phytother. Res.* **2012**, *26*, 579-586.

43. Brkljaca, R.; Urban, S. *J. Liq. Chromatogr. Rel. Technol.* **2011**, *34*, 1063-1076.

44. Dias, D. A.; White, J. M.; Urban, S. *Nat. Prod. Commun.* **2009**, *4*, 157-172.

45. Krucker, M.; Lienau, A.; Putzbach, K.; Grynbaum, M. D.; Schuler, P.; Albert, K. *Anal. Chem* **2004**, *76*, 2623-2628.

46. Gronquist, M.; Meinwald, J.; Eisner, T.; Schroeder, F. C. *J. Am. Chem. Soc.* **2005**, *127*, 10810-10811.

47. Sprogoe, K.; Staerk, D.; Jaeger, A. K.; Adersen, A.; Hansen, S. H.; Witt, M.; Landbo, A. -. R.; Meyer, A. S.; Jaroszewski, J. W. *J. Nat. Prod.* **2007**, *70*, 1472-1477.

48. Lambert, M.; Wolfender, J. -.; Staerk, D.; Christensen, S. B.; Hostettman, K.; Jaroszewski, J. W. *Anal. Chem.* **2007**, *79*, 727-735.

49. Nugroho, A. E.; Morita, H. *J. Nat. Med.* **2014**, *68*, 1-10.

50. Neff, S. A.; Lee, S. U.; Asami, Y.; Ahn, J. S.; Oh, H.; Baltrusaitis, J.; Gloer, J. B.; Wicklow, D. T. *J. Nat. Prod.* **2012**, *75*, 464-472.

51. Schmidt, L. E.; Deyrup, S. T.; Baltrusaitis, J.; Swenson, D. C.; Wicklow, D. T.; Gloer, J. B. *J. Nat. Prod.* **2010**, *73*, 404-408.

52. Jiao, P.; Mudur, S. V.; Gloer, J. B.; Wicklow, D. T. *J. Nat. Prod.* **2007**, *70*, 1308-1311.

53. Rodriguez, R. J.; Jr., J. F. W.; Arnold, A. E.; Redman, R. S. *New Phytol.* **2009**, *182*, 314-330.

54. Sy, A. A.; Swenson, D. C.; Gloer, J. B.; Wicklow, D. T. *J. Nat. Prod.* **2008**, *71*, 415-419.

55. Shim, S. H.; Baltrusaitis, J.; Gloer, J. B.; Wicklow, D. T. *J. Nat. Prod.* **2011**, *74*, 395-401.

56. Wicklow, D. T.; Jordan, A. M.; Gloer, J. B. *Mycol. Res.* **2009**, *113*, 1433-1442.

57. Dowd, P. F.; Johnson, E. T.; Vermillion, K. E.; Berhow, M. A.; Palmquist, D. E. *Entomol. Exp. Appl.* **2011**, *141*, 208-215.

58. Dowd, P. F.; Johnson, E. T.; Pinkerton, T. S. *J. Agric. Food Chem.* **2007**, *55*, 3421-3428.

59. Buchl, G.; White, J. D.; Wogan, G. N. *J. Am. Chem. Soc.* **1965**, *87*, 3484-3489.

60. Zhu, J.; Porco, J. A. *Org. Lett.* **2006**, *8*, 5169-5171.

61. Philips, M. R.; Cox, A. D. *J. Clin. Invest.* **2007**, *117*, 1223-1225.

62. Blias, L. A.; Apsimon, J. W.; Blackwell, B. A.; Greenhalgh, R.; Miller, J. D. *Can. J. Chem.* **1992**, *40*, 1281-1287.

63. Savard, M. E.; Miller, J. D.; Salleh, B.; Strange, R. N. *Mycopathologia* **1990**, *110*, 177-181.

64. Grove, J. F.; Hitchcock, P. B. *J. Chem. Soc. Perkin Trans. I* **1991**, 997-999.

65. Shier, W. T.; Abbas, H. K. *Toxicon* **1992**, *30*, 1295-1298.

66. Jerram, W. A.; McInnes, A. G.; Maass, W. S. G.; Smith, D. G.; Taylor, A.; Walter, J. A. *Can. J. Chem.* **1975**, *53*, 727-737.

67. Kingsland, S. R.; Barrow, R. A. *Aust. J. Chem* **2009**, *62*, 269-274.

68. Phillips, N. J.; Goodwin, J. T.; Fraiman, A.; Cole, R. J.; Lynn, D. G. *J. Am. Chem. Soc.* **1989**, *111*, 8223-8231.

69. Singh, S. B.; Zink, D. L.; Goetz, M. A.; Dombrowski, A. W.; Polishook, J. D.; Hazuda, D. J. *Tetrahedron Lett.* **1998**, *39*, 2243-2246.

70. Bloch, P.; Tamm, C. *Helv. Chim. Acta* **1981**, *64*, 304-315.

71. Roy, K.; Chatterjee, S.; Deshmukh, S. K.; Vijayakumar, E. K. S.; Ganguli, B. N.; Fehlhaber, H. W. *J. Antibiot.* **1996**, *49*, 1186-1187.

72. Arai, K.; Yoshimura, T.; Itatani, Y.; Yamamoto, Y. *Chem. Pharm. Bull.* **1983**, *31*, 925-933.

73. Holler, U.; Gloer, J. B.; Wicklow, D. T. *J. Nat. Prod.* **2002**, *65*, 876-882.

74. Kimura, Y.; Nakahara, S.; Fujioka, S. *Biosci. Biotech. Biochem.* **1996**, *60*, 1375-1376.

75. Keromnes, J.; Thouvenot, D. *Appl. Environ. Microbiol.* **1985**, *49*, 660-663.

76. Rao, A. V. R.; Reddy, E. R.; Sharma, G. V. M.; Yadagiri, P.; Yadav, J. S. *Tetrahedron* **1986**, *42*, 4523-4532.

77. Inoue, M.; Takaenaka, H.; Tsurushima, T.; Miyagawa, H.; Ueno, T. *Tetrahedron Lett.* **1996**, *37*, 5731-5734.

78. Zheng, C. J.; Yu, H. E.; Kim, E. H.; Kim, W. G. *J. Antibiot.* **2008**, *61*, 633-637.

79. Nicolaou, K. C.; Nilewski, C.; Hale, C. R. H.; Ioannidou, H. A.; El Marrouni, A.; Koch, L. G. *Angew. Chem. Int. Ed.* **2013**, *52*, 8736-8741.

80. Marrero, J. G.; Harwood, L. M. *Tetrahedron Lett.* **2009**, *50*, 3574-3576.

81. Jurjevic, Z.; Peterson, S. W.; Horn, B. W. *IMA Fungus* **2012**, *3*, 59-79.

82. Kingston, D. G. I.; Chen, P. N.; Vercellotti, J. R. *Phytochemistry* **1976**, *15*, 1037-1039.

83. Fuscher, J. Ph.D. Thesis: Beeinflussung der Sekundarstoffbildung bei *Aspergillus ochraceus* durch Variation der Kulturbedingungen sowie Isolierung, Strukturaufklarung und Biosynthese der neuen Naturstoffe, University of Göttingen, Göttingen, Germany, 1995 (Prof. A. Zeeck).

84. Sugie, Y.; Hirai, H.; Inagaki, T.; Ishiguro, M.; Kim, Y.; Kojima, Y.; Sakakibara, T.; Sakemi, S.; Sugiura, A.; Suzuki, Y.; Brennan, L.; Duignan, J.; Huang, L.; Sutcliffe, J.; Kojima, N. *J. Antibiot.* **2001**, *54*, 911-916.

85. Tsukamoto, S.; Kato, H.; Samizo, M.; Nojiri, Y.; Onuki, H.; Hirota, H.; Ohta, T. *J. Nat. Prod.* **2008**, *71*, 2064-2067.

86. Kato, H.; Yoshida, T.; Tokue, T.; Nojiri, Y.; Hirota, H.; Ohta, T.; Williams, R.; Tsukamoto, S. *Angew. Chem. Int. Ed.* **2007**, *46*, 2254-2256.

87. Tsukamoto, S.; Kato, H.; Greshock, T. J.; Hirota, H.; Ohta, T.; Williamn, R. M. *J. Am. Chem. Soc.* **2009**, *131*, 3834-3835.

88. Lu, X.; Shi, Q.; Zheng, Z.; Ke, A.; Zhang, H.; Huo, C.; Ma, Y.; Ren, X.; Li, Y.; Lin, J.; Jiang, Q.; Gu, Y.; Kiyota, H. *Eur. J. Org. Chem.* **2011**, *2011*, 802-807.

89. Li, G.; Yang, T.; Luo, Y.; Chen, X.; Fang, D.; Zhang, G. *Org. Lett.* **2009**, *11*, 3714-3717.

90. Li, G.; Li, L.; Yang, T.; Chen, X.; Fang, D.; Zhang, G. *Helv. Chim. Acta* **2010**, *93*, 2075-2080.

91. Kassaee, M. Z.; Arshadi, S.; Ahmadi-Taheri, N. *J. Mol. Struct.* **2005**, *715*, 107-115.

92. Vogel, E.; Gunther, H. *Angew. Chem. Int. Ed.* **1967**, *6*, 385-476.

93. Bock, C. W.; George, P.; Stezoxski, J. J.; Glusker, J. P. *Struct. Chem.* **1988**, *1*, 33-39.

94. Dowd, P. F. *Entomol. Exp. Appl.* **1988**, *47*, 69-71.

95. Plattner, R. D. *J. Chem. Res.* **1988**, 2461-2473.

96. Sudakin, D. *Toxicol. Lett.* **2003**, *143*, 97-107.

97. Freeman, G. *J . Gen. Microbiol.* **1955**, *12*, 213-221.

98. Sy-Cordero, A. A.; Graf, T. N.; Adcock, A. F.; Kroll, D. J.; Chen, Q.; Swanson, S. M.; Wani, M. C.; Pearce, C. J.; Oberlies, N. H. *J. Nat. Prod.* **2011**, *74*, 2137-2142.

99. Amagata, T.; Morinaka, B.; Amagata, A.; Tenney, K.; Valeriote, F.; Lobkovsky, E.; Clardy, J.; Crews, P. *J. Nat. Prod.* **2006**, *69*, 1560-1565.

100. Marfey, P. *Carlsberg Res. Commun.* **2007**, *49*, 591-596.

101. Bhushan, R.; Bruckner, H. *Amino Acids* **2004**, *27*, 231-247.

102. Faden, A.; Movsesyan, V.; Knoblach, S.; Ahmed, F.; Cernak, I. *Neuropharmacology* **2005**, *49*, 410-424.

103. Zhou, Y.; Debbab, A.; Mandi, A.; Wray, V.; Schultz, B.; Muller, W.; Kassack, M.; Lin, W.; Kurtan, T.; Proksch, P.; Aly, A. *Eur. J. Org. Chem.* **2013**, *2*, 894-906.

104. Krasnof, S.; Keresztes, I.; Gillilan, R.; Szebenyi, D.; Donzelli, B.; Churchill, A.; Gibson, D. *J. Nat. Prod.* **2007**, *70*, 1919-1924.

105. Frehenhagen, A.; Molleyres, L.; Bohlendorf, B.; Laue, G. *J. Antibiot.* **2006**, *59*, 267-280.

106. Flesch, P.; Stockinger, G. *Fresenius Z. Anal. Chem* **1988**, *330*, 152-154.

107. Soledade, M.; Pedras, C.; Taylor, J. L. *J. Org. Chem.* **1993**, *58*, 4778-4780.

108. Snowden, R. L.; Grenno, R.; Vial, C. *Flavour Fragr. J.* **2005**, *20*, 372-380.

109. Qu, S.; Kolodziej, E. P.; Cwiertny, D. M. *Environ. Sci. Technol.* **2012**, *46*, 13202-13211.

110. Schiffer, B.; Daxenberger, A.; Meyer, K.; Meyer, H. H. D. *Environ. Health Perspect.* **2001**, *109*, 1145-1151.

111. Card, M. L.; Chin, Y. -.; Lee, L. S.; Khan, B. *J. Agric. Food Chem.* **2012**, *60*, 1480-1487.

112. Webster, J. P.; Kover, S. C.; Bryson, R. J.; Harter, T.; Mansell, D. S.; Sedlak, D. L.; Kolodziej, E. P. *Environ. Sci. Technol.* **2012**, *46*, 3803-3810.

113. Orn, S.; Yamani, S.; Norrgren, L. *Arch. Environ. Contam. Toxicol.* **2006**, *51*, 237-243.

114. Jensen, K. M.; Makynen, E. A.; Kahl, M. D.; Ankley, G. T. *Environ. Sci. Technol.* **2006**, *40*, 3112-3117.

115. Khan, B.; Lee, L. S.; Sassman, S. A. *Environ. Sci. Technol.* **2008**, *42*, 3570-3574.

116. Jain, N.; Allan, G.; Linton, O.; Tannenbaum, P.; Chen, X.; Gunnet, J.; Demarest, K.; Lundeen, S.; Murray, W.; Sui, Z. *Bioorg. Med. Chem. Lett.* **2009**, *19*, 3977-3980.

117. Food and Drug Administration Environmental Assessment- NADA- Revalor (trenbolone acetate and estradiol) Cattle Ear Implant. *http://www.fda.gov/ucm/groups/fdagov-public/@fdagov-av-gen/documents/document/ucm072272.pdf*2012).

118. Woodward, R. B. *J. Am. Chem. Soc.* **1941**, *63*, 1123-1126.

119. Fieser, L. F.; Fieser, M.; Rajagopalan, S. *J. Org. Chem.* **1948**, *13*, 800-806.

120. Kolodziej, E. P.; Qu, S.; Forsgren, K.; Long, S. A.; Gloer, J. B.; Jones, G.; Schlenk, D.; Baltrusaitis, J.; Cwiertny, D. M. *Environ. Sci. Technol.* **2013**, *47*, 5031-5041.

121. Qu, S.; Kolodziej, E. P.; Long, S. A.; Gloer, J. B.; Patterson, E. V.; Baltrusaitis, J.; Jones, G. D.; Benchetler, P. V.; Cole, E. A.; Kimbrough, K. C.; Tarnoff, M.; Cwiertny, D. M. *Science* **2013**, *342*, 347-351.

122. Simpson, A. J.; Simpson, M. J.; Soong, R. *Environ. Sci. Technol.* **2012**, *46*, 11488-11496.

123. Bullock, E.; Roberts, J. C.; Underwood, J. G. *J. Chem. Soc* **1962**, 4179-4183.

124. Qian-Cutrone, J.; Huang, S.; Shu, Y.; Vyas, D.; Fairchild, C.; Menendez, A.; Krampitz, K.; Dalterio, R.; Klohr, S.; Gao, Q. *J. Am. Chem. Soc.* **2002**, 14556.